
Electrophosphorescent Materials for use in Organic Light Emitting Devices

Hugo Bronstein

A thesis submitted in partial fulfilment of the requirements for the degree of Doctor of
Philosophy in Chemistry

Imperial College London

January 2009

Declaration

The work performed in this thesis was carried out in the Chemistry Department, Imperial College London, between October 2005 and September 2008 and is the work of the author unless otherwise stated.

Contents

Declaration	2
Abstract	6
Acknowledgements	7
Publications	8
Abbreviations	9
Chapter 1: Introduction	12
1.1 <i>Organic light emitting devices</i>	13
1.1.1 Discovery	13
1.2 <i>Energy level diagram</i>	14
1.2.1 Anode.....	15
1.2.2 Hole transport layer (HTL)	15
1.2.3 Cathode	16
1.2.3 Electron transport layer (ETL).....	16
1.2.4 Emissive layer (EML)	16
1.3 <i>Quantum efficiency</i>	17
1.4 <i>Phosphorescent complexes and singlet-triplet harvesting</i>	18
1.4.1 Emission from phosphorescent complexes	19
1.5 <i>Host-guest systems</i>	20
1.6 <i>Mechanisms of energy transfer</i>	21
1.6.1 Radiative energy transfer	22
1.6.2 Förster energy transfer ^{9,13,24}	22
1.6.3 Dexter energy transfer (electron exchange excitation transfer) ^{9,13,24}	22
1.6.4 Charge trapping ^{9,13,24}	23
1.7 <i>Developments in OLED technology</i>	23
1.8 <i>Fine tuning of emissive properties</i>	25
1.9 <i>Solution processability and preventing phase separation</i>	26
1.10 <i>Red emitting phosphorescent iridium complexes</i>	28
Chapter 2 : Investigation into the phosphorescence of a series of substituted iridium(III)bis(phenylisoquinoline)(acac) complexes	31
2.1 <i>Introduction</i>	32
2.2 <i>Synthesis</i>	35
2.2.1 Target materials.....	35
2.2.2 Synthesis of bromo substituted complexes.....	36
2.2.2.1 Synthesis of bromo substituted ligands	36
2.2.2.2 Preparation of bromo substituted iridium complexes.....	37
2.2.3 Synthesis of fluorenyl substituted iridium complexes.....	39
2.2.3.1 Synthesis of fluorenyl substituted ligands	39
2.2.3.2 Complexation of fluorenyl substituted ligands.....	40
2.3 <i>Photophysical properties of iridium complexes</i>	42
2.3.1 UV-Vis absorption spectra	42
2.3.1.1 Bromo substituted iridium complexes.....	42
2.3.1.2 Fluorenyl substituted iridium complexes.....	43
2.3.2 Solution photoluminescence spectra	43

2.3.2.1 Bromo substituted iridium complexes.....	43
2.3.2.2 Fluorenyl substituted iridium complexes.....	44
2.3.2.3 Quantum yields.....	45
2.3.3 Experimental measurements of energy levels	46
2.3.4 DFT and TDDFT calculations	47
2.3.4.1 Comparison of DFT optimization and X-ray crystal structure.....	47
2.3.4.2 Comparison of experimental and calculated energy levels	49
2.3.4.3 Comparison of singlet and triplet excited states	52
2.3.4.4 DFT and TD-DFT calculations of bromo substituted iridium complexes.....	55
2.3.4.5 DFT calculations of fluorenyl substituted iridium complexes.....	58
2.3.4.6 Note on the effect of the complex structure on the quantum yields.....	61
2.4 Conclusions.....	61
Chapter 3: Polymeric iridium(III)bis(phenylisoquinoline)(acac) complexes	63
3.1 Introduction	64
3.1.1 Non conjugated polymer backbones.....	64
3.1.2 Conjugated Polymer backbones.....	65
3.1.2.1 Use of bis(phenylisoquinoline)iridium complexes in polymeric materials	66
3.1.3 Importance of energy level matching.....	68
3.1.4 Aim of this study.....	70
3.1.5 Materials to be used	71
3.2 Synthesis.....	72
3.2.1 Synthesis of AB monomers.....	72
3.2.1.1 Synthesis of AB fluorene monomer	72
3.2.1.2 Synthesis of AB 2,7 carbazole monomer	73
3.2.1.3 Synthesis of 3,6 Carbazole Monomer	74
3.2.2 Synthesis of conjugated iridium complexes by AB polymerizations.....	74
3.2.2.1 Analysis of the polymers	76
3.2.2.2 End group analysis	80
3.2.3 Synthesis of polymer complexes by a macromonomer approach.....	81
3.2.3.1 Synthesis of F8BT monomers.....	81
3.2.3.2 Synthesis of conjugated iridium complexes via the macromonomer approach.....	84
3.2.3.3 Analysis of the polymer complexes	84
3.2.3.4 End group analysis	87
3.3 Photophysical properties	87
3.3.1 UV-Vis absorption.....	87
3.3.2 Photoluminescence	88
3.3.3 Energy Levels of Polymers.	91
3.3.4 Discussion of the emission properties of the polymer-iridium complexes	92
3.4 Conclusions.....	97
Chapter 4: Alternating and random copolymers of iridium complexes and oligofluorenes	98
4.1 Introduction.....	99
4.1.1 Triplet-Triplet (T-T) Annihilation.....	99
4.1.1.1 Encapsulation.....	100
4.1.1.2 Copolymers incorporating iridium complexes and conjugated polymers	101
4.1.2 Synthetic Strategy.....	103
4.2 Synthesis.....	104
4.2.1 Synthesis of monodisperse macromonomers	105
4.2.2 Synthesis of polydisperse macromonomers.....	107
4.2.2.1 Analysis of macromonomers	108
4.2.2.2 End group analysis	110
4.2.2.3 UV-Vis absorption of macromonomers	110
4.2.3 Synthesis of Alternating Copolymers.....	111
4.2.4 Calculating Iridium loading in the alternating copolymers.....	114
4.2.4.1 End group analysis	116

4.2.5 Synthesis of random copolymers.....	117
4.2.6.1 End group analysis	119
4.3 <i>Photophysical properties of the alternating and random copolymers</i>	120
4.3.1 Absorption Spectroscopy.....	120
4.3.2 Solution photoluminescence of the alternating and random copolymers.....	121
4.3.2.1 Solution quantum yields of the alternating and the random copolymers.....	124
4.3.3 Thin film photoluminescence measurements of the alternating and random copolymers ..	126
4.3.3.1 Thin Film Quantum Yields of the Alternating and the Random Copolymers	128
4.4 <i>Conclusions</i>	129
Chapter 5: Asymmetric “Multifunctional” Iridium Complexes.....	130
5.1 <i>Introduction</i>	131
5.1.1 Multifunctional iridium complexes.....	131
5.1.2 Multifunctional polymeric/dendritic materials	132
5.1.3 Synthetic plan	134
5.1.4 Asymmetric iridium complexes	134
5.1.5 Target materials.....	137
5.2 <i>Synthesis</i>	137
5.2.1 Well defined complexes	137
5.2.2 Synthesis of the asymmetric iridium complex.....	138
5.2.3 Completion of asymmetric multifunctional iridium complex.....	139
5.2.4 Synthesis of asymmetric regioismer.....	140
5.2.5 Synthesis of symmetric carbazole substituted iridium complex	142
5.2.6 Photophysical properties of asymmetric complex	143
5.3 <i>Asymmetric polymeric iridium complexes</i>	145
5.3.1 Boronic acid protecting groups.....	146
5.3.1.1 Acid labile boronic acid protecting group	146
5.3.1.2 Base labile boronic acid protecting group	146
5.3.1.3 Strategy	147
5.3.2 Synthesis of protected fluorene units	147
5.3.3 Attempted synthesis of protected asymmetric iridium complex	149
5.3.4 Modification of synthetic route.....	151
5.3.5 Synthesis of functionalized asymmetric iridium complex	152
5.3.6 Alternative strategy for synthesis of asymmetric polymeric iridium complexes.....	155
5.3.7 Synthesis	156
5.4 <i>Conclusions</i>	163
Chapter 6: Experimental Procedures	164
6.1 <i>Materials</i>	165
6.2 <i>Measurements</i>	165
6.2.1 Absorption and Emission Spectroscopy.....	165
6.2.2 Theoretical Methods	166
6.2.3 Cyclic Voltammetry.....	166
6.3 <i>Experimental For Chapter 2</i>	167
6.4 <i>Experimental for Chapter 3</i>	183
6.5 <i>Experimental for Chapter 4</i>	197
6.6 <i>Experimental For Chapter 5</i>	212
Chapter 7: References.....	229
Appendix A.....	242
Appendix B.....	246
Appendix C.....	247

Abstract

A series of novel regioisomeric iridium complexes based on [iridium(III)bis(1-phenylisoquinolino-*N,C*²)(acetylacetonate)] bearing either bromine or fluorenyl substituents were synthesized and their photophysical properties probed. Observed variations of the emission wavelength are caused by changes to the HOMO and LUMO energy levels which were measured by cyclic voltammetry and optical spectroscopy. The effect of the substituents, in their various positions, on the frontier orbitals were investigated with density functional theory (DFT), which was validated through comparison of predicted energetic properties with those measured.

Polymeric analogues of the small complexes were synthesized bearing a range of conjugated polymers with different triplet energy levels. It was found that the trends observed in the well defined complexes were maintained in the polymeric ones. Furthermore, the thin film phosphorescent quantum yield was observed to vary significantly depending on the attached polymer due to the amount of triplet energy back transfer that could occur.

The effect of having multiple complexes incorporated into a polymer chain was subsequently investigated. It was found that maintaining the complexes a maximum distance apart led to significantly more efficient emission in solution and thin film which was believed to be due to a reduction in triplet-triplet annihilation.

Finally, the synthesis of novel asymmetric bis-cyclometallated iridium complexes bearing different cyclometallating ligands is presented which could allow tailoring of ligands to specific roles such as hole or electron transport. Brief photophysical studies were performed demonstrating the participation of both ligands in emission processes. Synthetic steps towards polymeric analogues are also presented and their limitations discussed.

Acknowledgements

Firstly, I would like to thank Dr. Charlotte Williams, my supervisor, for giving me the opportunity to carry out this work and for her help and support throughout. I would also like to thank Prof. Richard Friend, Dr. Kiril Kirov and Dr. Chris Finlayson, my collaborators in Cambridge University, for their helpful discussions and suggestions, and for their hard work in device preparation and photophysical studies.

I would like to thank Pete Haycock and Dick Shephard for running an excellent NMR service, Andy White for the X-ray crystallography and explanations, John Barton for the mass spectrometry and Matt Harvey for the outstanding HPC service.

I am very grateful to Dr. Paul Knight who taught me how to do chemistry and for making the lab everything it is. I would also like to thank Dr. Nick Evans for his helpful comments and suggestions and for explaining lots of things to me.

Thanks to all the members of the Williams group past and present: Anita, Linda, Sven, Min, Ash, Harry, Turkey, Ping, Mike, Katherine, Jenny and Ros. In particular I would like to thank Rachel for listening to my complaints and putting up with me working next to her for 3 years, and Coco for his love of Genesis and Jeff Wayne.

I am extremely grateful to the following people who helped me in various areas of which I had little knowledge and were very patient with me and for letting me use their equipment. Dr. Paul Wilde – cyclic voltammetry; Dr. Henry Rzepa – Gaussian; Siva – integrating sphere.

Finally, I would like to thank all my friends and family for putting up with me over the last 3 years and for all their support. I am eternally grateful to my parents and Pablo for always being there for me, and Arwen for looking after me and being everything I could wish for.

Publications

The following publications have arisen from the work described in this thesis and can be found in Appendices B and C.

1. Investigation into the phosphorescence of a series of regioisomeric iridium(III) complexes

Bronstein, H. A.; Finlayson, C. E.; Kirov, K. R.; Friend, R. H.; Williams, C. K. *Organometallics* **2008**, *27*, 2980.

2. Charge recombination in organic photovoltaic devices with high open-circuit voltages

Westenhoff, S.; Howard, I. A.; Hodgkiss, J. M.; Kirov, K. R.; Bronstein, H. A.; Williams, C. K.; Greenham, N. C.; Friend, R. H. *J. Am. Chem. Soc.* **2008**, *130*, 13653.

Abbreviations

27PCz	poly(<i>N</i> -octyl-2,7-carbazole)
36PCz	poly(<i>N</i> -octyl-3,6-carbazole)
°	degrees
δ	chemical shift
μ	micro
Å	angstrom
approx	approximately
aq.	aqueous
Ar	aromatic
br	broad
Bu	butyl
C	Celcius
calcd.	calculated
CI	chemical ionisation
d	doublet
DFT	density functional theory
DP	degree of polymerisation
EML	emissive layer
Et	ethyl
ETL	electron transporting layer
eq.	equivalents
ESI	electrospray ionisation
F8BT	poly(9,9'-dioctylfluorene- <i>co</i> - benzothiadiazole)
FAB	fast atom bombardment
g	grams
GPC	gel permeation chromatography
h	hours
HTL	hole transporting layer
HOMO	highest occupied molecular orbital
Hz	Hertz
<i>i</i>	iso

IR	infra red
<i>J</i>	coupling constant
L	litre
LUMO	lowest unoccupied molecular orbital
m	milli, multiplet, minutes
m.p.	melting point
M	molar
M_n	number averaged molecular weight
M_w	weight averaged molecular weight
MALDI-TOF	matrix assisted laser desorption ionisation – time of flight
MHz	megahertz
MS	mass spectrometry
Me	methyl
mol	moles
<i>n</i>	neo
NMR	nuclear magnetic resonance
OLED	organic light emitting device
PDI	polydispersity
PFO	poly(9,9-dioctylfluoren-2,7-diyl)
Ph	phenyl
Piq	phenylisoquinoline
PL	photoluminescent
ppm	parts per million
Ppy	phenylpyridine
q	quartet
s	second, singlet
SEC	size exclusion chromatography
soln	solution
SOMO	singly occupied molecular orbital
<i>t, tert</i>	tertiary
t	triplet, time
T	temperature
TD-DFT	time dependant – density functional theory

T_g	glass transition temperature
T_m	melting temperature
THF	tetrahydrofuran
TMS	trimethylsilyl
Tol	toluene
UV-Vis	ultraviolet-visible
w/v	weight by volume
w/w	weight by weight

Chapter 1: Introduction

1.1 Organic light emitting devices

Organic Light Emitting Devices (OLEDs) emit visible light on application of an electric current. As the name suggests, the difference between OLEDs and conventional LEDs is the use of organic components in their construction.

A typical OLED is constructed as shown below (Fig. 1.1), and the basic working principle is that electrons are injected from the cathode; whilst holes are injected from the anode. The holes and electrons travel through the various layers until they reach the emissive layer where they can recombine and emit light; a phenomenon known as electroluminescence.

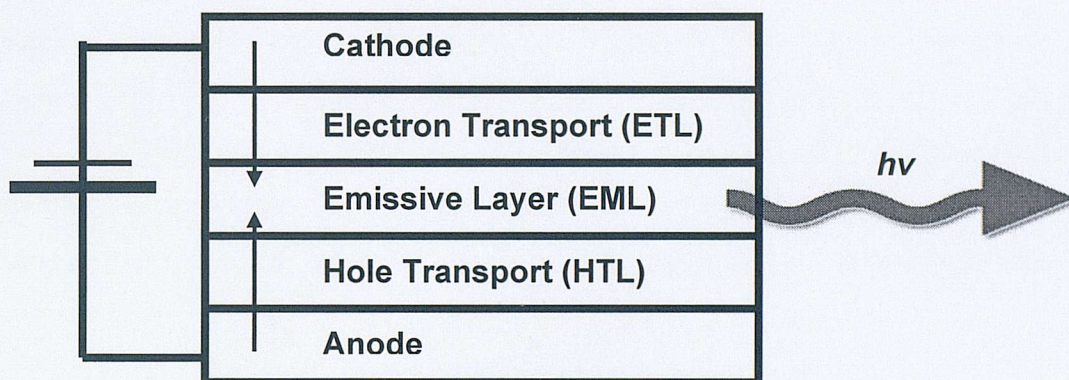


Figure 1.1: Typical OLED construction

1.1.1 Discovery

The discovery of the OLED is attributed to Tang *et al* in 1987 who used a double organic layer comprising of aromatic diamine layer, and a layer of fluorescent complex tris(8-hydroxyquinoline)aluminium(III) (Alq_3) 1.1 sandwiched between an indium tin oxide (ITO) anode and a metal cathode.¹

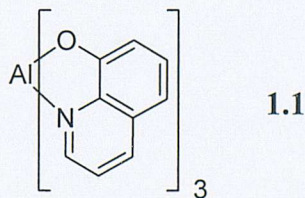
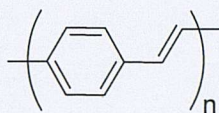


Figure 1.2: Tris(8-hydroxyquinoline)aluminium(III) (Alq_3)

Another early example of an OLED was developed in 1990 by Burroughes *et al*, where a layer of conjugated polymer poly(1,4-phenylenevinylene) (PPV) **1.2** spin coated between two electrodes displayed electroluminescence.²



1.2

Figure 1.3: poly(1,4-phenylenevinylene) (PPV)

1.2 Energy level diagram

Construction of an OLED requires the consideration of the energy levels of the materials used in order to ensure efficient transport of electrons and holes and that the charge recombination event occurs in the correct section of the device. The energy level diagram (Fig. 1.4) shows the frontier orbital energy levels of an ideal OLED and demonstrates the movement of electrons and holes through the device. An enormous amount of investigation has been carried out in order to develop and identify suitable materials that possess the required electronic properties for each layer in an OLED.

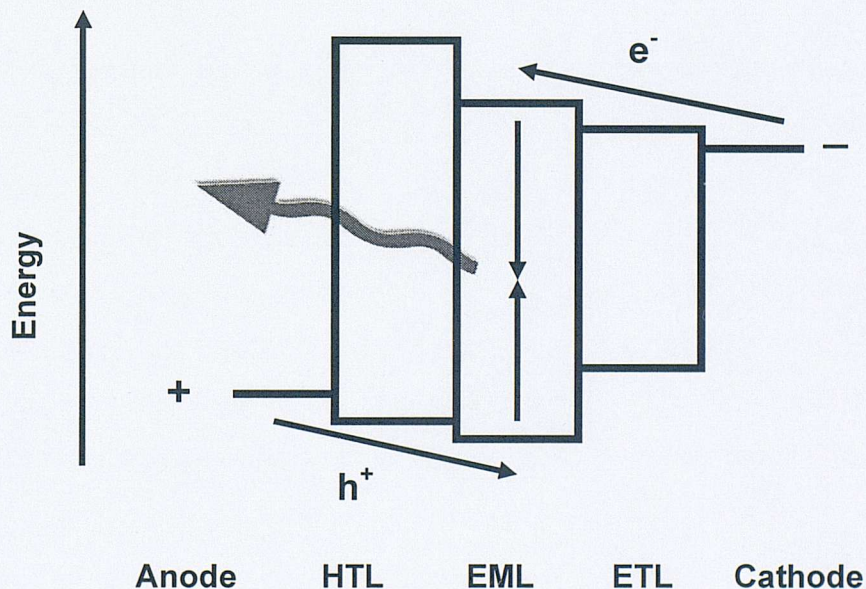


Figure 1.4: Energy level diagram of an OLED

Other layers are often applied to further enhance the operation of the devices, which can perform various other functions such as hole, electron or exciton blocking layers. The roles of all the layers are to carry electrons and holes onto the emissive layer and confine them there, maximising the possibility of radiative recombination (i.e. light emission). The specific requirements of the individual layers are discussed below.

1.2.1 Anode

The anode is typically a glass substrate covered with a conducting, transparent electrode such as indium tin oxide (ITO); it is often subsequently coated (frequently by spin coating) with a hole-conducting polymer such as poly[3,4-ethylenedioxythiophene/poly[styrene sulfonate] (PEDOT:PSS) **1.3**.

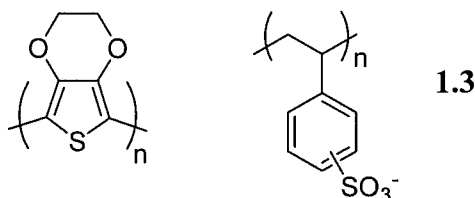


Figure 1.5: poly[3,4- ethylenedioxythiophene]/poly[styrene sulfonate] (PEDOT:PSS)

The purpose of the PEDOT:PSS is typically to improve the surface smoothness and compatibility with subsequent organic layers allowing facile injection of holes.^{3,4} Furthermore, these layers must be transparent allowing the generated light to escape.

1.2.2 Hole transport layer (HTL)

In order to facilitate the movement of holes from the anode to the emissive layer, a hole transporting layer (HTL) is applied. HTLs must possess good thermal stability and hole transport ability; and the layer must have suitable frontier energy levels to enable hole injection from the anode to the HTL, and then from the HTL to the emissive layer (EML). This requires it to have a HOMO energy level between that of the anode and the emissive layer. A typical material used as a hole transport layer is *N,N'*-bis(3-methylphenyl)-*N,N'*-diphenyl-(1,1'-biphenyl)-4,4'-diamine (TPD) **1.4**, although a huge library of HTL compounds, both well defined and polymeric, have been developed.^{3,5}

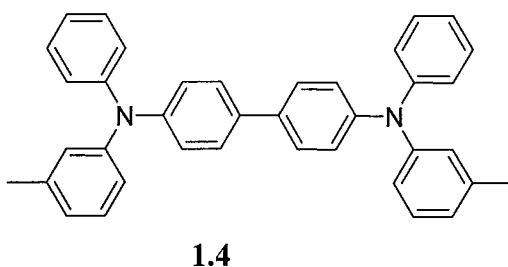


Figure 1.6: *N,N'*-bis(3-methylphenyl)-*N,N'*-diphenyl-(1,1'-biphenyl)-4,4'-diamine (TPD)

1.2.3 Cathode

The cathode is usually a low-work function metal, which is useful for electron injecting; Ca and Al are commonly used as cathodes.³

1.2.3 Electron transport layer (ETL)

The electron transport material should have a reversible electrochemical reduction, with a sufficiently high reduction potential; this facilitates electron transport which can be thought of as a series of redox processes within the organic film. As in the case of HTLs, the ETL should have suitable HOMO and LUMO energy levels relative to those of the other layers, allowing minimization of the barrier for electron injection and reducing the turn-on/operating voltage.

High electron mobility is also desirable to move the charge recombination zone away from the cathode and improve the exciton generation rate. Finally, a high glass transition temperature (T_g) and thermal stability are useful to withstand the heating encountered during OLED operation.

Tris(8-hydroxyquinoline)aluminum(III) (Alq_3) **1.1** is one of the most commonly used electron transport materials, although as in the case of HTLs, a huge library of compounds has also been developed.⁶

1.2.4 Emissive layer (EML)

The emissive layer is the region where the transported electrons and holes recombine to form either singlet or triplet excitons (bound electron and hole pairs). The emission colour and the efficiency of the device depend on the properties of the emissive layer, which can be either a single compound or a blend. Extensive investigations into the factors affecting the emissive properties of this layer, and the compounds used therein have been performed, the results of which will be briefly outlined below.

1.3 Quantum efficiency

The external quantum efficiency (η_{EL} or EQE) of an OLED can be described by the following equation.

$$\eta_{EL} = \chi_S \eta_{PL} \eta_C \gamma$$

Where the fraction of excitons formed as singlet excitons is χ_S , η_{PL} is the intrinsic (or internal) photoluminescence efficiency (or quantum yield), the light output coupling fraction η_C is the fraction of emitted photons captured by the detector, and $\gamma \leq 1$ measures losses present in electroluminescence, but not in photoluminescence.^{7,8}

Exciton spin statistics have a huge impact on the external quantum efficiency of electroluminescence in an OLED. Singlet excitons are states with an antisymmetric spin and a total spin quantum number $S = 0$. The quantum mechanically allowed decay of a singlet exciton to the ground state gives rise to fluorescence, within nanoseconds. Triplet states have an even symmetry, with $S = 1$, and the decay to the singlet ground state is quantum mechanically forbidden, resulting in phosphorescence with lifetimes in the microsecond to second regime. As a consequence of the corresponding multiplicities of the spin angular momentum states (i.e. $mS = 0$ for $S = 0$ and $mS = -1, 0, 1$ for $S = 1$) and the random nature of non geminate recombination in electroluminescent devices, simple statistics predicts that only 25% of the injected charges result in a singlet exciton, whereas 75% give triplet excitons. Thus, uncorrelated electrons and holes form triplet states with a threefold higher probability than singlet states.^{8,9}

Assuming the light output coupling fraction, $\eta_C \sim 1/2n^2 \sim 20\%$, for a glass substrate with index of refraction, $n = 1.5$,^{7,10} it is possible to obtain some theoretical maximum external efficiencies.

If only singlets are radiative in fluorescent materials then $\eta_{PL} = 25\%$ and η_{EL} is limited to 5%. However, using phosphorescent materials, which harvest both singlet and triplet excitons, η_{PL} can approach 100%, in which case we can anticipate an upper limit for η_{EL} of 20%.

However, it must be noted that experimental studies on the actual values of the singlet to triplet ratio have been found to vary from the idealized values mentioned above. In

particular, it has been suggested that polymeric materials can have a singlet to triplet ratio as high as 1:1.^{11,12}

As calculating the internal quantum efficiency (η_{PL}) involves the construction and testing of a device, workers typically measure the photoluminescent quantum efficiency ($\Phi_{\text{Ph}} = \text{number of photons emitted/number of photons absorbed}$) of materials that are to be used in the emissive layer in either solution or solid state. Although this figure does not correlate exactly with the internal quantum efficiency, it is assumed that the higher the photoluminescent quantum yield, the better this material will perform in an OLED.

1.4 Phosphorescent complexes and singlet-triplet harvesting

In order to utilize the generated triplet excitons and improve the efficiencies of OLEDs, researchers turned to heavy metal-containing complexes, which relax transition selection rules through spin orbit coupling, allowing phosphorescence to occur. Furthermore, rapid intersystem crossing from excited singlet states to triplet states allows the usage of potentially all the generated excitons (i.e. 100% internal quantum efficiency), in what is known as singlet-triplet harvesting. These compounds typically have high photoluminescence quantum yields ($\Phi_{\text{Ph}} > 20\%$), even at room temperature, which is necessary considering that the external quantum efficiency directly depends on the internal quantum yield, as demonstrated by the above equation. A variety of heavy metals have been investigated as phosphorescent materials including complexes of Os(II), Ir(III), Pt(II/IV), Ru(II).^{3,9,13-16}

An early example which demonstrated the potential of these materials was an OLED fabricated by Baldo *et al*, where the phosphorescent 2,3,7,8,12,13,17,18-octaethyl-21*H*,23*H*-porphine platinum(II) (PtOEP) **1.5** was incorporated into an Alq₃ host, to achieve an external quantum efficiency of 4%.¹⁷

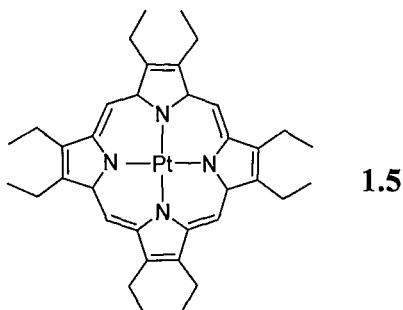


Figure 1.7: 2,3,7,8,12,13,17,18-octaethyl-21*H*,23*H*-porphine platinum(II) (PtOEP)

Another impressive example was the incorporation of *fac*-tris(2-phenylpyridine)iridium(III) **1.6** in a 4,4'-bis(carbazol-9-yl)biphenyl (CBP) **1.7** host to produce a green emitting OLED, with an external quantum efficiency of 8%.¹⁸ The high solution phosphorescence quantum yield ($\Phi_{\text{Ph}} = 40\%$) of complex **1.6** and its impressive performance in OLEDs resulted in iridium-containing complexes being the most commonly used in this field.¹⁹⁻²¹

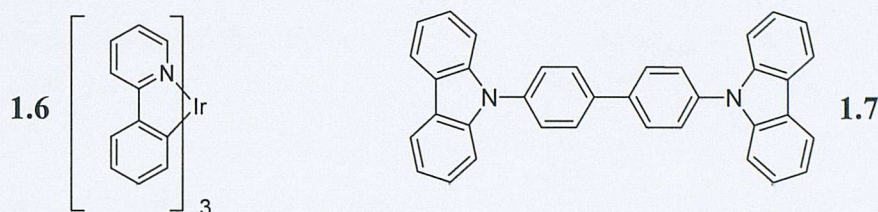


Figure 1.8: *fac*-tris(2-phenylpyridine)iridium(III) ($\text{Ir}(\text{ppy})_3$) and 4,4'-Bis(carbazol-9-yl)biphenyl (CBP)

1.4.1 Emission from phosphorescent complexes

In a seminal paper by the Thompson group, a large number of phosphorescent iridium complexes were synthesized and their emissive properties investigated. The compounds all featured intense $^1\text{MLCT}$ (metal to ligand charge transfer) and $^3\text{MLCT}$ absorption bands as a result of the selection rule relaxation produced by the presence of the heavy iridium atom. Emission was observed to originate from either a $^3\text{MLCT}$ or $^3(\pi-\pi^*)$ state or a mixture of the two, depending on their respective energies. The emissive state was assigned depending on whether vibronic fine structure was observed in emission ($^3(\pi-\pi^*)$) or not ($^3\text{MLCT}$). The consequence of this vibronic coupling was a large observed Stokes shift for complexes which emitted from the $^3(\pi-\pi^*)$ state.²⁰

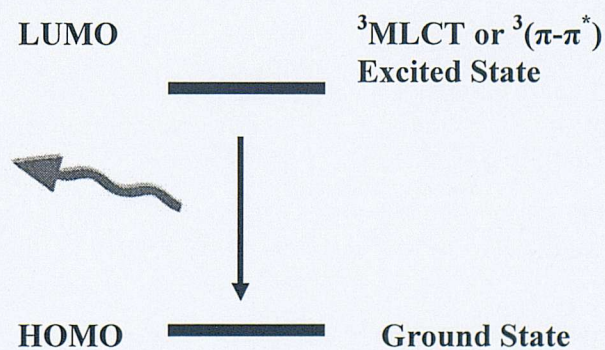


Figure 1.9: Emission process in phosphorescent iridium complexes

1.5 Host-guest systems

Transition metal complexes such as *fac*-tris(2-phenylpyridine)iridium(III) (Ir(ppy)₃) **1.6** exhibit a series of very desirable materials properties: emission wavelengths covering the entire visible spectrum depending on which complex is used, high phosphorescence quantum yields and appropriate lifetimes. However, severe concentration quenching is observed for most pure layers of phosphorescent complexes. This is due to non-radiative deactivation of the excited state through phenomena such as triplet-triplet annihilation.²²

Consequently, phosphorescent complexes are usually blended into suitable host materials (small molecules or polymers), from which the excitation energy is transferred to the guest which subsequently decays radiatively.²³

The importance of selecting the appropriate host material and the correct host doping concentration is vital. The lowest excited state in the blend must reside on the emissive guest material in order for emission to be as efficient as possible. This is not necessarily trivial, as the triplet energy level of the host is often not known. Incorrect matching of energy levels results in significantly reduced emission efficiency due to energy transfer from the guest back onto the host. This has been observed in host-guest systems of blue emitting iridium complex FIrpic **1.8** in CBP **1.7**, which has a photoluminescence quantum yield of 40%, compared to ~100% in a blend with *m*-bis-(*N*-carbazolyl)benzene (mCP) **1.9** due to the latter's higher triplet energy level.²²

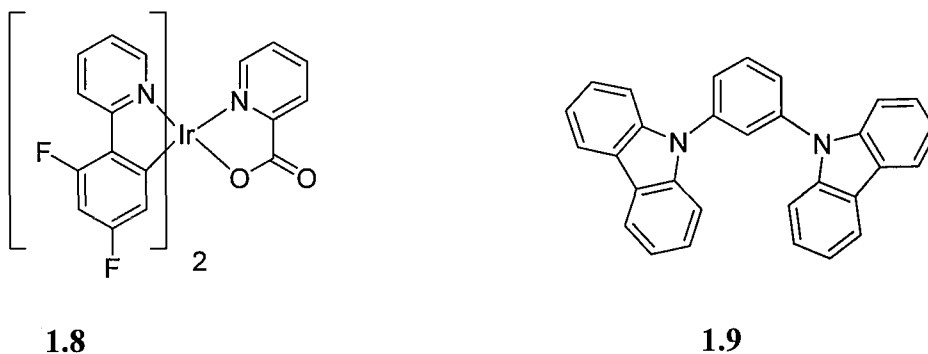


Figure 1.10 : Bis(4,6-difluorophenylpyridinato)iridium(III)(picolate) (FIrpic) and *m*-bis-(*N*-carbazolyl)benzene (mCP)

A blend of 1.5 mol % Ir(ppy)₃ **1.6** in CBP **1.7** has an emission quantum yield of ~100%, whereas at 40 mol% this is reduced to 30%, and a neat film has negligible emission quantum yield. The reduction in emission quantum yields is due to self quenching effects and highlights the importance of obtaining the correct dopant concentration.²²

Assuming the correct matching of energy levels, the energy transfer processes which can occur in a host-guest system are illustrated in Fig. 1.11. Either a singlet (S_1) or triplet (T_1) exciton that is generated on the host material can be transferred onto the guest material; the subscript 1 indicates that it is the lowest (or first) excited state. Singlets (S_1) on the guest can then relax to the triplet (T_1) state (intersystem crossing), which is the lowest excited state. Finally, the T_1 state relaxes radiatively emitting the observed photons.

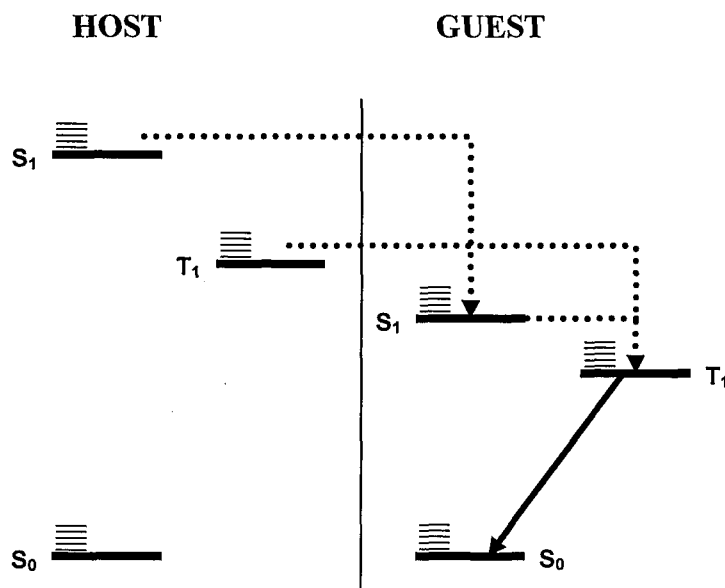


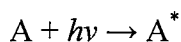
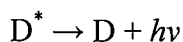
Figure 1.11: Energy transfer processes in a Host-Guest system

1.6 Mechanisms of energy transfer

Energy transfer from the host to the guest can only occur through certain mechanisms. The following list describes these main mechanisms and with what transitions they are associated. These mechanisms are general and not specific to host-guest systems and so the host will be referred to as the donor (D), and the guest the acceptor (A).

1.6.1 Radiative energy transfer

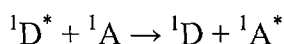
This is where the light emitted from a donor (D) is reabsorbed by the acceptor (A), where * indicates an excited state.^{9,24}



No direct interaction of the donor with the acceptor is involved. The process requires that the emission spectrum of D and the absorption spectrum of A overlap. Consequently, the efficiency of the transfer is governed by the photoluminescence yield of the donor molecules and the absorption ability of the acceptor, i.e. the extinction coefficient.

1.6.2 Förster energy transfer^{9,13,24}

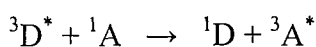
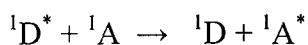
Förster transfer is a long range (40 Å -100 Å), non-radiative, dipole-dipole coupling of donor (D) and acceptor (A) molecules. It requires that the transitions from the ground to the excited states be quantum mechanically allowed for both D and A species, which means this mechanism only transfers energy to the singlet state of the acceptor molecule via:



The efficiency of this transfer mechanism depends on the oscillator strengths and the spectral overlap of the relevant transitions.

1.6.3 Dexter energy transfer (electron exchange excitation transfer)^{9,13,24}

Dexter transfer is a short-range process where excitons diffuse from D to A sites *via* intermolecular electron exchange. It also requires an overlap of the wavefunctions of the energy donor and the energy acceptor. In contrast to Förster transfer, Dexter processes require only that the total spin of the D-A pair be conserved via:



Thus, Dexter transfer permits both singlet-singlet and triplet-triplet transfers. However, Förster transfer dominates singlet-singlet transfer at low acceptor concentrations because it is faster over long distances, whereas Dexter transfer is the dominant mechanism in triplet-triplet energy transfer.

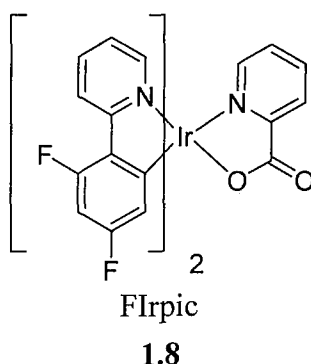
1.6.4 Charge trapping^{9,13,24}

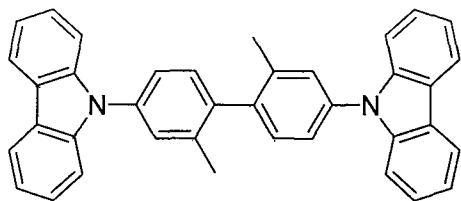
In a charge trapping mechanism, the exciton is generated by sequential trapping of a hole and then an electron on the guest complex. This mechanism is most favorable if the HOMO and LUMO energy levels of the guest are within those of the host. It is not necessary for both of these requirements to be fulfilled as a guest with HOMO above that of the host could trap a hole to form a cationic excited state which subsequently acts as an electron trap. Charge trapping and localization onto the guest complex requires overlap of the molecular orbitals of the host and guest molecules. There is evidence to suggest that when the above criteria are fulfilled, charge trapping is the dominant mechanism in exciton formation.^{25,26}

1.7 Developments in OLED technology

Following much optimization, researchers have been able to produce red, green and blue devices that approach the theoretical upper limit of ~20% EQE.

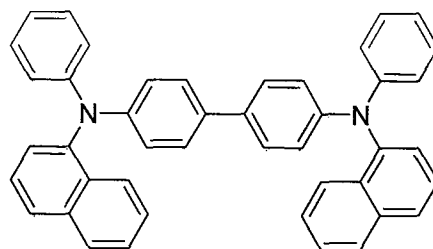
In 2003, workers produced a blue emitting OLED with an external quantum efficiency of 10.4%, by using a blend of **1.8** in 4,4'-bis-(9-carbazolyl)-2,2'-dimethyl-biphenyl (CDPB) **1.10** in a device with the following configuration.²⁶





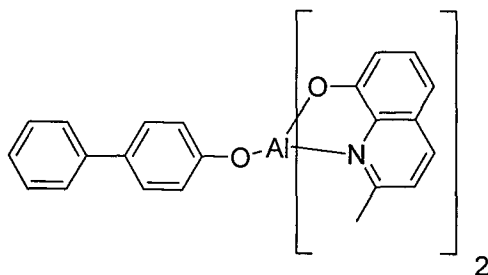
4,4'-bis-(9-carbazolyl)-2,2'-dimethylbiphenyl (CDBP)

1.10



4,4'-bis[N-(1-naphthyl)-N-phenyl-amino]biphenyl (NPB)

1.11



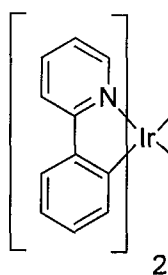
bis(2-methyl-8-quinolinolate)4-phenylphenolate (BALq)

1.12

Figure 1.12: Materials used in the highly efficient blue OLED construction

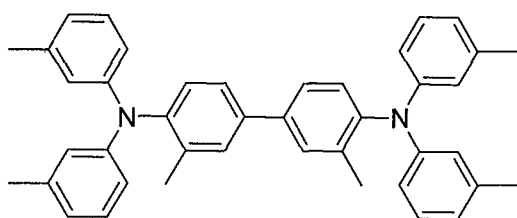
Adachi *et al*⁷ reported an exceptionally efficient green OLED with a maximum external efficiency of 19%, which corresponds to an internal quantum efficiency of nearly 100%.

ITO | HMTPD | TAZ + **1.13** | Alq₃ | Mg:Ag



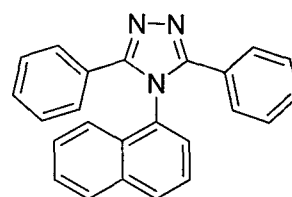
iridium(III)bis(phenylpyridine)(acetylacetonate)

1.13



4,4'-bis[N,N'-(3-tolyl)amino]-3,3'-
dimethyl biphenyl (HMTPD)

1.14

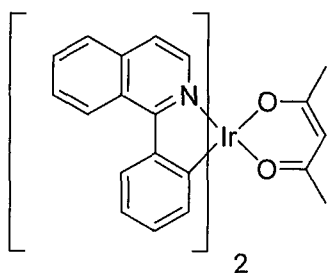
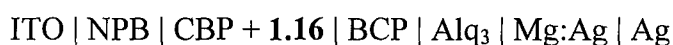


3-phenyl-4-(1'-naphthyl)-5-
phenyl-1,2,4-triazole (TAZ)

1.15

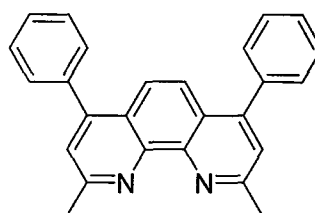
Figure 1.13: Materials used in the green OLED

A red emitter displaying very good emissive properties in an OLED is **1.16**, which had an efficiency of 9.21%.²⁷ This complex will also be the subject of the subsequent investigation in this thesis due to its desirable emission properties.



Iridium(III)bis(1-phenylisoquinoline)
(acetylacetonate) [piq₂Ir(acac)]

1.16



Bathocuproine (BCP)

1.17

Figure 1.14: Materials used in the red OLED

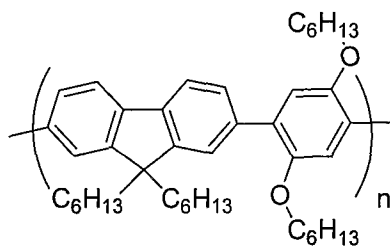
1.8 Fine tuning of emissive properties

Although it has been possible to obtain efficient red, green and blue OLEDs, a substantial amount of work has been conducted on fine tuning the emissive properties of particular complexes. This is typically done to improve the colour purity or quantum yield of the emission and probe the underlying photophysical processes occurring in the complexes.²⁸⁻³¹

In-depth density functional theory (DFT) and time dependent DFT (TD-DFT) calculations have revealed the nature of the ground and excited states of Ir(ppy)₃ **1.6** and experimentally measured parameters such as phosphorescent lifetime have been reproduced successfully from theory.³² In an impressive paper, Avilov and co-workers successfully managed to rationalise the observed emission differences in a series of substituted bis(phenylpyridine)iridium derivatives.³³

1.9 Solution processability and preventing phase separation

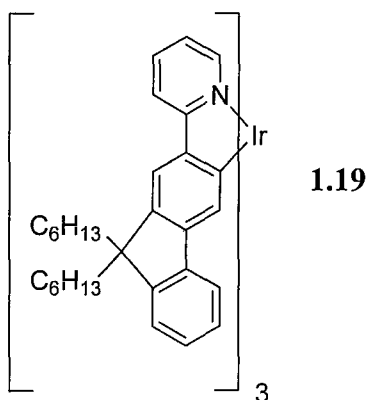
A further development in the field of OLED technology is the suppression of phase separation that can occur in the host-guest emissive layer. Such phase separation results in an increased aggregation of the emissive guest phosphors and reduced emission efficiency, as has been observed experimentally in thin films of **1.6** in poly((9,9'-di-*n*-hexyl-2,7-fluorene-alt-1,4(2,5 di-*n*-hexyloxy) phenylene) (PFHP) by atomic force microscopy.³⁴

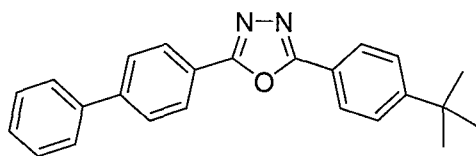


1.18

Figure 1.15: Poly (9,9'-di-*n*-hexyl-2,7-fluorene-alt-1,4(2,5 di-*n*-hexyloxy) phenylene) (PFHP)

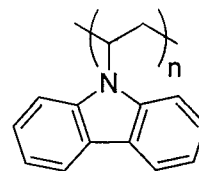
Attempts to prevent phase separation in host guest systems have included the attachment of solubilizing functional groups onto the guest complex. The presence of long alkyl chains in complex **1.19** reduces its crystallinity, allowing construction of efficient OLEDs where the emissive layer contains blends of poly(*N*-vinylcarbazole) (PVK) **1.21** and 2-(biphenyl-4-yl)-5-(4-*tert*-butylphenyl)-1,3,4-oxadiazole **1.20** (fig. 1.16).³⁵





2-(biphenyl-4-yl)-5-(4-*tert*-
butylphenyl)-1,3,4-oxadiazole

1.20



poly(*N*-vinylcarbazole) (PVK)

1.21

Figure 1.16: An amorphous iridium complex and materials used in the OLED

An added benefit of the increased solubility of guest complexes (for example by attachment of long alkyl chains) is the ability to solution process the device, i.e. the emissive layer can be deposited as a thin film by spin coating or inkjet printing methods. A solution of host and guest can be directly formulated into an OLED without the need for expensive metal evaporation techniques. Ultimately such properties should allow display sizes of significantly larger sizes and lower costs to be produced. However, the construction of elaborate device architectures (i.e. devices with multiple layers of materials), such as those mentioned above, by solution processing techniques is problematic due to the need for solvent orthogonality.

Emissive guest complexes have also been incorporated into dendrimers and polymers to prevent phase separation and reduce the effects of concentration quenching.³⁶⁻³⁹ Furthermore, if the attached dendrimer or polymer is a material that can function as an appropriate host, it becomes possible to create ‘host-free’ materials that do not require blending for use in OLEDs, allowing for greatly simplified device construction.

Lo and coworkers reported a green emitting OLED from a very simple host-free device which possessed an external quantum efficiency of 13.6% (fig. 1.17).⁴⁰

ITO | **1.22** | TPBI | Ca | Al

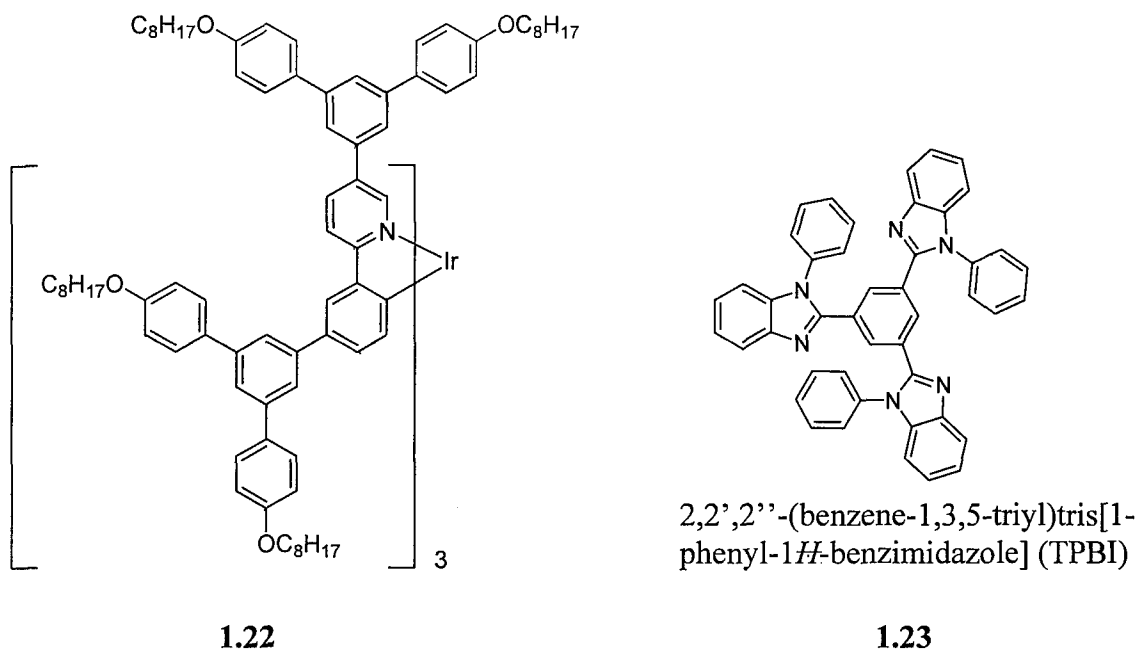


Figure 1.17: Materials used in 'host-free' OLED

An extremely impressive “host-free” device was prepared by Chien *et al*, where an osmium complex was incorporated into a polyfluorene type polymer **1.24** and spin coated into a device; it showed a remarkable external quantum efficiency of 18% and red emission (fig. 1.18).⁴¹

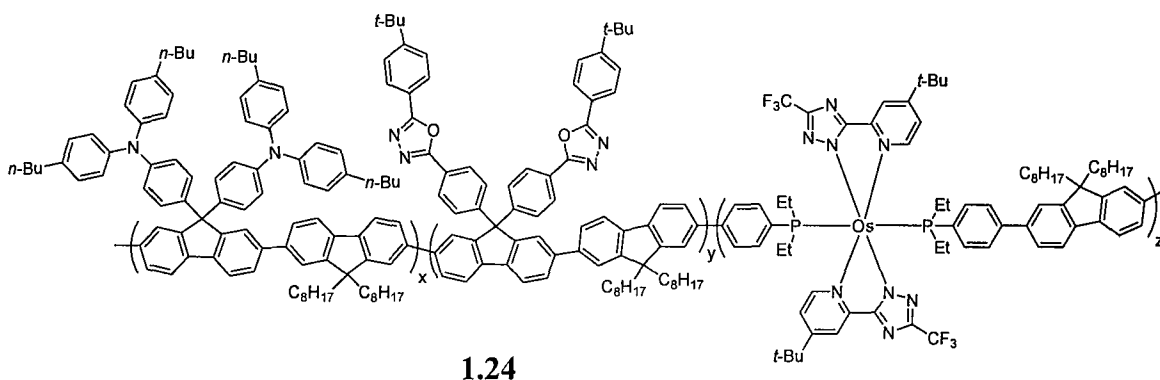
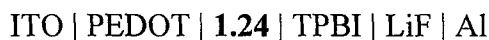


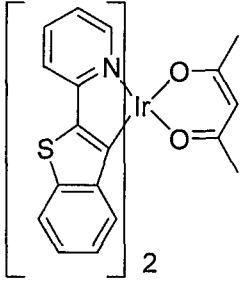
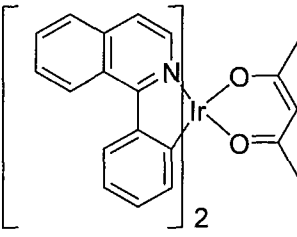
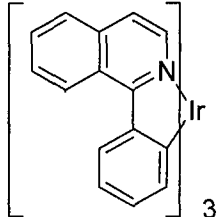
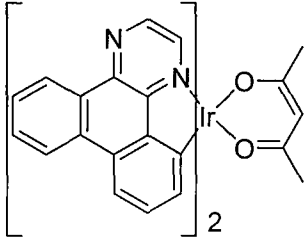
Figure 1.18: Red emitting electrophosphorescent polymer

1.10 Red emitting phosphorescent iridium complexes

The focus of this thesis will be on red phosphorescent iridium complexes for use in OLEDs. It is worth noting that red emitting complexes have been investigated far less extensively than their green emitting counterparts. A fundamental issue with obtaining

efficient red emission is the energy gap law, which states that the non-radiative decay rate constant increases as the energy gap between excited and ground state decreases (i.e. as the emission colour shifts to the red region of the electromagnetic spectrum).⁴² In practice this means that red emitting compounds suffer from lower photoluminescence quantum yields, which can result in less efficient OLEDs.²⁹

A brief overview of the best performing iridium based red emitters is shown in table 1.1, alongside their solution maximum emission wavelength and their solution quantum yield.

Compound	Name	Emission max. /nm	Solution quantum yield (Φ_{Ph}) /%
1.25 	[btp ₂ Ir(acac)] ²⁰	612	21
1.16 	[piq ₂ Ir(acac)] ²⁷	622	20
1.26 	[piq ₃ Ir] ⁴³	621	22
1.27 	[dbq ₂ Ir(acac)] ⁴⁴	618	53

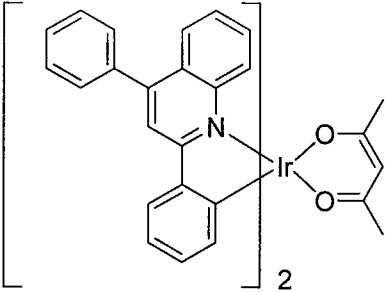
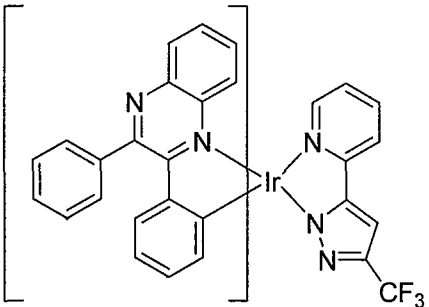
1.28		[dpq ₂ Ir(acac)] ⁴⁵	614	14
1.29		[dpqx ₂ Ir(fppz)] ²⁹	642	40

Table 1.1: Red phosphorescent iridium complexes

It can be seen that to achieve red emitting iridium complexes it is necessary to have an extended π system, which reduces the energy gap between the HOMO and the LUMO levels.^{20,27,29,43,45} Predominantly, bis-cyclometallated complexes have been used, although **1.26** (a tris complex) has also demonstrated good performance in OLEDs.⁴³ Acetyl acetonate (acac) is the most commonly used ancillary ligand, although again there are exceptions (**1.29**).²⁹ There has also been significant work done on each of these complexes to further fine-tune their emissive properties and optimize their performance (see chapter 2).

It was decided to further investigate [piq₂Ir(acac)] **1.16** as a phosphorescent emitter for use in OLEDs. This compound was chosen for its good emission colour and photoluminescent quantum yield, and for its ease of synthesis which should allow facile modification for probing its photophysical properties. Furthermore, as mentioned earlier, OLEDs constructed using this material as a dopant have displayed excellent emissive properties and efficiencies.²⁷

**Chapter 2 : Investigation into the
phosphorescence of a series of
substituted
iridium(III)bis(phenylisoquinoline)(acac)
complexes**

2.1 Introduction

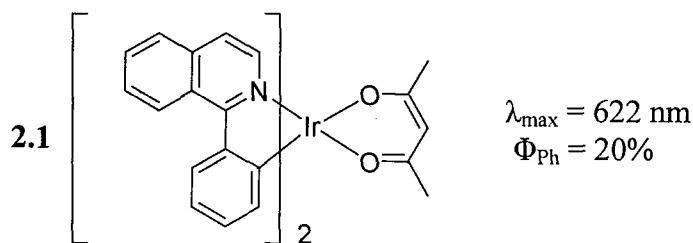


Figure 2.1: [Iridium(III)bis(1-phenylisoquinolinato-*N,C*²)(acetylacetonate)]

Su *et al*²⁷ reported the first synthesis of [iridium(III)bis(1-phenylisoquinolinato-*N,C*²)(acetylacetonate)] in 2003. It displayed an emission maximum (λ_{\max}) of 622 nm, and a solution phosphorescence quantum yield (Φ_{Ph}) of 20%. Incorporation of this phosphor into an optimized OLED produced a device with an impressive external quantum efficiency of 9.21%. Furthermore, the external quantum efficiencies remained high over a wide range of current. Subsequent to this publication several other investigations into the properties and uses of this complex were reported.⁴⁶⁻⁴⁸ Efforts were predominantly directed towards tuning the emission wavelength in an attempt to improve the colour purity.

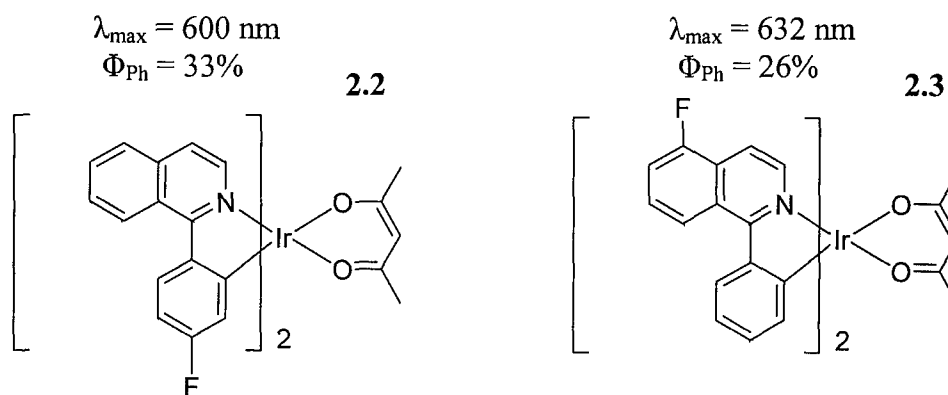


Figure 2.2: Fluorinated [Iridium(III)bis(1-phenylisoquinolinato-*N,C*)(acetylacetonate)] complexes

The same authors published a paper further investigating the properties of the complex bearing fluorine atoms at several different positions (Fig.2.2).⁴⁹ It was found that depending on the position of the fluorine atom, the emission wavelength varied significantly and either a red or a blue shift could be obtained. Typically, fluorine substitution increased the solution emission quantum yield, which is a common phenomenon in phosphorescent materials, and is attributed to decreasing the number of C-H bonds in the molecule that can allow non-radiative decay through vibronic coupling. All the derivatives synthesized in this publication gave extremely good performances when incorporated into an OLED. However, despite a thorough

investigation into the effects of fluorine substitution, an in-depth analysis of the origins of the varying optical properties was not undertaken.

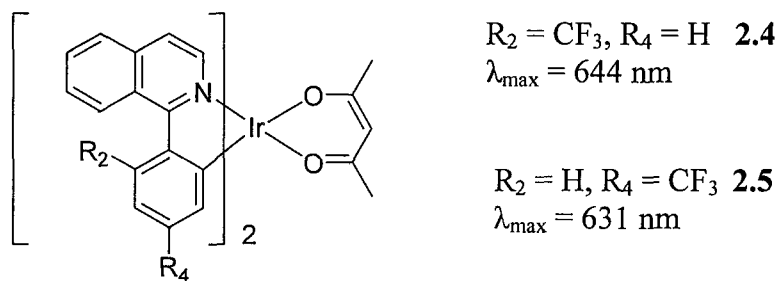


Figure 2.3: Regioisomeric substituted iridium complexes

Fang and coworkers^{50,51} published a series of investigations into the effects of regioisomerism on the emissive properties of substituted phenylisoquinoline iridium complexes. A large number of substitutions were performed at varying positions, often in conjunction with other substitutions (Fig. 2.3). Impressive quantum yields were reported, although they were measured against Ir(Piq)₃ **2.6** as a standard, quoting its solution quantum yield as 60%, in contrast to Okada *et al*^{43,52} who published the original synthesis of Ir(Piq)₃ **2.6** and reported the solution quantum yield to be 22%. Consequently, we find the results obtained by Fang *et al* to be questionable. Furthermore, the complicated nature of the substitution variations made elucidating individual effects difficult.

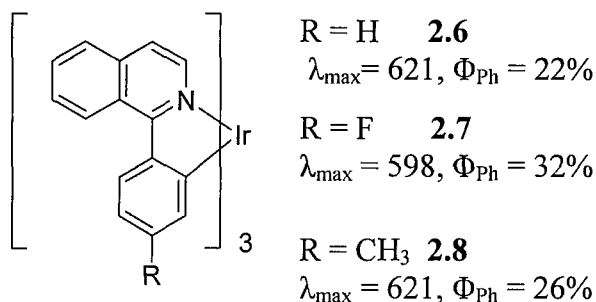


Figure 2.4: Substituted tris(1-phenylisoquinoline)iridium complexes

As mentioned above, researchers from the Ueno group published an impressive paper on the chemistry of Ir(Piq)₃.⁴³ Emissive properties were found to depend on the Hammett constants of the varying substituents (Fig. 2.4). However, only brief *ab initio* studies were undertaken to truly understand the photophysical processes involved. Furthermore, due to the differences between tris and bis cyclometallated iridium complexes, it is not known whether their substituent effects are the same.

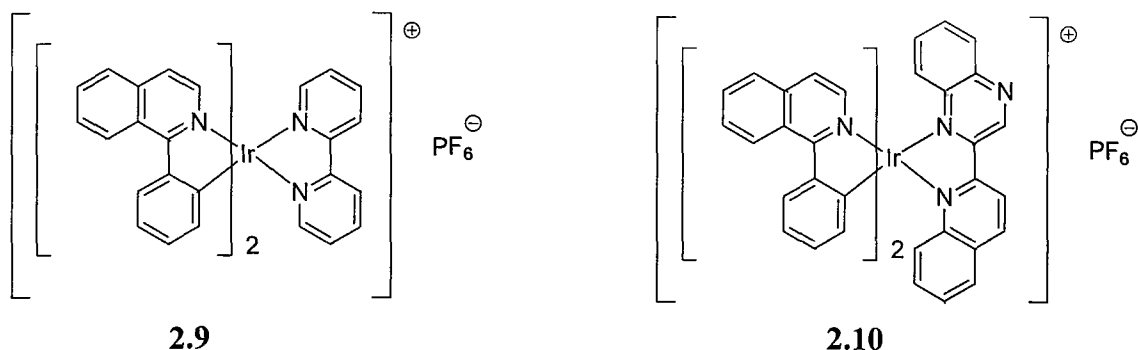


Figure 2.5: Variation of ancillary ligand in iridium complexes

A very thorough investigation into the effects of varying the ancillary ligand in bis(phenylisoquinoline)iridium cationic complexes was undertaken by Zhao *et al.*⁵³ It was shown that the emission wavelength could be varied by a large range (586 - 732 nm) and the underlying photophysical processes were investigated thoroughly. However, the emission quantum yields for these complexes were very poor.

Despite the multiple attempts at obtaining structure-property relationships of substituted phenylisoquinoline complexes, there has yet to be an investigation that is carried out in a thorough and systematic fashion.

Another reason for investigating the effects of substitution on these metal complexes is to elucidate the optimal position to attach moieties which possess properties that could improve device performance in other manners. For instance, small molecule phosphors such as these often possess substituents that can improve hole or electron injection. Alternatively, phosphors can be incorporated into dendrimers or polymers in order to simplify device fabrication and prevent T-T annihilation.

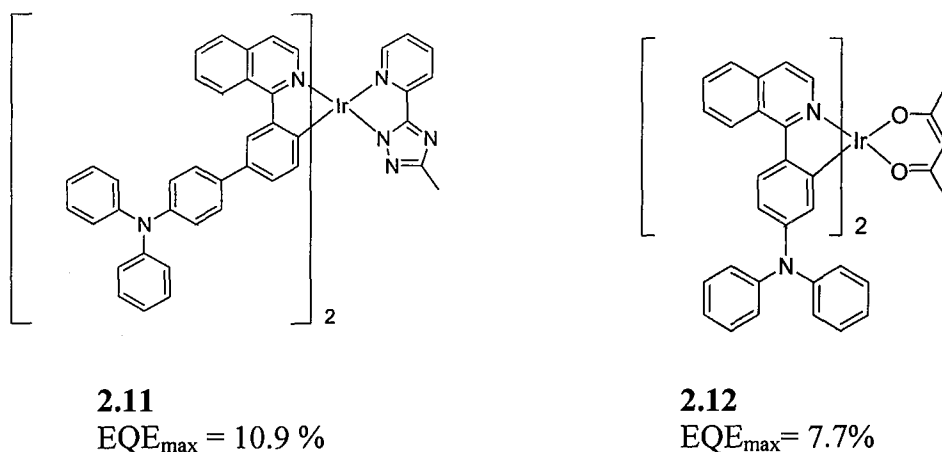


Figure 2.6: Similar iridium complexes with significantly different EQE efficiencies

Complexes **2.11** and **2.22** were reported by workers in the Cao group in separate publications.^{54,55} Both are similar in ligand structure, incorporating an aryl amine substituent but different ancillary ligands. Both of these materials display good characteristics when incorporated in OLEDs with similar structure and doping concentrations. However, there does not appear to be any rationale as to why the substituent is attached in their respective positions. Consequently, due to differences in ancillary ligand and the slight difference in substituent structure, it is not possible to elucidate the origin of the differences in OLED performance.

There are several reports in the literature of phenylisoquinoline iridium complexes that are attached to polymeric materials (see Chapter 3). At the time of writing, covalent attachment to the polymeric materials has only been attempted through the ancillary ligand.⁵⁶⁻⁶¹ Other attachment sites have not been investigated, in particular direct linkage into the cyclometallating ligand, which has shown promising results in other iridium complexes.^{39,62}

Consequently, the aim of this work is to investigate the effects of substitution on the emission properties of a series of bis(1-phenylisoquinoline) iridium complexes, and to elucidate if any of these substitution sites can be identified as the most beneficial site for attachment of moieties that may aid the emissive properties of OLEDs developed from these materials.

2.2 Synthesis

2.2.1 Target materials

It was decided to investigate the effect of bromine substitution on the emission properties of complex **2.1** for two reasons. Firstly, it possesses both inductive electron withdrawing effects, and mesomeric type donating properties. Consequently, the complex can be subjected to a variety of electronic effects allowing detailed study of its emissive properties. Secondly, aromatic bromine compounds undergo a variety of cross-coupling reactions, allowing facile future access to a wide range of ligands.

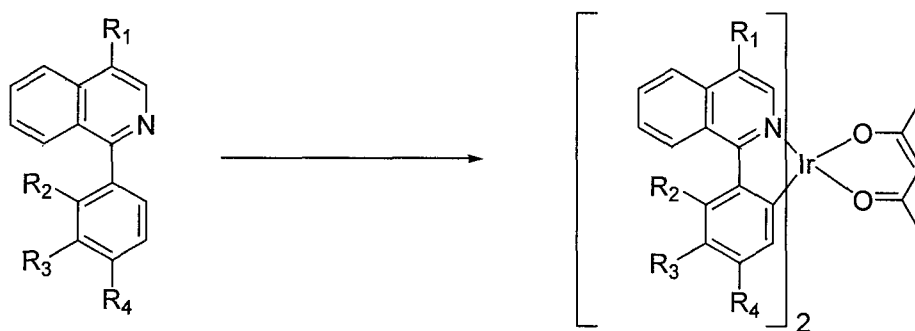


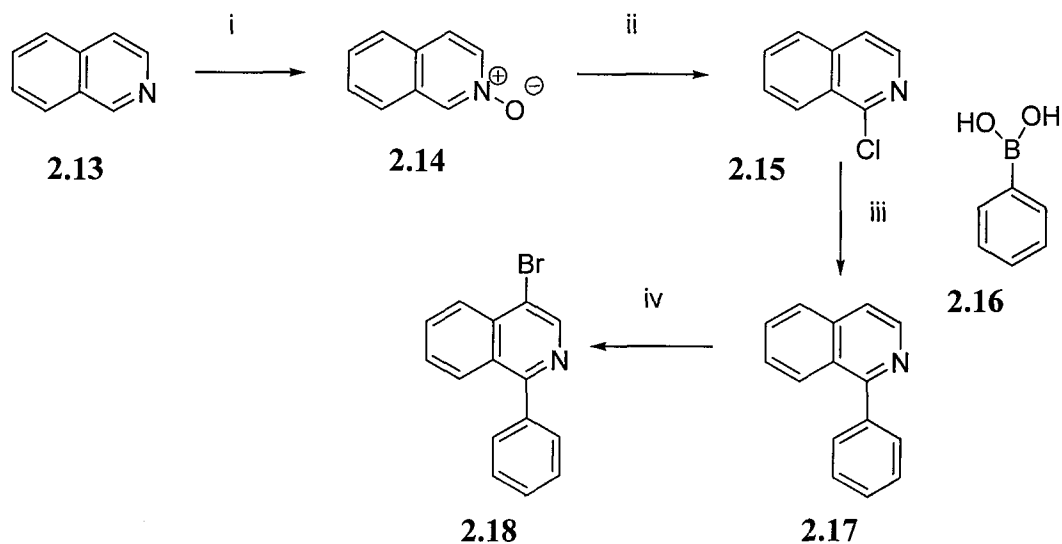
Figure 2.7: Target syntheses

The following ligands will be synthesized where the R groups (R_1 - R_4) will be either Br atoms or another substituent. In order to simplify discussion the following labeling scheme has been developed. R_1 = isoquinoline ring, R_2 = 1,2 position relative to C-C bond between the phenyl and isoquinoline rings, R_3 = 1,3 position relative to C-C bond, R_4 = 1,4 position relative to C-C bond. This labeling system will be used throughout this work.

2.2.2 Synthesis of bromo substituted complexes

2.2.2.1 Synthesis of bromo substituted ligands

The target bromo substituted phenylisoquinoline ligands (**2.18**, **2.26-2.28**) were prepared according to the schemes outlined in Fig. 2.8 and 2.9.



Reagents and conditions: i) mCPBA, DCM, 0 °C, 67%; ii) POCl₃, DCM, Reflux, 73%; iii) Pd(OAc)₂, PPh₃, Tol, TEAOH(aq), 89%; iv) Br₂, Nitrobenzene, Reflux, 84%

Figure 2.8: Synthesis of 4-bromo-1-phenylisoquinoline

The oxidation of isoquinoline **2.13** and subsequent conversion to 1-chloroisoquinoline **2.15** was facile and proceeded in good yields in accordance with previously published procedures.⁶³ Suzuki coupling of **2.15** with phenyl boronic acid **2.16** afforded phenyl isoquinoline **2.17** in excellent yield.⁵² Typically aromatic chlorides are not particularly susceptible towards palladium catalyzed coupling reactions; however, the presence of the nitrogen atom activates the 1 position, significantly increasing its reactivity. Selective bromination of the isoquinoline ring was achieved by refluxing with bromine in nitrobenzene, in a procedure adapted from the literature,⁶⁴ to afford 4-bromo-1-phenylisoquinoline **2.18** as a white crystalline solid, in very good yield (84%).

The syntheses of the 1-(bromo)-phenylisoquinolines, **2.26-2.28**, were achieved using a procedure developed by Funabashi *et al*⁶⁵ The appropriate bromo substituted benzoyl chloride, **2.20-2.22**, was reacted with (\pm)-2-amino-1-phenylethanol to afford the corresponding amide, **2.23-2.25**, in quantitative yields. Subsequent cyclization using phosphorus oxy chloride and phosphorus pentoxide was achieved in reasonable yield to afford 1-(2-bromo)-phenylisoquinoline **2.26** (70%), 1-(3-bromo)-phenylisoquinoline **2.27** (75%) and 1-(4-bromo)-phenylisoquinoline **2.28** (61%). The novel ligands were fully characterized by ¹H and ¹³C NMR, mass spectrometry, and elemental analysis.

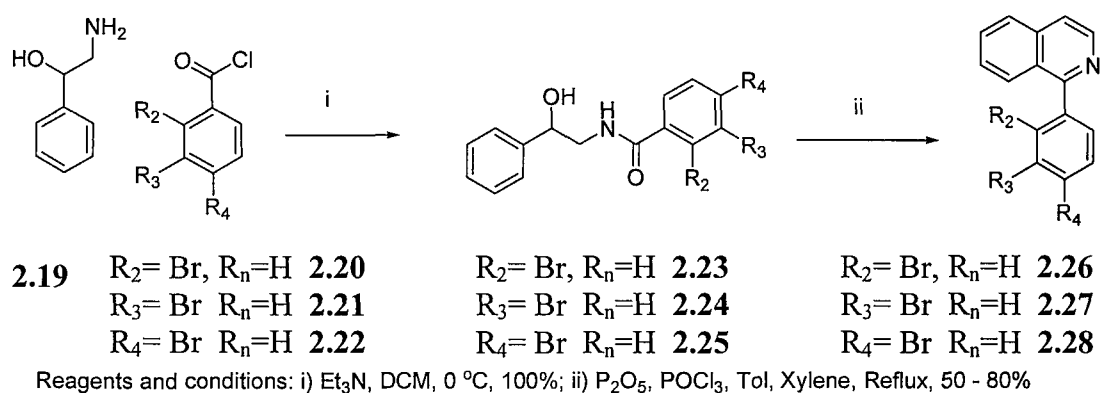
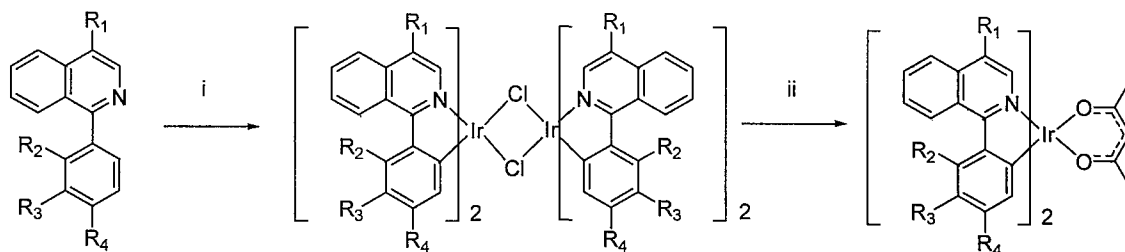


Figure 2.9: Synthesis of 1-(bromophenyl)-isoquinoline ligands

2.2.2.2 Preparation of bromo substituted iridium complexes

The target iridium complexes were prepared by complexation of the appropriate bromo-substituted ligand with iridium trichloride and subsequent cleavage of the chloro bridged dimer using acetyl acetone, according to the methods outlined in Fig. 2.10.



Reagents and conditions: i) $\text{IrCl}_3 \cdot x\text{H}_2\text{O}$, 2-ethoxyethanol, H_2O , 110°C ; ii) acetylacetonate, Na_2CO_3 , 2-ethoxyethanol, 110°C , 50-80% (2 steps)

$R_n = \text{H}$	2.17	$R_n = \text{H}$	2.29	$R_n = \text{H}$	2.34
$R_1 = \text{Br}, R_n = \text{H}$	2.18	$R_1 = \text{Br}, R_n = \text{H}$	2.30	$R_1 = \text{Br}, R_n = \text{H}$	2.35
$R_2 = \text{Br}, R_n = \text{H}$	2.26	$R_2 = \text{Br}, R_n = \text{H}$	2.31	$R_2 = \text{Br}, R_n = \text{H}$	2.36
$R_3 = \text{Br}, R_n = \text{H}$	2.27	$R_3 = \text{Br}, R_n = \text{H}$	2.32	$R_3 = \text{Br}, R_n = \text{H}$	2.37
$R_4 = \text{Br}, R_n = \text{H}$	2.28	$R_4 = \text{Br}, R_n = \text{H}$	2.33	$R_4 = \text{Br}, R_n = \text{H}$	2.38

Figure 2.10: Synthesis of bromo substituted iridium complexes

Ligands **2.17**, **2.18**, **2.26-2.27** were reacted with $\text{IrCl}_3 \cdot x\text{H}_2\text{O}$ to yield chloro-bridged dimeric complexes **2.29-2.33** under standard conditions.^{20,27,43} Due to the extremely low solubility of these complexes, purification was not possible. Subsequent cleavage of the dimers was achieved by reaction with acetyl acetone, in the presence of base and heat. Column chromatography was used to purify the respective iridium complexes. Thus the unsubstituted isomer, **2.34**, and the four novel bromine substituted bis(bromophenylisoquinoline) iridium complexes, **2.35-2.38**, were isolated as red solids in reasonable yields (50-80%).

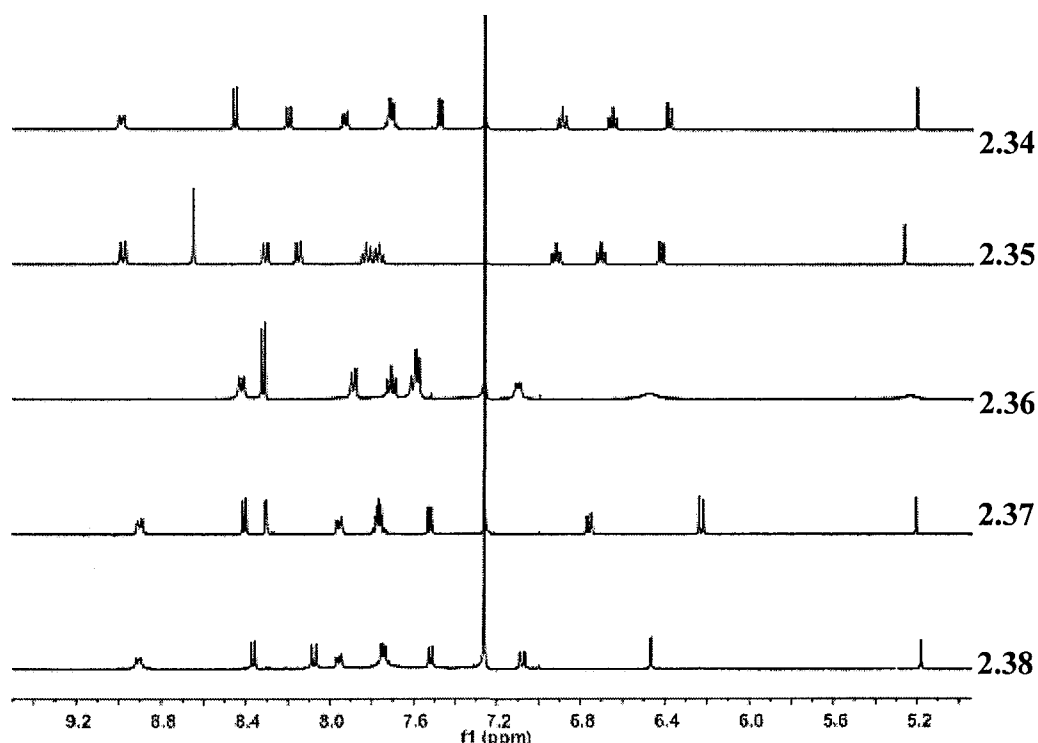


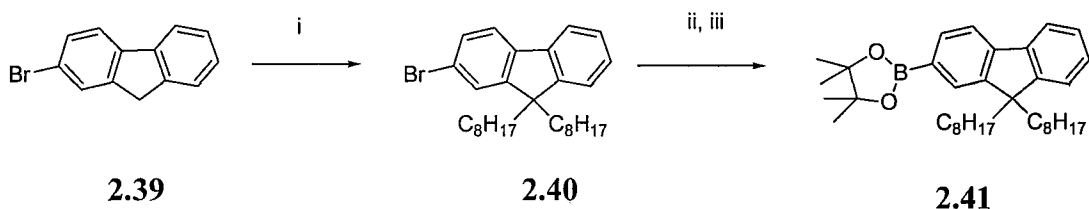
Figure 2.11: ^1H NMR spectra of 2.34-2.38

Fig. 2.11 shows the aromatic section of the ^1H NMR spectra of complexes **2.34**–**2.38**. The singlet at ~ 5.2 ppm corresponds to the H in the middle of the acac ancillary ligand. The simplicity of the spectra and the integration confirm the symmetrical nature of the ligand environment. The signal at ~ 8.9 ppm is assigned as H-8 by analogy to a similar complex reported in the literature⁶⁶ and is deshielded due to the ring current effects of the phenyl ring. Complex **2.36** has a significantly broadened spectrum which is due to the bromo substituent clashing sterically with the isoquinoline ring, resulting in the observed fluxionality on the NMR time scale. The novel bromo substituted complexes were also characterized by ^{13}C NMR, mass spectrometry and elemental analysis.

2.2.3 Synthesis of fluorenyl substituted iridium complexes

Having synthesized the bromine substituted ligands, the ligand library can be quickly doubled through the use of a Suzuki coupling reaction. It was decided to attach a fluorene unit onto the ligand in order to investigate the effects this would have on the optical properties of the complexes. Fluorene was chosen as it has been used frequently, in both monomeric and polymeric form, in OLED materials with great success.^{62,67-71} 9,9'-Dioctyl-9*H*-fluorene was chosen as it has two solubilizing alkyl chains which allow solution processability. Iridium complexes are frequently covalently bound to polyfluorene or other conjugated polymers in efforts to suppress phase separation (see Chapter 3), and so these well-defined small molecules will be used to discover the optimal site of attachment of a polyfluorene chain.

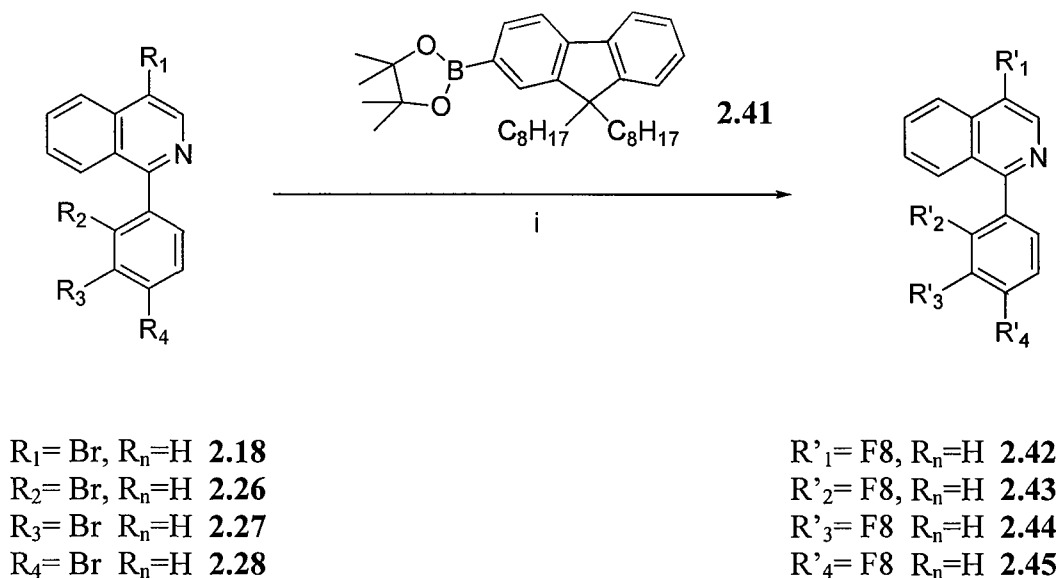
2.2.3.1 Synthesis of fluorenyl substituted ligands



Reagents and conditions: i) bromooctane, TBAB, Tol, $\text{NaOH}_{(\text{aq})}$, Reflux, 70%; ii) $n\text{BuLi}$, THF, $-78\text{ }^\circ\text{C}$; iii) 2-Isopropoxy-4,4',5,5'-tetramethyl-1,3,2-dioxaborolane, $-78\text{ }^\circ\text{C} \rightarrow$ room temperature, 89%

Figure 2.12: Synthesis of 2-(9,9'-dioctyl-9*H*-fluoren-2-yl)-4,4',5,5'-tetramethyl-1,3,2-dioxaborolane

The alkylation of commercially available 2-bromofluorene **2.39**, followed by a metal-halogen exchange and addition of 2-isopropoxy-4,4',5,5'-tetramethyl-1,3,2-dioxaborolane afforded 2-(9,9'-dioctyl-9*H*-fluoren-2-yl)-4,4',5,5'-tetramethyl-1,3,2-dioxaborolane **2.41** in excellent yield (89%).³⁹

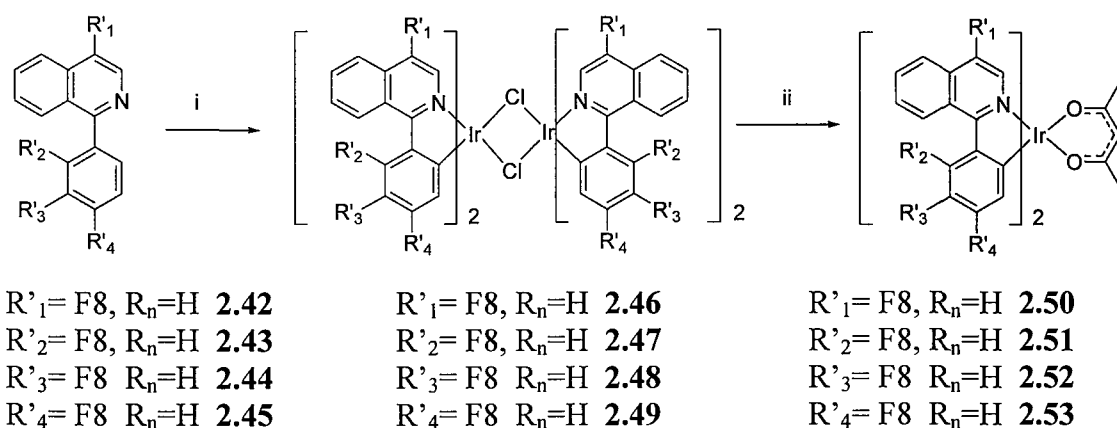


Reagents and conditions: i) Pd(OAc)₂, PPh₃, Tol, TEAOH_(aq), Reflux, 80 - 90%

Figure 2.13: Synthesis of fluorenyl substituted 1-phenylisoquinolines

A Suzuki coupling reaction between the previously synthesized bromo phenylisoquinoline ligands, **2.18**, **2.26-2.28**, and the boronic ester substituted fluorene moiety **2.41** provided the novel ligands **2.42-2.45**, where F8 represents a 9,9'-dioctyl-9H-fluorene-2-yl substituent.

2.2.3.2 Complexation of fluorenyl substituted ligands



Reagents and conditions: i) IrCl₃·xH₂O, 2-ethoxyethanol, H₂O, 110 °C; ii) acetylacetonate, Na₂CO₃, 2-ethoxyethanol, 110 °C, 50 -70% (2 steps)

Figure 2.14: Synthesis of fluorenyl substituted iridium complexes

The complexation of the novel ligands **2.42-2.45** was achieved by reaction with iridium trichloride to form the μ-chloro bridged dimers **2.46-2.49**, followed by dimer cleavage with acetyl acetonate, under basic conditions. These reactions provided access to the

four desired new regioisomeric complexes **2.50-2.53**. The complexes were purified by column chromatography allowing isolation of the complexes in high purity. The novel complexes were fully characterised by ^1H and ^{13}C NMR, mass spectrometry and elemental analysis.

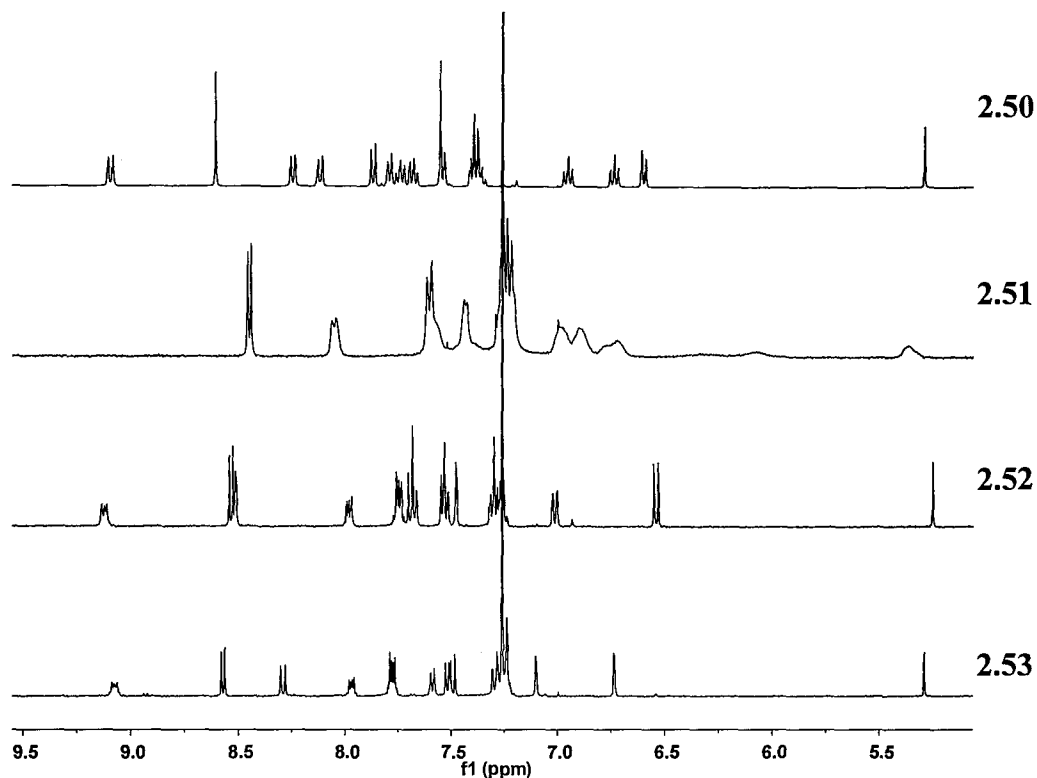


Figure 2.15: ^1H NMR spectra of fluorenyl substituted iridium complexes

Fig 2.15 shows the aromatic section of the ^1H NMR spectra of the novel complexes. The H-8 signal is again visible in complexes **2.50**, **2.52** and **2.53** although it is now at ~ 9.2 ppm. Significant spectral broadening is observed for **2.52**; this is analogous to the bromo substituted complex **2.36** and is again attributed to the steric interaction of the substituent and the isoquinoline ring.

2.3 Photophysical properties of iridium complexes

2.3.1 UV-Vis absorption spectra

2.3.1.1 Bromo substituted iridium complexes

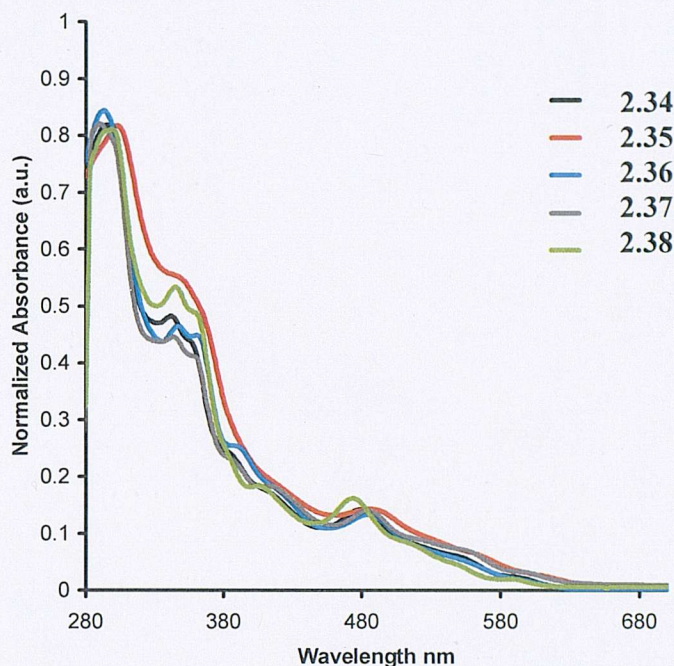


Figure 2.16: Normalized solution UV-Vis absorption spectra of 2.34-2.38 (DCM, $\sim 10^{-5}$ M)

Fig. 2.16 shows the solution UV-Vis absorption spectra of the parent complex **2.34** and the novel bromo substituted complexes **2.35-2.38**. The spectra are all assigned by analogy to related literature iridium(III)bis(cyclometallated) complexes.²⁷ The introduction of bromine substituents has little effect on the absorption spectra of complexes **2.35-2.38** compared to the unsubstituted analogue **2.34**. The intense absorption bands between 250 and 350 nm (molar absorption coefficient, $\epsilon = 10,000 - 60,000 \text{ M}^{-1}\text{cm}^{-1}$) are attributed to $^1\pi-\pi^*$ transitions between 1-phenylisoquinolinato centered states. The weaker absorption bands ($\epsilon = 1000 - 6000 \text{ M}^{-1}\text{cm}^{-1}$) in the range 350 - 440 nm are assigned to the spin allowed metal-to-ligand charge transfer transitions, $^1\text{MLCT}$, and those at 450 - 500 nm to the spin forbidden metal-to-ligand charge transfer transitions, $^3\text{MLCT}$ which gain intensity through the strong spin-orbit coupling.

2.3.1.2 Fluorenyl substituted iridium complexes

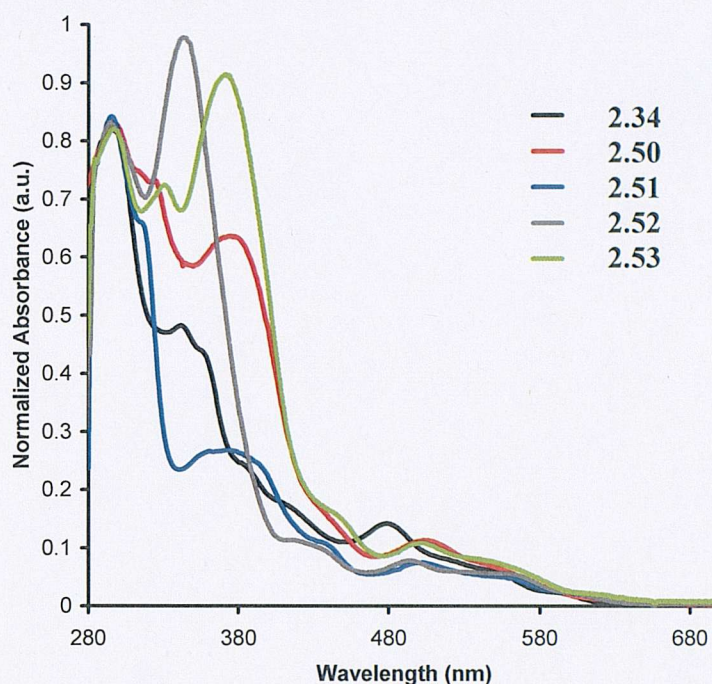


Figure 2.17: Normalized solution UV-Vis absorption spectra of **2.50-2.53** (DCM, $\sim 10^{-5}$ M)

Substitution of the 1-phenylisoquinolinato ligands with fluorenyl groups significantly alters the absorption spectra for **2.50-2.53** (Fig. 2.17). As for **2.34-2.38**, the intense absorption bands between 250 and 300 nm are attributed to $^1\pi-\pi^*$ transitions of 1-phenylisoquinolinato centered states. The absorption bands between 320 and 400 nm are attributed to $^1\pi-\pi^*$ transitions of the fluorenyl substituents. Complexes **2.50**, **2.51** and **2.53** display red-shifted fluorenyl absorption peaks, for **2.51** this peak is also of significantly reduced relative intensity. These red-shifts indicate extended conjugation, i.e. orbital overlap between the fluorenyl substituents and the iridium complex. The weaker MLCT absorption bands in the range 450-600 nm are also red-shifted compared to **2.34**.

2.3.2 Solution photoluminescence spectra

2.3.2.1 Bromo substituted iridium complexes

The solution photoluminescence spectra of the bromo substituted complexes are shown below (Fig 2.18). The unsubstituted complex **2.34** has an emission maximum at 623 nm, close to that reported previously (622 nm).²⁷ Complexes **2.35**, **2.36** and **2.37** all display

red-shifted emissions, whilst complex **2.38** displays a blue-shift. The λ_{max} varies in the order $2.35 > 2.36 > 2.37 > 2.34 > 2.38$.

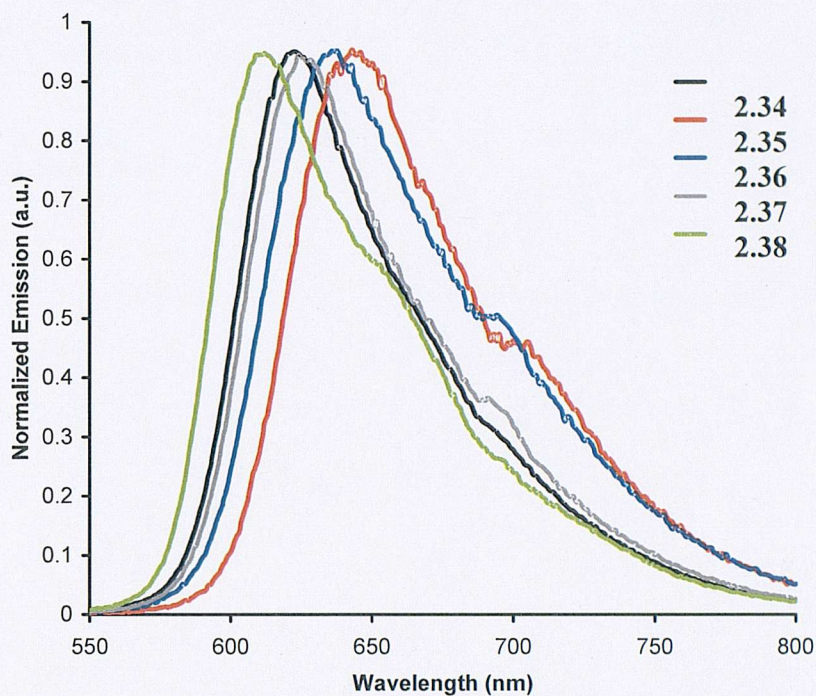


Figure 2.18: Normalized solution photoluminescence spectra of 2.34-2.38 (DCM, Max Abs~0.1, 350 nm excitation)

2.3.2.2 Fluorenyl substituted iridium complexes

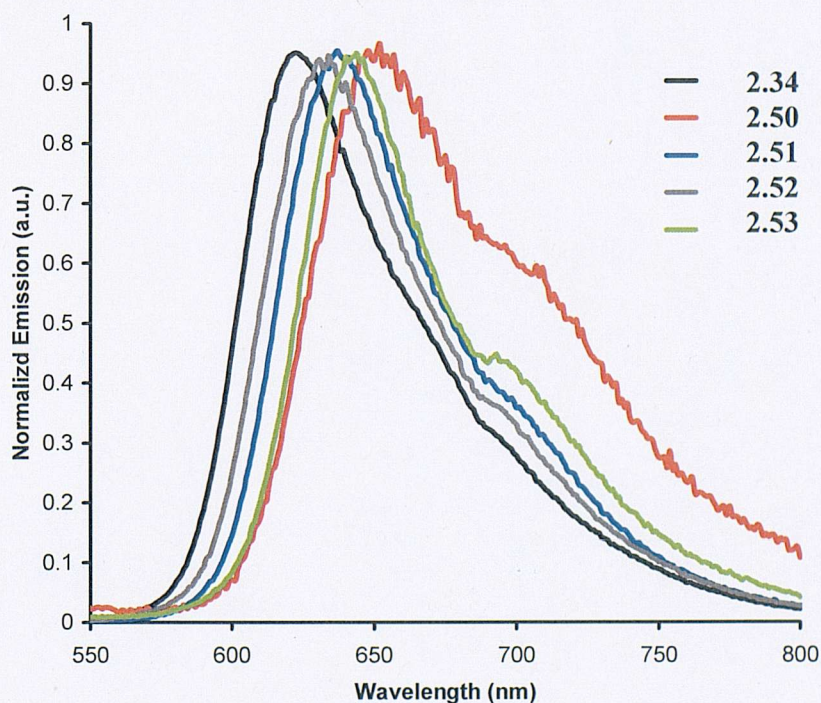


Figure 2.19: Normalized solution photoluminescence spectra of 2.50-2.53 (DCM, Max Abs~0.1, 350 nm excitation)

The influence of the site of substitution on the shift in the emission differs between the bromine and fluorenyl substituted complexes. For the fluorenyl substituents, all substituents cause a red-shift and the order of emission wavelength is **2.50>2.53>2.51>2.52>2.34**.

2.3.2.3 Quantum yields

Compound	Emission Wavelength (λ_{\max})/nm	Quantum Yield ^a (Φ_{Ph}) / %
2.34	623	20
2.35	646	12
2.36	637	7
2.37	626	14
2.38	612	10
2.50	653	7
2.51	637	3
2.52	634	15
2.53	644	6

Table 2.1: Quantum yields of iridium complexes

a) measured in degassed DCM solutions using **2.34** as the standard.²⁷

The solution phosphorescence quantum yields, Φ_{Ph} , of **2.35-2.38** and **2.50-2.53** are shown above (Table 2.1). All complexes show moderate quantum yields ($\Phi_{\text{Ph}} = 6 - 15\%$). Substitution in the 3-phenyl position (**2.37** and **2.52**) leads to the highest quantum yields for all the substituted complexes, the origin of this phenomenon and an interpretation of all the observed photophysical data will be discussed below.

2.3.3 Experimental measurements of energy levels

In order to understand the variation in optical properties of the regioisomers, it was important to establish the energy levels of the frontier molecular orbitals. The orbital energies were determined by cyclic voltammetry and absorption spectroscopy. A measure for the HOMO energy, E_{HOMO} , is the ionization potential;⁷² here the ionization potential was calculated from the half-wave oxidation potential ($E_{1/2}^{\text{Ox}}$) as determined by cyclic voltammetry, conducted in DCM solution. All complexes showed single, reversible one-electron oxidation peaks. Ferrocene was used as an internal standard and the half-wave oxidation potentials were converted to values for E_{HOMO} using methodology developed by D'Andrade *et al* who calculated the relationship between the ionization and oxidation potentials in closely related iridium complexes.⁷²

No reduction processes were detected within the solvent cathodic limit. Therefore, the optical energy gap of the complexes was measured from the absorption onset in the absorption spectra and this was used to obtain the LUMO energy, E_{LUMO} .

Compound	$E_{1/2}^{\text{Ox}}$ /V ^a	E_{HOMO} /eV ^b	ΔE /eV ^c	E_{LUMO} /eV ^d
2.34	0.36	-5.11	1.99	-3.12
2.35	0.52	-5.33	1.92	-3.41
2.36	0.52	-5.33	1.96	-3.37
2.37	0.48	-5.27	1.97	-3.3
2.38	0.56	-5.38	2.02	-3.36
2.50	0.35	-5.09	1.88	-3.21
2.51	0.36	-5.1	1.95	-3.15
2.52	0.33	-5.06	1.95	-3.11
2.53	0.42	-5.19	1.93	-3.26

Table 2.2: HOMO and LUMO energy levels of complexes

a) Measured from solution (DCM) CV using Fc as an internal standard. b) Calculated using method by D'Andrade *et al*. c) Estimated from UV-Vis spectrum absorption onset. d) $E_{\text{LUMO}} = E_{\text{HOMO}} + \Delta E$

Both the nature of the substituents and their positions on the phenyl ring exert a significant influence over the orbitals' energies and therefore over the optical properties. It is interesting to note the similarities in the trend in HOMO and LUMO for the Br substituted complexes **2.35-2.38** compared to the fluorenyl substituted complexes **2.50-2.53** (Fig 2.20).

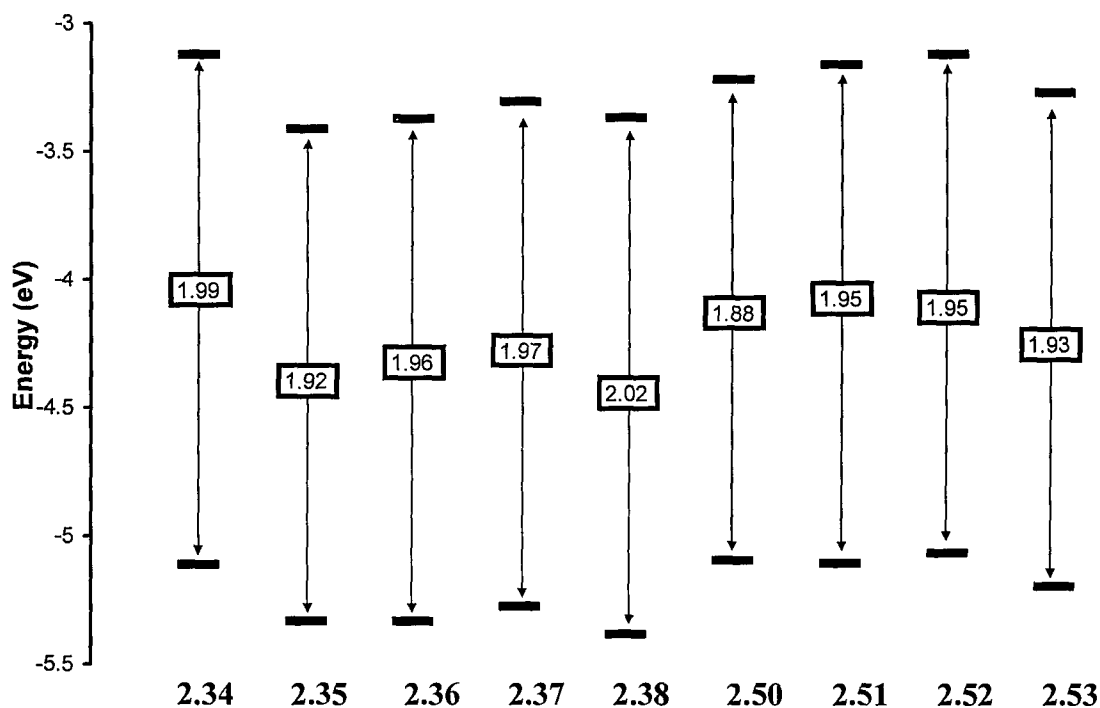


Figure 2.20: HOMO-LUMO energy level diagram of complexes

The variation in the frontier energy levels will be rationalised in the subsequent section. The value indicated by the square margin corresponds to the HOMO-LUMO energy gap, as measured from the UV-Vis absorption onset. These values are found to decrease with an increase in red-shifted emission from the complexes, which is as expected.

2.3.4 DFT and TDDFT calculations

2.3.4.1 Comparison of DFT optimization and X-ray crystal structure

In order to understand the variation in optical properties of the regioisomers, it was important to establish the properties of the frontier molecular orbitals. Density functional theory (DFT) and Time Dependent Density Functional theory (TD-DFT) calculations, using the B3LYP functional, with the LANL2DZ basis set for the Ir atom, and the 6-31G(d) basis set for the ligand atoms, were used to optimize the complex geometries and model the linear combination of atomic orbitals (LCAO) and the spatial

distribution of the molecular orbitals. Despite the wide usage of the aforementioned level of calculation,^{28,33,73-76} only a limited number of investigations into the validity of the chosen basis sets have been reported.^{33,77} Consequently, it was deemed important to demonstrate the applicability of these methods to the complexes to which they would be applied.

A single crystal of **2.37** was grown from a solution of hot toluene. The bond lengths and angles of the crystal structure are compared to those obtained from the ground state optimized geometry of the corresponding structure.

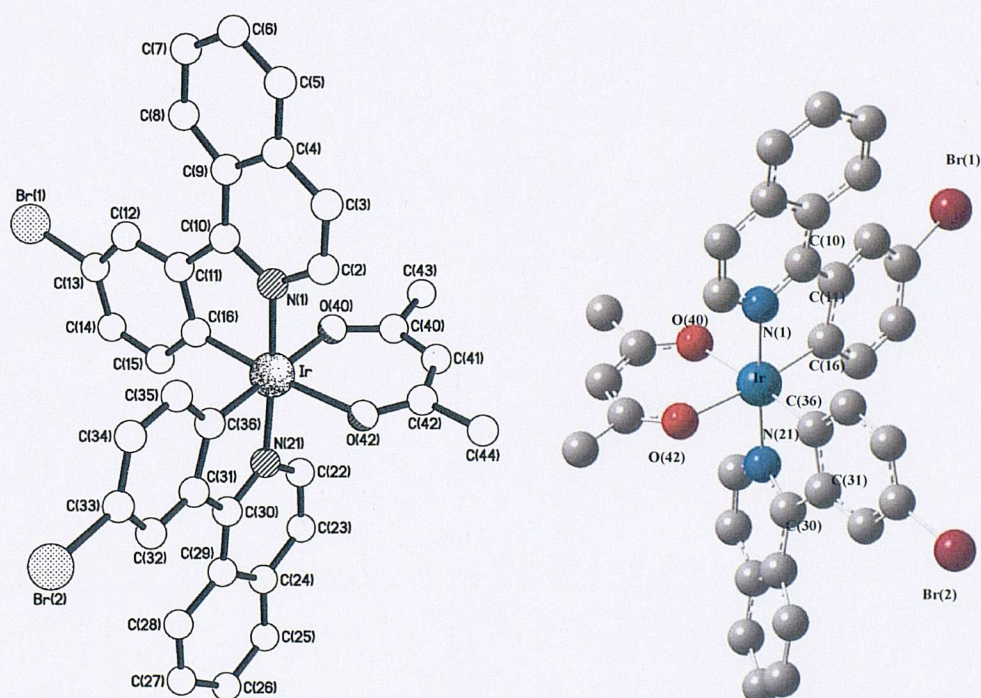


Figure 2.21: Comparison of X-ray crystal structure and DFT optimized ground state of **2.37**

The X-Ray crystal structure confirms the trans orientation of the N atoms, and the cis orientation of the ancillary ligand (acac), as has been verified by many other researchers.^{27,48,50,51} The geometry around the metal centre is best described as distorted octahedral with similar bond lengths for the cyclometallating C and N atoms (~ 2 Å), and slightly longer lengths for the Ir-O bonds (~ 2.15 Å). Full crystallographic data are presented in Appendix A.

Bond	X-ray crystal structure bond length /Å	DFT bond length / Å	Bond Angle	X-ray crystal structure angle /°	DFT angle / °
C(16)-Ir	1.97	2.00	C(36)-Ir-C(16)	89.4	93.4
C(36)-Ir	1.98	2.06	O(42)-Ir-O(40)	88.6	86.3
N(1)-Ir	2.02	2.06	C(36)-Ir-O(42)	93.3	91.4
N(21)-Ir	2.03	2.06	C(16)-Ir-O(40)	89.0	89.3
C(10)-C(11)	1.48	1.47	N(1)-Ir-C(16)	79.4	79.7
C(30)-C(31)	1.49	1.47	N(1)-Ir-C(36)	98.7	97
O(40)-Ir	2.16	2.20	N(21)-Ir-C(36)	79.3	79.7
O(42)-Ir	2.14	2.20	N(21)-Ir-C(16)	97.1	99.5
C(13)-Br(1)	1.90	1.92	C(10)-C(11)	0.8	11.2
C(33)-Br(2)	1.91	1.92	C(30)-C(31)	2.2	10.6

Table 2.3: Comparison of selected bond lengths and angles from X-ray structure and DFT optimized geometry

Table 2.3 shows that there is a very good agreement between the experimentally obtained bond lengths and those from the optimized ground state geometry. There is less agreement in the bond angles, as was already noted by Nie *et al.*,⁷⁷ although this may be due to the geometries being optimized as single molecules and packing effects being ignored in DFT. Such crystal packing effects are likely to have a significant impact on the bond angles measured from the X-ray crystal structure.

2.3.4.2 Comparison of experimental and calculated energy levels

It is vital to ensure a good match between the experimentally determined energy levels and those predicted by the DFT and TD-DFT calculations. The ground state singlet optimized geometry gave values for the HOMO frontier orbital energy level, and the

vertical excitation energy to the lowest excited triplet state obtained by TD-DFT was summed to the HOMO to obtain a value for the LUMO energy level.

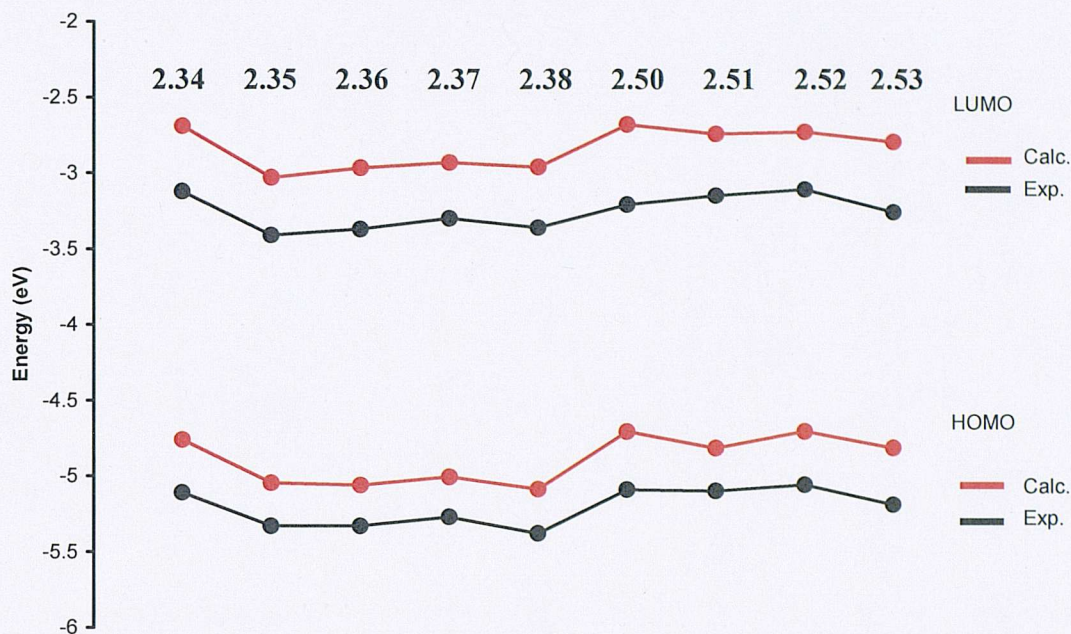


Figure 2.22: Comparison of experimental (Cyclic Voltammetry and UV-Vis absorption onset) and theoretical (DFT/TDDFT) energy levels

Despite the absolute values of the calculated frontier orbitals being significantly different from the experimentally derived ones, the trend in the relative energies of the various complexes gives an exceedingly good agreement.

The calculated energies of the first vertical transitions ($S_0 \rightarrow T_1$) according to TD-DFT are shown below (Fig 2.23). They are directly compared to the absorption onsets of the UV-Vis spectra of the relevant complexes, showing a good agreement in the trends of the transition energy despite a difference in the absolute values. The TD-DFT calculated value for the first vertical absorption of complex **2.52** is significantly lower than those calculated for the other complexes. The cause of this is not known.

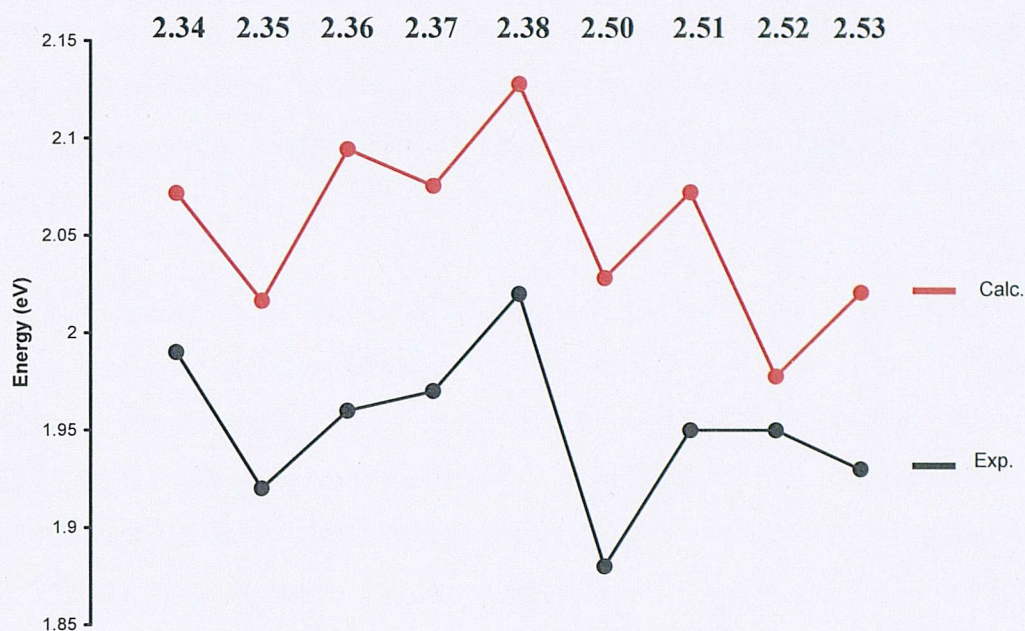


Figure 2.23: Comparison of theoretical and experimental $S_0 \rightarrow T_1$ vertical transition energy

Compound	Transition	Orbitals	Contribution / %	Energy / eV
2.34	$S_0 \rightarrow T_1$ MLCT + LLCT	HOMO \rightarrow LUMO	62	2.0716
2.35	$S_0 \rightarrow T_1$ MLCT + LLCT	HOMO \rightarrow LUMO	63	2.0163
2.36	$S_0 \rightarrow T_1$ MLCT + LLCT	HOMO \rightarrow LUMO	59	2.0943
2.37	$S_0 \rightarrow T_1$ MLCT + LLCT	HOMO \rightarrow LUMO	63	2.0756
2.38	$S_0 \rightarrow T_1$ MLCT + LLCT	HOMO \rightarrow LUMO	58	2.1278
2.50	$S_0 \rightarrow T_1$ MLCT + LLCT	HOMO \rightarrow LUMO	61	2.0282
2.51	$S_0 \rightarrow T_1$ MLCT + LLCT	HOMO \rightarrow LUMO	61	2.0722
2.52	$S_0 \rightarrow T_1$ MLCT + LLCT	HOMO \rightarrow LUMO	66	1.9775
2.53	$S_0 \rightarrow T_1$ MLCT + LLCT	HOMO \rightarrow LUMO	59	2.0206

Table 2.4: TD-DFT orbital contribution and energy of $S_0 \rightarrow T_1$ transition

The calculated first vertical transitions of the all the complexes are predominantly (~60%) HOMO \rightarrow LUMO (Table 2.4) and as such the other contributions (which are typically transitions of similar energy e.g. HOMO \rightarrow LUMO+1) will be ignored, due to their small participation (<15%). This means that rationalizing the energy levels of only the frontier orbitals can explain the observed changing emission wavelengths in the complexes.

The exact nature of the transition can be probed by employing a Mulliken population analysis in order to calculate the relative contributions of the atomic orbitals to the frontier molecular orbitals. Table 2.5 shows the respective contributions to the HOMO and LUMO of each portion of the relevant complex. Population analysis reveals that the HOMO (S_0) has only ~40% metal character. There is at least an equal contribution to the HOMO from the phenyl portion of the cyclometallating ligand (i.e. entirely ligand π -orbital based). The LUMO (at the singlet ground state optimized geometry) predominantly consists of ligand character with the largest contribution localized on the isoquinoline section (~70%). Consequently, the lowest energy transition should be considered a combination of a MLCT and a LLCT (ligand to ligand charge transfer).

Compound	Iridium	Isoquinoline	Phenyl	acac
HOMO contribution (%)				
2.34	42.7	8.6	44.5	4.2
LUMO contribution (%)				
2.34	4.1	77.7	17.7	0.5

Table 2.5: Mulliken population analysis of HOMO and LUMO for 2.34

2.3.4.3 Comparison of singlet and triplet excited states

A final consideration is the nature of the electronic transitions being considered. The estimation of the LUMO energy in cyclometallated iridium complexes by using the absorption onset in the UV-Vis spectra, and by TD-DFT as previously demonstrated, is common throughout the literature.⁷³ However, the transitions calculated by both these methods relate to absorptions from the ground state to the first triplet excited state. Consequently, the energies obtained by these methods do not take into account the

geometry relaxation that occurs following the electronic excitation. As emission occurs from the relaxed excited triplet state back to the ground state, it is necessary to evaluate the effect of geometry relaxation on the frontier orbitals.

The first triplet excited state of complex **2.34** was optimized without any symmetry constraints and is displayed next to the singlet ground state for comparison (Fig 2.24). The two lowest singly occupied molecular orbitals (SOMOs) of the optimized triplet excited state are shown below alongside the HOMO and LUMO of the optimized singlet ground state.

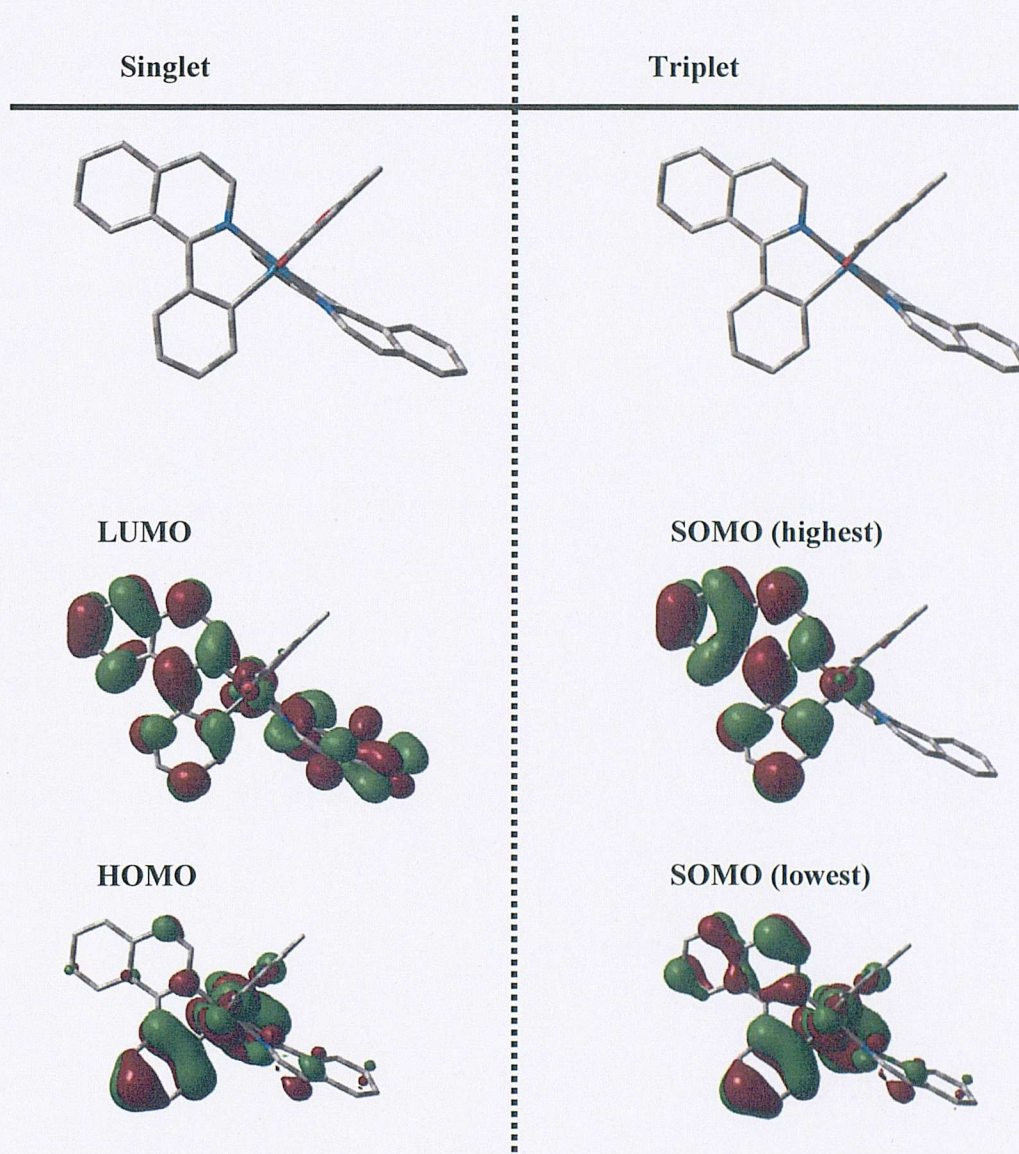


Figure 2.24: Comparison of singlet and triplet ground and excited state MO contributions

The LUMO of the optimized singlet state is predominantly (>90%) ligand based with a small contribution from the iridium metal orbitals. The highest SOMO is almost

identical in character with the exception that it is only localized on one ligand. It should be noted that in both cases, there is an absence of orbital density (i.e. a node) on the carbon at the 3-position of the phenyl ring. The HOMO of the optimized singlet ground state is predominantly phenyl (~40%) and iridium metal (~40%) based. The lowest SOMO of the optimized triplet excited state is also predominantly phenyl and metal based, although there is now a significant contribution from the isoquinoline portions of one of the ligands.

$$E(S_0 \rightarrow T_1^{\text{TDDFT}}) - \Delta(E^{\text{Total}T_1^{\text{Opt}}} - E^{\text{Total}S_0^{\text{Opt}}}) = \text{Relaxation Energy}$$

$$2.0716\text{eV} \quad - \quad 2.015\text{eV} \quad = 0.074 \text{ eV}$$

Subtracting the difference in total energy between the triplet optimized excited state ($E^{\text{Total}T_1^{\text{Opt}}}$) and the singlet optimized ground state ($E^{\text{Total}S_0^{\text{Opt}}}$) from the vertical absorption energy from the TDDFT calculations ($E(S_0 \rightarrow T_1^{\text{TDDFT}})$) gives a calculated geometry relaxation energy of 0.074 eV.

The small difference in geometry and the similarities in the distribution of the electron density between the HOMO and LUMO of the optimized singlet ground state and the SOMOs of the optimized triplet excited state indicate that factors that affect the energy of the absorption transition are likely to similarly affect the emission transition. Consequently, due to the significant difficulties associated with the optimization of the triplet excited states, only singlet optimized ground state geometries of the other complexes were calculated and it is assumed that the distribution of the electron density in the MO plots can be used to rationalise the emission properties of the complexes.

2.3.4.4 DFT and TD-DFT calculations of bromo substituted iridium complexes

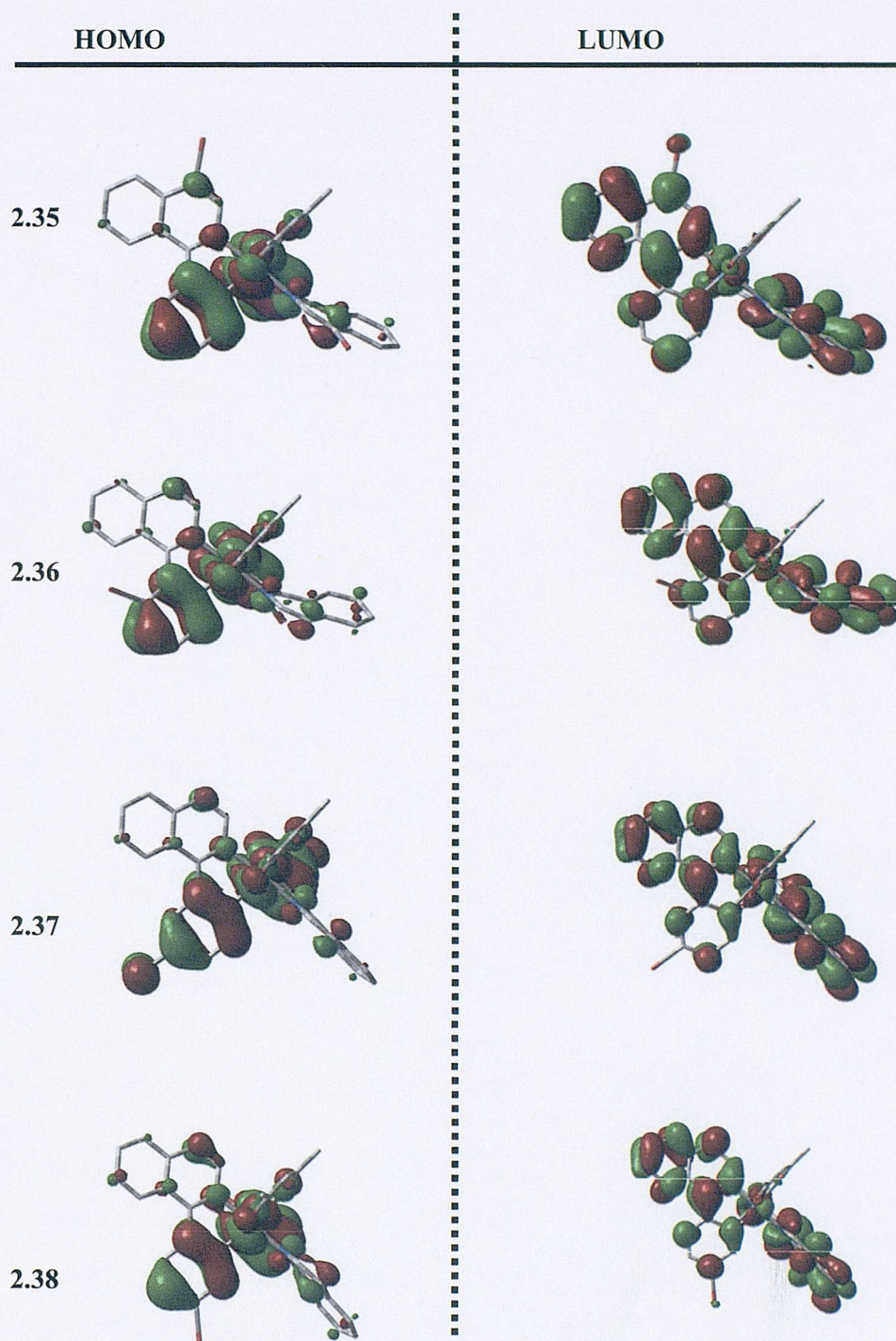


Figure 2.25: HOMO and LUMO orbital plots for bromo substituted complexes

The HOMO and LUMO densities of complexes 2.35-2.38 are shown above (Fig. 2.25). They are all similar to those of the unsubstituted complex 2.24 with the exception that

participation of the bromine atom can now be observed in some of the orbitals. Mulliken population analysis reveals the extent of participation of the bromine atom on either the HOMO or the LUMO (Table 2.6). This data, in conjunction with the experimentally measured energy levels, can be used to rationalise the observed differences in emission wavelengths of the complexes.

Compound	Iridium	Isoquinoline	Phenyl	acac	Bromine
HOMO contribution / %					
2.35	40.0	9.3	45.4	4.2	1.1
2.36	40.4	8.3	45.9	4.3	1.1
2.37	38.1	8.2	42.6	4.0	7.1
2.38	39.4	11.1	44.6	4.0	0.9
LUMO contribution / %					
2.35	3.9	76.0	18.1	0.4	1.6
2.36	4.3	73.4	21.1	0.5	0.7
2.37	3.9	75.4	20.2	0.4	0.1
2.38	3.8	75.5	19.2	0.4	1.2

Table 2.6: Mulliken population analysis of HOMO and LUMO for bromo substituted complexes

The bromine substituted regioisomers have significantly lower E_{HOMO} and E_{LUMO} than the unsubstituted complex **2.34** (Fig. 2.20). This is due to the inductive, electron withdrawing effect of the bromine atom stabilizing the frontier orbitals, resulting in a net lowering of E_{HOMO} and E_{LUMO} . For complex **2.35**, the Br substituent exerts an inductive effect which affects the LUMO to a greater extent than the HOMO, due to the greater proportion of LUMO density in close proximity to it. Despite, mesomeric donation from the Br 4p atomic orbitals (1.6%), which will slightly increase the energy of the LUMO, the overall result is a large observed red-shift in emission due to the inductive effect.

In contrast, the Br substituent on complex **2.38** is attached to the phenyl ring, and the HOMO is mostly localized on the phenyl rings of the ligand. Consequently, the

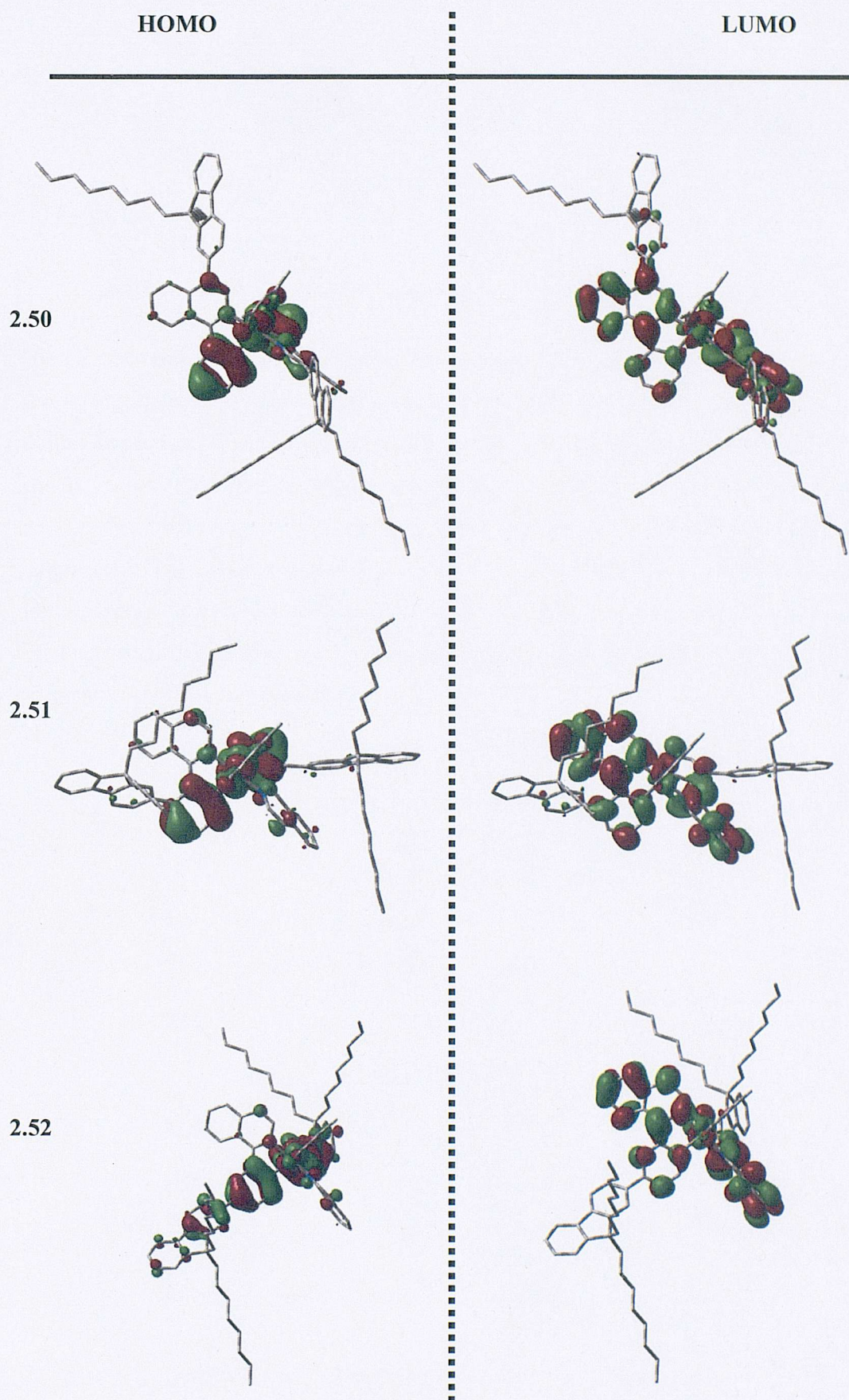
inductive electron withdrawing effect of the bromine substituent affects the HOMO to a greater extent than the LUMO. A small contribution to the LUMO from the Br 4p atomic orbitals (1.2%) can be seen above, which further increases the LUMO energy, resulting in a net separation of its frontier orbitals which results in the observed blue-shift in emission relative to **2.34**.

The HOMO and LUMO levels of **2.37** are lowered less than **2.38**. As in the case of **2.38**, it would be reasonable to expect a similar blueshift due to the large inductively withdrawing effect on the HOMO. However, the large mesomeric donation from the Br atom (7.1%), which can be clearly seen, leads to a destabilization of the HOMO; a similar destabilization was observed by Avilov *et al.* who carried out DFT and TD-DFT calculations on fluorinated phenyl pyridine iridium cyclometallates.³³ The presence of a node in the LUMO at the 3-position means the LUMO is less affected by the inductive effect of the bromine than **2.38**. Overall, there is a small decrease in energy gap predominantly caused by the large mesomeric destabilization of the HOMO by the Br atom.

Complex **2.36** displays a moderately large redshift. It is not believed that this is a direct result of mesomeric or inductive electronic effects. The unfavourable steric interactions between the Br substituent and the isoquinoline ring are believed to cause a large torsion angle between the C-C bond linking the isoquinoline and phenyl units. This increased torsion leads to a reduction in the HOMO-LUMO energy gap by forcing an increase in orbital overlap between the ligand and the metal orbitals which produces the observed red-shift. Similar bathochromic shifts have been observed by Fang *et al* in bis(1-phenylisoquinoline)iridium(III)(acac) complexes.⁵⁰

The order of increasing emission wavelengths (**2.38**<**2.34**<**2.37**<**2.36**<**2.35**) have been rationalised by three main contributions (inductive, mesomeric and torsion) and the relative contribution of each of these effects, to either the LUMO or the HOMO, depends significantly on the site of substitution.

2.3.4.5 DFT calculations of fluorenyl substituted iridium complexes



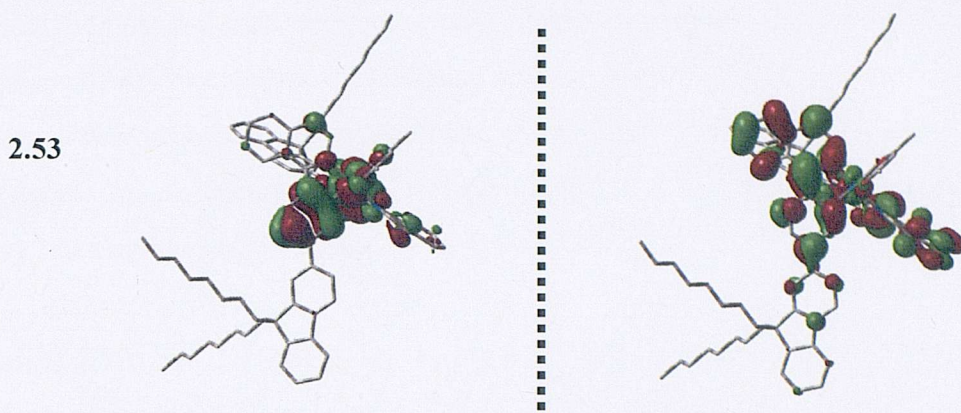


Figure 2.26: HOMO and LUMO orbital plots for fluorenyl substituted complexes

The HOMO and LUMO densities for the fluorenyl substituted complexes are shown above (Fig. 2.26). The phenylisoquinolinato core of the complexes again shows a very similar distribution of orbital density when compared to the unsubstituted complex **2.34**. The extension of the frontier orbitals onto the fluorenyl substituents through conjugation can clearly be seen in several of the plots. As in the case of the bromine derivatives the magnitude of the interaction and whether it affects the HOMO or the LUMO depends on its position. Mulliken population analysis (Table 2.7) again reveals numerical values for the observable difference in densities, which can be used to rationalise the differences in emission wavelength.

Compound	Iridium	Isoquinoline	Phenyl	acac	Fluorenyl
HOMO contribution / %					
2.50	40.9	9.6	43.4	3.9	2.1
2.51	39.5	7.2	45.7	3.3	4.3
2.52	31.4	6.5	39.4	2.8	19.9
2.53	37.4	11.2	43.9	3.7	3.9
LUMO contribution / %					
2.50	3.7	69.8	16.9	0.4	9.2
2.51	4.0	70.1	21.0	0.5	4.4
2.52	3.4	76.8	19.1	0.4	0.3
2.53	3.8	69.9	19.1	0.5	6.7

Table 2.7: population analysis of HOMO and LUMO for fluorenyl substituted complexes

The E_{HOMO} and E_{LUMO} for the fluorenyl substituted complexes **2.50-2.53** are similar to those of the unsubstituted derivative **2.34**. This is because the fluorenyl substituents do not exert inductive electron withdrawing effects. The DFT calculations show that the frontier molecular orbitals have significant coefficients on the fluorenyl rings. Fluorenyl substituents in conjugation with the phenyl ring result in a stabilization of the LUMO energy level and a destabilization of the HOMO energy.

Complex **2.50**, has a significantly lowered LUMO, which is due to large mesomeric stabilization by the fluorenyl group (9.2%). A small contribution to the HOMO can also be seen (2.1%), and, these two effects combined manifest as a significant reduction in the energy gap, and consequently a large redshift in emission.

Complex **2.52** has a raised HOMO energy, but its LUMO is unchanged from **2.34**. DFT calculations show that the LUMO of **2.52** has the same distribution as **2.34** (i.e. predominantly localised on the isoquinoline ring but with a node at the 3-phenyl position). The fluorenyl substituent in **2.52** therefore cannot strongly influence the LUMO energy. However, DFT shows that its HOMO is significantly delocalized onto the fluorenyl substituent (19.9%). This results in its higher HOMO energy and the bathochromic shift in the emission.

Conversely, **2.53** has a HOMO that does not have a large amount of fluorenyl contribution (3.9%), but its LUMO energy is lower due to significant delocalization onto the fluorenyl substituents (6.7%). Experimentally this is observed in the bathochromic shift in its emission. In general, the stabilizing effect on the LUMO by fluorenyl substituents has a greater magnitude than the destabilizing of the HOMO; therefore a greater bathochromic shift occurs in the emission of **2.50** and **2.53** relative to **2.52**.

Complex **2.51** also has considerable steric interactions between the fluorenyl substituent and the isoquinoline ring analogous to complex **2.36**. It displays moderate contributions from the fluorenyl substituent to both the HOMO (4.3%) and LUMO (4.4%). However, it must be noted that the emission maxima of complex **2.51** is identical to that of complex **2.36**. Consequently, it is believed that the predominant mechanism of emission wavelength variation in these complexes is due to orbital interactions caused by the steric clash of the 2-position with the isoquinoline ring system.

Using DFT it has also been possible to rationalize the various trends in emission wavelengths in fluorenyl substituted iridium complexes. The order of increasing emission wavelength of **2.34<2.52<2.51<2.53<2.50** can be rationalized by the effects of extra conjugation on either the HOMO or LUMO, and by steric effects.

2.3.4.6 Note on the effect of the complex structure on the quantum yields

The comparison of the solution quantum yields with the relative contributions to the HOMO and LUMO, calculated from the population analysis, shows that, overall, complexes that have substituents that contribute the least to the LUMO have the largest quantum yields. Due to the absence of LUMO density at the 1,3 position, substitution at this position prevents significant mesomeric interactions between the substituent and the LUMO. It is tentatively proposed that this increased localization of the excited state minimizes quenching processes leading to non-radiative transitions (e.g. bond vibrations) relative to complexes bearing substituents on positions that can contribute significantly to the LUMO. However, the investigations required to verify this are beyond the scope of this thesis.

2.4 Conclusions

A series of novel regioisomeric bromine and fluorenyl substituted bis(1-phenylisoquinolino)iridium(III)(acac) complexes have been synthesized and fully characterized. Their photophysical properties have been probed by absorption and emission spectroscopy, and their differences rationalized by consideration of the energy levels of their respective HOMO and LUMO frontier orbitals. The underlying causes of the variation of the energy levels have been investigated using DFT and TD-DFT calculations, the use of which has been validated by comparison to the experimental data.

The investigation has revealed that the variation of the emissive properties of the complexes depends on the steric and electronic influence of the substituent, and on its position with respect to the density of the HOMO and LUMO orbitals.

Bromine substituents exert both an inductive withdrawing effect, and a mesomeric donating effect, which can be utilised to either red or blue shift the emission of the complexes in a range of 612 - 646 nm.

Fluorenyl substituents result in a red-shift of the emission, which is a result of the extension of conjugation between the ligand orbitals and the fluorene unit. By varying the position of the substituent, the emission wavelength can be fine-tuned in the region of 634 - 653 nm.

Substitution at the 1,2 position results in significant steric interactions between the substituent and the isoquinoline ring, which results in a red-shift in emission, which is believed to be a result of the increased torsion present in the molecule.

Measurement of the solution quantum yields of the novel complexes reveals significant variation depending on the position of the substituent. Substitution at the 1,3 position results in the least loss of quantum efficiency relative to the unsubstituted complex, and implies that this is the optimal position for attachment of a polymer chain. The majority of the results found in this chapter have been published in the literature,⁷⁸ and can be found in Appendix B.

Chapter 3: Polymeric iridium(III)bis(phenylisoquinoline)(acac) complexes

3.1 Introduction

The small molecules presented in the previous chapter display desirable optical properties for use in OLEDs. However, a significant drawback of these types of molecules is the need for vacuum deposition in order to manufacture the LED. This is a costly procedure, and limits the potential size of a created display. Furthermore, it has recently been suggested that, in the case of bis-cyclometalated iridium complexes, sublimation is not an innocent technique and can cause isomerisation.⁷⁹

In an attempt to avoid the use of sublimation, other workers have doped small molecules (guests) into polymer matrices (host). This practice has yielded extremely effective and efficient OLEDs, and allows solution deposition of multiple layers.⁸⁰⁻⁸² Although significant improvements in device efficiency using blended systems are reported, their performance can suffer from a number of undesirable factors including phase separation, and aggregation induced phosphorescence quenching.³⁴

In order to suppress these shortcomings workers have attached the emissive phosphors in a conjugated fashion to the polymer matrix. This prevents the possibility of phase separations, and has also been shown to reduce the effect of concentration quenching through aggregation of the phosphor. Several different strategies have been attempted which will be outlined below.

3.1.1 Non-conjugated polymer backbones

Tokito *et al* published a series of non-conjugated polymers (Fig. 3.1) containing pendant charge transporting carbazole units and emissive iridium complexes. Variation of the incorporated iridium complex gave access to red, green and blue OLEDs which displayed impressive external quantum efficiencies (5-9%).⁸³

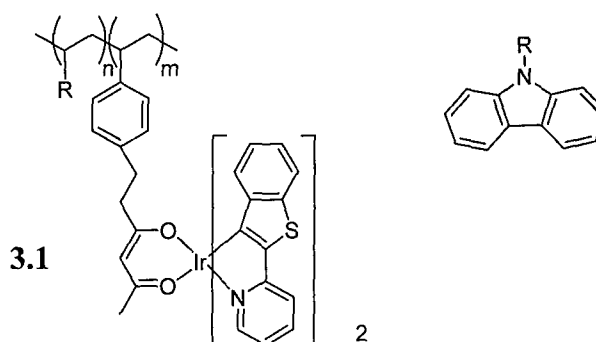


Figure 3.1: Non-conjugated polymer containing pendant iridium complexes

More recently, Haldi *et al*, have reported a series of polymers derived from the polymerization of norbornenes with pendant charge transporting groups and iridium complexes (Fig. 3.2) showing EQEs in the range of (1-4%).⁸⁴

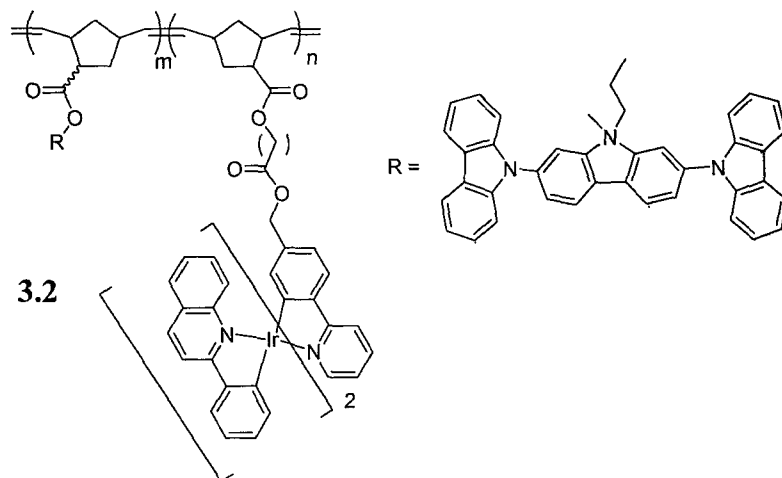


Figure 3.2: Non conjugated electrophosphorescent polymer derived from norbornene

A significant drawback of the non-conjugated approach is that the polymer backbone is non-conducting. Consequently, the operating voltages of the OLEDs are typically too high for practical purposes.

3.1.2 Conjugated Polymer backbones

Many workers have used conjugated polymers as host materials in efforts to exploit the desirable electrical properties they possess.

Chen *et al* reported an electrophosphorescent polyfluorene chain containing pendant iridium complexes and charge transporting units (Fig. 3.3), displaying reasonable external quantum efficiencies (1-3 %) in an OLED.⁶⁷

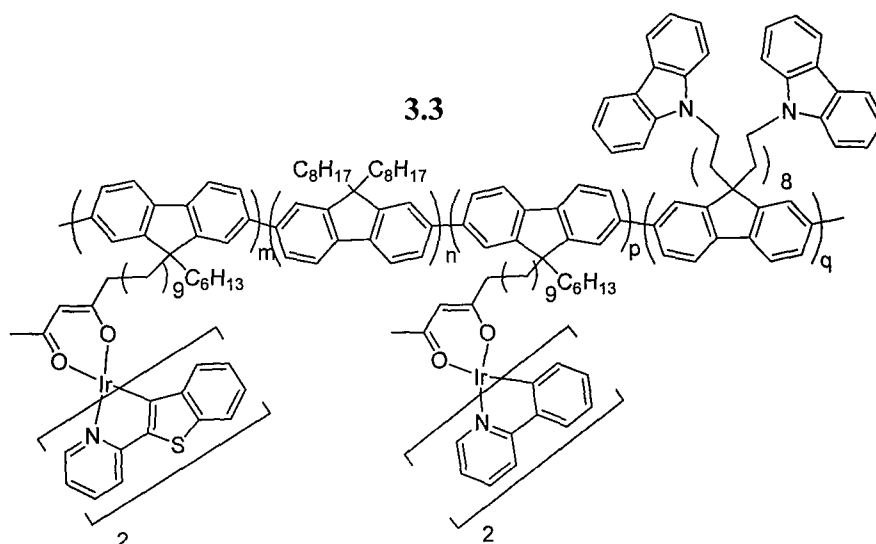


Figure 3.3: Conjugated polymer containing pendant iridium complexes

Zhen *et al* demonstrated a series of iridium containing polyfluorenes, linked through the cyclometallating ligand of the complex. OLED external efficiencies of around 4-5% were obtained.⁶²

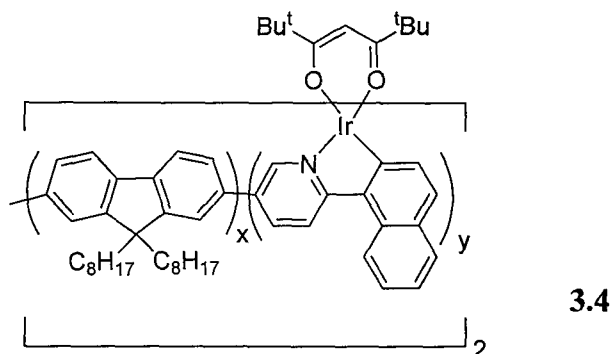


Figure 3.4: Iridium complex incorporated into polyfluorene chain

3.1.2.1 Use of bis(phenylisoquinoline)iridium complexes in polymeric materials

There have been several examples of the use of phenylisoquinoline iridium derivatives in polymeric materials as outlined below.

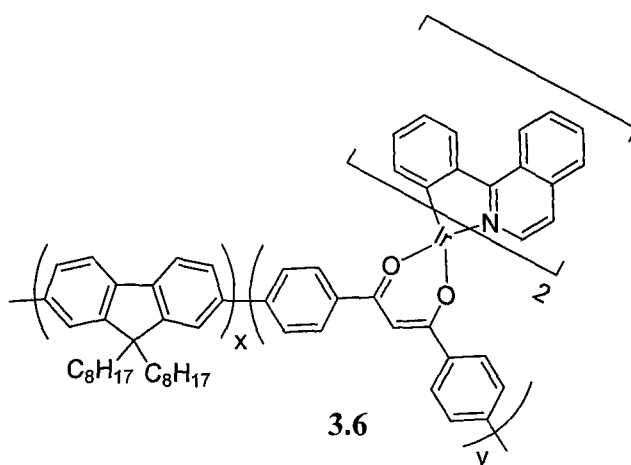
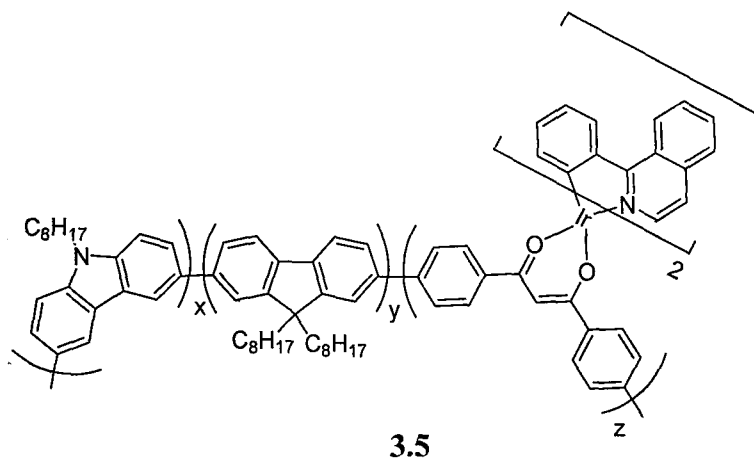


Figure 3.5: Bis(phenylisoquinoline)iridium complex incorporated into conjugated polymers

Zhang *et al* reported the synthesis of fluorene-alt-carbazole oligomers containing phenylisoquinoline iridium complexes linked through the ancillary ligand **3.5**. Despite good synthetic methodology, the polymers had poor performance when incorporated in OLEDs. They attributed the low electroluminescent quantum efficiencies (0.2 - 0.6%), in a variety of device configurations, to triplet energy back transfer onto the poly fluorene-alt-carbazole chain.^{59,60} An analogous series of polymers with a polyfluorene backbone **3.6** were also synthesized. Reasonable thin film photoluminescent quantum yields ($\Phi_{\text{Ph}} = 10 - 20\%$) were reported, along with modest EQEs (0.5% - 2%). Interestingly, the emissive efficiencies were found to vary significantly depending on whether the iridium complex was incorporated into, or on the end of the polyfluorene backbone.⁸⁵

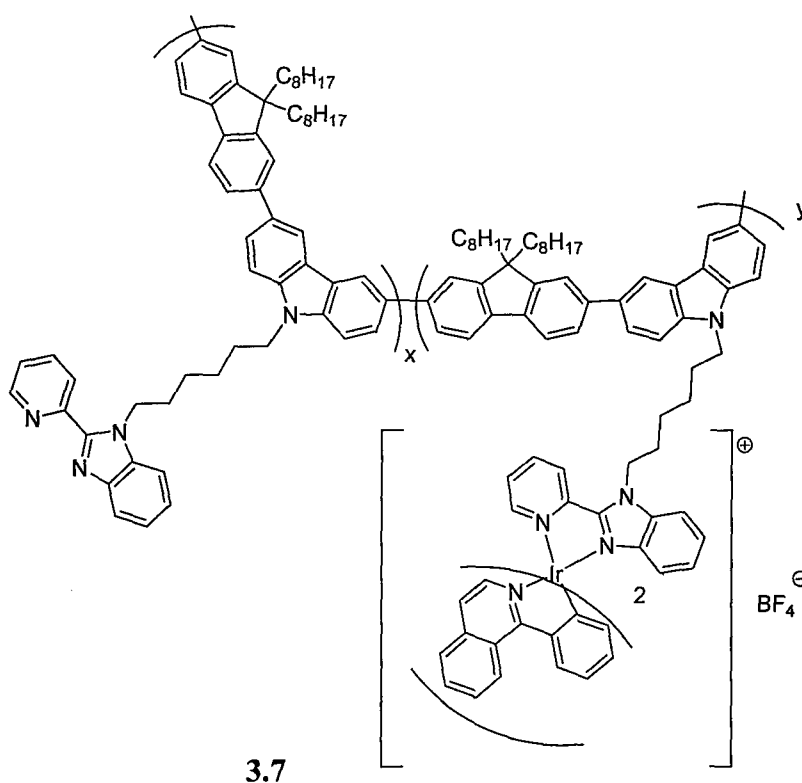


Figure 3.6: Fluorene-alt-carbazole polymer with pendant cationic iridium complexes

A recent report of charged phenylisoquinoline iridium complex containing polymers displayed impressive maximum EQEs of 7.3% with an iridium complex molar loading of 2.6%. A novel synthetic method was used whereby the backbone polymers were synthesized with an ancillary ligand attached to them, which was subsequently complexed by reaction with an iridium μ -chloro bridged dimer. To date, these polymers give the best OLED performance for an iridium phenylisoquinoline complex containing polymer.⁵⁶

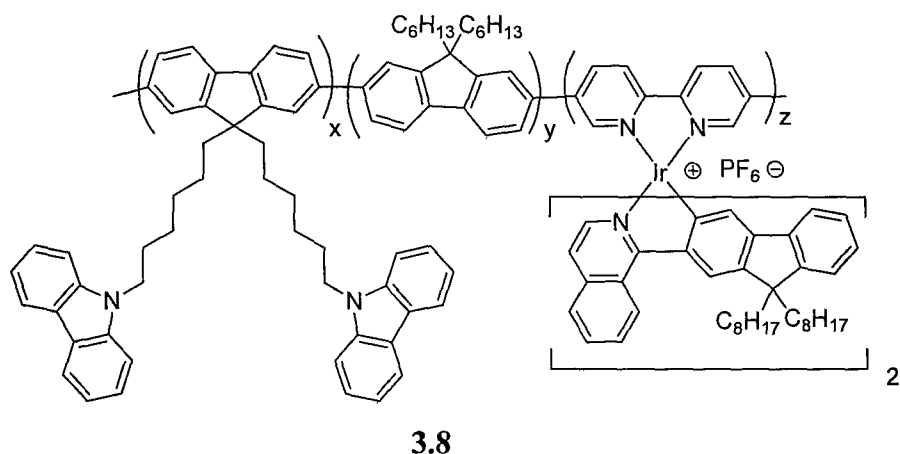


Figure 3.7: Cationic iridium complexes incorporated into polyfluorene containing pendant charge transport units

Workers in the Huang group reported a series of charged phenylisoquinoline iridium complex derivatives incorporated into a polyfluorene backbone. As in the previous example, the complex was attached through the ancillary ligand, except that in this case it is attached in a conjugated fashion as opposed to a tether. Only modest thin film photoluminescence quantum yields were obtained ($\Phi_{\text{Ph}} = 2 - 10\%$) and there were no reported OLED devices.^{57,61}

3.1.3 Importance of energy level matching

Despite the numerous synthetic methods developed to produce metal complex-containing polymers, the measured external efficiencies have not been remarkably high. There has not yet been a significant amount of work demonstrating the best method of attaching the metal complex onto the polymer host. Furthermore, in contrast to the OLEDs based on blended systems, there has not been much consideration of the nature of the polymer used as the backbone, in order to ensure a correct matching of energy levels between the conjugated polymer and the phosphorescent iridium complex. This is extremely important, as the energy levels of the frontier orbitals on the complex must be within those of the polyfluorene chain in order for efficient emission from the complex to occur.

Sandee *et al* reported a series of polyfluorene containing iridium complexes which highlighted the importance of the relative triplet energy levels of the donor and acceptor in order to provide efficient emission. Oligomer **3.09** displayed only modest emission

quantum yields ($\Phi_{\text{Ph}} \sim 1\%$) due to the high triplet energy of the $\text{Ir}(\text{ppy})_2$ moiety. Oligomer **3.10**, however, displayed much higher emission quantum yields ($\Phi_{\text{Ph}} \sim 25\%$), due to more efficient energy transfer from oligomer chain to the iridium complex, and the reduced triplet energy back transfer due to the lower energy triplet excited state of the iridium moiety relative to the oligofluorene chain.³⁹

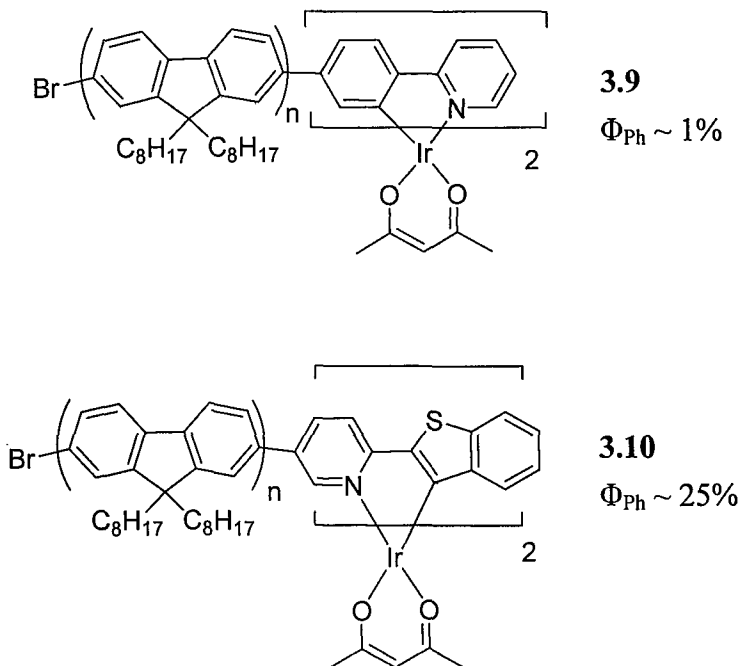


Figure 3.8: Polyfluorenes containing a single iridium complex

Evans *et al* demonstrated improved emission efficiencies in a system where an iridium phosphor is attached through a tether to a polyfluorene chain, suppressing the amount of triplet energy back transfer via Dexter transfer that can occur due to its distance dependency.³⁸ This further demonstrates the importance of considering the relative triplet energies of the donor and the acceptor.

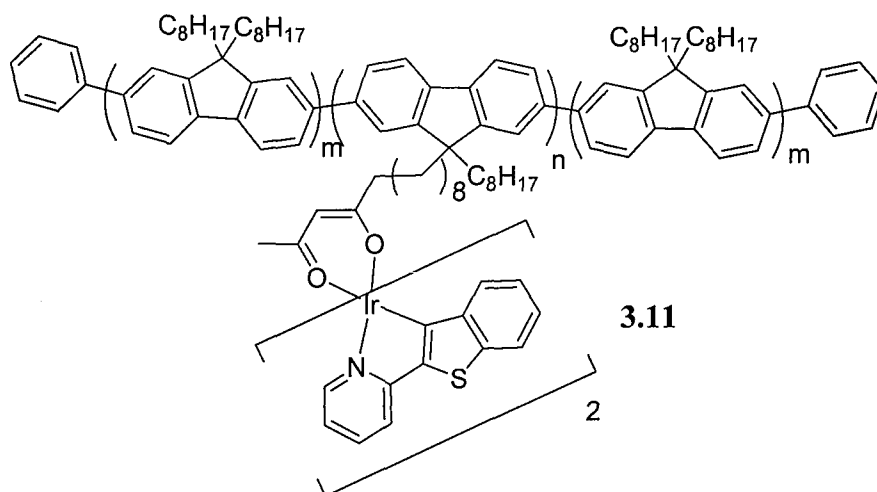


Figure 3.9: Polyfluorene containing a pendant iridium complex

Two recent reports in the literature have attempted to increase the triplet energy level of the polymer backbone in an attempt to improve device efficiencies by reducing triplet energy back transfer.^{86,87} This has been done by using polymers with only a limited amount of conjugation which reduces results in a larger band-gap.

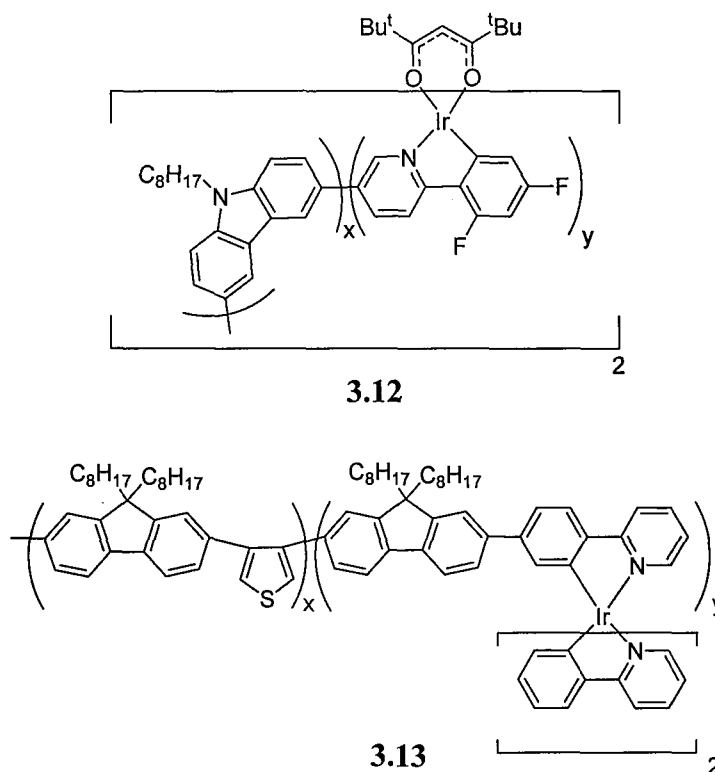


Figure 3.10: High triplet energy polymers containing iridium complexes

Due to the significant variation in the polymer structures, iridium complexes and site of attachment used in the aforementioned studies, it remains extremely difficult to identify the various benefits and drawbacks of incorporating an emissive metal complex into a polymer chain.

3.1.4 Aim of this study

The aim of this study is to synthesize polymeric iridium complexes with a range of conjugated polymers in order to investigate the benefits of these systems. Furthermore, the site of attachment of the polymer chain will be varied in order to elucidate an optimum regiochemistry for these materials.

3.1.5 Materials to be used

In the previous chapter a series of regioisomeric bromine-substituted iridium complexes were synthesized. The following complexes will be used in this study as they provide facile access to polymeric complexes through Suzuki polycondensations.

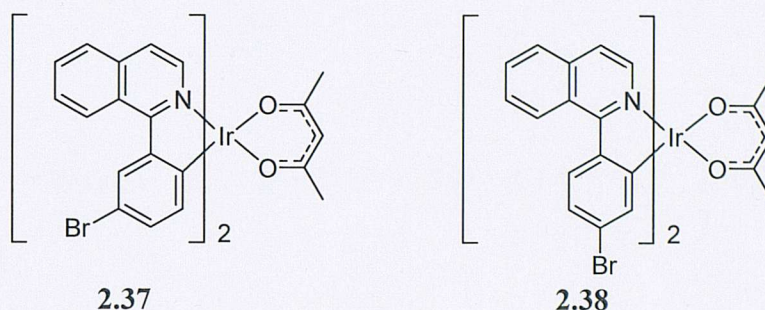


Figure 3.11: Previously synthesized bromo substituted iridium complexes

In order to simplify the system to be investigated, the target polymers will contain only one iridium complex with two polymer chains attached to it, they will be prepared using the protocols developed by Sandee *et al* for related iridium-polyfluorene complexes (Fig. 3.8).³⁹ In order to synthesize the required polymers, an A-B type conjugated monomer needs to be prepared which can subsequently be attached to the iridium complex through a chain extension reaction, as demonstrated in figure 3.12. In this example, by adding 20 equivalents of the A-B monomer, each A-A unit will end up with two polymer chains attached, each with an average length of 10 units.

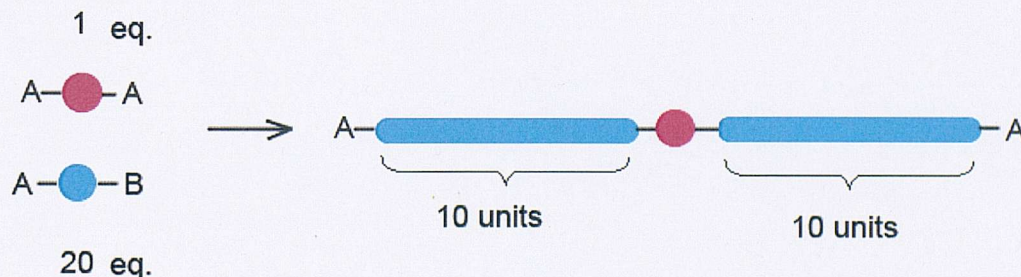


Figure 3.12: Synthetic plan for AB polymerization

The four polymers to be investigated in this study are poly(9,9-dioctylfluorene-2,7-diyl) (PFO), poly(N-octyl-2,7-carbazole) (27PCz), poly(N-octyl-3,6-carbazole) (36PCz) and poly(9,9'-dioctylfluorene-*co*-benzothiadiazole) (F8BT). All four of these polymers, or

related derivatives have been used extensively in OLED preparations and possess attractive photophysical properties.^{86,88-91}

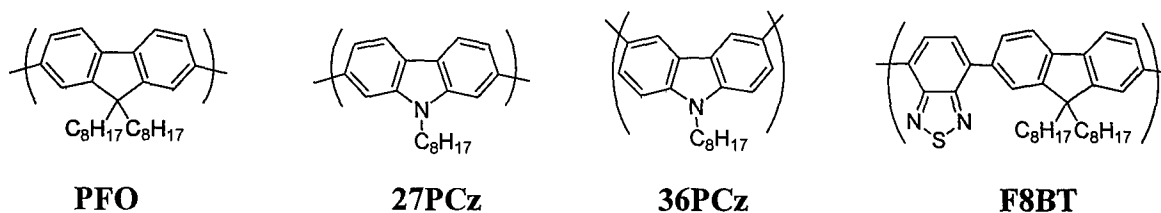
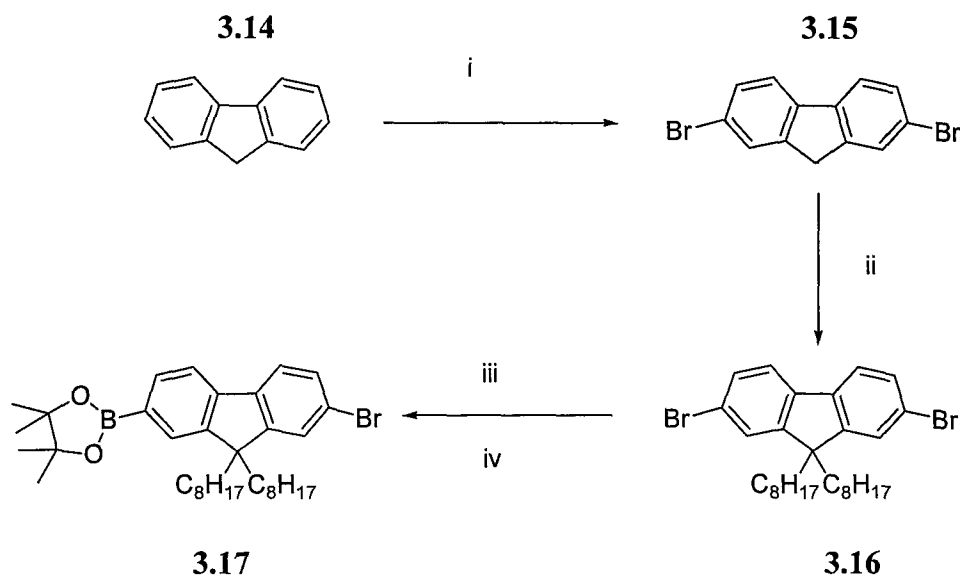


Figure 3.13: Polymers that will be attached to iridium complexes

3.2 Synthesis

3.2.1 Synthesis of AB monomers

3.2.1.1 Synthesis of AB fluorene monomer



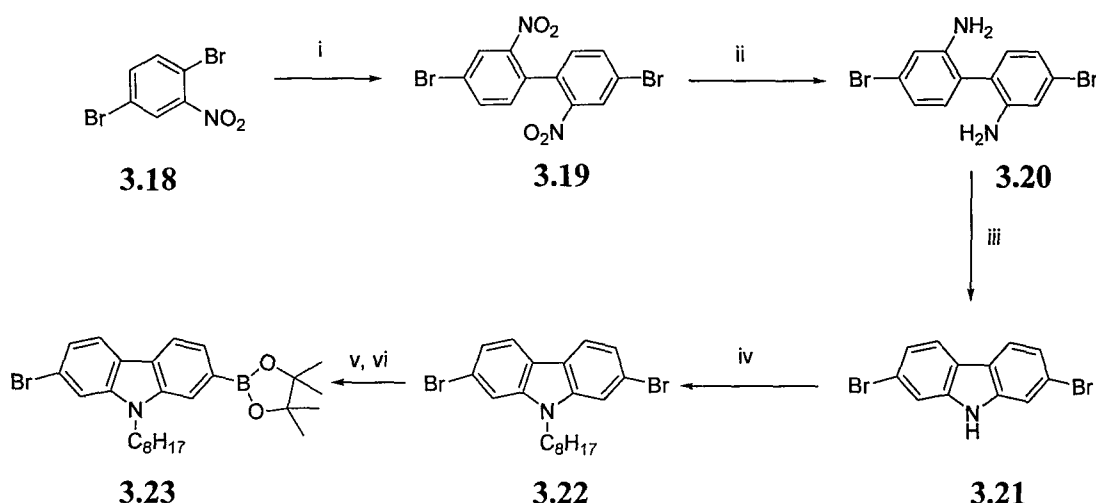
Reagents and conditions: i) Br_2 , I_2 , DCM, $0\text{ }^\circ\text{C}$, 83%; ii) bromooctane, TBAB, $\text{NaOH}_{(\text{aq})}$, Tol, Reflux, 87%, iii) $n\text{BuLi}$, THF, $-78\text{ }^\circ\text{C}$; iv) 2-isopropoxy-4,4',5,5'-tetramethyl-1,3,2-dioxaborolane, $-78\text{ }^\circ\text{C} \rightarrow$ room temperature, 52%

Figure 3.14: Synthesis of an AB fluorene monomer

Synthesis of the AB fluorene monomer **3.17** was achieved using 1 equivalent of *n*-butyl lithium, at $-78\text{ }^\circ\text{C}$, followed by the addition of 2-isopropoxy-4,4',5,5'-tetramethyl-1,3,2-dioxaborolane, in a similar manner to that described by Sandee *et al.*³⁹ The lithiation is not selective for the dibromo substituted fluorene and consequently a distribution of dibromo, mono-bromo mono-borylated and di-borylated fluorene units were observed.

Removal of the undesired species was facile via column chromatography, although a further side-product co-eluted with the desired AB monomer. Analysis of the ^1H NMR spectra revealed that a small amount (2-10%) of 2-(9,9'-dioctyl-9*H*-fluoren-2-yl)-4,4',5,5'-tetramethyl-1,3,2-dioxaborolane **2.41** was present. This species has also been observed by other groups attempting a similar synthesis.⁹² The origin of the dehalogenation was unidentified and could not be avoided despite multiple attempts under varying reaction conditions and reagents. Isolation of pure AB **3.17** monomer was finally achieved through multiple recrystallizations of the mixture and in a moderate yield (52 %).

3.2.1.2 Synthesis of AB 2,7 carbazole monomer



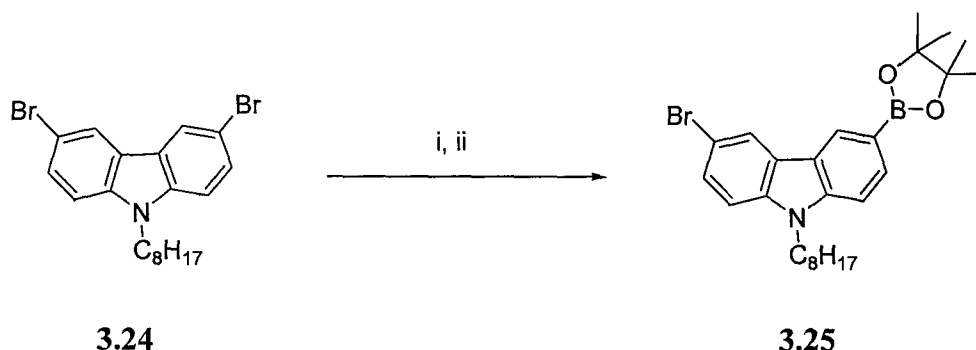
Reagents and conditions: i) Cu, DMF, 125 °C, 98%; ii) Sn, HCl, EtOH, 100 °C, 92%; iii) H_3PO_4 , 200 °C, 85%; iv) bromooctane, K_2CO_3 , DMF, 80 °C, 82%; v) $n\text{BuLi}$, THF, -78 °C; vi) 2-Isopropoxy-4,4,5,5-tetramethyl-1,3,2-dioxaborolane, -78 °C \rightarrow room temperature, 77%

Figure 3.15: Synthesis of an AB 2,7-carbazole monomer

The presence of the nitrogen atom at the bridgehead position in a carbazole molecule directs any attempt at bromination to the 3,6 positions instead of the desired 2,7 positions. Consequently, a multistep synthesis is required in order to synthesize the 2,7 AB carbazole monomer **3.23**. An Ullman coupling selectively homocouples the 2-position of 2,5 dibromo nitrobenzene **3.18**, in high yields (98%). Reduction of the nitro groups using Sn/HCl afforded compound **3.20**, in quantitative yields. Subsequent cyclization, under acidic conditions, affords the more thermodynamically stable 2,7 dibromocarbazole, **3.21**, in moderate yields (85%), as reported by several other groups.³⁹ The alkylation and subsequent mono-borylation reactions were facile and proceeded in good yields, to afford pure 2-bromo-9-octyl-7-(4,4',5,5'-tetramethyl-1,3,2-

dioxaborolan-2-yl)-9*H*-carbazole **3.23** (77%) as verified by ^1H , ^{13}C NMR, mass spectrometry and elemental analysis. In contrast to the AB fluorene unit **3.17**, dehalogenation during the introduction of the boronic ester was not observed.

3.2.1.3 Synthesis of 3,6 Carbazole Monomer



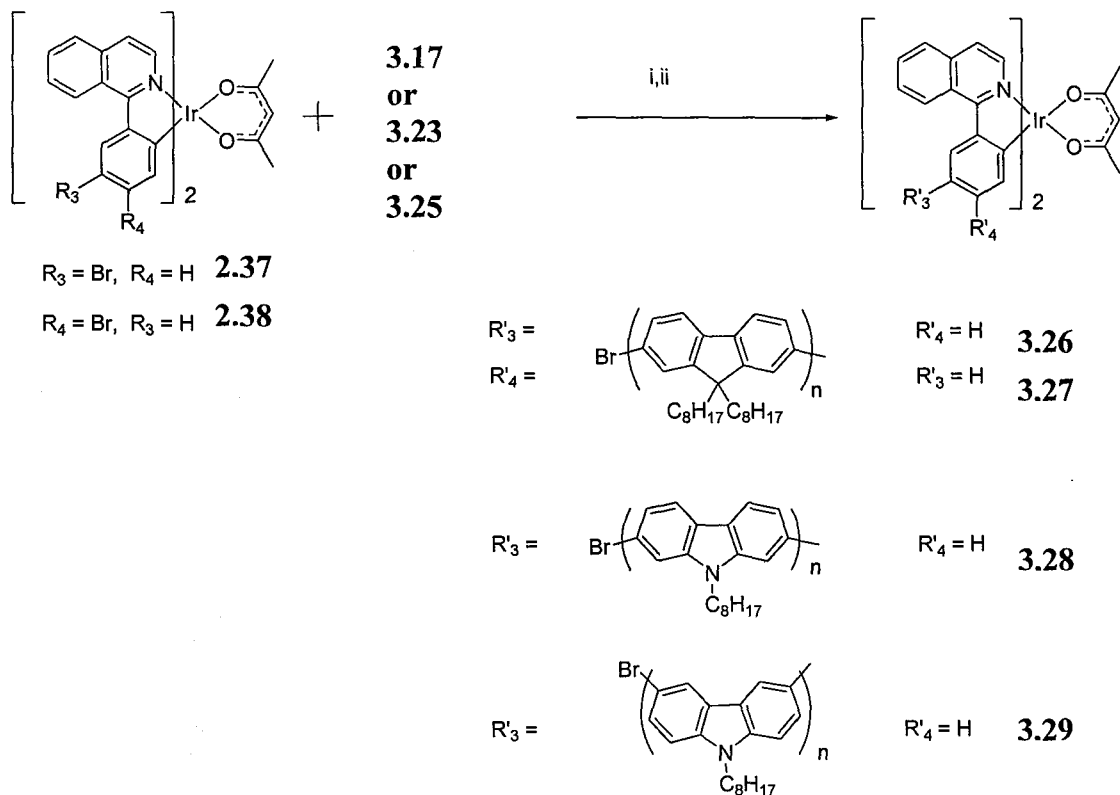
Reagents and conditions: i) $n\text{BuLi}$, THF, $-78\text{ }^\circ\text{C}$; ii) 2-Isopropoxy-4,4,5,5-tetramethyl-1,3,2-dioxaborolane, $-78\text{ }^\circ\text{C} \rightarrow$ room temperature, 68%

Figure 3.16: Synthesis of an AB 3,6-carbazole monomer

Synthesis of the AB 3-bromo-9-octyl-6-(4,4',5,5'-tetramethyl-1,3,2-dioxaborolan-2-yl)-9*H*-carbazole **3.25** monomer was achieved *via* identical conditions to those described above, in good yields. (The 3,6-dibromo-9-octyl-9*H*-carbazole **3.24** was synthesized by Mr Colin Keyworth by direct bromination of the alkyl carbazole). Dehalogenation was also not observed in this case, and the novel AB type monomer was fully characterized by ^1H , ^{13}C NMR, mass spectrometry and elemental analysis.

3.2.2 Synthesis of conjugated iridium complexes by AB polymerizations

Having synthesized a range of AB type monomers, chain extension polymerizations originating from the desired iridium complexes were attempted.



Reagents and conditions: i) Pd(OAc)₂, PCy₃, Tol, TEOAH, 90 °C; ii) acac, Na₂CO₃, Tol, 2-ethoxyethanol, 90°C, 40-60%

Figure 3.17: AB polymerizations

Iridium complexes **2.37** or **2.38** were reacted with 18 equivalents of the required AB monomer, according to the conditions developed by Sandee *et al.*³⁹ This corresponds to a molar feed ratio of iridium complex to monomer of 5%, which is typical for iridium-polymer complexes. The reaction conditions are typical for Suzuki polycondensations and employ a tricyclohexylphosphine (PCy₃) ligand which has been observed to substantially accelerate coupling reactions relative to the more commonly used triphenylphosphine (PPh₃).⁹³ Subsequent to the coupling reactions, the isolated material is heated in the presence of an excess acetyl acetone, under basic conditions, in an analogous manner to that previously reported.³⁹ In this work, the aforementioned procedure was adopted for all polymerizations involving an iridium complex as it was found to impart enhanced solubility and visually improve the aspect of the isolated material. It is not known if the process is necessary for the re-introduction of the ancillary ligand (acac), or whether it merely removes palladium impurities, as the crude isolated materials, in all cases, were too insoluble to characterize by NMR spectroscopy.

All compounds were isolated as red powders, which were purified by multiple precipitations into methanol. The oligofluorenyl iridium complex derivatives **3.26** and

3.27 displayed good solution processability, in contrast to compounds **3.28** and **3.29** which were extremely insoluble.

3.2.2.1 Analysis of the polymers

The novel polymers were analyzed by GPC, NMR spectroscopy, MALDI-TOF mass spectrometry and elemental analysis. The results will be discussed below.

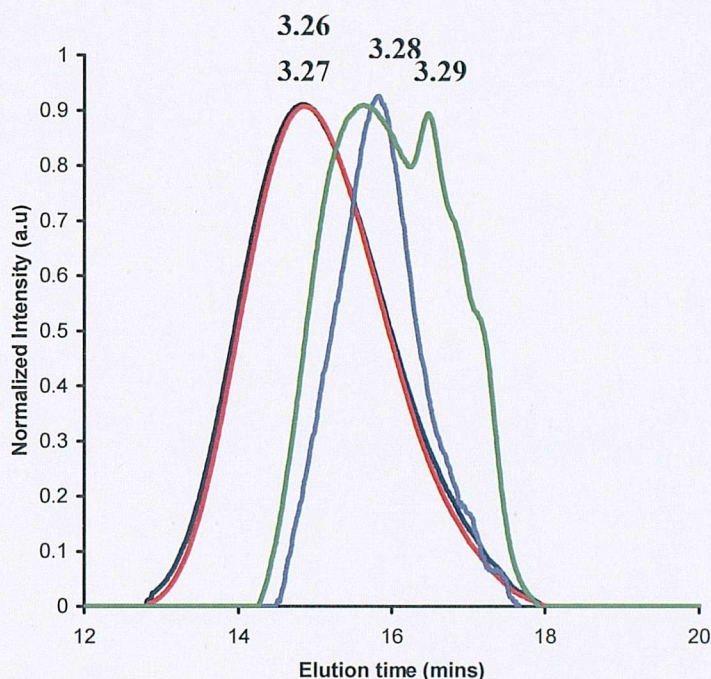


Figure 3.18: GPC(PS) trace of synthesized polymers (PS standards, THF eluent)

Figure 3.18 shows the GPC chromatogram of the synthesized polymers. The molecular weight data obtained from these measurements cannot be considered absolute, as the nature of the synthesized polymers differs greatly from polystyrene (PS) which is used as the calibration standard for the GPC instrument. It has been proposed that for rigid rod polymers, such as polyfluorene, the actual molecular weight (M_n) is approximately half of the value reported by the GPC, when PS standards are used.⁹⁴ However, GPC is still an extremely valuable tool as it allows an indication of the relative lengths of different polymers of the same general type. The two regiosomers **3.26** and **3.27** were polymerized in identical fashions and yielded oligomers with almost identical molecular weights. In contrast, the oligocarbazole derivatives **3.28** and **3.29**, have much longer elution times (i.e lower molecular weights) indicating that the polymerizations did not proceed as effectively as the oligofluorenyl analogues. This is perhaps not unexpected

as the synthesis of high molecular weight polycarbazoles is problematic due to solubility problems.^{88,89}

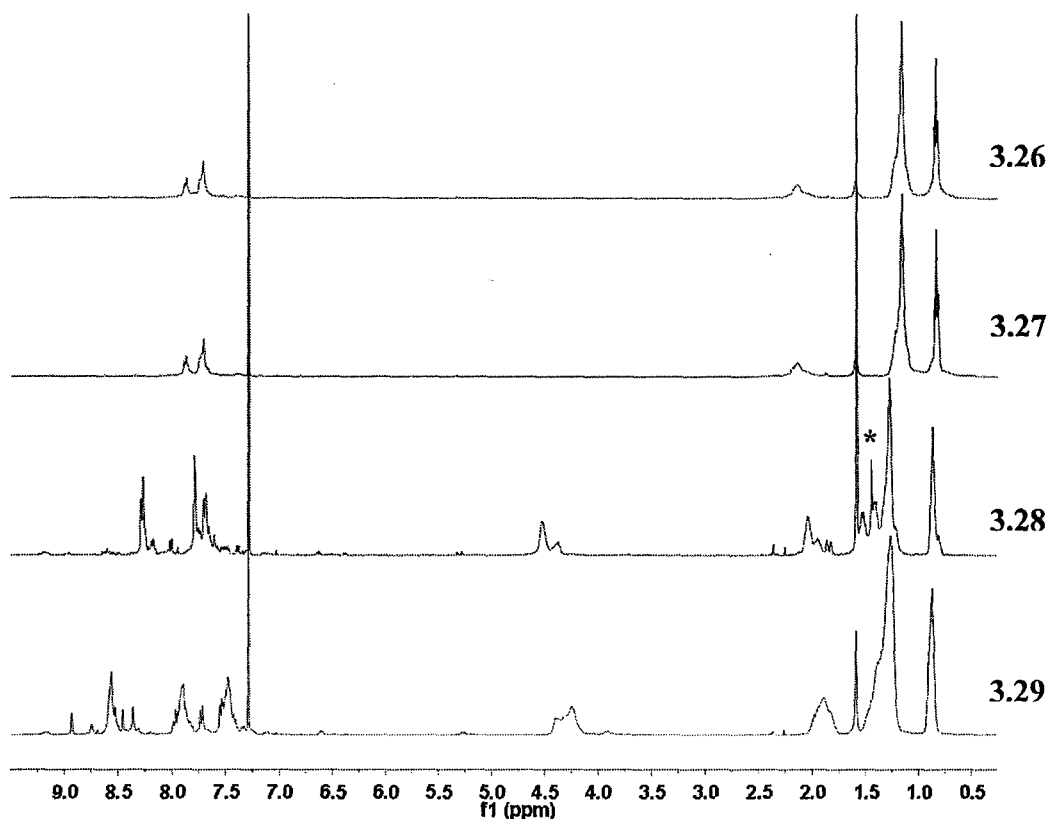


Figure 3.19: ^1H NMR of iridium complex containing polymers

The ^1H NMR spectra of the novel polymers are shown in figure 3.19. The large broad signals in the aromatic region (7.5 - 8.0 ppm for **3.26** and **3.27**; 7.4 - 8.0 and 8.2 - 8.4 ppm for **3.28**; 7.2 - 8.0 and 8.4 - 8.6 ppm for **3.29**) correspond to signals originating from the aromatic protons of the polymer backbone. The resonances at between 0.5 - 2.0 ppm correspond to the alkyl chain protons (and some residual H_2O is visible at 1.56 ppm). The broad peaks at 4 - 4.5 ppm in **3.28** and **3.29** correspond to the protons on the first carbon of the alkyl chain which are deshielded due to their proximity to the N atom of the carbazole unit.

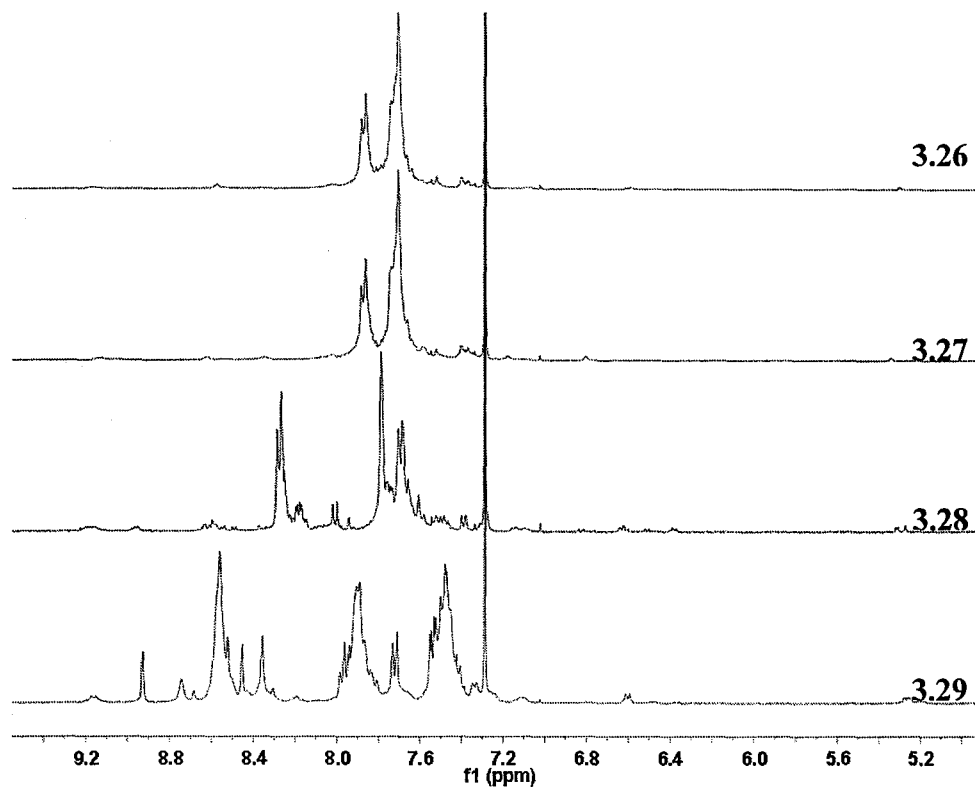


Figure 3.20: Aromatic portion of ^1H NMR of iridium complex containing polymers

On closer inspection (Fig. 3.20) of the aromatic region of the spectrum, it is possible to identify signals originating from the iridium complex. Small peaks can be observed which correspond well with the well defined fluorenyl substituted iridium complexes **2.52** and **2.53** synthesized in chapter 2.

Compound	Yield /%	M_n^a kDa	M_w^a kDa	PDI ^a	Iridium complex molar feed ratio /% ^b	Iridium complex molar incorporation /% ^c	Average chain length / n^c
3.26	55	11.0	21.7	1.96	5	3	15
3.27	58	12.1	21.3	1.76	5	3	15
3.28	40	2.9	3.9	1.36	5	7	7
3.29	46	2.3	3.6	1.57	5	3.5	13

Table 3.1: Analysis of iridium complex containing polymers

a) Determined from GPC, using THF as eluent, and PS standards; b) From reaction stoichiometry; c) Determined from ^1H NMR.

Table 3.1 summarizes the results of the polymerizations performed above. The iridium molar % incorporation was calculated by integration of the H-8 resonance (~9.2 ppm) and comparing it to the alkyl chain resonances (0.8 – 1.5) in the ^1H NMR spectrum. Such analysis of the integrals also yielded an average value of the oligomer chain length (n) attached to each metal complex. The results show that there is preferential Suzuki homo-coupling between 2,7 fluorenyl- or 3,6 carbazole monomers because the % iridium incorporation is lower than what the stoichiometry dictates. This is a phenomenon known as composition drift and will be discussed in the subsequent chapter.

In contrast, the poly 2,7 carbazole iridium derivative **3.28** has a higher iridium complex molar incorporation than the stoichiometry intended and a lower than expected degree of polymerization. This is due to the extremely low solubility of the oligomer chain causing precipitation during the reaction. The low solubility is caused by the presence of only one solubilizing alkyl chain at the bridgehead position of the monomer unit; in contrast to the two octyl chains attached the fluorenyl monomer. This does not occur with 3,6-derivative **3.29** as the polymer is less rigid (the 3,6-linkages confer a significant degree of twisting to the polymer structure) which facilitates solubility. The ^1H NMR spectra (Fig. 3.20) of the 2,7 oligocarbazole iridium complex **3.28** also shows evidence of an unsymmetrical oligomeric species with only one oligomer chain attached to the metal complex. This can be seen by the peaks at ~8.9 ppm, which correspond to the H-8 protons on a ligand with a bromine atom attached. These are assigned by analogy to the ^1H NMR spectra of asymmetric complexes that will be presented in Chapter 5. Problems associated with the solubility of carbazole derivatives are often encountered and the obtained molecular weights for these compounds are similar to those found by other groups working with poly(2,7-carbazole).⁸⁸

In the case of the 3,6-carbazole oligomer **3.29**, this solubility problem is not encountered due to the more flexible backbone. Consequently, there is only a negligible amount of the unsymmetrical oligomeric iridium complex. The singlet peak observed at ~8.9 ppm is not believed to originate from an unsymmetrical complex due to the absence of the other peaks corresponding to this moiety (~6.9 and 6.4 ppm). Instead, this peak is assigned to the first carbazole unit attached to the iridium complex, such an assignment is in agreement with the integration. The lower molecular M_n , by GPC, of the oligo 3,6-carbazole derivative, **3.29**, compared to the oligo 2,7-carbazole material,

3.28, is probably due to the greater flexibility of the backbone of the former oligomer. Thus, a lower M_n is observed by GPC (**3.29** is less rigid rod like than **3.28**) despite there being a higher degree of polymerization, according to NMR spectroscopy.

3.2.2.2 End group analysis

Polymers **3.26-3.29** were analyzed by MALDI-TOF mass spectrometry, using a dithranol matrix, in order to further investigate the composition. In all cases, only peaks corresponding to oligomers that did *not* contain incorporated iridium complexes were observed. This implies that the analytical method used is not suitable for the direct observation of polymer-iridium complexes. However, the presence of oligomeric chains not attached to a complex implies that estimate value for the average chain length (n) is likely to be an overestimate due to the fact it is derived from the assumption that all polymeric material is attached to a complex.

Polymers **3.26** and **3.27** displayed several series of peaks corresponding to either di-H terminated or α -H- ω -Br oligofluorenes, 4 - 12 repeat units long. This implies that any unreacted boronic ester groups are completely hydrolyzed by the end of the reaction, and may also explain the reason for the non-complete incorporation of iridium complex into the polymer. The presence of some di-H terminated oligofluorenes indicates that dehalogenation is also occurring during the reaction conditions. Both of these phenomena have been observed previously in polyfluorene synthesis via Suzuki coupling.⁹⁵ It is reasonable to assume that the polymers containing iridium complexes (that are not visible by MALDI-TOF mass spectrometry) will also contain a mixture of -H and -Br termini.

Polymer **3.28** displayed several series' of peaks corresponding to free α -boronic ester- ω -(H or Br) oligomer chains. The residual boronic ester groups can be seen in the ^1H NMR and are indicated with an asterisk (Fig. 3.19). Oligo 2,7-carbazole peaks were observed up to 13 repeat units.

Polymer **3.29** only displayed a small number peaks corresponding to di-H terminated 3,6-carbazole oligomers indicating that hydrolysis of the unreacted boronic ester groups is complete, and that significant dehalogenation is occurring.

3.2.3 Synthesis of polymer complexes by a macromonomer approach

Synthesis of an AB type F8BT monomer was not possible despite multiple attempts. Consequently, it was decided to adopt a strategy whereby the polymer chain would be synthesized first and then attached to the iridium phosphor.

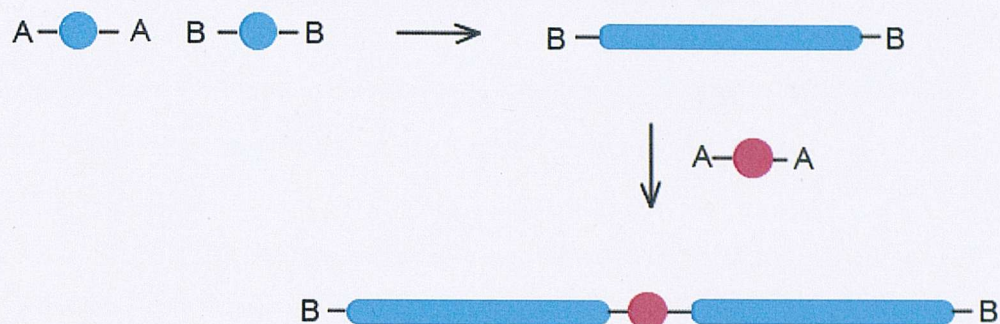
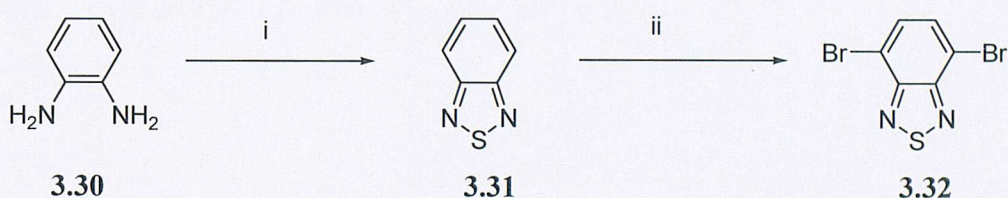


Figure 3.21: Synthetic plan for synthesis of iridium complex containing F8BT polymer

In order for this strategy to be used, an A-A + B-B type polymerization of the F8BT oligomer would first be performed, and a second Suzuki coupling reaction would be used to attach the macromonomer onto the metal complex.

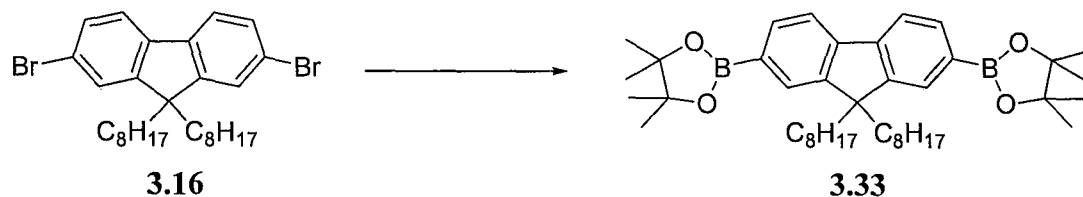
3.2.3.1 Synthesis of F8BT monomers



Reagents and conditions: i) SOCl_2 , H_2SO_4 , Reflux, 95%; ii) Br_2 , $\text{HBr}_{(\text{aq})}$, Reflux, 64%

Figure 3.22: Synthesis of benzothiadiazole A-A monomer

The synthesis of the bromo substituted benzothiadiazole moiety was achieved by refluxing 1,2 phenyl diamine 3.30 in thionyl chloride, followed by bromination as described in the literature.^{96,97} Both reactions proceeded in pleasing yields (95%, 64%).



Reagents and conditions: i) $nBuLi$, THF, $-78\text{ }^\circ\text{C}$; ii) 2-Isopropoxy-4,4,5,5-tetramethyl-1,3,2-dioxaborolane, $-78\text{ }^\circ\text{C} \rightarrow$ room temperature, 81%

Figure 3.23: Synthesis of fluorene B-B monomer

The synthesis of **3.33** was achieved using conditions described in the literature,³⁸ which afforded the product as white crystals in good yield (81%)

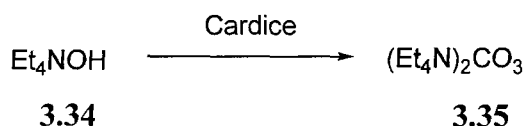
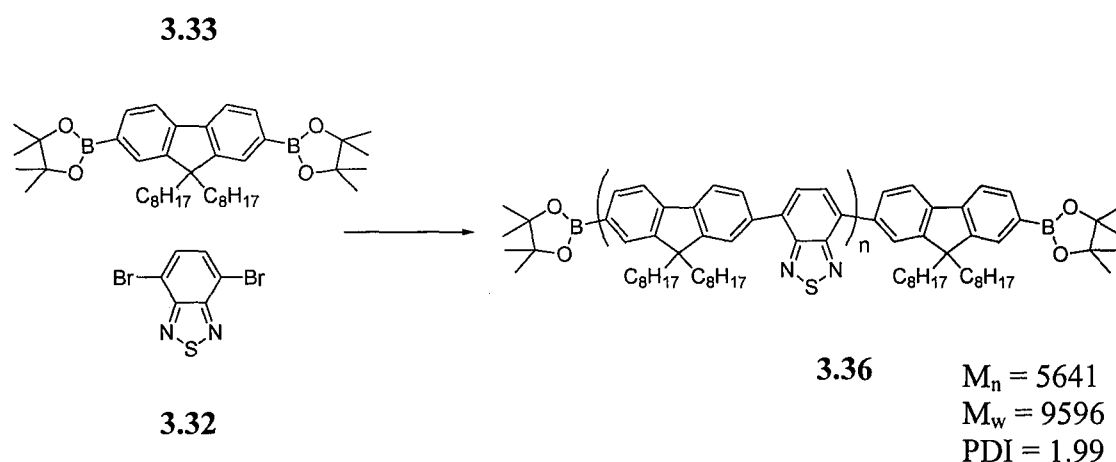


Figure 3.24: Synthesis of bis(tetraethylammonium)carbonate

The synthesis of F8BT, as described in the literature, utilizes an uncommon base (**3.35**) in the Suzuki polycondensation.⁹⁸ It was decided to synthesise and employ bis(tetraethylammonium)carbonate, **3.35**, as other groups have reported excellent results when using this base for the synthesis of F8BT. The base was prepared by the addition of cardice to an aqueous solution of tetraethyl ammonium hydroxide **3.34**, followed by concentration *in vacuo* to afford the desired compound **3.35**.⁹⁹



Reagents and conditions: $Pd(PPh_3)_4$, TEAC, THF, Tol, Reflux, 61%

Figure 3.25: Synthesis of F8BT polymer

In order to control the chain length of the synthesized F8BT oligomer, **3.36**, and to ensure that both termini are end-capped by boronic ester substituted fluorene units, 1.2 equivalents of **3.33** were reacted with 1 equivalent of the bromo substituted benzothiadiazole **3.32**. The F8BT oligomer **3.36** was isolated as yellow fibers, in good

yield (61%). Assuming both chain ends are terminated by boronic esters, integration of the ^1H NMR spectrum (Fig. 3.29) determined the chain length (n) to be approximately 8 units.

The GPC chromatogram is shown in Fig. 3.28. A clear ascension of peaks can be observed which correspond to an increasing number of repeat units in the polymer.

End group analysis of the F8BT macromonomer by MALDI-TOF mass spectrometry (Fig 3.26) shows a major series of peaks that correspond to the desired product containing two boronic ester groups. Due to the lower propensity of heavier molecular weight oligomers to “fly” in mass spectrometry, this method cannot be used to estimate the average chain length. A smaller series of peaks can be seen at lower molecular weights which correspond to a α -H- ω -boronic ester terminated F8BT oligomer.

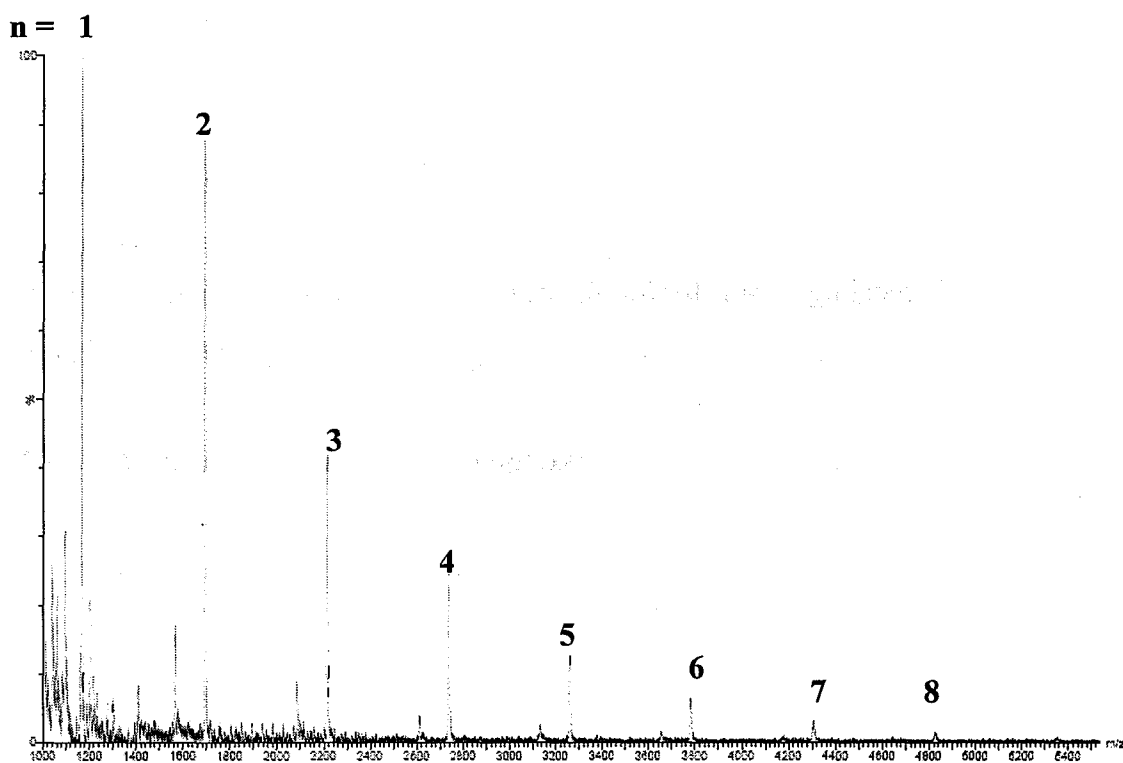
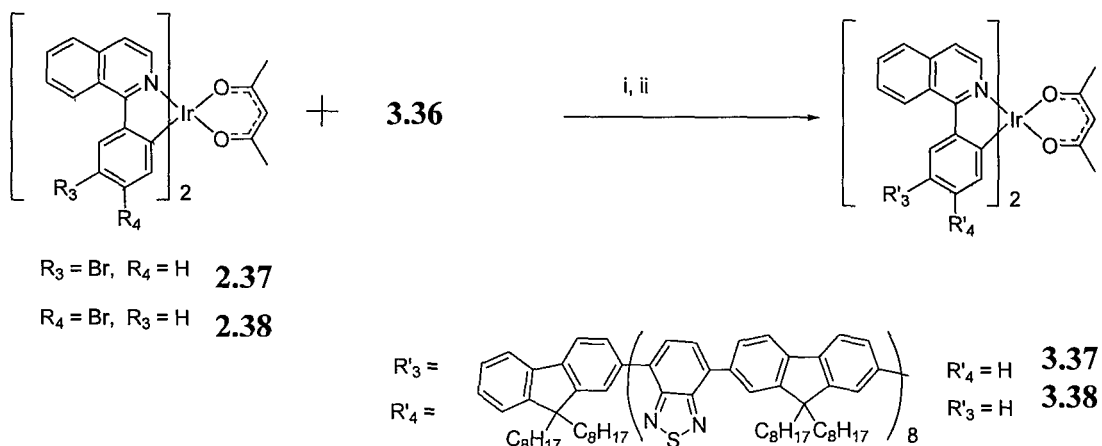


Figure 3.26: MALDI-TOF mass spectrum of F8BT polymer (n = repeat units)

3.2.3.2 Synthesis of conjugated iridium complexes via the macromonomer approach



Reagents and conditions: i) $\text{Pd}(\text{OAc})_2$, PCy_3 , Tol, TEAOH, 90°C ; ii) acac, Na_2CO_3 , Tol, 2-ethoxyethanol, 90°C , ~70%

Figure 3.27: Synthesis of iridium complex containing polymer via macromonomer approach

The F8BT iridium complexes were synthesized by reaction of 2.5 equivalents of **3.36** with 1 equivalent of the iridium complex, **2.37** or **2.38**. The reason for the slight excess of the macromonomer was to minimize the possibility of an A-A + B-B type polymerization occurring which would yield more than one iridium complex per chain (see Chapter 4). Excess, unreacted macromonomer was removed by washing the isolated yellow powders with hexane, to afford the regioisomeric F8BT-iridium complexes, **3.37** and **3.38**.

3.2.3.3 Analysis of the polymer complexes

The GPC trace of the starting macromonomer **3.36**, and the resulting products **3.37** and **3.38** are shown below. As anticipated, the molecular weights for **3.37** and **3.38** are almost double that of **3.36**, indicating the success of this methodology.

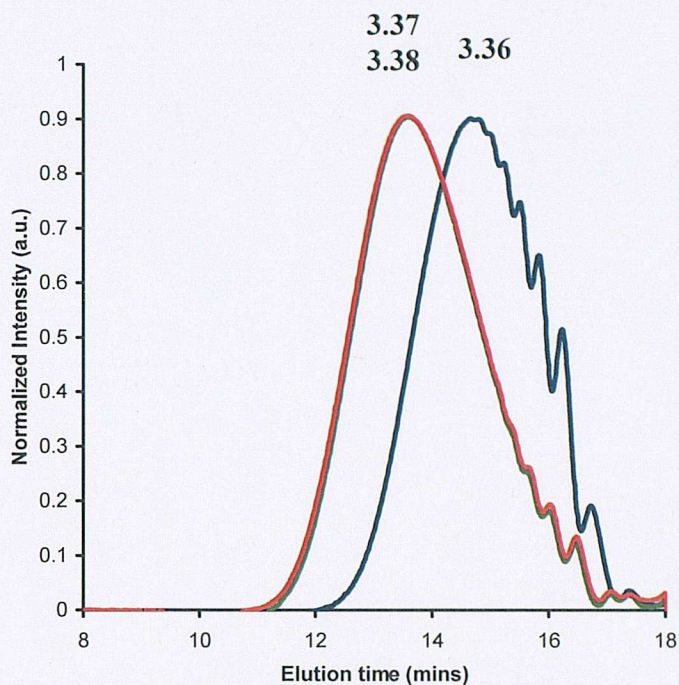


Figure 3.28: GPC trace of F8BT polymers (PS standards, THF eluent)

Compound	M_n 3.36 ^a	Yield / %	M_n ^a	M_w ^a	PDI ^a	Feed ratio / % ^b	Incorporation ratio / % ^c
3.37	5641	72	12205	27175	2.23	5	4
3.38	5641	69	12975	28499	2.20	5	4

Table 3.2: Analysis of F8BT polymers

a) Determined from GPC, using THF as eluent, and PS standards; b) From reaction stoichiometry; c) Determined from ^1H NMR.

The ^1H NMR spectra (Fig. 3.29) reveal the absence of boronic ester termini (~ 1.4 ppm), indicating that hydrolysis of the end groups occurred during the reaction, a phenomenon that is commonly observed for related complexes.^{95,100,101} The iridium complex molar incorporation ratio was estimated by integration of the H-8 peaks (~ 9.2 ppm) and comparison to those originating from the alkyl chains (0.5 – 1.4 ppm).

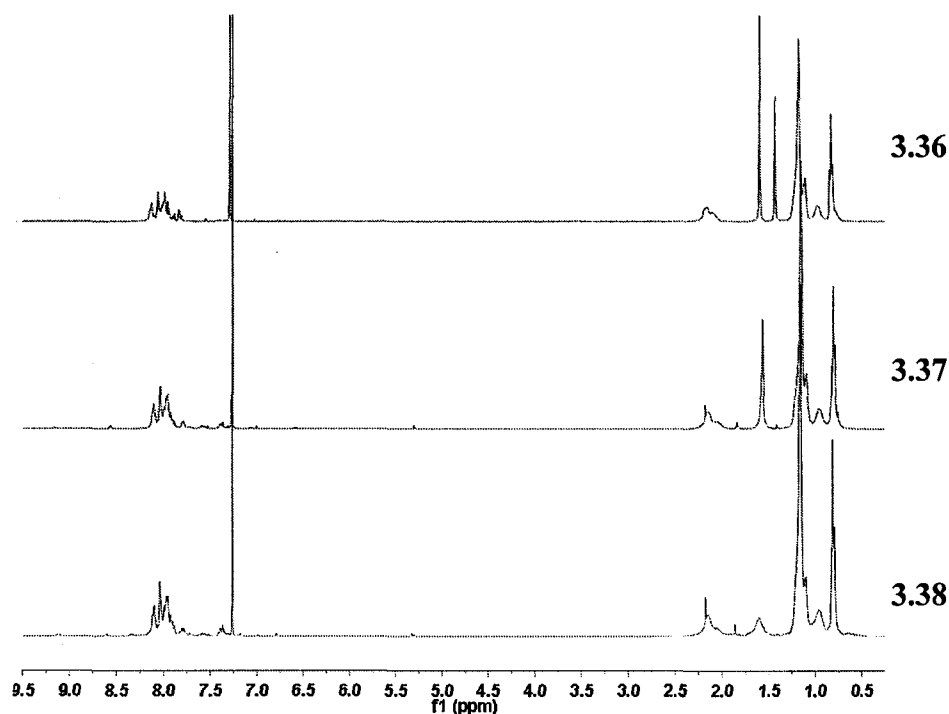


Figure 3.29: ^1H NMR spectra of F8BT polymers

A close up of the aromatic section of the ^1H NMR spectra is shown below (Fig. 3.30). The presence of the H-8 peaks (at ~ 9.2 ppm in both cases) confirms the presence of the complex, and its chemical shift implies that the complex is covalently bound to the oligomer. This is assigned by analogy to the well defined complexes synthesized in the previous chapter, which displayed an increase in chemical shift on going from a bromine substituent (~ 8.9 ppm) to a fluorenyl group (~ 9.2 ppm).

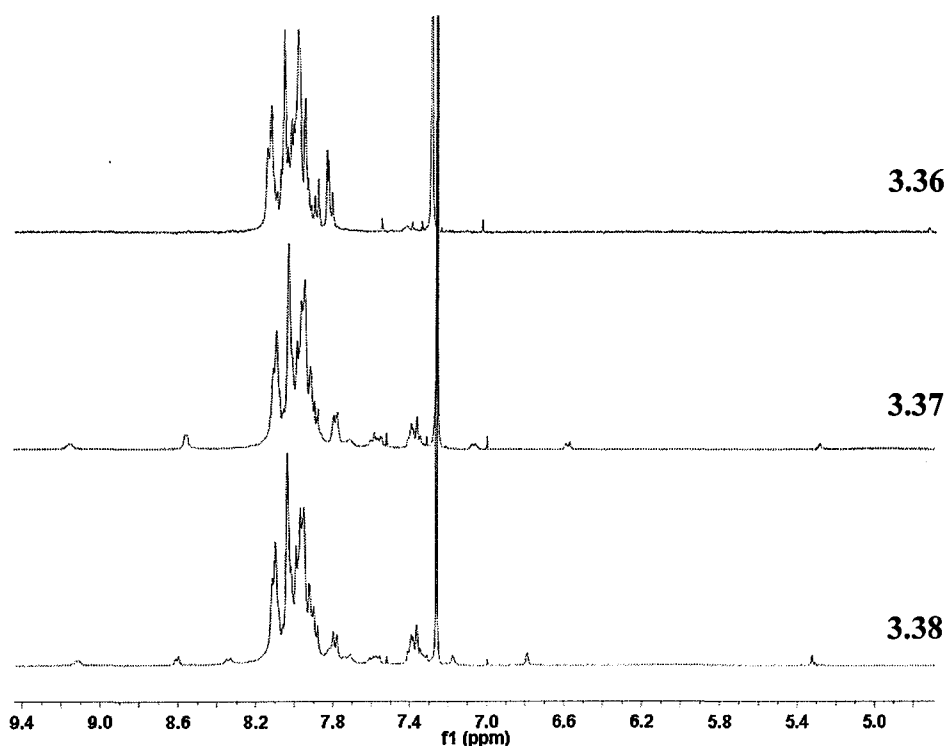


Figure 3.30: Aromatic section of ^1H NMR spectra of F8BT polymers

3.2.3.4 End group analysis

Polymers **3.37** and **3.38** were analyzed by MALDI-TOF mass spectrometry. As seen previously (Section 3.2.2.2) the only observable signals originated from oligomers lacking any iridium complexes. Di-H terminated F8BT oligomers, with repeat units ranging from 1-5, were observed in both cases, indicating that hydrolysis of the boronic ester end groups had occurred, as also indicated by ^1H NMR spectroscopy. The presence of unattached F8BT oligomers explains why a lower than expected iridium molar % incorporation was obtained.

3.3 Photophysical properties

3.3.1 UV-Vis absorption

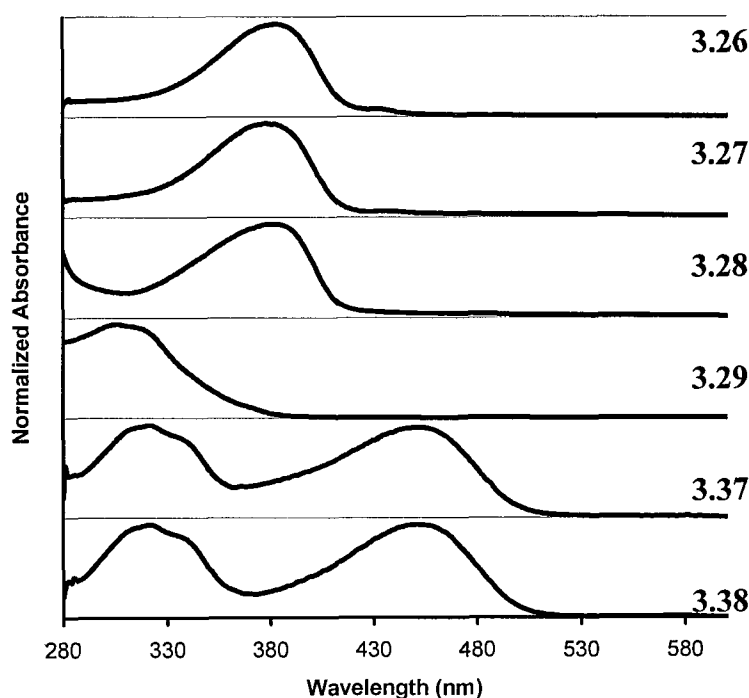


Figure 3.31: UV-Vis absorption spectra of iridium complex containing polymers (DCM, $\sim 10^{-5}\text{M}$)

Fig 3.31 shows the solution UV-VIS absorption spectra of the new polymers. In every case, the only visible absorptions are those corresponding to $\pi\text{-}\pi^*$ transitions of the conjugated backbone. This is unsurprising as the molar incorporation of the iridium complex in every case is low, and consequently its transitions are masked by those of the bulk material. Oligomers **3.26** - **3.28** display identical absorption maxima, at ~ 375 nm. A small red-shifted feature is visible in the polyfluorene derivatives **3.26** and **3.27**, at ~ 430 nm. This is probably due to aggregation of some of the polyfluorene chains in solution.¹⁰² This feature is not present in the 2,7 carbazole derivative **3.28**, which may be due to the shorter chain length lessening the extent of any aggregation. The

absorption maxima of the oligo 3,6 carbazole derivative, **3.29**, is at a significantly higher energy (~ 300 nm). This is due to the lack of conjugation through the carbazole moiety leading to a larger energy gap. There are two main features present in the F8BT derivatives **3.37** and **3.38**. The higher energy feature (~ 330 nm) corresponds to absorption of the fluorene part of the F8BT chain, whilst the lower energy feature (~ 450 nm) corresponds to absorption of the benzothiadiazole portion of the chain.

3.3.2 Photoluminescence

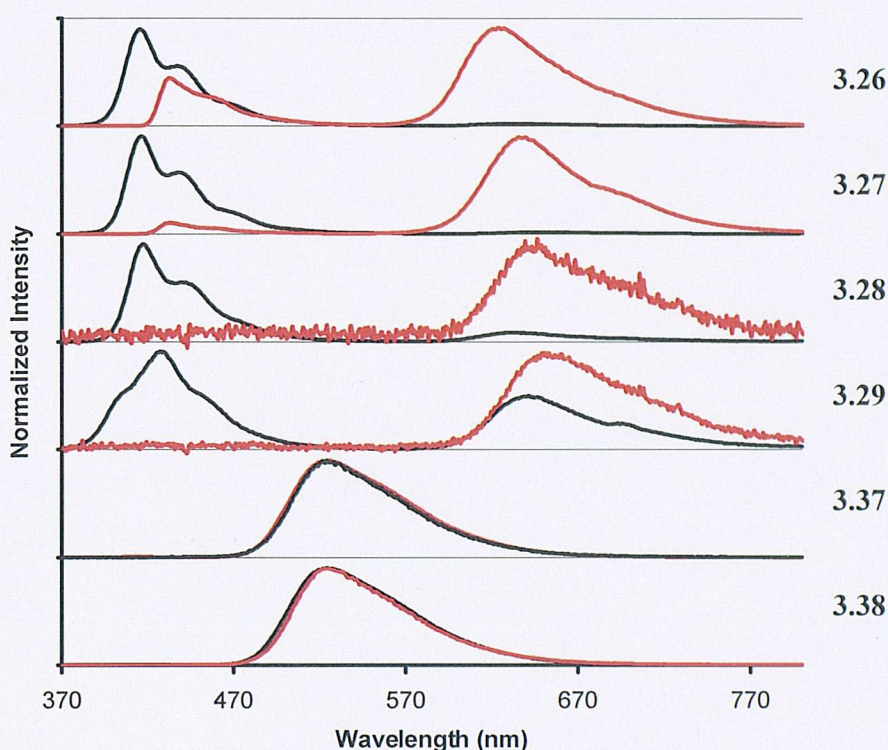


Figure 3.32: Solution (black) and thin film (red) photoluminescence spectra of polymers (Soln: DCM, Max. Abs. ~ 0.1 , 350 nm excitation; Film: 375 nm excitation)

Figure 3.32 shows the solution (black) and thin film (red) photoluminescence spectra of the synthesised polymers. The solution photoluminescence spectra of all the compounds are dominated by emission from the oligomer backbone. In the case of the polyfluorene, and polycarbazole derivatives, **3.26-3.29**, strong blue emission is observed that corresponds very well with previously reported emission maxima for the corresponding polymer backbones. The F8BT derivatives, **3.37** and **3.38**, display yellow/green emission, also corresponding to emission from the F8BT main chain, however, the intensity is extremely weak. Compounds **3.26-3.29** also displayed red emission originating from the iridium complex. For both the oligofluorene, **3.26** and **3.27**, and the oligo 2,7 carbazole, **3.28**, derivatives only a small fraction of red emission was observed

($\Phi_{\text{Ph}} < 1\%$). This is due to incomplete energy transfer from the oligomer chain onto the iridium phosphor. However, in the case of the oligomer **3.29**, a significant proportion of the total emission originated from the iridium complex ($\Phi_{\text{Ph}} = 9\%$). It is possible that due to the more twisted nature of the oligomer chain, a larger amount of energy transfer can occur from polymer-iridium as a greater proportion of the chain is in close proximity to the emissive centre. In the case of the oligo F8BT iridium compounds, **3.37** and **3.38**, there was no emission from the iridium complex.

In the thin films, the molecules are in greater proximity to one another, and consequently, energy transfer from the oligomers to the iridium complexes can occur in an intra- or intermolecular fashion. This typically results in a significantly increased proportion of emission from the iridium complex.^{38,39} In the case of the oligofluorene containing materials **3.26** and **3.27**, a small amount of residual polymer emission is visible. However, the dominant emission now originates from the iridium complex, indicating the efficient transfer of excitons from the oligofluorene chain onto the emissive phosphor. The residual oligofluorene emission is red-shifted, which indicates the presence of aggregation in the thin film.³⁶ It is interesting to note that the two emission maxima of the iridium complexes in the thin film are slightly blue-shifted relative to their emission in solution. This is possibly the result of the aggregation of the oligofluorene chains, reducing the amount of orbital overlap between the iridium complex orbitals and the oligofluorene chain. Pleasingly, the emission of compound **3.27** is red-shifted relative to **3.26**, as was observed in the previous chapter for the well-defined small molecule complexes. Furthermore, the 1,3 oligofluorene substituted iridium complex **3.26** displayed a similar enhanced quantum yield ($\Phi_{\text{Ph}} = 20\%$) relative to the 1,4 oligofluorene substituted complex **3.27** ($\Phi_{\text{Ph}} = 10\%$), indicating that the trends observed in the previous chapter are maintained in the polymeric analogues.

There is no residual polymer emission in the oligo 2,7 carbazole iridium compound **3.28**. This is likely to be due to the increased mol % of iridium present in this compound, caused by the shorter chain length. The phosphorescence emission maxima of both the oligocarbazole compounds, **3.28** and **3.29**, are red-shifted relative to the solution measurements. This is often seen and is the result of aggregation of the emissive units causing an increase in orbital overlap, and a reduction of the energy gap.^{40,58,103} The emission of **3.29** is red-shifted relative to **3.28**, which is likely to be due to mesomerically donating properties of the N atom which can increase the level of the

HOMO leading to a red-shift in emission. The quantum yield (Φ_{Ph}) of **3.28** is 20%, which is identical to that of its oligofluorene analogue **3.26**. However, in the case of the oligo 3,6 carbazole derivative **3.29**, the quantum yield is significantly higher ($\Phi_{\text{Ph}} = 35\%$). In the case of the F8BT-iridium complexes **3.37** and **3.38**, only very weak emission originating from the F8BT chain was observed, as was the case in solution. No emission from the iridium phosphor was observed, and an explanation for this will be outlined below.

Solution			
Compound	Fluorescence emission max./ nm	Phosphorescence emission max./ nm	Phosphorescence Quantum Yield (Φ_{Ph}) /% ^a
3.26	417	635	< 1
3.27	417	650	< 1
3.28	417	635	< 1
3.29	429	643	9
3.37	524 (v. weak)	N/A	N/A
3.38	524 (v. weak)	N/A	N/A

Table 3.3: Solution photoluminescent data for iridium complex containing polymers
 a) measured in degassed DCM solution, using $[\text{Ir}(\text{Piq})_2(\text{acac})]$ as standard, $\Phi_{\text{Ph}} = 20\%$, Excitation wavelength = 350 nm.

Thin Film			
Compound	Fluorescence emission max./ nm	Phosphorescence emission max./ nm	Phosphorescence Quantum Yield (Φ_{Ph}) /% ^a
3.26	434	624	20
3.27	434	639	10
3.28	N/A	643	20
3.29	N/A	653	35
3.37	524 (v. weak)	N/A	N/A
3.38	524 (v. weak)	N/A	N/A

Table 3.4: Thin film photoluminescent data for iridium complex containing polymers
 a) measured using an integrating sphere

3.3.3 Energy Levels of Polymers.

In order to explain the significant differences observed in the quantum efficiencies of these compounds, the energy levels of the frontier orbitals were investigated by cyclic voltammetry.

Compound	$E_{\text{onset}}^{\text{Ox}}$ /V ^a	E_{HOMO} /eV ^b	ΔE /eV ^c	E_{LUMO} /eV ^d
3.26	0.92	-5.72	2.94	-2.78
3.27	0.92	-5.72	2.94	-2.78
3.28	0.92	-5.72	2.94	-2.78
3.29	0.98	-5.78	3.23	-2.55
3.37	0.77	-5.57	2.38	-3.19
3.38	0.77	-5.57	2.38	-3.19

Table 3.5: Electrochemical data for synthesized polymers

a) Measured from solution (DCM) CV using Fc as an internal standard. b) Calculated using $E_{\text{HOMO}}(\text{eV}) = -(E_{\text{onset}}^{\text{Ox}}(\text{V}) + 4.8)$ c) Estimated from UV-Vis spectrum absorption onset. d) $E_{\text{LUMO}} = E_{\text{HOMO}} + \Delta E$

The oxidation potential (HOMO, see chapter 1) of the materials was measured by cyclic voltammetry, under identical conditions to those described in the previous chapter. All polymers displayed irreversible single electron oxidations. In contrast to the previous chapter, the onset of the oxidation wave was used to calculate the oxidation potential, as the oligomers contain a variety of different chain lengths which could lead to a variety of different potentials. This is a commonly used practice for the measurement of oxidation potentials of polymers.¹⁰⁴⁻¹⁰⁶ The energy level of the HOMO was calculated using the equation $E_{\text{HOMO}} = -(E_{\text{onset}}^{\text{Ox}} + 4.8)$, as the method used in the previous chapter has not been validated for polymeric materials.^{107,108} No reduction peaks were observed within the cathodic limit, and the UV-Vis absorption onset was summed to the oxidation potential, in an estimate of the LUMO energy. The experimentally measured values for these compounds correspond to the energies for the frontier orbitals of the oligomer chain, as it is the bulk of the material. The actual HOMO and LUMOs of the compounds are those corresponding to the emissive red phosphor, although these are

not visible by cyclic voltammetry due to the low percentage incorporation of iridium in the materials. According to the experimentally measured energy levels (Fig. 3.33), it can clearly be seen that the 3,6 carbazole derivative **3.29** has the biggest energy gap (3.23 eV), followed by the oligofluorene **3.26-3.27**, and oligo 2,7 carbazole **3.28** compounds (2.94 eV), and finally the iridium complex-F8BT molecules **3.37-3.38** have the smallest energy gap (2.38 eV). The measured energy gap corresponds to the absorption transition from the ground state to produce a singlet excited state.

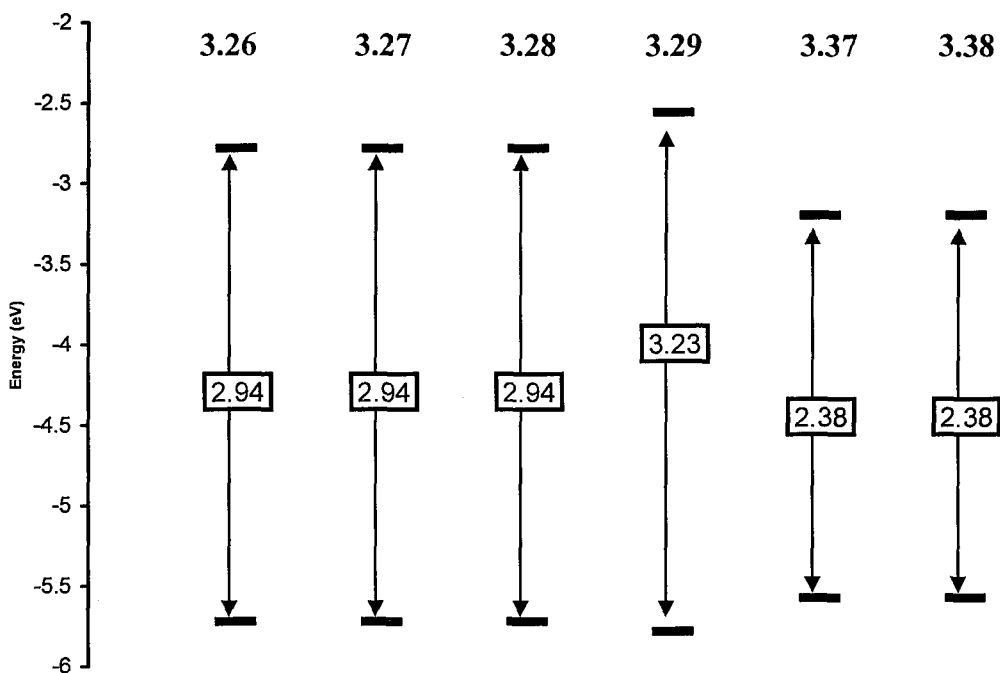


Figure 3.33: Energy level diagram of polymers

3.3.4 Discussion of the emission properties of the polymer-iridium complexes

As mentioned previously (see introduction): Under photoexcitation an exciton generated on a host type material has to be transferred onto the emissive phosphor guest. In materials where a conjugated polymer is attached to an emissive complex, the polymer portion acts as the host (due to its larger concentration) and the attached complex functions as the guest. The fate of this exciton determines the photoluminescence quantum efficiency. In order to demonstrate this, the following three examples will be considered.

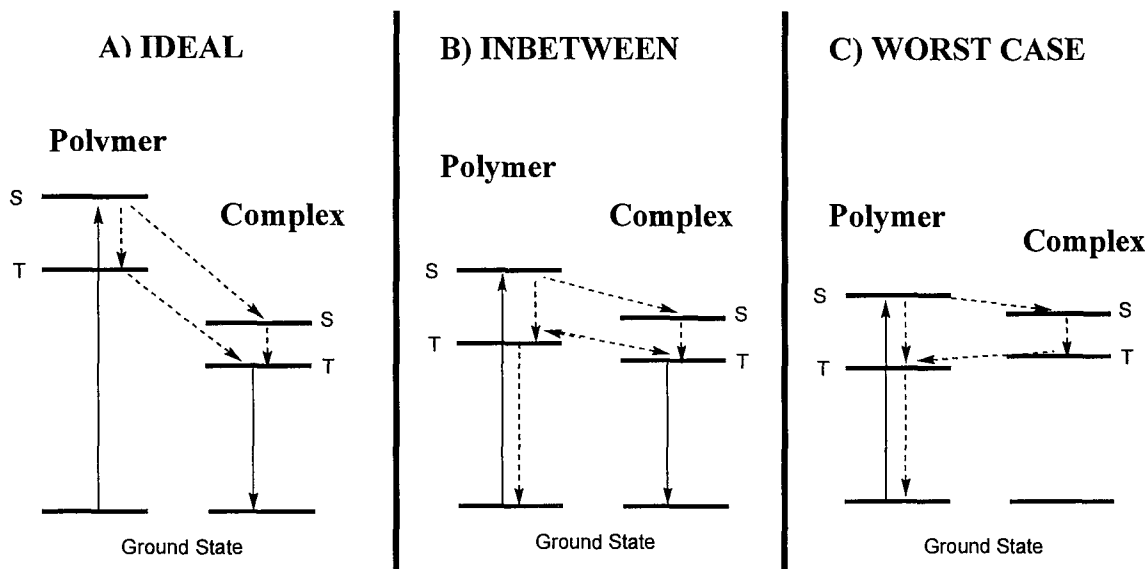


Figure 3.34: Energy transfer in polymer-complex systems

The three Jablonski diagrams above (fig. 3.34) represent three different scenarios of either a host-guest blend, or a host compound covalently attached to a guest. In each case it is assumed that the same guest molecule (i.e iridium complex in this case) is used, and that its energy levels remain the same. It is also assumed to have a small S-T energy gap. The energy levels of the host material are the variable and they are assumed to have a large S-T energy gap.¹⁰⁹ In the 'ideal case' (A), a singlet exciton is generated on the host material. The exciton can either i) directly be transferred to the S (Singlet) excited state on the guest molecule which then intersystem crosses to the T (Triplet) state of the guest, or ii) intersystem cross to the T state of the host, and then be transferred directly to the T state on the guest. Phosphorescence from the guest triplet state then leads to efficient emission. In the 'in-between' case (B), the S and T states of the host material are similar in energy to those on the guest molecule. The same processes as above occur, however, due to the similarity in energy of the two T states, an equilibrium is established, and some of the energy is "back transferred" onto the host material. Deactivation occurs by both phosphorescence and internal conversion leading to less efficient emission. In the 'worst' case (C), the T state of the host material is below that of the guest material. This results in complete triplet-energy back-transfer onto the host. Deactivation only occurs via internal conversion, leading to very inefficient or no emission at all.

In reality, the processes involved are significantly more complicated as the amount of energy transfer depends greatly on the relative rates at which the various processes occur.

Furthermore, in the case of the materials synthesised, the energy levels of host and guest cannot be separated as in the diagram, as the energy levels of the guest molecule spread out onto those of the host. Despite this, it is possible to plot Jablonski diagrams from the experimental measurements. Only the 1,3 regioisomers will be considered as it has already been shown that varying the substitution pattern can affect the quantum yield for reasons unrelated to energy transfer from host-guest and triplet energy back transfer.

The energy gap, measured from the UV-Vis absorption onset, can be taken as the ground state to host singlet energy gap, and the thin film phosphorescence maxima as the guest triplet to ground state energy gap. Using literature reported values for the triplet energies of the host materials, the following plots can be made. The triplet energy of poly-2,7 carbazole has not yet been measured, although it can be estimated at 2.1 eV, according to an empirically derived equation.¹¹⁰ As no phosphorescence was observed for compound **3.37**, the emission maximum for compound **2.52** was used.

Compound	Polymer S /eV ^a	Polymer T /eV ^b	Complex T /eV ^c
3.26	2.94	2.1 ¹¹¹	1.99
3.28	2.94	2.1 ¹¹⁰	1.93
3.29	3.23	2.73 ⁹⁰	1.9
3.37	2.38	1.6 ¹¹²	1.95

Table 3.6: Lowest excited state energy levels

a) Obtained from UV-Vis absorption onset; b) Literature values obtained from respective reference; c) Obtained from emission maxima

As can be seen from the Figure 3.35, compounds **3.26** and **3.28** display energy level differences almost identical to the (B) ‘in-between’ regime. Both of these compounds displayed almost identical quantum yields; in both compounds the triplet energy levels of the attached oligomer are very close in energy to those of the metal complex, indicating that it is highly likely that there is a degree of triplet energy back transfer, reducing the photoluminescence efficiency. The Jablonski diagram for compound **3.29** is identical to the (A) ‘ideal’ regime, indicating that triplet energy back transfer is minimised when oligo(3,6 carbazole) is attached to the metal phosphor. The significantly higher quantum yield observed for this compound further demonstrates

that poly(3,6 carbazole) is an energetically favourable host material for bis(phenylisoquinoline)iridium emitters. Compound **3.37** has a Jablonski diagram that looks identical to the ‘worst’ case (C) scenario. This indicates that the majority of the generated excitons are transferred back onto the triplet level of the attached oligomer (in this case F8BT). This explains the lack of any observed phosphorescence for these oligomers, and the weak singlet emission observed from the F8BT backbone. It is clear that F8BT is not a suitable host for OLEDs in this case. However, the ability of this compound to exclusively produce triplets on the oligomer chain has generated substantial interest. Using this material, it has been possible to measure the rates of triplet diffusion and quenching in F8BT, which has wider implications for the field of organic photovoltaics (a copy of this publication is provided in appendix C).¹⁰⁹

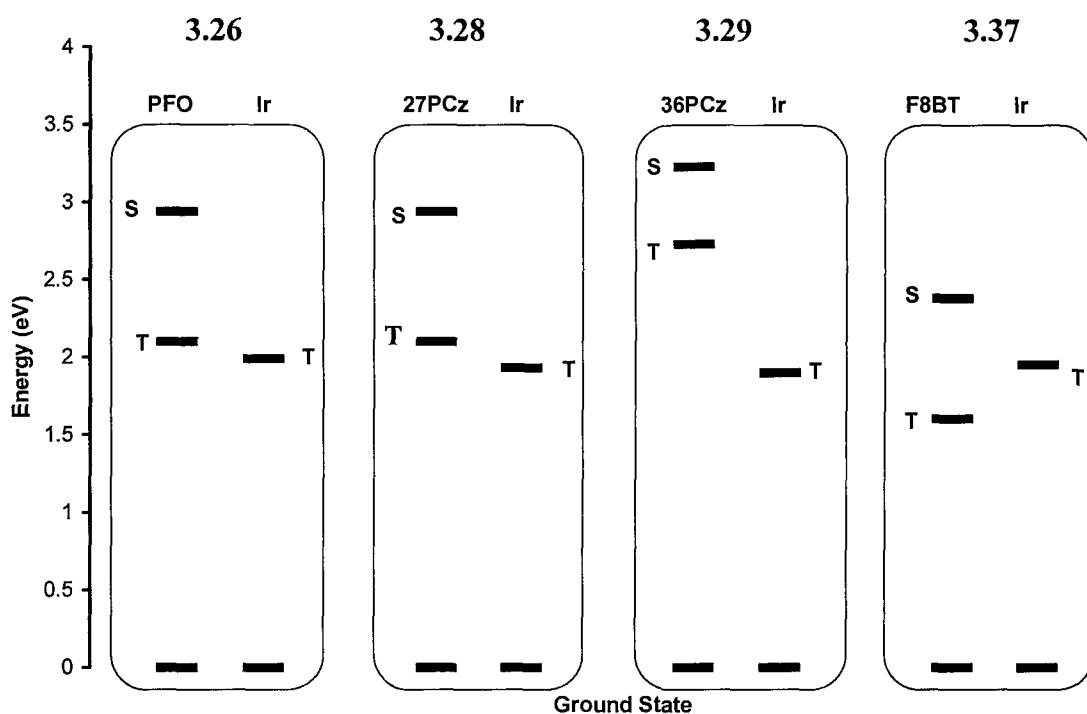


Figure 3.35: Jablonski diagram showing lowest excited states of synthesized polymers

There are a number of potential issues with the conclusions outlined above. Firstly, due to the differing degrees of polymerizations, and consequently, the varying levels of iridium molar concentration within the samples, it cannot be said conclusively that the differences in observed thin film quantum yield originate from the differences in the triplet energy level of the attached oligomers. It has been well documented that quantum efficiencies vary according to iridium concentration in a host guest system.²³ There are two main factors for this: incomplete energy transfer (at low iridium concentrations), and triplet-triplet annihilation (at high iridium concentrations). Incomplete energy transfer is visible in the oligofluorene samples, as residual singlet emission could be

seen in the thin film PL measurements. Neither of the oligocarbazole derivatives display any residual singlet emission in thin film measurements. Furthermore, the molar concentrations of iridium complex are high enough that triplet-triplet annihilation might be occurring.^{22,84,113} Finally, it is possible that differences in morphology could contribute to differences observed in the quantum efficiencies. The more “coil” like nature of the oligo(3,6 carbazole) material could potentially shield the emissive centre from other phosphors. This, in turn, would reduce any triplet-triplet annihilation that might be occurring, leading to an increase in emission efficiency. Despite this, the author finds it likely that the differences observed in emission efficiency of metal complex guests attached to the conjugated oligomer hosts are strongly affected by the relative triplet energy levels of the host and guest, allowing different amounts of triplet energy back transfer to occur.

Based on this study, it is clear that trends based on regioisomerism in small molecules (Chapter 1) are maintained in polymeric analogues. This is clearly seen by the differences in emission and quantum yield of compounds **3.26** and **3.27**, closely mirroring those of the small molecule analogues **2.52** and **2.53** synthesized in the previous chapter. It is also clear that the use of oligo(3,6 carbazole) as the polymeric component attached to bis(1-phenylisoquinoline)iridium complexes provides differences in energy levels that are favourable for phosphorescence compared to oligofluorene and oligo(2,7 carbazole). This is due to the limited conjugation in 3,6-carbazole oligomers providing a high triplet energy level. However, the low solubility of the 3,6 carbazole derivative limits its practical use. Both the oligo 2,7 carbazole and fluorene are reasonable hosts for the emissive phosphors being considered in this study. The lower triplet energy level of the polymers allows some triplet energy back transfer to occur, but still allows for reasonably strong phosphorescent emission. Oligo 2,7 carbazole displays very limited solubility which does not allow facile solution processing and as a consequence is not a suitable material for the construction of OLEDs. In contrast, oligo 2,7 fluorene displays excellent solubility and can be polymerized readily allowing facile thin film formation, suggesting it is the best of the tested materials for construction of conjugated polymers bearing emissive iridium complexes.

3.4 Conclusions

A series of novel polymeric iridium complexes were synthesized and fully characterized. The site of attachment of the polymer chain, and different types of polymer were investigated.

It was found that the site of attachment of the polymer chain mirrored behaviour observed in small molecule analogues synthesized in the previous chapter.

Polymers possessing different triplet energy levels were attached and it was observed that the emission phosphorescence quantum yield decreased significantly as the triplet energy of the polymer was reduced. This is believed to be due to back transfer of excitons from the complex onto the triplet energy level of the polymer.

It was found that polyfluorene was the polymer best suited for use in polymer iridium complexes due to its reasonably high triplet energy level, allowing good energy transfer from polymer to complex to occur, and due to its facile synthesis and good solution processability.

Chapter 4: Alternating and random copolymers of iridium complexes and oligofluorenes

4.1 Introduction

In blends of a phosphorescent guest in a conjugated host material it is important to introduce the optimum amount of guest in order to achieve the maximum possible emission efficiency.

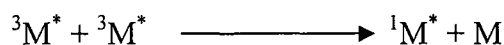
In general, at low concentrations, as the concentration of the guest is increased, the phosphorescence efficiency will increase. This is due to the greater amount of exciton transfer that can occur from host to guest, and due to the greater number of emissive centers.^{23,114} However, the long lifetime of the triplet excited state can result in saturation of emissive sites. At high guest concentration, this can allow triplet-triplet (T-T) annihilation to occur.^{25,115,116} Consequently, an ideal OLED would have a sufficiently high concentration of guest to allow complete energy transfer from the host, whilst not being high enough to succumb to the effects of T-T annihilation.

4.1.1 Triplet-Triplet (T-T) Annihilation

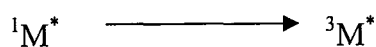
T-T annihilation is commonly seen in host-guest systems. Upon photoexcitation, T-T annihilation results in a decrease of the observed phosphorescent quantum yield. Under electroluminescence conditions, the number of triplets generated is greater and can result in a marked decrease in device efficiency. This effect is more pronounced at high current densities, and external quantum efficiencies are often observed to ‘roll off’ as the current is increased.^{49,58,117-119}

The mechanism of triplet-triplet annihilation is as follows:

Two triplet states ($^3M^*$) can have sufficiently long enough lifetimes to encounter one another before decaying radiatively. When this occurs, a new singlet excited state ($^1M^*$) and a ground state (M) are generated.



However, singlet excited states can undergo intersystem crossing (due to the heavy atom) and a new triplet excited state is generated



This triplet excited state can then undergo the usual radiative or non-radiative relaxation pathways (including a subsequent T-T annihilation)



As the efficiency of a phosphorescent material is directly dependant on the number of triplet states that decay radiatively, T-T can have significant detrimental effects.

The exact nature of the energetic processes occurring is still a matter of debate, although it is established that for T-T annihilation to occur, the two triplet states must be in close proximity. As the triplet exciton normally resides on the iridium complex, the best strategy to minimize T-T annihilation is to spatially separate all the complexes as much as possible. There is also the possibility of triplet diffusion, whereby a triplet can be generated or transferred onto the host material. The rate and magnitude of this effect is still not known.^{113,119-123}

Two main methods have been developed in order to minimize triplet-triplet annihilation: (1) Encapsulation of the phosphorescent complex into a dendrimer; and (2) incorporation of the complex into a conjugated polymer. This thesis is concerned with the use of iridium complexes and so only the literature pertaining to encapsulation/polymer complexes using iridium will be discussed.

4.1.1.1 Encapsulation

This method relies on the iridium complex being encapsulated within a dendrimer. Such materials are referred to as having an iridium core covalently attached to conjugated oligomer/polymer dendrons. This encapsulation strategy prevents the emissive iridium cores, where the triplet is localized, from coming into contact with one another. The encapsulating dendron can either be purely structural or can possess electron and/or hole transporting properties, which can aid charge transfer to and from the metal complex. A significant drawback of this approach is the extremely low synthetic yields and the large number of steps/purifications required to prepare the dendrimers.^{37,40,124-135}

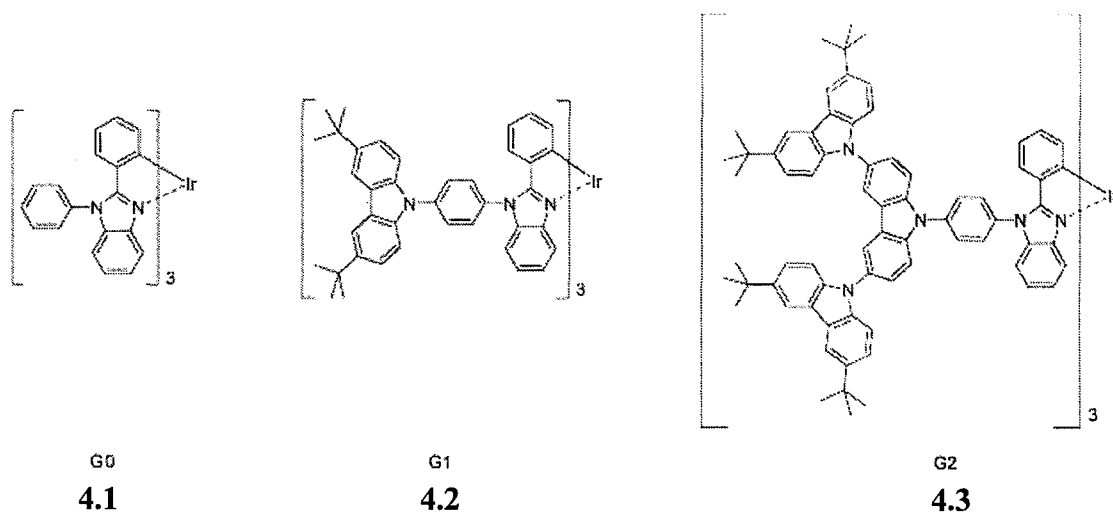


Figure 4.1: Increasing dendrimer generation

Ding *et al*¹²⁷ found that on increasing the dendrimer generation, the thin film photoluminescent quantum yield increased from 18% (G0), to 31% (G1), and 45% (G2) (Fig. 4.1).

4.1.1.2 Copolymers incorporating iridium complexes and conjugated polymers

The second method relies on the incorporation of the phosphorescent iridium complex into a conjugated polymer chain (host) and results in materials such as those illustrated in Figs. 4.2 and 4.3 and those described in chapter 3. The polymers are typically prepared by an A-A + B-B + B'-B' type statistical polymerization, where the desired guest material (iridium complex) is introduced in small percentages as the B'-B' monomer. This produces a polymer where the metal complex is incorporated at random intervals along the polymer backbone. Due to the low percentage loading of the B'-B' monomer it is assumed that the complexes are held sufficiently apart to minimize T-T annihilation. The benefits of these materials are that they can be synthesized in good to high yields in a single step, and could potentially allow for very simple device construction, as blending with a host is not required.^{8,30-52}

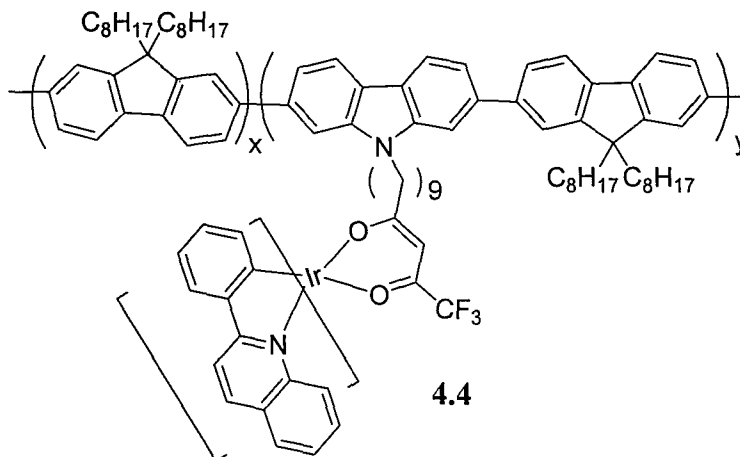


Figure 4.2: Tethered iridium complex containing polymer

Jiang *et al*⁶⁸ synthesized tethered copoly(fluorene-alt-carbazole) with iridium complexes attached to the carbazole moieties via an alkyl tether (Fig. 4.2). They showed excellent thin film photoluminescence quantum efficiencies (50-70%), with the best efficiencies deriving from the copolymer containing 2 mol% of iridium complex. Reasonable electroluminescence efficiencies were obtained (1-4%), with the best copolymers having an iridium complex loading of 0.5 mol%. However, at high current densities, the efficiency ‘gently decayed’ indicating that whilst T-T annihilation had been suppressed, it had not been completely prevented.

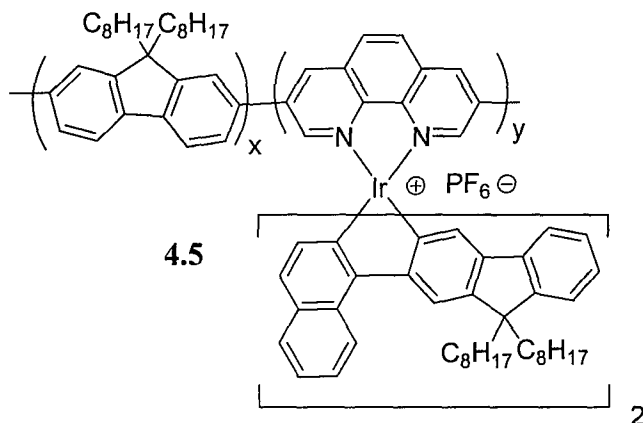


Figure 4.3: Polyfluorene attached to a cationic iridium complex

Liu *et al*¹³⁶ recently synthesized a series of polymers incorporating a charged iridium complex in a polyfluorene chain 4.5. The thin film phosphorescence quantum yield decreased rapidly as the concentration of iridium complex was increased, which was attributed to T-T annihilation.

It is apparent that although T-T annihilation can be reduced by incorporating the guest molecule into the host molecule covalently, it is still limiting the performances of this important type of material.

In order for the guest molecule to be incorporated at random intervals in an A-A + B-B + B'-B' polycondensation, the rate of reaction of B-B and B'-B' must be identical. If this is not the case, composition drift¹³⁷ can occur. This is where one type of molecule reacts preferentially over another and can result in incomplete incorporation of the desired monomer. It can also result in areas of higher and lower guest concentrations along the polymer backbone (see Fig. 4.4). Incomplete guest incorporation is often encountered and is not a significant problem as accurate guest concentrations can be calculated by integration of the ¹H NMR spectra and by using other analytical techniques such as ICP-MS (inductively coupled plasma-mass spectrometry).^{38,62,85,86,138,139}

An inhomogeneous polymer sample could present a much bigger problem in two main ways. In an inhomogeneous polymer, there will be areas where guest molecules will be closer to one another than anticipated. This could allow an increase in the amount of T-T annihilation, and consequently reduce the efficiency. Secondly, due to the larger amount of unoccupied host material in other areas of the polymer, energy transfer to the guest will be much less efficient.

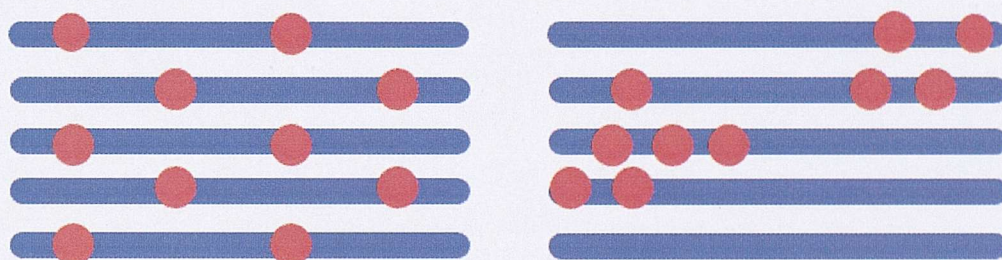


Figure 4.4: Homogenous (left) and inhomogeneous (right) Host-Guest polymers (blue = host, red = guest)

Due to the significantly different steric and electronic properties of a typical guest monomer to those of a typical host starting monomer, it is extremely unlikely that they will have equal rates of reactivity in a polymerization, and consequently, the likelihood of there being inhomogeneity within host containing polymers is high.

4.1.2 Synthetic Strategy

To investigate the magnitude of T-T annihilation and reduced energy transfer in randomly synthesized host-guest polymers, a series of oligomers (macromonomers) were prepared which were polymerized with a guest molecule to ensure that each guest

was maintained a set distance apart (Method 1). These alternating copolymers were then compared with a set of polymers synthesized via a traditional random method (Method 2).

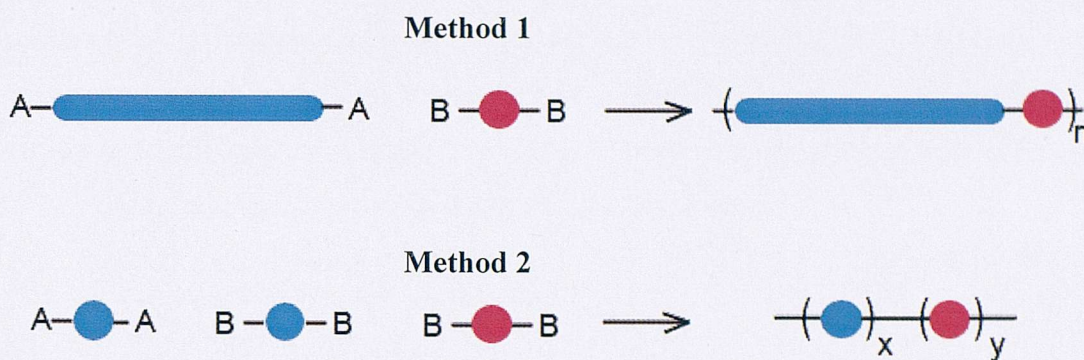


Figure 4.5: Different methods to make host-guest polymers

It was envisaged that by varying the oligomer length and consequently altering the host concentration within the sample it would be possible to elucidate the magnitude of T-T annihilation that might be occurring in these samples.

4.2 Synthesis

For this study, polyfluorene was selected as the host material as the previous chapter demonstrated its suitability, and as there is already a wealth of literature on the synthesis of well defined oligofluorenes.¹⁴⁰⁻¹⁴⁵ Furthermore, there were already several examples of polyfluorenes as the hosts for iridium complexes, as well as the preparation of polyfluorenes covalently attached to iridium complexes.^{41,67,146-148} Oligomer chain lengths of 3, 5, 10, 20, 40, and 80 units were selected as they would result in polymers containing a broad range of iridium complex concentrations (1 – 25 mol%) which would enable investigation of the concentration-phosphorescence activity relationship.

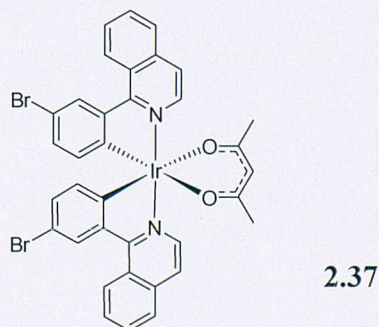


Figure 4.6: The iridium complex to be used in the copolymers

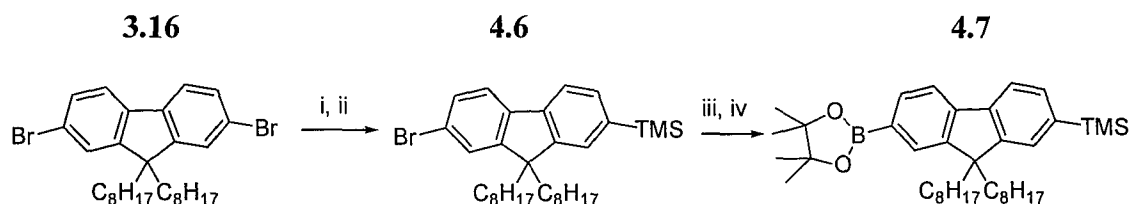
It was also decided to use the complex **2.37** as the guest complex, as the previous chapter has shown that oligofluorenes substituted at the 3-phenyl position of this

complex have significantly greater phosphorescence quantum yields than other regioisomers. Consequently, the influence of iridium complex loading in the copolymers should be easily detected.

Suzuki coupling was chosen as the method for copolymerizing the oligofluorene units with the iridium complex **2.37**, as the previous chapter has already shown this to be a feasible synthetic method. Furthermore, a significant proportion of host-guest polymers in the literature have been synthesized in this manner.^{38,39,60,62,78,85,136,138,146,149,150} Consequently, well defined oligofluorenes with two boronic ester end groups were required.

4.2.1 Synthesis of monodisperse macromonomers

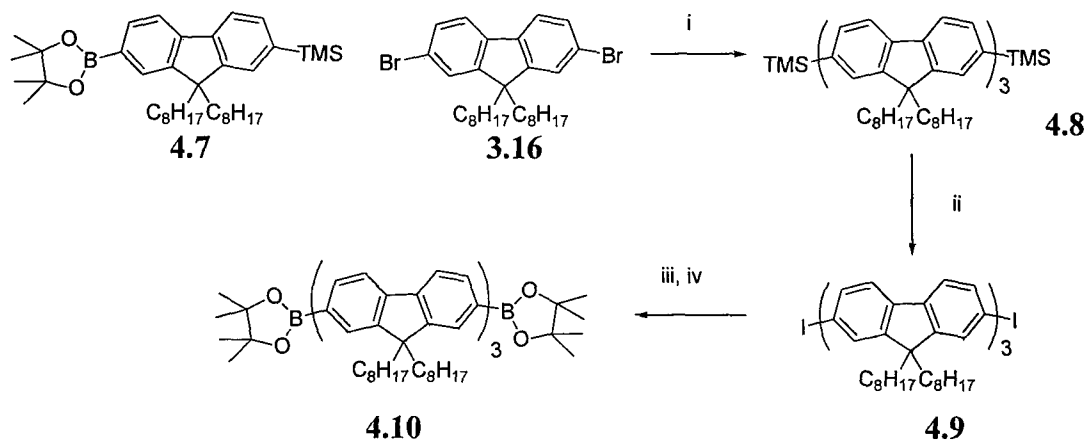
Substantial work has already been carried out by other groups on the synthesis of monodisperse oligofluorenes.^{39,143,145,151,152} These methodologies were adapted and used to synthesize the shorter ($m = 3,5$) oligofluorene chains (Fig. 4.7, 4.8, 4.9).



Reagent and Conditions: i) *n*BuLi, THF, -78 °C; ii) TMSCl, -78 °C → room temperature, 98% Crude;
 iii) *n*BuLi, THF, -78 °C; iv) 2-Isopropoxy-4,4,5,5-tetramethyl-1,3,2-dioxaborolane, -78 °C → room temperature, 61%

Figure 4.7: Synthesis of mono TMS protected, mono borylated fluorene

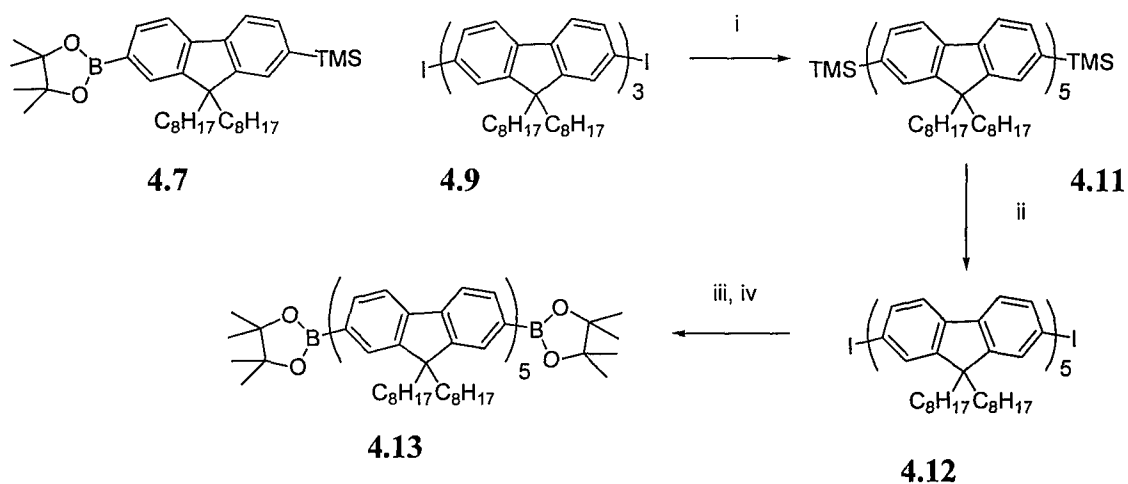
The synthesis of **4.6**, via a metal-halogen exchange reaction afforded a distribution of unreacted, mono, and di-substituted products. Due to the low polarity of these compounds, purification via chromatography proved problematic. It was decided to proceed with the subsequent borylation via another metal-halogen exchange using the crude reaction mixture. The products of this reaction were readily separable by chromatography and allowed isolation of pure **4.7** in good yields (61%).



Reagents and Conditions: i) Pd(OAc)₂, PPh₃, Toluene, aq. Et₄NOH, 90 °C, 85%; ii) ICl, DCM, 0 °C, 100%; iii) nBuLi, THF, -78 °C; iv) 2-Isopropoxy-4,4,5,5-tetramethyl-1,3,2-dioxaborolane, -78 °C → room temperature, 58%

Figure 4.8: Synthesis of fluorene trimer with boronic ester end groups

The synthesis of the TMS protected fluorene trimer **4.8** was achieved in a pleasing yield (85%) via a Suzuki condensation reaction using **3.16** and 2.2 equivalents of **4.7**. Deprotection of the trimethylsilyl groups using ICl occurred in quantitative yield and afforded the 2,7-diiodo substituted trimer **4.9** as a white crystalline solid. Subsequent conversion of the iodo groups to the required boronic esters was achieved via a metal halogen exchange, followed by addition of 2-isopropoxy-4,4',5,5'-tetramethyl-1,3,2-dioxaborolane. Purification *via* column chromatography allowed isolation of the desired macromonomer **4.10** in 58% yield.



Reagents and Conditions: i) Pd(OAc)₂, PPh₃, Toluene, aq. Et₄NOH, 90 °C, 76%; ii) ICl, DCM, 0 °C, 100%; iii) nBuLi, THF, -78 → 0 °C; iv) 2-Isopropoxy-4,4,5,5-tetramethyl-1,3,2-dioxaborolane, -78 °C → room temperature, 42%

Figure 4.9: Synthesis of fluorene pentamer with boronic ester end groups

The synthesis of the pentamer **4.13** was achieved using procedures identical to those described above. However, significantly more vigorous conditions were required to during the attachment of the boronic esters. Macromonomer **4.13** was isolated in a reasonable yield (32%) based on **4.9**. The novel macromonomers **4.10** and **4.13** were fully characterized by ^1H and ^{13}C NMR, mass spectrometry, GPC and elemental analysis.

4.2.2 Synthesis of polydisperse macromonomers

Although it would be desirable for all the monomers to be discrete monodisperse species such as **4.10** and **4.13**; the synthesis of these moieties becomes increasingly challenging as the chain length increases. Although there are literature examples of the synthesis of monodisperse oligofluorenes up to about 10 – 15 repeat units,^{143,153} it would be laborious and low yielding to continue these procedures up until 20 or even 40 repeat units.

Consequently, it was decided to synthesize these macromonomers via Suzuki polycondensation reactions (Fig. 4.10). Unfortunately this approach means that only the average distance between iridium units would be known, as polyfluorenes synthesized in this fashion typically have polydispersity indices of around 2.³⁸

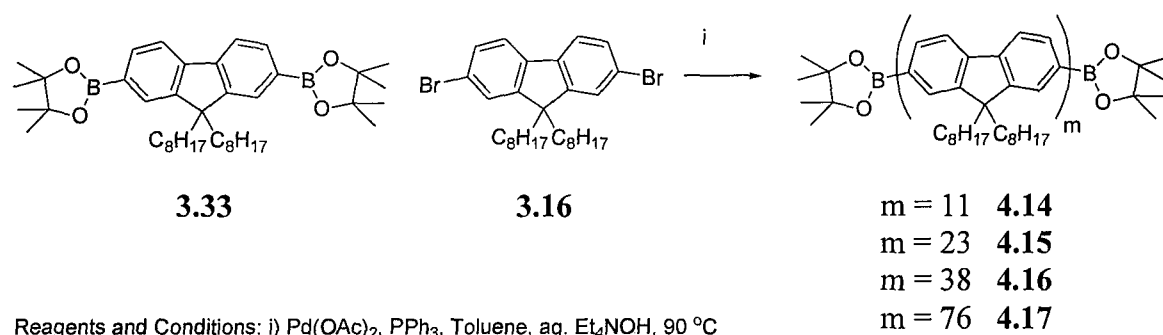


Figure 4.10: Synthesis of fluorene macromonomers with boronic ester end groups

These polymerizations were carried out using Suzuki coupling conditions described previously in the chapter. Purification of the crude macromonomers was achieved *via* multiple precipitations into methanol and allowed isolation of the macromonomers as greenish fibres. To control the chain length of these oligomeric macromonomers, the ratio of 9,9'-dioctyl-2,7-bis(4,4',5,5'-tetramethyl-1,3,2-dioxaborolan-2-yl)-9H-fluorene **3.33** to 2,7-dibromo-9,9'-dioctyl-9H-fluorene **3.16** was varied, in a manner similar to that devised by Evans *et al.*³⁸

4.2.2.1 Analysis of macromonomers

The chain length was calculated from the ^1H NMR spectrum of the resulting polymers. The NMR spectrum for macromonomer **4.15** is shown below (Fig. 4.15). The broad peaks present between 7.5 - 8 ppm correspond to the aromatic protons on the fluorene backbone. The signals at 2.5 - 2.0 and 1.25 - 0.5 ppm originate from the protons on the alkyl chains. The sharp singlet at ~ 1.4 ppm (indicated with an *) corresponds to the methyl groups on the boronic ester.

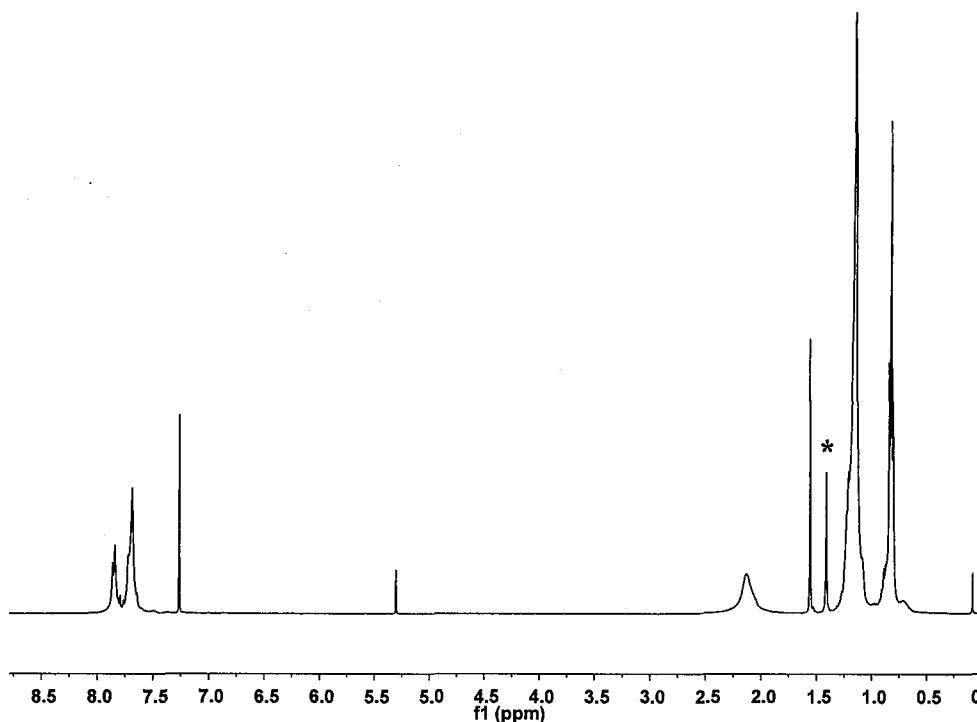


Figure 4.11: ^1H NMR of macromonomer **4.15**

Assuming the oligomers were completely end-capped at both ends with boronic ester groups, and comparing the integration of the peak at ~ 1.4 ppm (24H) with those of the alkyl chains allowed an estimation of the chain length (m) of the macromonomers. The chain length, determined by ^1H NMR, is compared to the theoretical value dictated by the stoichiometry, in Table 4.1, and is in exceedingly good agreement.

Ratio of 3.33 : 3.16	Product	m (theoretical) ^a	m (obtained) ^b	M _n ^c kDa	M _w ^c kDa	PDI ^c
1.2 : 1	4.14	11	11	3.6	5.6	1.6
1.1 : 1	4.15	21	23	11.6	26.8	2.3
1.05 : 1	4.16	41	38	24.2	58.7	2.4
1.025 : 1	4.17	81	76	37.0	102.5	2.8

Table 4.1: Macromonomer polymerization data

a) Dictated by stoichiometry; b) Estimated from ¹H NMR; c) From GPC using PS standards and THF as eluent

The GPC traces shown in Fig. 4.12 demonstrate the increasing molecular weight of the synthesized macromonomers. Compounds **4.10** and **4.13** are monodisperse, whilst the remaining oligomers comprise of a range of chain lengths and show broader peaks. It is interesting to note that it is possible to see the contribution of the fluorene pentamer **4.13** in the trace for **4.14** and **4.15**.

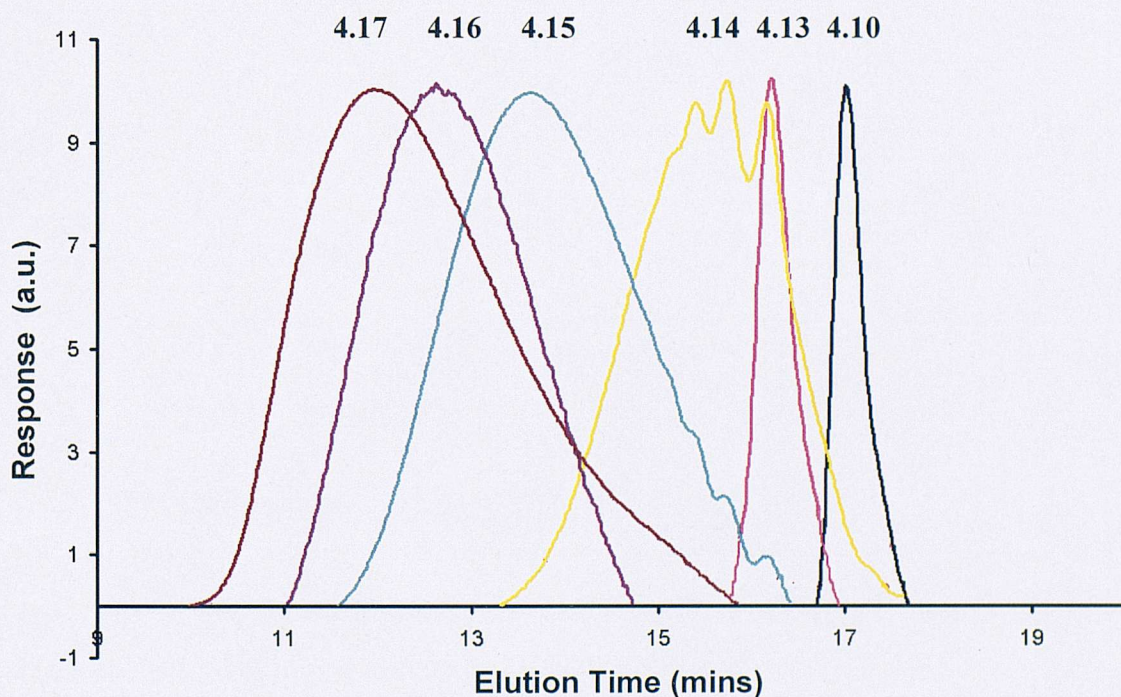


Figure 4.12: GPC elution peaks of oligofluorene macromonomers (PS standards, THF eluent)

4.2.2.2 End group analysis

MALDI-TOF mass spectrometry was performed on all the macromonomer samples. The monodisperse macromonomers **4.10** and **4.13** only displayed peaks corresponding to the desired product. In the disperse macromonomer samples **4.14** - **4.17** it was possible to observe increasing lengths of oligofluorene ($m = 3 - 15$), containing two boronic ester groups. Only odd chain lengths were observed as would be expected by the excess of **3.33** relative to **3.16**. An example of the MALDI-TOF spectrum for **4.15** is shown below (Fig. 4.13). It was also possible to observe a smaller series of peaks corresponding to α -boronic ester- ω -H oligofluorenes, and in some cases di-H terminated oligofluorenes. This indicates that loss of the boronic ester end group occurs either during the reaction or work-up procedures. Consequently, the obtained value of m is likely to be a slight overestimate.

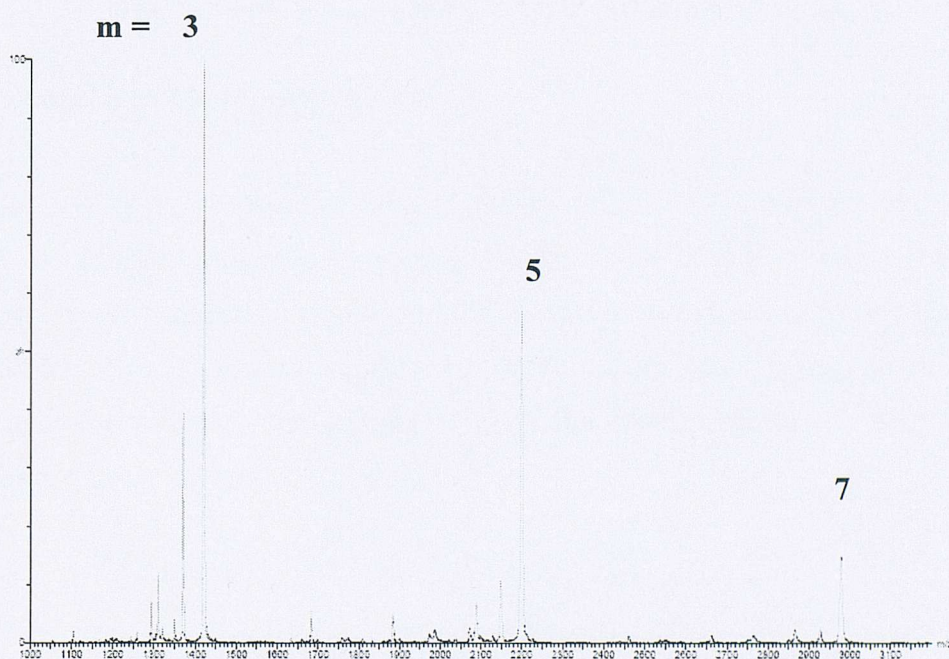


Figure 4.13: MALDI-TOF (Dithranol) mass spectrum of macromonomer **4.15**

4.2.2.3 UV-Vis absorption of macromonomers

The UV-Vis absorption spectra of the macromonomers are shown below (Fig. 4.14). The increasing λ_{max} corresponds to an increase in chain length (m) and is due to an increase in conjugation. These results are similar to those reported by other researchers.^{143,145}

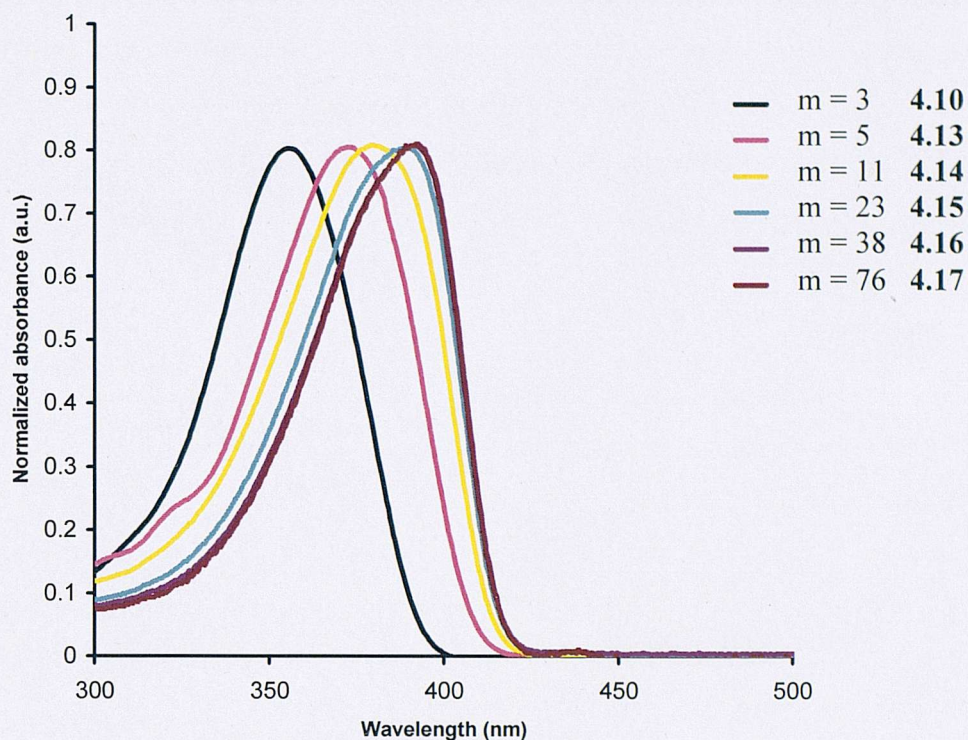
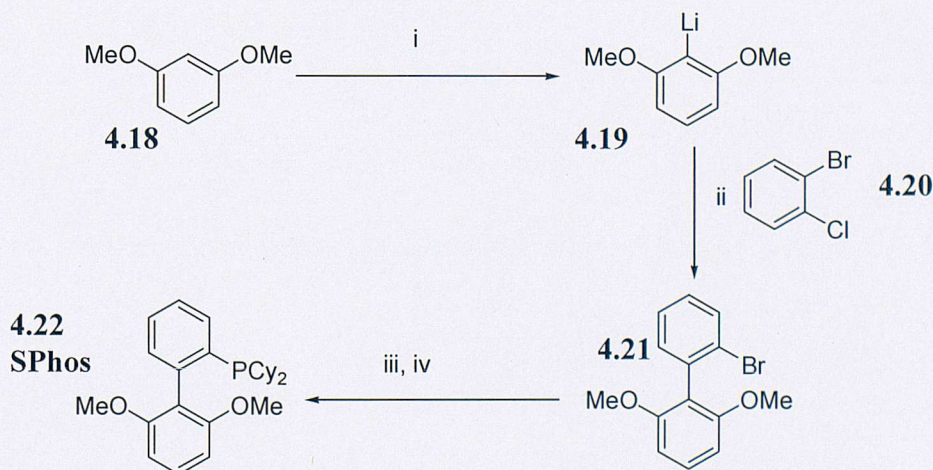


Figure 4.14: UV-Vis absorption of macromonomers (DCM, $\sim 10^{-5}$ M)

4.2.3 Synthesis of Alternating Copolymers

In order to react the synthesized fluorene macromonomers **4.10**, **4.13–4.17** with **2.37** a variety of catalyst systems were screened in a series of test reactions. Of these, Pd(OAc)₂, with 2 equivalents of SPhos **4.22** displayed the highest activity. SPhos **4.22** has recently been shown to significantly accelerate the rate of reaction in Suzuki couplings where one or both starting materials are either sterically or electronically unfavorable to normal reaction conditions.¹⁵⁴

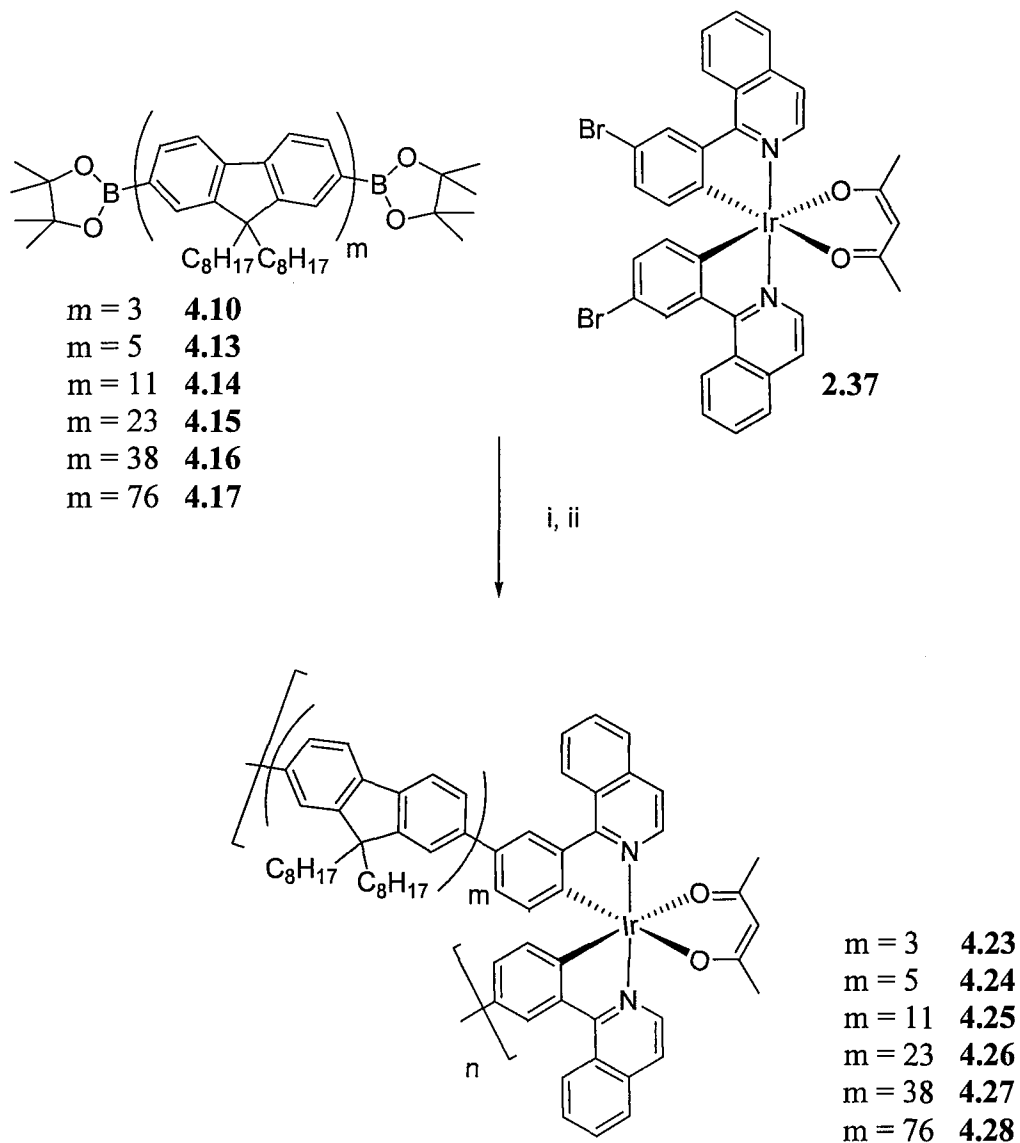


Reagents and conditions: i) nBuLi, THF, room temperature; ii) 0 °C, **4.20**;
iii) nBuLi, -78 °C; iv) Cy₂PCl, 51%

Figure 4.15: Synthesis of SPhos

The synthesis of SPhos **4.22** is shown in Fig. 4.15. It was performed as described in the literature¹⁵⁴ and afforded the product in a similar yield (51 %) to the reported synthesis.

Having identified suitable reaction conditions, the copolymerizations were performed as illustrated in Fig. 4.16.



Reagents and conditions: i) Pd(OAc)₂, SPhos, Tol, TEAOH_{aq}, 90 °C; ii) acac, Na₂CO₃, Tol, 2-ethoxyethanol, 90 °C, 60 - 90%

Figure 4.16: Synthesis of the alternating copolymers

The results of the polymerizations are shown in Table 4.2, and subsequently discussed.

Reactant	M_n 4.x ^a kDa	M_n 2.37 ^b kDa	Product	Yield /%	M_n ^c kDa	M_w ^c kDa	PDI ^c	n^d
4.10	1.0	0.2	4.23	75	12.6	26.1	2.1	13
4.13	2.3	0.2	4.24	85	29.6	61.2	2.1	14
4.14	3.6	0.2	4.25	91	31.2	72.6	2.3	9
4.15	11.6	0.2	4.26	89	42.3	104.0	2.4	4
4.16	24.2	0.2	4.27	88	71.3	157.9	2.2	3
4.17	37.0	0.2	4.28	-	37.5	102.3	2.7	1

Table 4.2: Alternating oligofluorene-iridium complex polymerization data

a) M_n of relevant reactant **4.x**; b) M_n of iridium complex **2.37** according to GPC; c) Determined by GPC using PS standards and THF as eluent; d) $n = M_n / (M_n(\text{reactant } \mathbf{4.x}) + M_n(\mathbf{2.37}))$

Due to the complex appearance of Fig. 4.16, the following cartoon (Fig. 4.17) represents the structure of the synthesized materials.

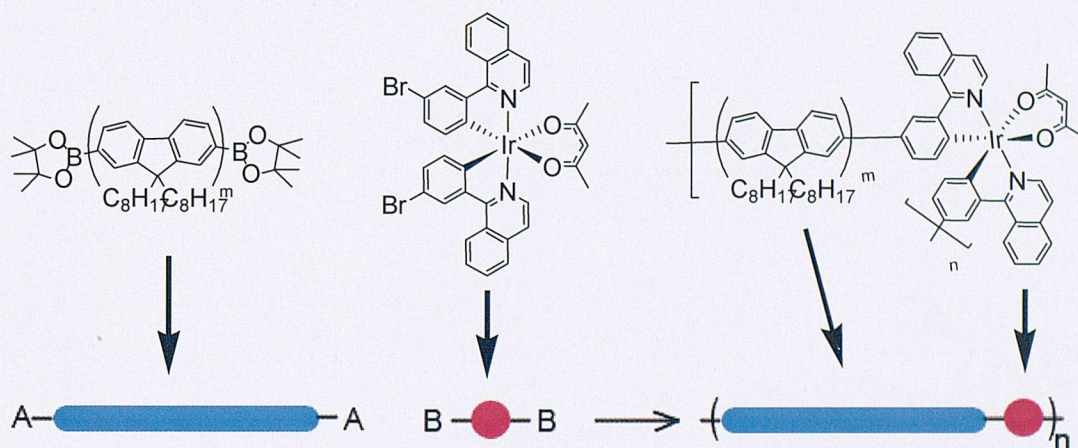


Figure 4.17: Representation of the structures of the alternating copolymers

The value m , is the chain length of the starting fluorene oligomer, and n is the total number of repeat units of the oligofluorene-iridium complex unit.

All polymerizations resulted in the isolation of red fibers in good yields. In order to calculate the degree of polymerization, GPC measurements were performed. As mentioned previously, GPC using PS standards is not capable of giving absolute

molecular weights (see Chapter 3).¹⁰² Consequently, the value of n was determined by dividing the molecular weight (M_n) of the new polymers by the sum of the molecular weights (M_n) of the starting monomers, all determined by GPC. The number of repeat units decreases with the increasing chain length of the starting oligomer. This was expected as the high molecular weights of the oligo/polyfluorenes caused precipitation of the copolymer as the reaction proceeded, effectively limiting the maximum possible molecular weight. Indeed, compound **4.17** did not undergo satisfactory polymerization probably due to the long chain length of the starting polyfluorene unit ($M_n = 37,000$) and consequently will not be investigated further.

4.2.4 Calculating Iridium loading in the alternating copolymers

The degree of polymerization in all the samples prepared is fairly low, and as such, the percentage of iridium within the product will be dependent on whether the chain termini are oligofluorene or iridium phosphors. In order to ascertain the correct iridium loading it was necessary to analyze the relative integrals in the ^1H NMR spectra of the copolymers (Fig. 4.18).

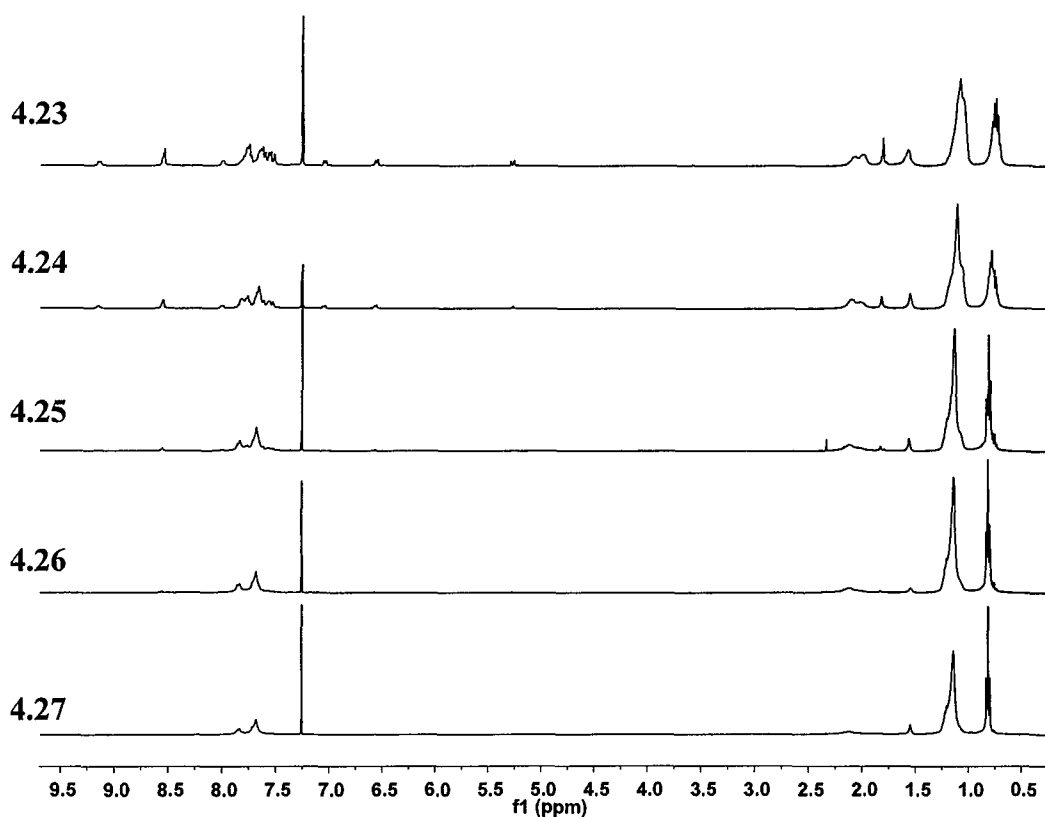


Figure 4.18: ^1H NMR spectra of the alternating copolymers

The ^1H NMR spectra of the synthesized copolymers are shown above (Fig 4.18). They are all similar in appearance to those of the starting macromonomers with the aromatic and alkyl peaks appearing unchanged. The peak at ~ 1.4 ppm is absent indicating consumption and/or hydrolysis of the boronic ester group. There are several new signals at around 9.2, 8.5, 8.0, 7.0 and 6.5 ppm which correspond to the aromatic protons of the iridium complex. The small peak at around 5.3 ppm corresponds to the acac-H on the ancillary ligand of the iridium complex. The peak at 1.8 ppm corresponds to the methyl signal of the acac group.

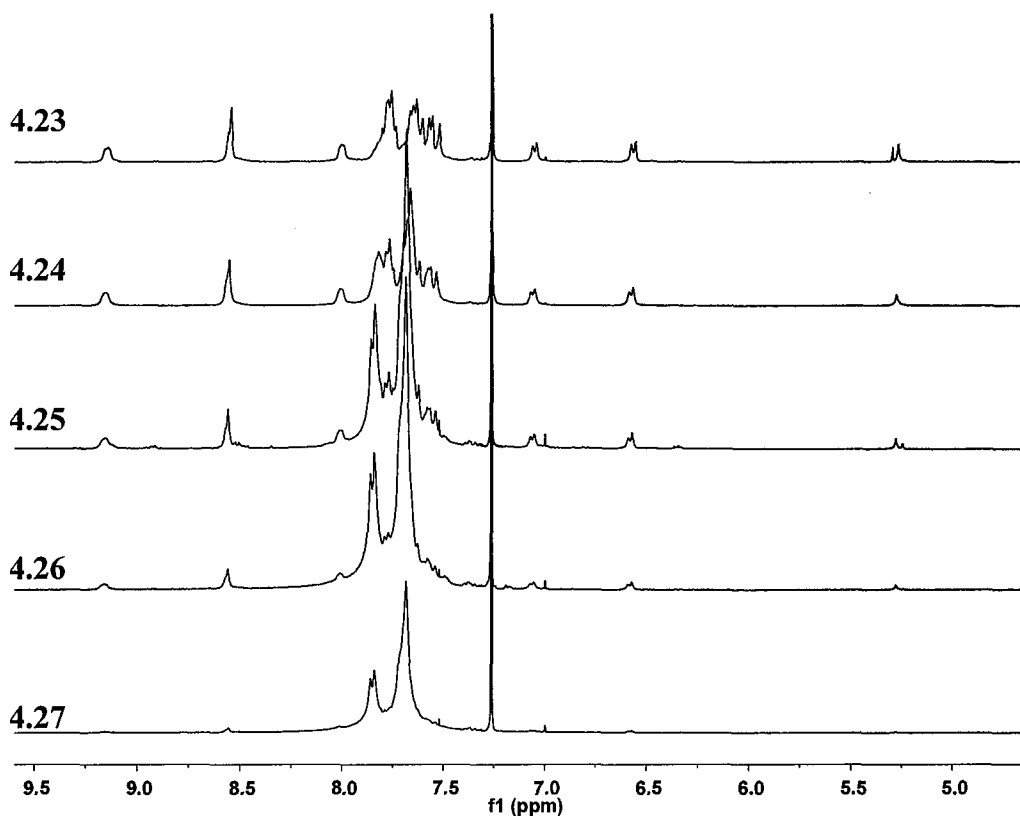


Figure 4.19: ^1H NMR spectra of the aromatic region of the alternating copolymers

The aromatic region of the NMR spectra is shown above (Fig. 4.19). The increasing amount of iridium complex incorporation is clearly visible on going from compound 4.27 to 4.23. The peak at ~ 9.2 ppm corresponds to H-8 in the iridium complex covalently bound to a fluorene oligomer (see Chapter 2 and 3). The small signal that is just visible in 4.25 at ~ 8.9 ppm corresponds to a bromo terminated iridium complex, which is due to an end-capping iridium complex. These were observed in all the polymer samples although the intensity of this peak varied, and in most cases was very small. As the degree of polymerization in all samples is low and all polymerizations were performed at a 1:1 ratio of iridium complex to oligofluorene, 50% of the endgroups should be bromo terminated iridium complexes. The observed value is much

lower, which implies that the majority of the end groups are oligofluorene chains. The reason for this is unclear, although it may be due to the presence of some contamination of the oligofluorene by α -boronic ester- ω -H oligofluorene segments, which were observed in the MALDI-TOF measurements which would act as end-capping groups.

Integration of the peak at 9.2 ppm relative to the peaks corresponding to the alkyl chains on the oligofluorenes was used to calculate the iridium complex concentration within the sample.

Compound	Iridium complex: fluorene units feed ratio ^a	Obtained ratio ^b	Iridium Complex mol% incorporation ^b
4.23	1:3	1:4	20
4.24	1:5	1:6	14.3
4.25	1:11	1:14	6.7
4.26	1:23	1:29	3.3
4.27	1:38	1:55	1.8

Table 4.3: Iridium complex incorporation ratio in alternating samples

a) Dictated by stoichiometry; b) Estimated from ¹H NMR

The propensity of these materials to show oligofluorene end groups results in an iridium complex incorporation ratio that is below that expected on the basis of the starting stoichiometry (feed ratio).

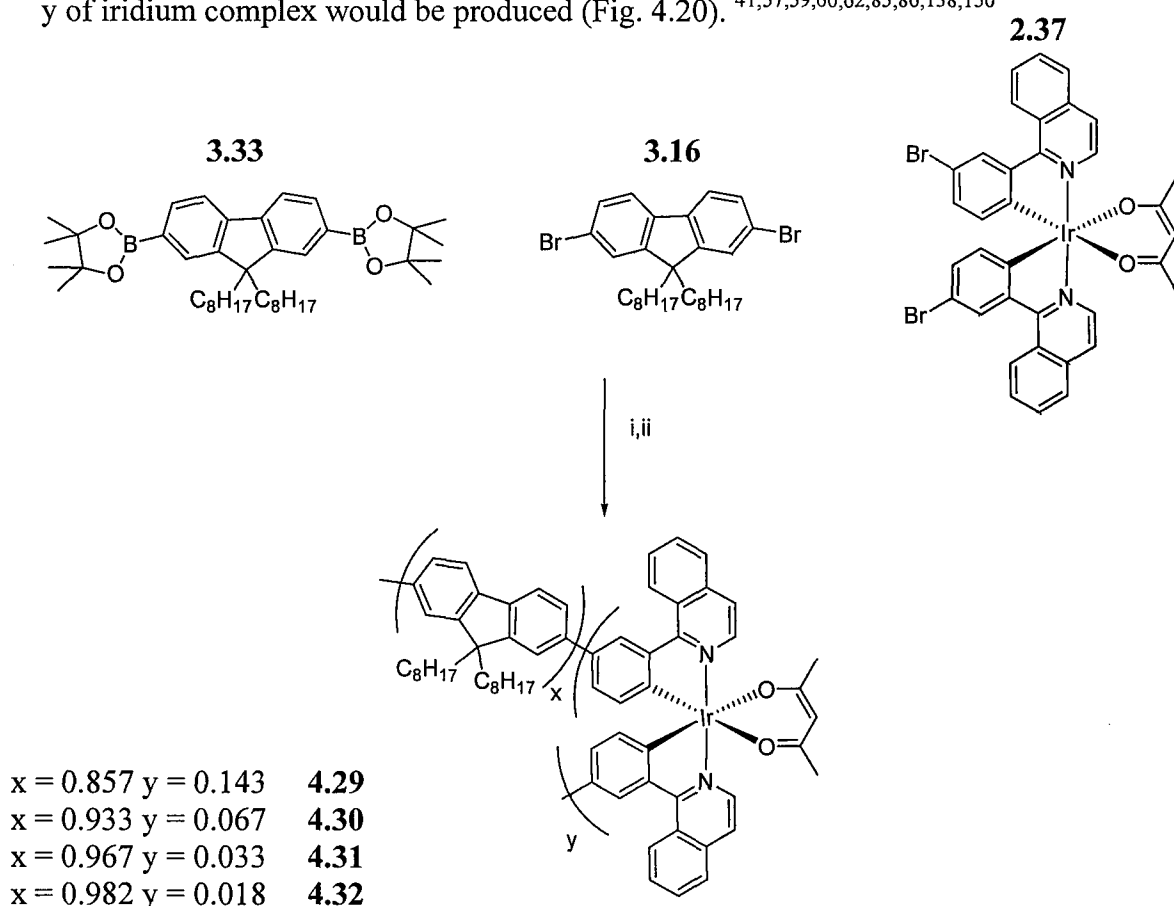
4.2.4.1 End group analysis

MALDI-TOF mass spectrometry on the synthesized iridium complex containing polymers only revealed residual di-H terminated fluorene oligomers as was observed in chapter 3, confirming that hydrolysis of any remaining boronic ester end groups was complete.

4.2.5 Synthesis of random copolymers

In order to compare the photophysical properties of the alternating copolymers with the random ones, it is necessary for the iridium loadings to be similar. Consequently, using the iridium incorporation percentages calculated above for the alternating copolymers, analogous random copolymers were targeted.

The copolymers were synthesized under conditions that are similar to many of those used in the literature to prepare such random copolymers, with the ratios of the reactants varied such that if the reaction went to completion, a polymer containing a mole fraction y of iridium complex would be produced (Fig. 4.20).^{41,57,59,60,62,85,86,138,150}

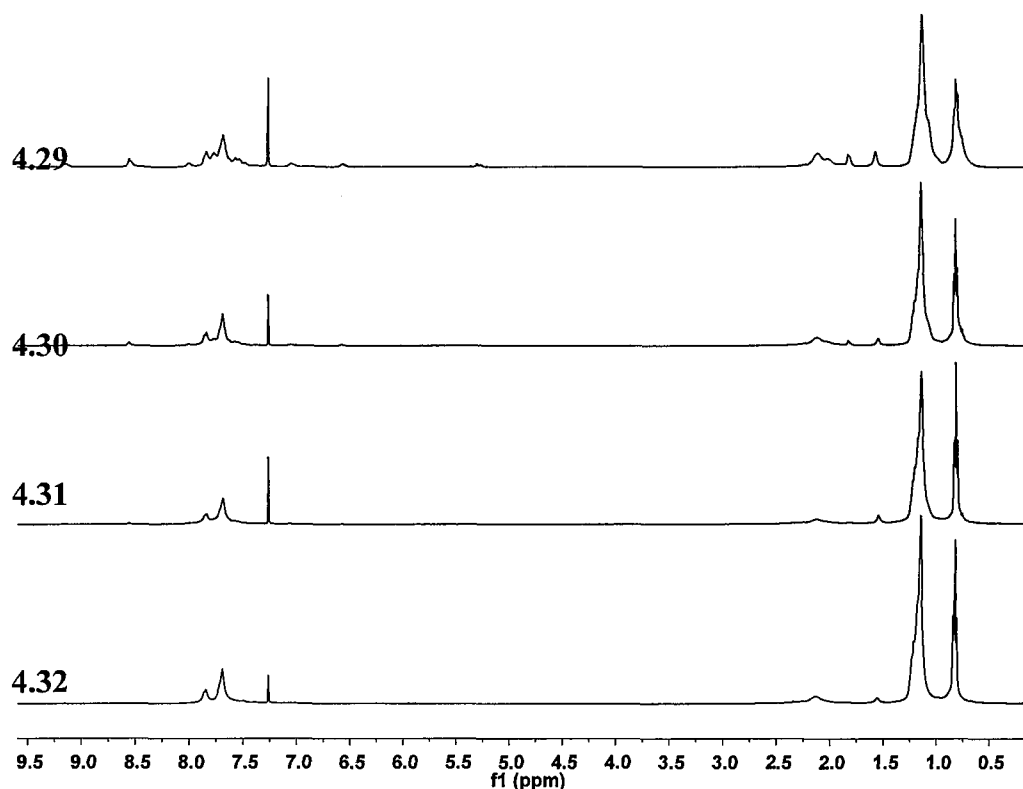


Reagents and conditions: i) Pd(OAc)₂, SPhos, Tol, TEAOH_{aq}, 90 °C; ii) acac, Na₂CO₃, Tol, 2-ethoxyethanol, 90 °C, 60 - 90%

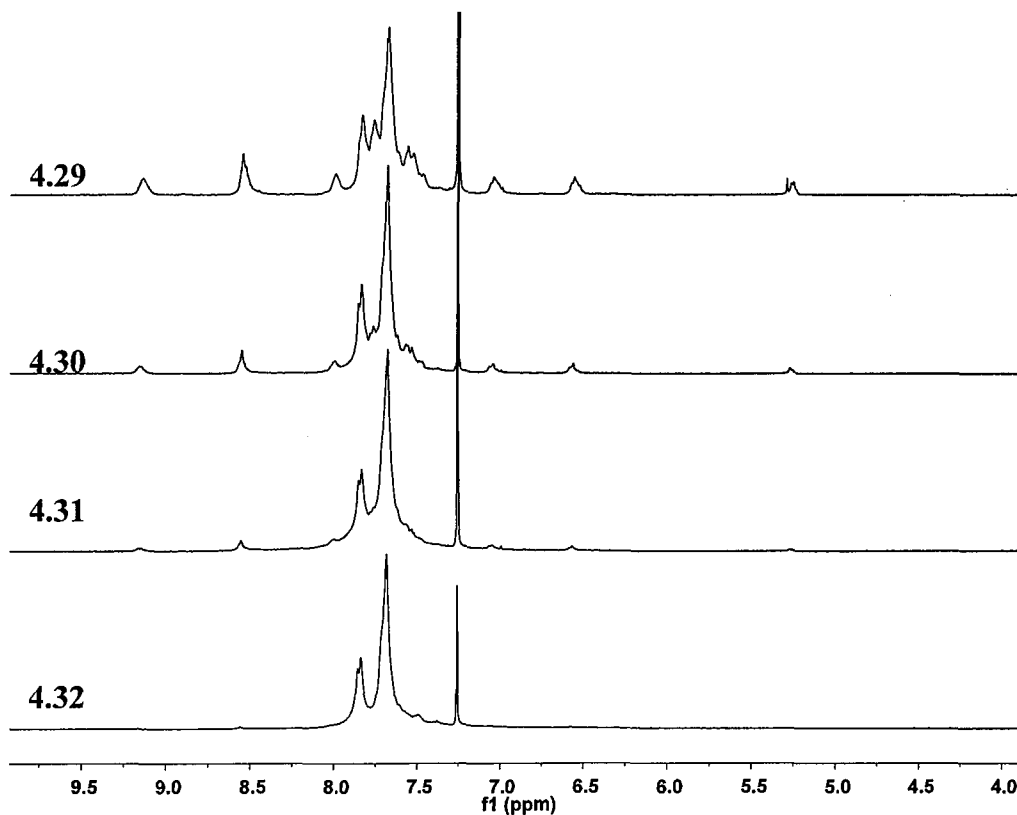
Figure 4.20: Synthesis of the random copolymers

The reactions all proceeded in good yields to afford red fibers. All the copolymers were characterized by NMR, GPC, and elemental analysis.

4.2.6 Calculating the iridium loading in the random copolymers

Figure 4.21: ^1H NMR spectra of the random copolymers

The ^1H NMR spectra of the random co-polymers are very similar to those of the alternating copolymers (Fig. 4.21 vs Fig. 4.18). A close up of the aromatic region is shown in Fig. 4.22.

Figure 4.22: ^1H NMR spectra of the aromatic region of the random copolymers

Integration of the iridium complex peak at ~9.2 ppm relative to those of the alkyl chains (~1.3 – 0.5 ppm) on the fluorene units was again used to estimate the percentage incorporation of the iridium complex (table 4.4). In contrast to the polymers synthesized *via* the macromonomer approach, there was no evidence of iridium complex terminated polymers. Furthermore, the signals originating from the iridium complex appeared broader than those synthesized by the previous method.

Polymer	Feed ratio / mol% (y) ^a	Yield / %	M _n ^b kDa	M _w ^b kDa	PDI ^b	Complex incorporation / mol% (y) ^c
4.29	14.3	70	9.9	27.6	2.8	12.8
4.30	6.7	82	43.9	98.7	2.2	6.1
4.31	3.3	93	72.2	195.5	2.7	3.1
4.32	1.8	88	49.0	108.4	2.2	1.1

Table 4.4: Random oligofluorene-iridium complex polymerization data

a) From reaction stoichiometry; b) Measured by GPC using PS standards and THF as eluent; c) Estimated from ¹H NMR

As can be seen from table 4.4, the actual incorporation ratio (y) is slightly lower than the feed ratio, which indicates that concentration drift is occurring. However, the extent of this phenomenon cannot be assessed as there are likely to be significant errors in the integration of these spectra. This is due to the broad nature of the peaks and in the cases of the polymers containing low iridium loading levels, the low signal to noise ratio.

However, a sufficiently large number of polymer samples, bearing a wide enough distribution of iridium loading concentrations has been prepared that will allow a thorough photophysical investigation into the differences between alternating and random iridium containing copolymers.

4.2.6.1 End group analysis

MALDI-TOF analysis of the randomly synthesized iridium complex containing polyfluorenes revealed several series of peaks that corresponded to either di-bromo, α -

bromo- ω -H, or di-H terminated oligofluorenes. The reason for the presence of the end-capping bromine atoms is a result of the random nature of the polymerization where it would now be possible to have either boronic ester (which are subsequently hydrolyzed) or bromine end groups.

4.3 Photophysical properties of the alternating and random copolymers

4.3.1 Absorption Spectroscopy

The UV-Vis spectra of the alternating iridium complex-oligofluorene polymers are shown below (Fig.4.23). The peak maxima (370 – 390 nm) increase in wavelength corresponding with the increasing length of the oligofluorene segments, as is the case for the oligofluorene macromonomers (Fig 4.14). The increase in absorption maxima of macromonomers **4.10** (fluorene trimer) and **4.13** (fluorene pentamer) compared to those of the copolymers **4.23** and **4.24** is due to the slight extension of conjugation onto the iridium complex aromatic ligand system. The peak shoulder that is visible at ~ 300 nm and the low intensity absorptions between 425 and 500 nm, correspond to absorption from the iridium complex ligand (π - π^* transition and MLCT transitions respectively) and decrease in intensity as the complex mol % decreases.

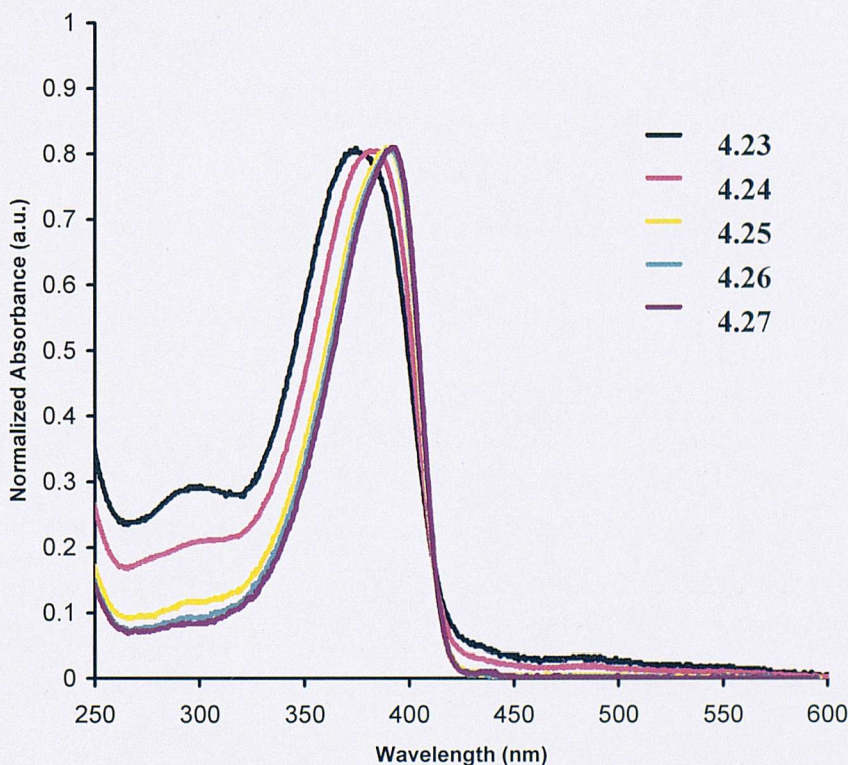


Figure 4.23: Absorption spectra of alternating copolymers (DCM, $\sim 10^{-5}$ M)

The UV-Vis spectra for the random copolymers are shown below (Fig. 4.24). As in the case of the alternating copolymers, the predominant absorption corresponds to the $\pi \rightarrow \pi^*$ transition of the oligofluorene chain. The maxima for **4.24**, which has the highest iridium complex incorporation, is at the same wavelength (384 nm) as that for **4.29** indicating that they have a similar oligofluorene chain length. This is not surprising as the two aforementioned compounds have very similar iridium complex molar concentrations (12.8% cf. 14.3%)

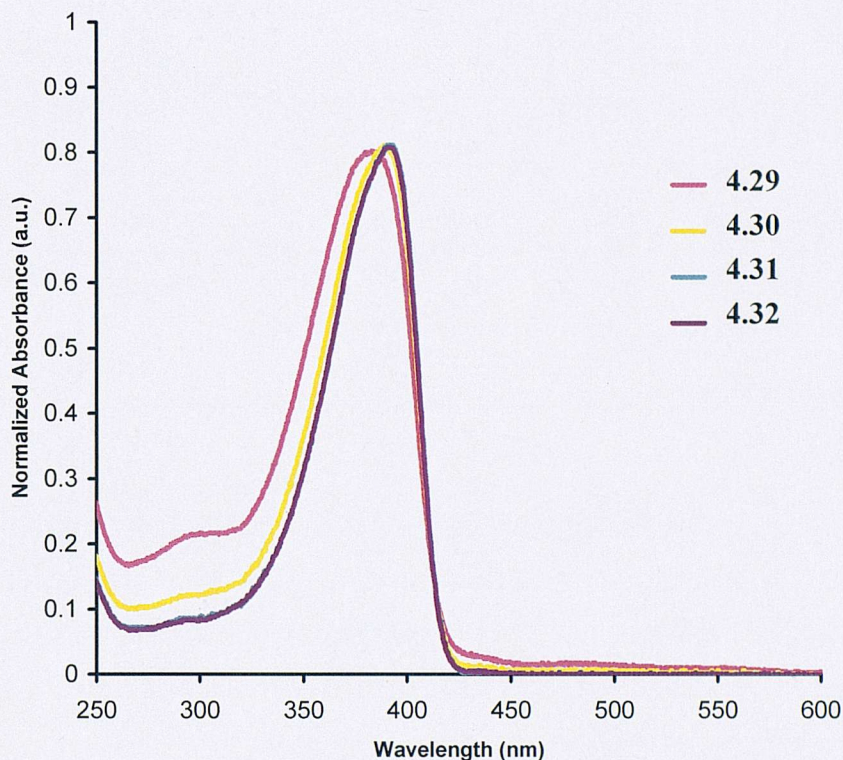


Figure 4.24: Absorption spectra of the random copolymers (DCM, $\sim 10^{-5}$ M)

4.3.2 Solution photoluminescence of the alternating and random copolymers

In order to ascertain the effect of maintaining the emissive phosphors at fixed intervals, in the alternating copolymers, solution photoluminescence (PL) measurements were performed. The benefits of solution measurements are that interchain effects are minimized due to the polymer chains being solvated. This prevents excitons being transferred from one chain to another as the energy transfer processes for this to occur are typically fairly short range (see Introduction), allowing a more detailed understanding of the differences between the two types of synthesized polymer. There is the possibility that the chains may collide or aggregate in solution but this was minimized by performing the measurements at high dilutions.

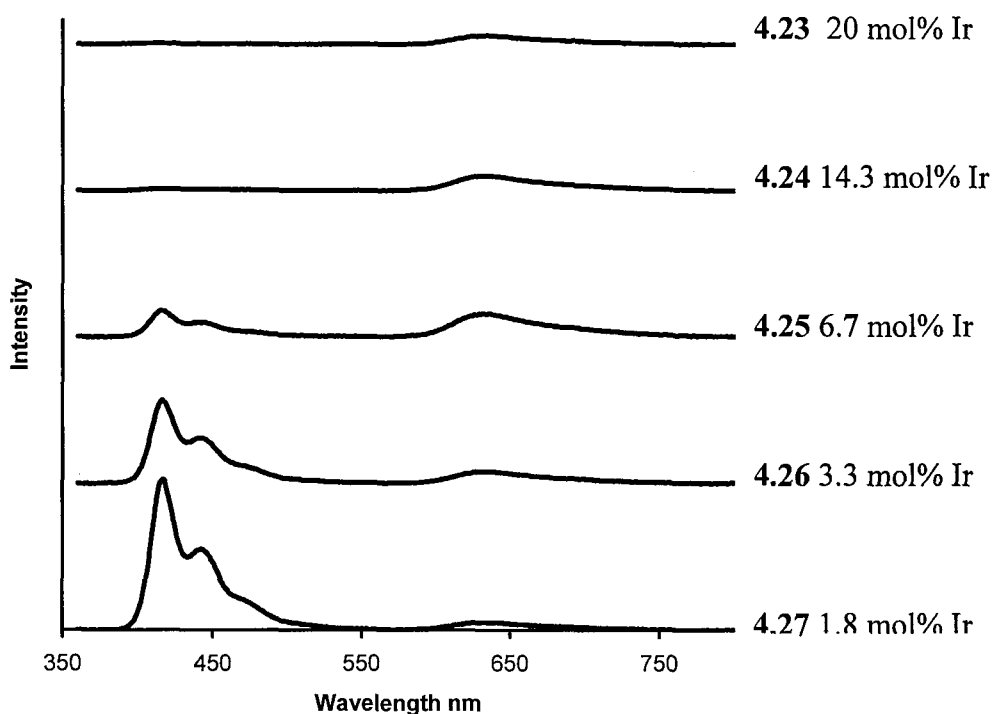


Figure 4.25: Photoluminescence spectra of the alternating copolymers (DCM, Max. Abs ~0.1, Ex. 350 nm)

Fig 4.25 shows the degassed solution PL spectra of the alternating copolymers. At low iridium loadings (4.27 and 4.26) emission is dominated by a peak at ~430 nm, which corresponds to fluorescence from the oligofluorene main chain. This is due to the low concentration of the iridium complex resulting in incomplete energy transfer from the oligofluorene segments onto the metal complex. As the amount of iridium incorporation increases, the emission from the oligofluorene main chain decreases until there is complete transfer of the oligofluorene excitons onto the iridium phosphor, at iridium molar % of 14.3% and higher.

The emission from the iridium complex can be seen at ~630 nm. The red emission is visible in all the copolymer samples, but reaches its maximum intensity in polymer 4.25 which contains 6.7 mol% of the iridium complex.

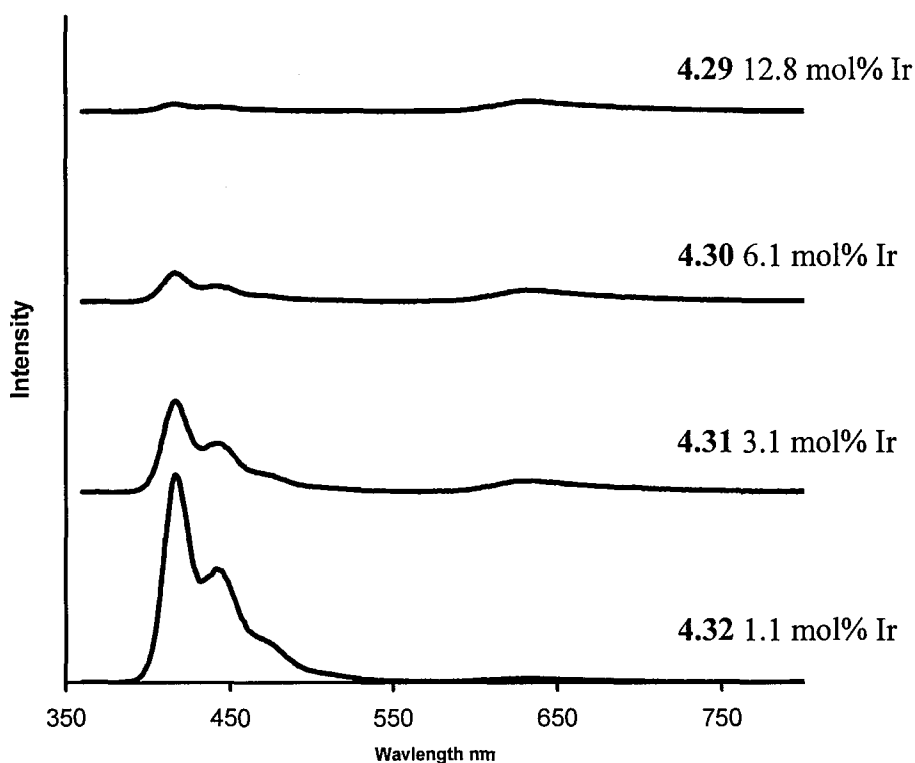


Figure 4.26: Photoluminescence spectra of the random copolymers (DCM, Max. Abs. \sim 0.1, Ex. 350 nm)

Fig. 4.26 displays the solution PL emission spectrum of the random copolymers. It is again possible to observe emission from the oligofluorene segments (\sim 430 nm) and the iridium complex (\sim 650 nm). In contrast to the alternating copolymers, the oligofluorene emission is visible in all samples, and there is lower intensity emission from the iridium complex relative to the oligofluorene. This is likely to be a consequence of the random copolymers being less homogenous. This would result in these samples containing regions with significantly less iridium complex percentage loading than others and as such showing poor energy transfer onto the iridium complex.

4.3.2.1 Solution quantum yields of the alternating and the random copolymers

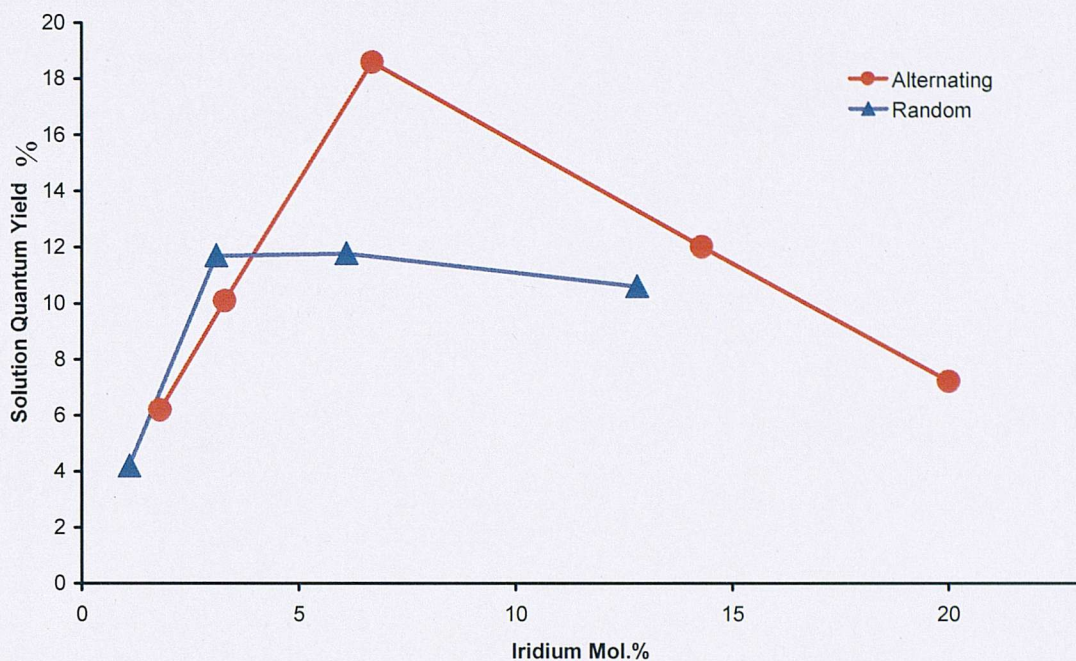


Figure 4.27: Solution phosphorescence quantum yield vs iridium mol% (DCM, $(\text{piq}_2)\text{Ir}(\text{acac})$ standard, $\Phi_{\text{ph}} = 20\%$, Ex. 350 nm)

Fig 4.27 shows the variation in solution phosphorescence quantum yield (PLQY) of the various copolymer samples measured against a standard ($[(\text{piq})_2\text{Ir}(\text{acac})]$ PLQY ($\Phi_{\text{ph}} = 20\%$)²⁷). At low iridium incorporations (< 5 mol%), both types of copolymer display a similar increase in quantum yield as the loading increases. This behavior is typical in both iridium containing polymers and iridium/polymer blends. The increase in quantum yield is due to an increase in energy transfer from host to guest due to the greater availability of guest molecules. The low level of iridium concentration means that in the random polymers it is unlikely that iridium phosphors have been incorporated near each other, so triplet-triplet annihilation is unlikely. At an iridium concentration of 6.7% the alternating copolymer quantum yield reaches a maximum of approx. 19%, compared to $\sim 10\%$ for the random copolymer analogue. This significant difference in efficiency is likely to be caused by two effects. i) Increased energy transfer in the alternating samples due to the regular presence of iridium complexes along each polymer chain. i.e in the random copolymer samples it is possible there are sections without any iridium complex incorporation and excitons generated in these sections cannot be transferred to an iridium complex. ii) Reduced T-T annihilation in the alternating polymers. In the same manner that in the random samples there are polymer chains with decreased iridium concentrations; there will be polymer chains with a greater than average number of

iridium complexes. This increased local concentration and proximity of guest molecules can allow for greater T-T annihilation and consequently a lower phosphorescent efficiency. Above 7 mol% iridium loading the PL efficiency of both types of copolymer decreases, this is likely to be a consequence of the increased proximity of the guest molecules leading to an increase in T-T annihilation.

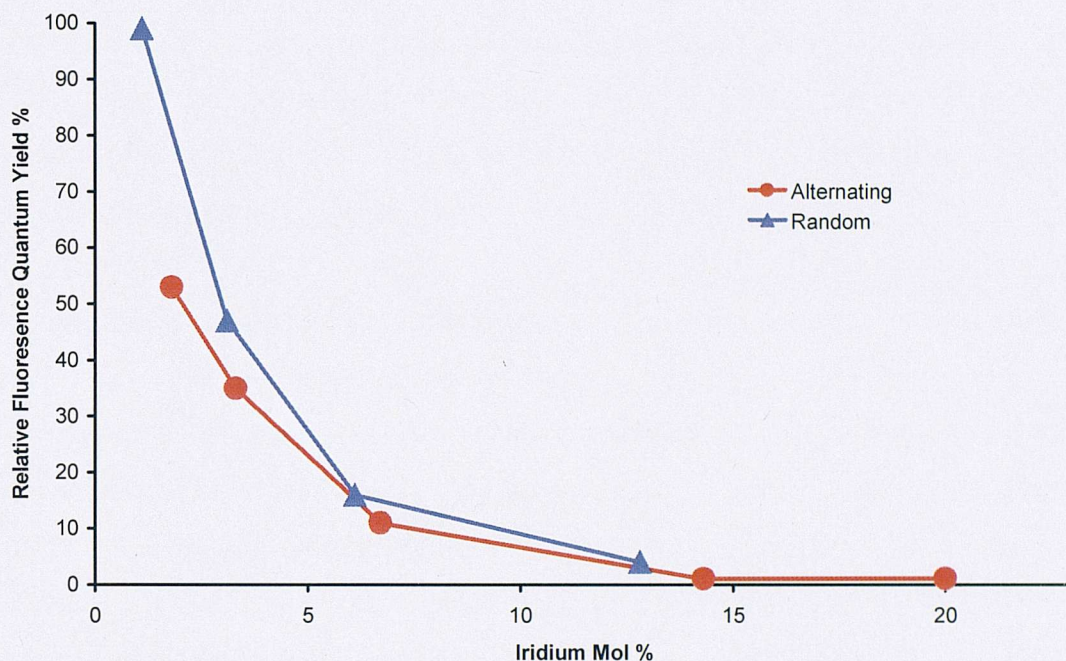


Figure 4.28: Relative fluorescence (~ 430 nm) solution quantum yield vs iridium mol% (DCM, $(\text{piq}_2)\text{Ir}(\text{acac})$ standard, $\Phi_{\text{ph}} = 20\%$, Ex. 350 nm)

Fig 4.28 shows the relative proportion of the emission which is due to fluorescence (i.e. from the oligofluorene chains) vs phosphorescence (i.e. from the iridium phosphors). These numbers are not absolute quantum yields as the standard used has a different emission wavelength (622 nm), and corrections to adjust for variations in instrument sensitivity have not been performed. However, they are useful as they indicate the extent of energy transfer from oligofluorene to iridium complex. At low iridium loadings there is almost twice as much singlet emission from the random copolymers than the alternating ones. Again, this is probably due to the inhomogeneous nature of the random copolymer resulting in areas on the polymer chains with little iridium content, preventing efficient transfer onto the iridium complex. At higher iridium molar concentrations, the relative fluorescence quantum yields are similar (and low) due to the increased quantity of the iridium phosphor onto which excitons can be transferred.

4.3.3 Thin film photoluminescence measurements of the alternating and random copolymers

Although solution measurements give insight into the extent of T-T annihilation and the efficiency of the energy transfer from fluorene to iridium complex, OLEDs are solid state devices, and so conclusions drawn from solution measurements may not necessarily be applicable. In thin films, polymer chains are in close proximity and as such, interchain interactions occur and are important. This allows increased energy transfer from host to guest. However, thin films also increase the proximity of guest molecules to one another leading to an increase in T-T annihilation and other concentration quenching effects.

The thin film PL spectra of the alternating copolymers are shown below (Fig. 4.29). It is immediately obvious that the emission from the oligofluorene segments is absent in all but the sample with the lowest iridium molar concentration **4.27**. This indicates that the energy transfer from the oligofluorene to the iridium complex is much more efficient than in solution. This is expected as excitons can now be transferred in an inter- or intramolecular fashion to the iridium complex. As in the case of the solution PL measurements, the intensity of the emission increases with increasing iridium mol% until it reaches a maximum at 6.7% loading. After this point, T-T annihilation becomes dominant and the intensity of the emission decreases.

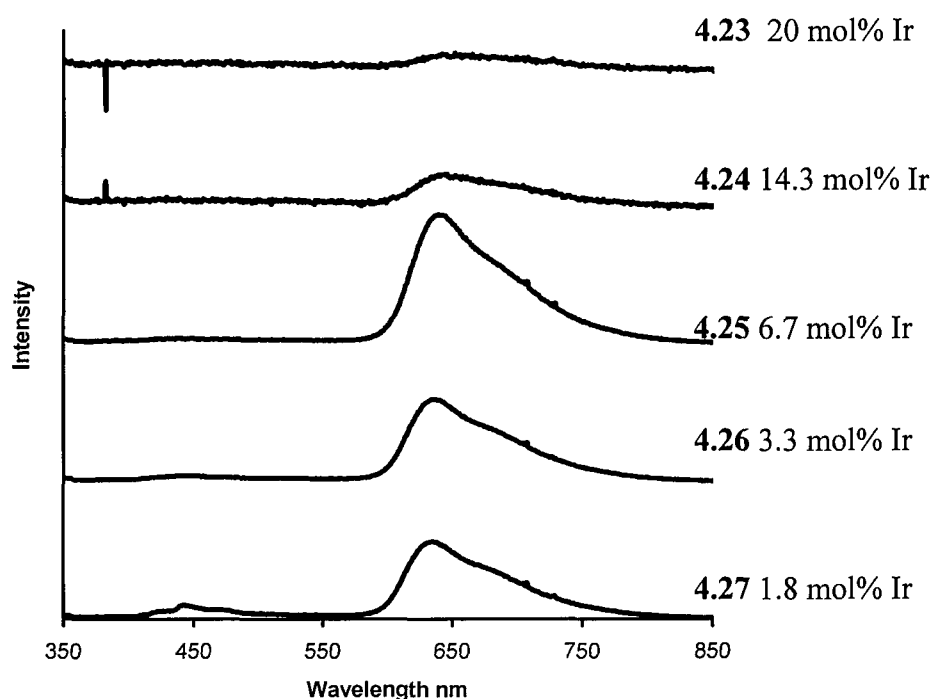


Figure 4.29: Thin film photoluminescence spectra of the alternating copolymers (integrating sphere, Ex. 325 nm)

Fig 4.30 shows the thin film PL spectra of the random copolymers. As in the case of the alternating copolymers, emission from the oligofluorene segments is drastically reduced. The phosphorescence emission intensity increases as the iridium mol% is increased, although the maximum intensity is reached at a lower concentration than the alternating samples (3.1% cf 6.7%). This indicates that in the solid state, the decreased homogeneity of the random copolymers allows T-T annihilation to become significant at lower iridium loading levels.

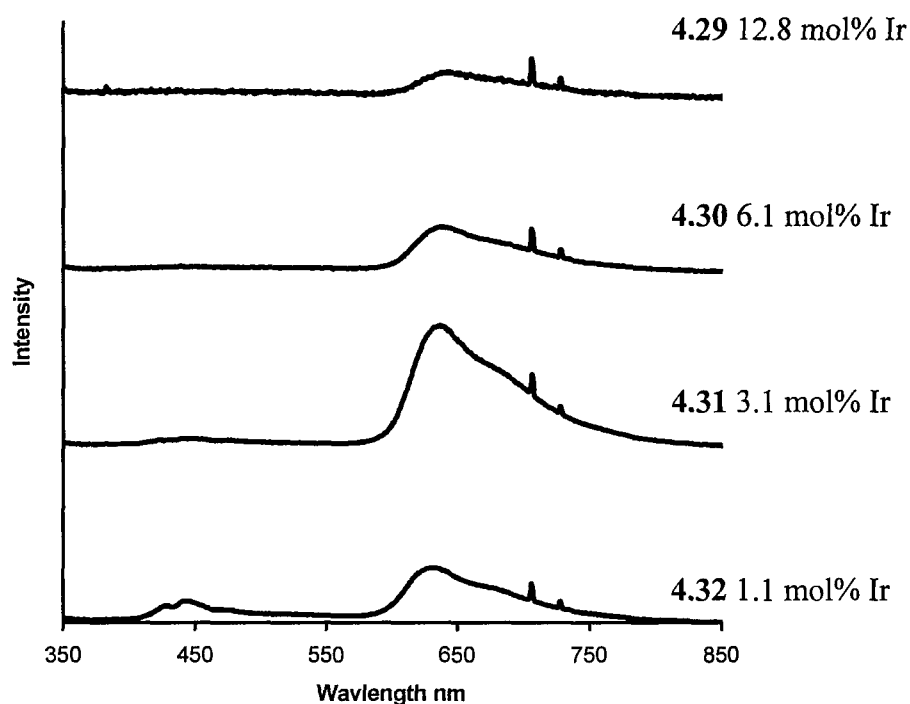


Figure 4.30: Thin film photoluminescence spectra of the random copolymers (integrating sphere, Ex. 325 nm)

4.3.3.1 Thin Film Quantum Yields of the Alternating and the Random Copolymers

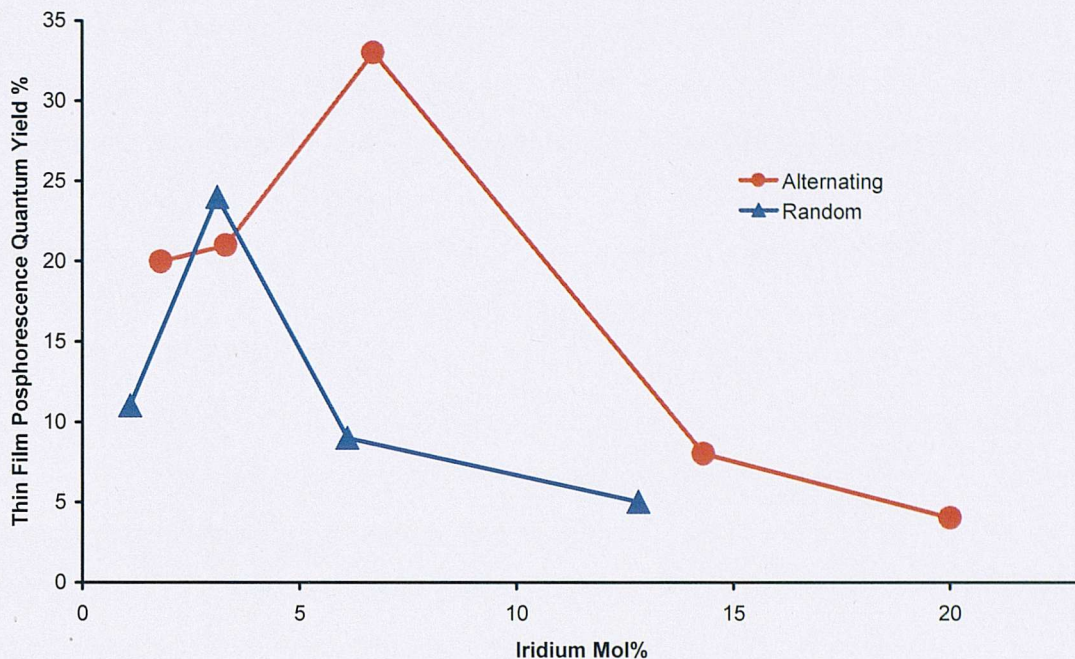


Figure 4.31: The variation of the thin film phosphorescence quantum yields with iridium mol% (integrating sphere, Ex. 375 nm)

Fig 4.31 shows the thin film phosphorescence quantum yields as measured using an integrating sphere. Due to the nature of the experiment, these values are absolute as they are not measured against a standard, as in the case of the solution quantum yields.

Overall it can clearly be seen that the quantum yields of the alternating copolymers are greater than those of the randomly synthesized ones. In the case of the alternating copolymers, there is a clear maximum ($\Phi_{\text{Ph}} \sim 35\%$) at an iridium loading of 6.7%. In the random copolymers, the maximum ($\Phi_{\text{Ph}} \sim 25\%$) occurs at a lower iridium loading level (3.1 mol%). The reason for this is almost certainly due to the reduced T-T annihilation in the alternating copolymers relative to the random ones. The fixed distances between the phosphors in the solid state ensures that T-T annihilation is kept to a minimum whereas in the case of the random samples, the inhomogeneous distribution of the guest molecules increases the amount of T-T annihilation. At high iridium loadings, as observed in the solution measurements, the T-T annihilation is prevalent in both sample types, significantly reducing the efficiency.

4.4 Conclusions

A series of novel iridium complex-poly/oligofluorene copolymers have been synthesized and fully characterized. The molar incorporation of the complex in the copolymer was varied between 1 – 20 mol %, to obtain the most efficient emission.

By varying the method of synthesis, it was possible to study the effect of having the incorporated iridium complex at either fixed or random intervals along the copolymer chain. Pre-synthesizing an oligofluorene chain segment and subsequent copolymerization with the iridium complex provided access to alternating copolymers (i.e. where the iridium complexes were positioned at fixed intervals along the oligo/polyfluorene chain). In contrast, a one-pot, 3 component A-A, B-B, B'-B' type polymerization produced the analogous random copolymers - i.e. where the iridium complexes were distributed randomly along the oligo/polyfluorene chain.

All the co-polymers displayed excellent energy transfer from the oligofluorene segments onto the iridium complex, resulting in strong red (~650 nm) phosphorescence, and negligible fluorescence from the polymer backbone in the thin film.

In solution measurements, it was found that the polymers containing an iridium complex at fixed intervals (alternating copolymers) displayed significantly more efficient emission, which is thought to be due to an improved spatial separation of the phosphorescent complexes, which results in a decrease in triplet-triplet annihilation.

In thin film measurements, an optimum emission quantum yield of ~35% was obtained at an iridium complex molar incorporation of 6.7% for the alternating copolymers. This is significantly greater than the optimum emission quantum yield of ~25% obtained at 3.1 mol% for the random copolymers. These findings clearly illustrate the benefits of maintaining the iridium complexes as far apart as possible and highlight the importance of the copolymer structure in determining PL efficiency. It should be mentioned that such alternating copolymer structures have only been rarely described in the literature,¹⁵⁵ and there are no examples using iridium complexes.

Chapter 5: Asymmetric

“Multifunctional” Iridium Complexes

5.1 Introduction

Much work has been conducted into the design of novel materials that facilitate the transport and injection of electrons and holes into OLEDs. It is necessary to have a balance of electrons and holes reaching the emissive layer simultaneously, in order to generate the maximum number of excitons which can decay radiatively.^{6,156-158}

A small amount of work has been conducted into the synthesis of emissive phosphors that possess either electron and/or hole transporting moieties to enhance the transport and trapping of charge on the phosphor.^{41,74,82,159-164}

5.1.1 Multifunctional iridium complexes

Ho *et al* synthesized a bis(fluorenyl pyridine)iridium complex **5.1** with an end-capping carbazole unit in an attempt to increase the hole transport properties of the complex. OLEDs prepared with this material displayed excellent emissive properties, although it was not unambiguously demonstrated that this was due to the incorporation of the hole transporting units.¹⁶¹

A more recent publication by the same authors demonstrated a carbazolyl pyridyl iridium complex containing a trifluoromethyl pyridyl substituent **5.2**. The carbazolyl unit is proposed to increase the hole transporting ability of the molecule, whilst the trifluoromethyl group was attached in an effort to increase the electron mobility, and suppress non-radiative decay. High efficiency orange OLEDs were prepared demonstrating the suitability of the iridium complex, although, as before, the role of the various “components” was not thoroughly investigated.⁷⁴

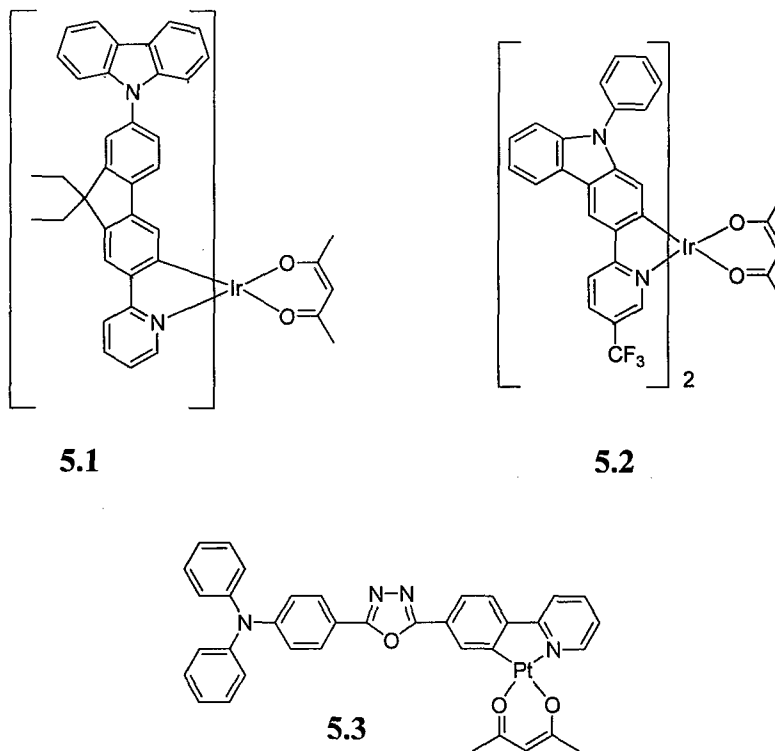


Figure 5.1: Multifunctional metal complexes

A thorough investigation into multifunctional cyclometallated platinum complexes was undertaken by He *et al.* Hole transporting triarylamino groups and electron transporting oxadiazole were attached to a phenyl pyridyl cyclometallated platinum complex **5.3**. OLEDs constructed with complex **5.3** and other similar derivatives displayed simultaneous singlet and triplet emission resulting in white light emission at certain driving voltages.¹⁶²

5.1.2 Multifunctional polymeric/dendritic materials

Similar efforts to synthesize multifunctional polymeric and dendritic compounds have been undertaken.^{41,82,159,164} The benefits of incorporation of the emissive phosphor into a host type compound have been previously discussed, and extra hole and electron transporting units are incorporated with a view to further simplifying device construction.

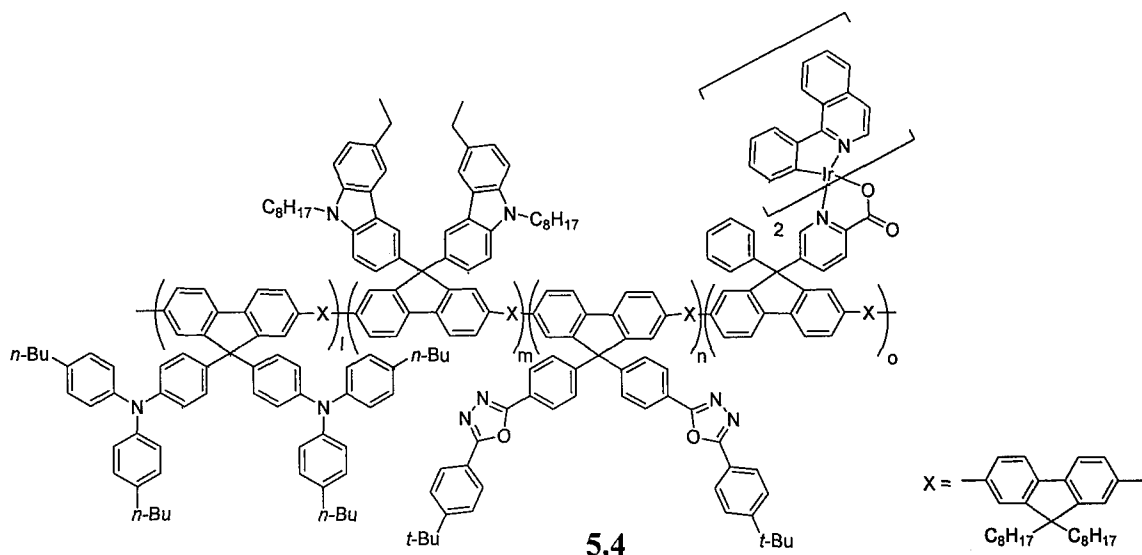


Figure 5.2: Multifunctional electrophosphorescent polymer

Yang *et al* reported the synthesis of a highly elaborate red electrophosphorescent polymer **5.4**, containing polyfluorene as a conducting polymer backbone, with pendant hole transporting triarylamine and carbazole units, electron transporting oxadiazole units and emissive phenyl isoquinoline iridium phosphors. A simple OLED device constructed from polymer **5.4** gave good efficiencies of $\sim 9\%$.¹⁵⁹

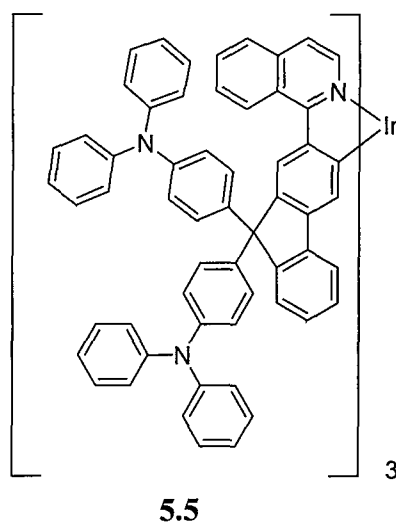


Figure 5.3: Multifunctional iridium dendrimer

A phenylisoquinoline iridium based dendrimer containing charge transporting triarylamine dendrons was developed by Zhou *et al*. The triarylamine units were attached in efforts to reduce the barrier for hole injection, and incorporation of **5.5** into an OLED afforded a red emitting device with a respectable 7% efficiency.⁸²

5.1.3 Synthetic plan

The presence of two cyclometallating ligands in the iridium complexes, discussed in previous chapters, and the potential benefits of hole and electron transporting units, as highlighted above, lends itself to the idea of synthesizing an asymmetric iridium complex where a hole transporting moiety is attached to one ligand, and an electron transporting moiety is attached to another. Consequently, one ligand would be tailored towards trapping holes on the emissive core, and the other, electrons, with the ultimate goal being to increase exciton generation on the phosphor.

If the attached hole and electron transporting units are polymeric, then it is possible that microphase separation of the hole and electron transporting units could occur leading to various film morphologies typical of diblock co-polymers. The effect of copolymer morphology has been extensively studied in the field of organic photovoltaics and found to have a significant effect on performance, but has been largely ignored in the construction of OLEDs. This is perhaps surprising as the transport of charge through a thin film depends extensively on its morphology.¹⁶⁵⁻¹⁶⁸

5.1.4 Asymmetric iridium complexes

An area of iridium complex coordination chemistry that has received little attention is that of asymmetric complex synthesis. Several investigations have been carried out on the variation of the ancillary ligand in bis cyclometallated complexes and this has been found to have significant effects on the photophysical properties.^{31,169-172} The emissive iridium complexes, however, typically possess either two or three identical cyclometallating ligands and thus far there has been little investigation into the synthesis or effect of having different ligands in a single complex.¹⁷³⁻¹⁷⁵

There have been very few reported syntheses of tris-cyclometallating asymmetric iridium complexes. Typically the reported syntheses are low yielding and are prone to ligand scrambling. The use of low reaction temperatures and silver salts has allowed isolation of a few examples of tris cyclometallated iridium complexes with different ligands.^{131,176-181}

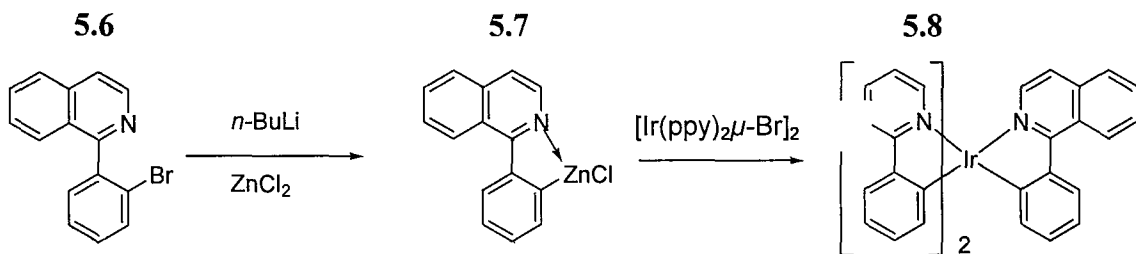


Figure 5.4: Synthesis of asymmetric tris-cyclometallated iridium complexes

A higher yielding method of synthesizing asymmetric tris iridium complexes was developed by Huo *et al* where a ligand with a 1,2 substituted bromine atom **5.6** is treated with butyllithium and then zinc chloride to generate complex **5.7**. Subsequent reaction with a bromo bridged iridium complex allows isolation of the mer tris asymmetric iridium complex **5.8**, in high yields.¹⁷⁶

Photophysical and theoretical studies on these types of compounds have revealed that emission only originates from the mixed metal-ligand orbitals with the lowest energy, and the remaining ligands do not participate in emission. In the above case only red-emission is observed (due to the iridium-phenyl isoquinoline portion), as opposed to green emission (originating from the iridium-phenylpyridine portion), as might be expected.^{131,176,177,179}

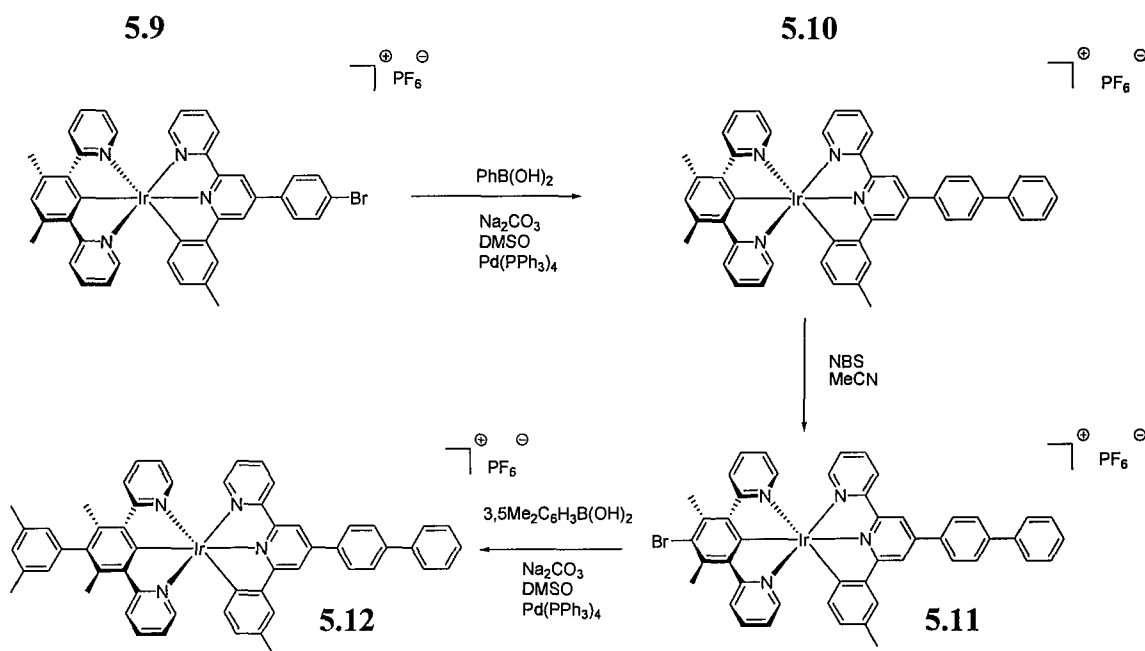


Figure 5.5: Stepwise synthesis of asymmetric iridium complex

Impressive work on asymmetric iridium complex synthesis has been undertaken by the Williams group.¹⁸²⁻¹⁸⁵ A range of charged and neutral asymmetric complexes containing

two different tridentate ligands have been developed. Furthermore, selective functionalization of these complexes has been demonstrated allowing attachment of different groups at different positions through cross coupling reactions (5.9 – 5.12). Unfortunately, photodegradation is observed for the neutral complexes limiting their potential use in OLEDs.¹⁸⁵

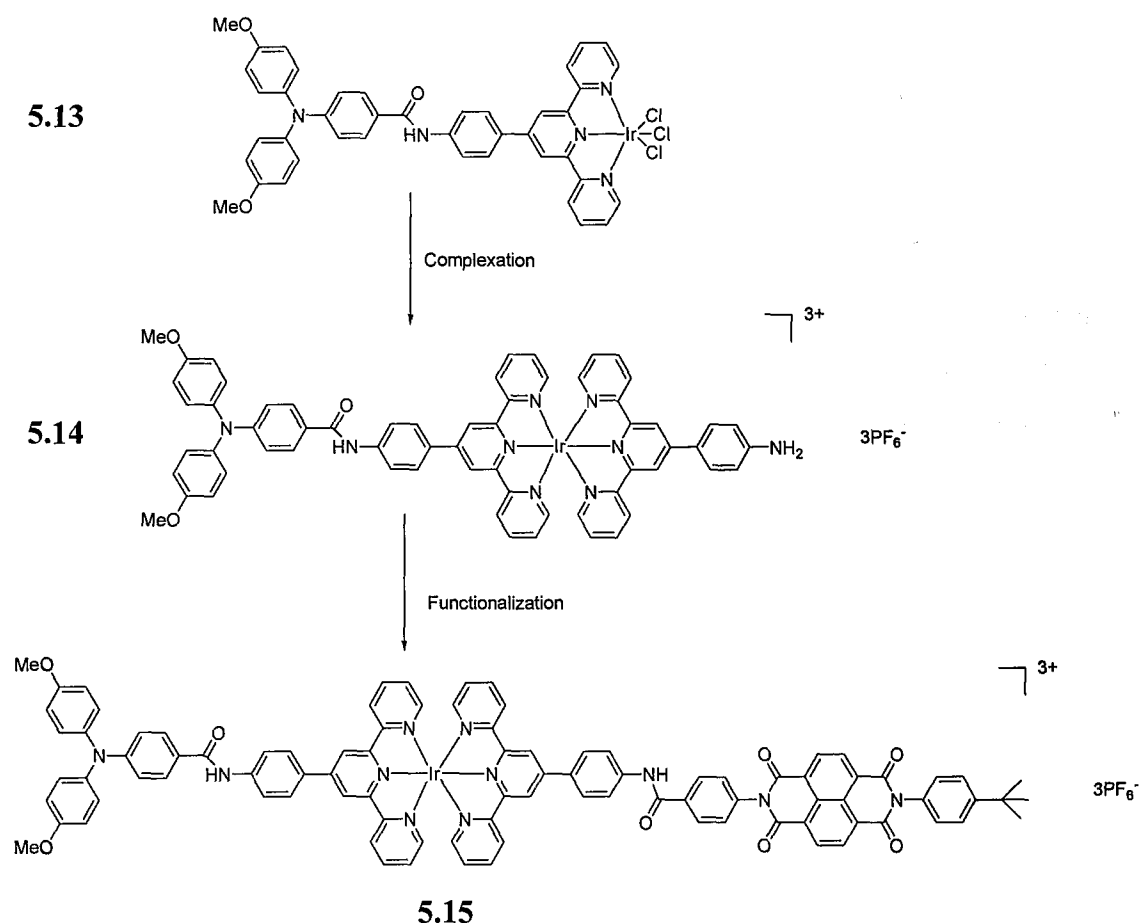


Figure 5.6: Synthesis of asymmetric donor-iridium complex-acceptor assembly

An excellent example of a multifunctional asymmetric iridium complex was synthesized by Flamigni *et al.* A brief overview of the synthesis is shown above (Fig. 5.6). A donor substituted ligand was complexed to iridium 5.13; followed by another ligand 5.14. Finally an acceptor unit was attached to the second ligand through an amide linker 5.15, with moderate yields over all the steps. The asymmetric complex was used to study the generation of a charge separated state.¹⁸⁶

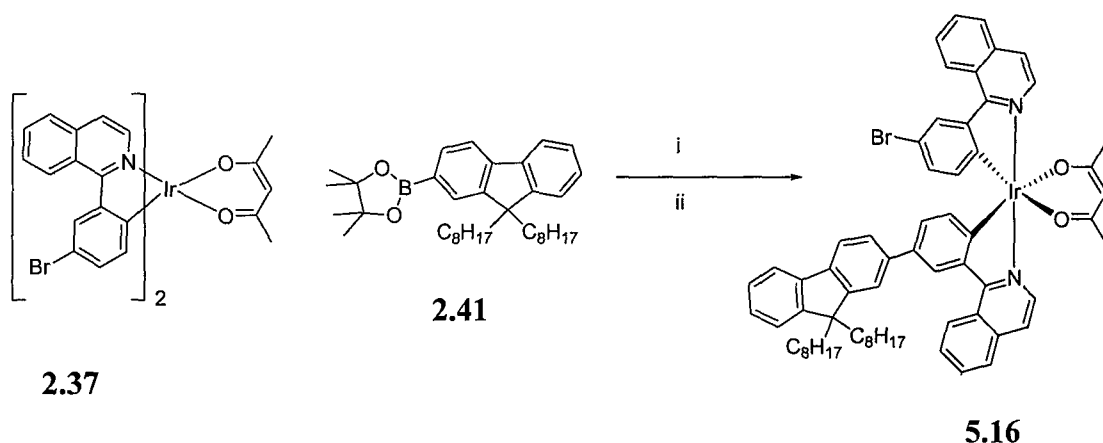
5.1.5 Target materials

As the chemistry of phenylisoquinoline iridium complexes has been extensively studied in this work, it was decided to use these in attempts to synthesize novel asymmetric multifunctional complexes. The Suzuki coupling of bromo substituted iridium complexes has also been demonstrated throughout this work and allows further functionalization of the complexes. It was decided to use Suzuki coupling chemistry to synthesize the novel complexes. The aim of this study is to develop new synthetic methods towards asymmetric materials, and as a consequence fluorene and carbazole units will be used in the synthesis of these novel compounds as their chemistry is well known. Although polyfluorene and polycarbazole have desirable electronic properties with differing electron and hole transporting properties, they are not electronically the best polymers which could be used.^{6,156} As a result, this study is intended to be a proof of principle which, if successful, could be applied to different polymeric materials to optimize the electronic properties of these systems.

5.2 Synthesis

Before any attempts at synthesizing polymeric complexes, it is important to establish if it is possible with the use of a model compound. Thus, the first synthetic target is an asymmetric multifunctional well defined iridium complex.

5.2.1 Well defined complexes



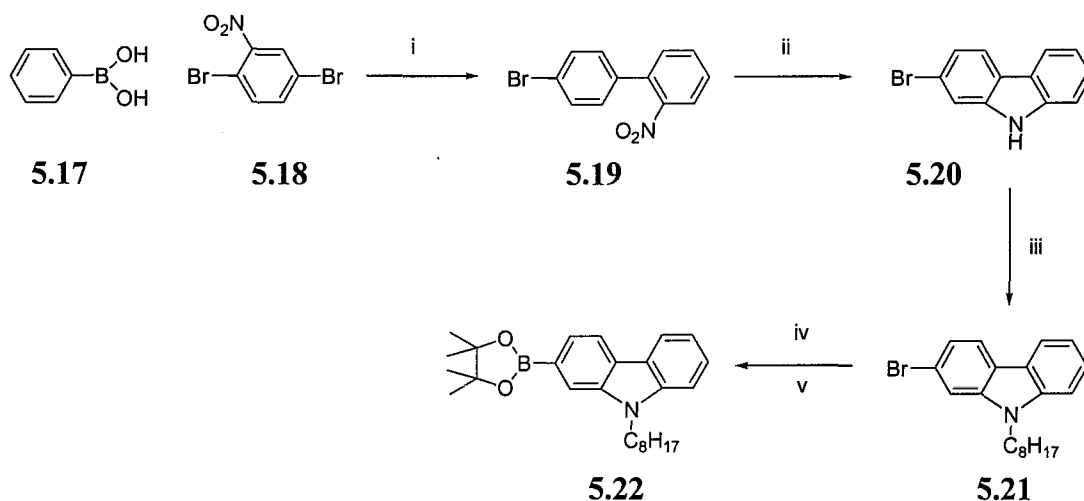
Reagents and conditions: i) Pd(OAc)₂, PPh₃, Tol, TEAOH_(aq), 90 °C; ii) acetylacetonate, Na₂CO₃, Tol, 2-ethoxyethanol, 110 °C, 45%

Figure 5.7: Synthesis of asymmetric iridium complex

The reaction of the previously synthesized complex, **2.37**, with one equivalent of mono boronic ester functionalized fluorene moiety, **2.41**, afforded a distribution of starting material **2.37**, mono fluorenyl substituted complex, **5.16**, and di-fluorenyl substituted complex, **2.52**, in approximately 20%, 20% and 40% yields respectively. All three complexes possess very similar polarities and purification via column chromatography was extremely challenging. The non statistical distribution of products indicates an increase in reactivity towards Suzuki coupling of complex **5.16** relative to the starting material **2.37**. It is believed that the reason for this is the proximity of another bromine group on the same complex which can undergo an intramolecular oxidative addition reaction with the palladium catalyst. Similar preferential Suzuki coupling reactions have been observed in aryl halides bearing multiple halogen substituents.^{187,188} It was found that the yield of complex **5.16** could be increased by using 1.5 equivalents of the fluorenyl moiety **2.41** resulting in its complete consumption and allowed isolation of the desired complex in 45% yield out of a maximum possible 50%. The ¹H NMR spectrum of complex **5.16** is shown below (Fig. 5.10) and will be subsequently discussed.

5.2.2 Synthesis of the asymmetric iridium complex

Having synthesized an unsymmetrical complex with a remaining bromine group **5.16**, further substitution through another coupling reaction can be achieved. It was decided to use a carbazole derivative. Carbazole compounds typically have reasonable hole transporting abilities, and its structural similarity to fluorene was planned to allow simple ¹H NMR analysis of the asymmetric complexes.¹⁶³

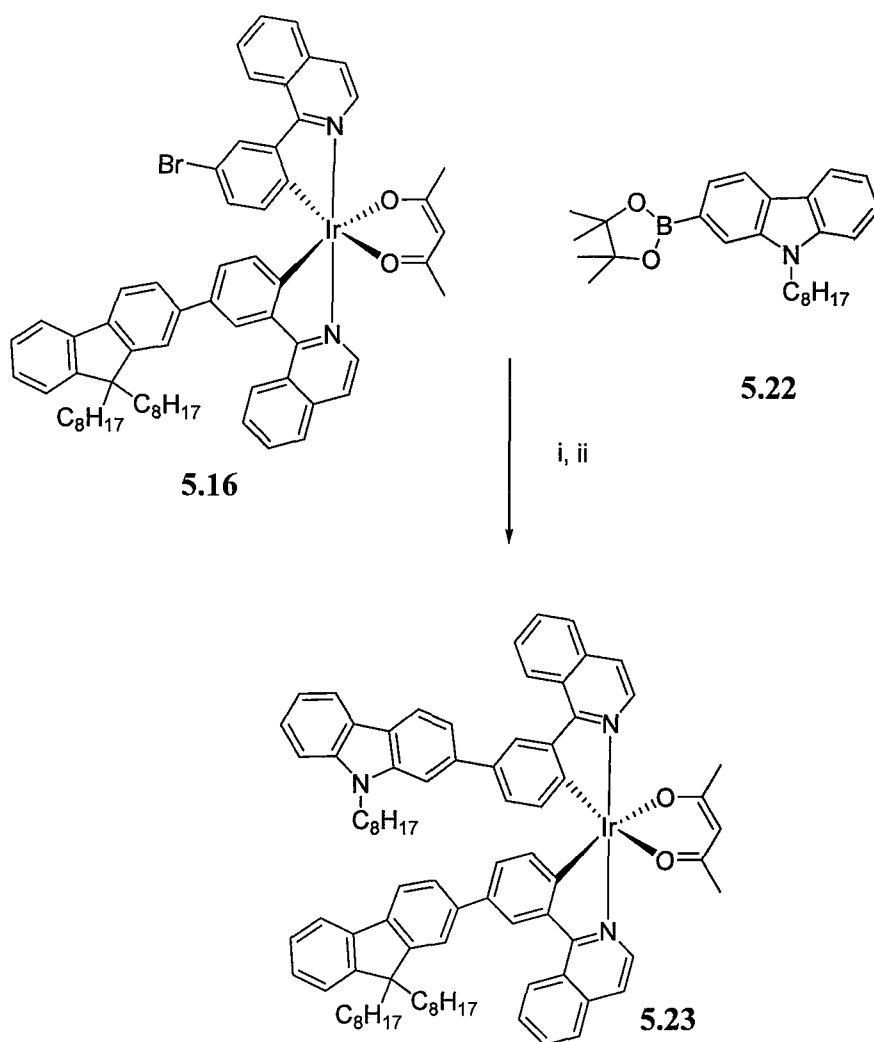


Reagents and conditions: i) Pd(PPh₃)₄, Tol, 2M Na₂CO_{3(aq)}, 90 °C; ii) PPh₃, *o*-dichlorobenzene, reflux, 20%; iii) bromooctane, K₂CO₃, DMF, 80 °C, 78%; iv) *n*-BuLi, THF, -78 °C v) 2-Isopropoxy-4,4,5,5-tetramethyl-1,3,2-dioxaborolane, -78 °C → room temperature, 83%

Figure 5.8: Synthesis of 2-boronic ester substituted carbazole

In order to prepare the asymmetric iridium complex, a boronic ester substituted carbazole was prepared. The Suzuki coupling of phenyl boronic acid **5.17** and di-bromo nitrophenyl **5.18** afforded a mixture of **5.19** and a number of side-products which were inseparable by all attempted methods. Similar results were obtained by Tavasli *et al*¹⁸⁹ who attributed the impurities to other coupling products. Subsequent cyclization to afford the mono-bromo substituted carbazole **5.20** was achieved in a modest 20% yield, over 2 steps. Alkylation, under basic conditions, afforded **5.21** as white crystals in excellent yield. Conversion to the boronic ester substituted carbazole compound, **5.22**, was achieved in good yield using identical conditions to those for the fluorene analogue.

5.2.3 Completion of asymmetric multifunctional iridium complex



Reagents and conditions: i) Pd(OAc)₂, PPh₃, Tol, TEAOH_(aq), 90 °C; ii) acetylacetonate, Na₂CO₃, Tol, 2-ethoxyethanol, 110 °C, 87%

Figure 5.9: Synthesis of multifunctional asymmetric iridium complex

Suzuki coupling of complex **5.16** with the carbazole moiety **5.22** afforded the completed unsymmetrical complex **5.23** in good yield. To the best of our knowledge, this is the first example of a bis cyclometallated iridium complex with differing bidentate cyclometallating ligands.

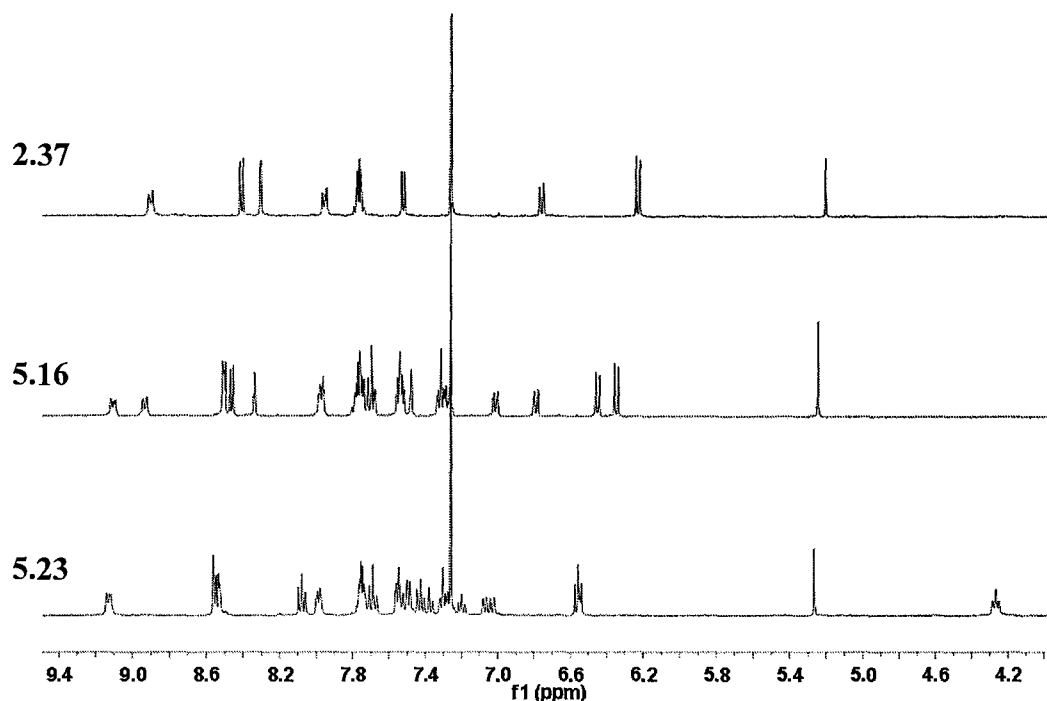
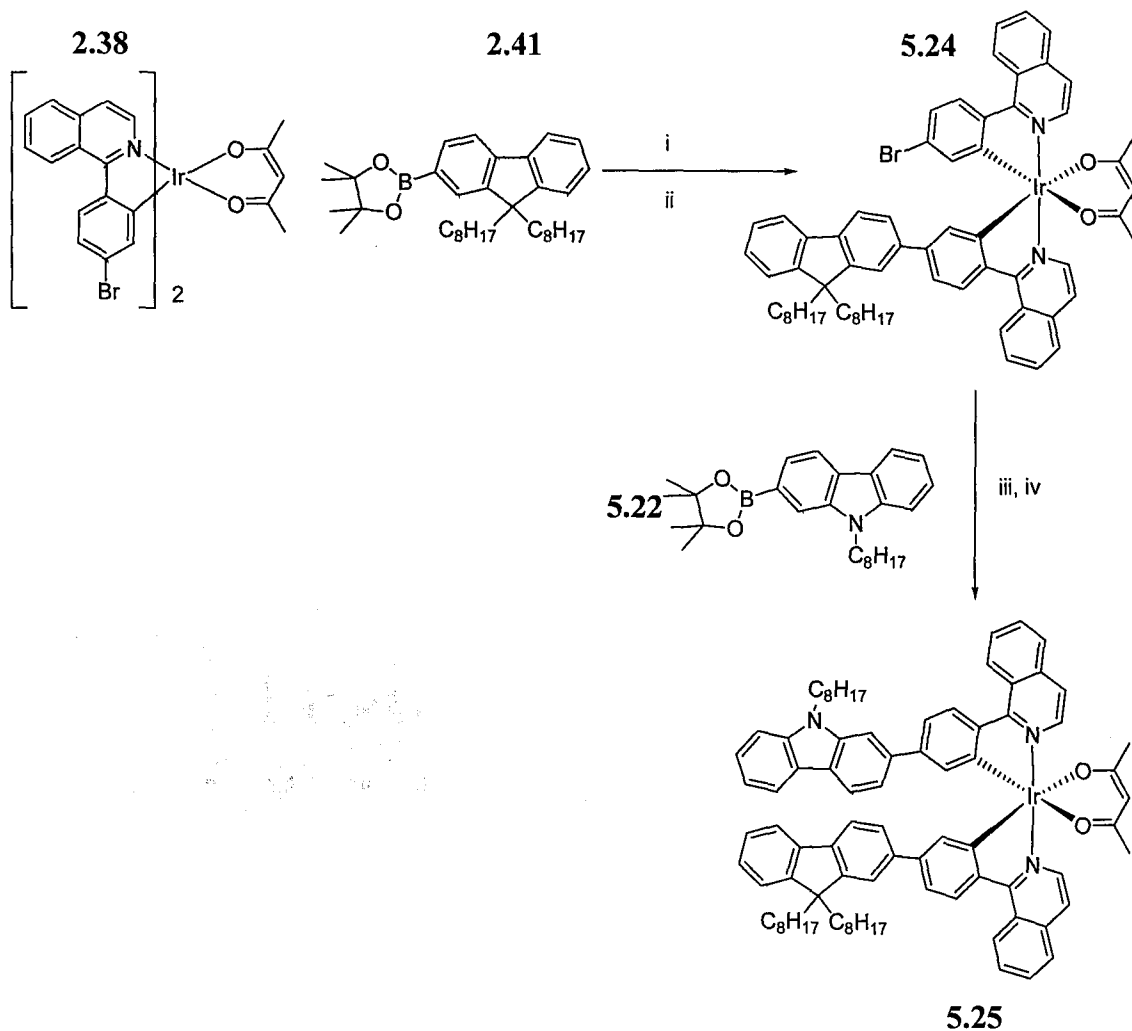


Figure 5.10: ^1H NMR spectra of asymmetric complexes

The ^1H NMR spectra of the starting material **2.37** and the two unsymmetrical iridium complexes **5.16** and **5.23** are shown above (Fig. 5.10). The protons on the two ligands of complex **5.16** are in significantly different environments which results in two sets of peaks being visible. The peaks at ~ 9 ppm (H-8) are very useful diagnostically and demonstrate the obvious asymmetry present in complex **5.16**. Introduction of the carbazole substituent reduces the amount of asymmetry present in the complex due to the structural similarity of the two ligands. As a consequence, only a single multiplet is observed at ~ 9 ppm which integrates to 2 protons. The peak at ~ 4.2 ppm corresponds to the protons on the first carbon of the alkyl chain of the carbazole unit, which are strongly deshielded due to the electron withdrawing effect of the N atom.

5.2.4 Synthesis of asymmetric regioisomer

In order to demonstrate the generality of this synthesis, it was repeated using a different iridium precursor complex.



Reagents and conditions: i) Pd(OAc)₂, PPh₃, Tol, TEAOH_(aq), 90 °C; ii) acetylacetonate, Na₂CO₃, Tol, 2-ethoxyethanol, 110 °C, 43%; iii) Pd(OAc)₂, PPh₃, Tol, TEAOH_(aq), 90 °C; iv) acetylacetonate, Na₂CO₃, Tol, 2-ethoxyethanol, 110 °C, 89%

Figure 5.11: Synthesis of regioisomeric asymmetric complex

Inspection of the ¹H NMR spectra (Fig. 5.12) of complexes **2.38** and **5.24** reveals the significant asymmetry produced by the incorporation of one fluorene unit, clearly identified by the two signals at ~ 9 ppm which integrate to 1 H atom each. An unidentified impurity in this sample can be seen in the ¹H NMR spectrum. Attachment of the carbazole substituent increases the similarity of the environments for the protons and only a single multiplet is observed at ~9 ppm, which has an integral corresponding to 2 protons and resulting in an overall simplification of the spectrum. Column chromatography allowed isolation of pure **5.25** as verified by ¹H and ¹³C NMR, mass spectrometry and elemental analysis.

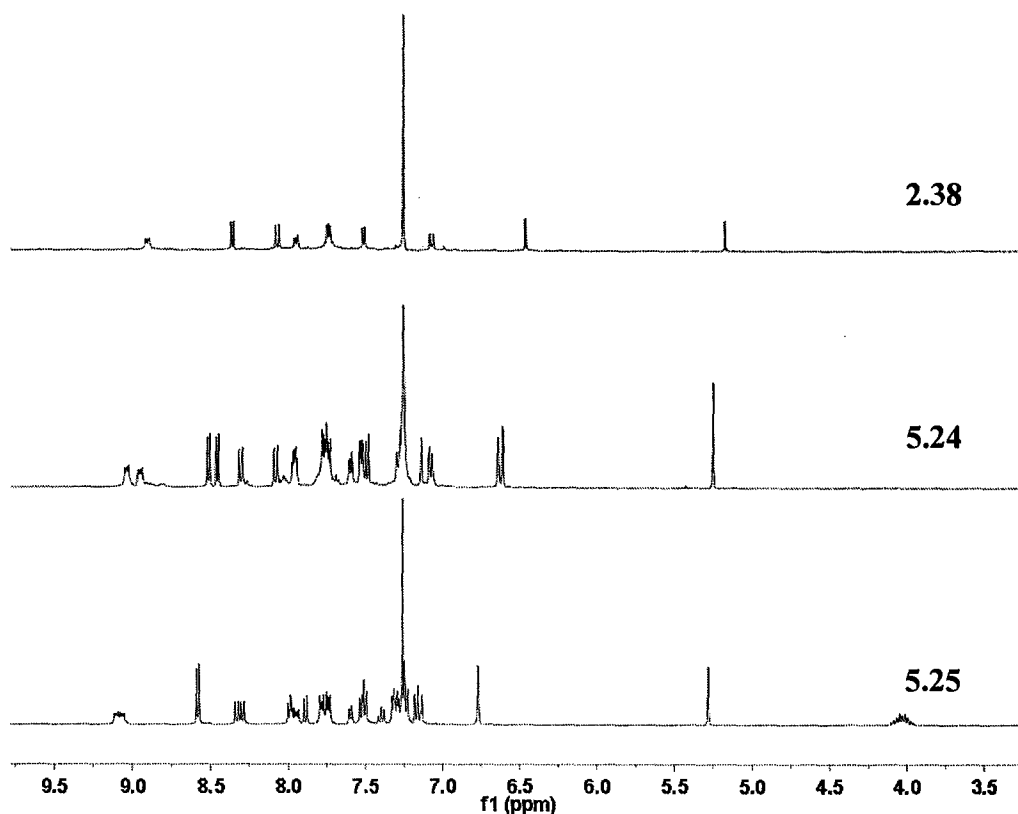
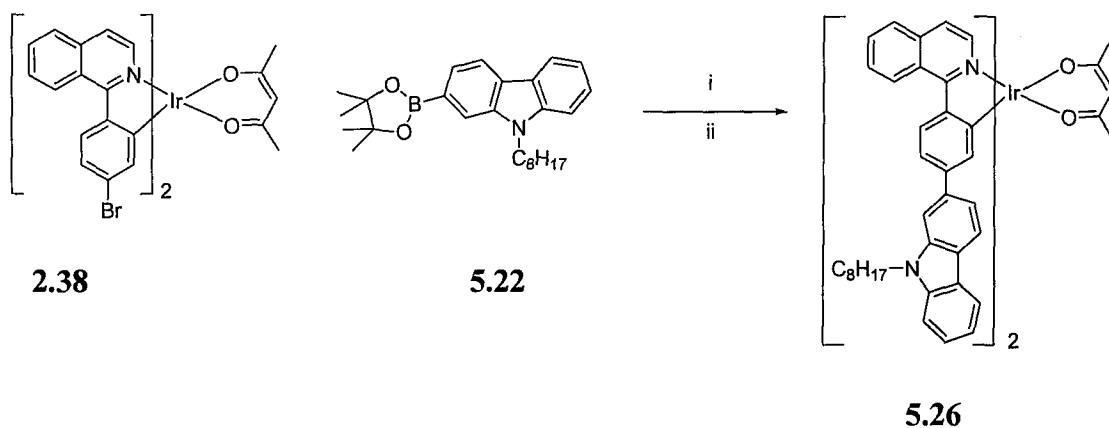


Figure 5.12: NMR spectra of asymmetric complexes

5.2.5 Synthesis of symmetric carbazole substituted iridium complex

In order to probe the photophysical properties of the novel asymmetric complexes, it is useful to have the symmetrical equivalents for use as standards. The synthesis of the difluorenyl substituted iridium complex **2.53** has been shown previously (see Chapter 2). The synthesis of the dicarbazole analogue **5.26** is shown below.



Reagents and conditions: i) Pd(OAc)₂, PPh₃, Tol, TEAOH_(aq), 90 °C; ii) acetylacetonate, Na₂CO₃, Tol, 2-ethoxyethanol, 110 °C, 76%

Figure 5.13: Synthesis of carbazole substituted iridium complex

A Suzuki coupling of bromo substituted complex **2.38** and the boronic ester functionalized carbazole moiety **5.22** afforded the novel bis(carbazole substituted)iridium complex in good yield **5.26** (76%). The ^1H NMR spectrum is shown below (Fig. 5.14) and the multiplet originating from the protons on the carbon adjacent to the bridgehead nitrogen atom can clearly be seen at ~ 4 ppm. The new compound was fully characterized by NMR, mass spectrometry and elemental analysis.

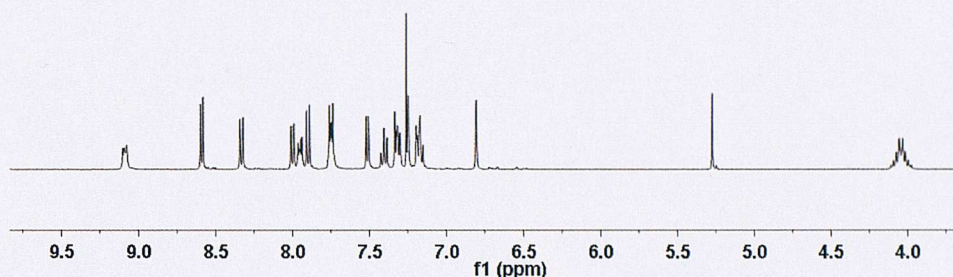


Figure 5.14: NMR spectrum of carbazole substituted iridium complex

5.2.6 Photophysical properties of asymmetric complex

The photophysical properties of the novel asymmetric complex were investigated in order to ascertain whether the one of the ligands is redundant during emissive processes as has been observed in the literature for asymmetric tris cyclometallated iridium complexes.^{131,176,177,179}

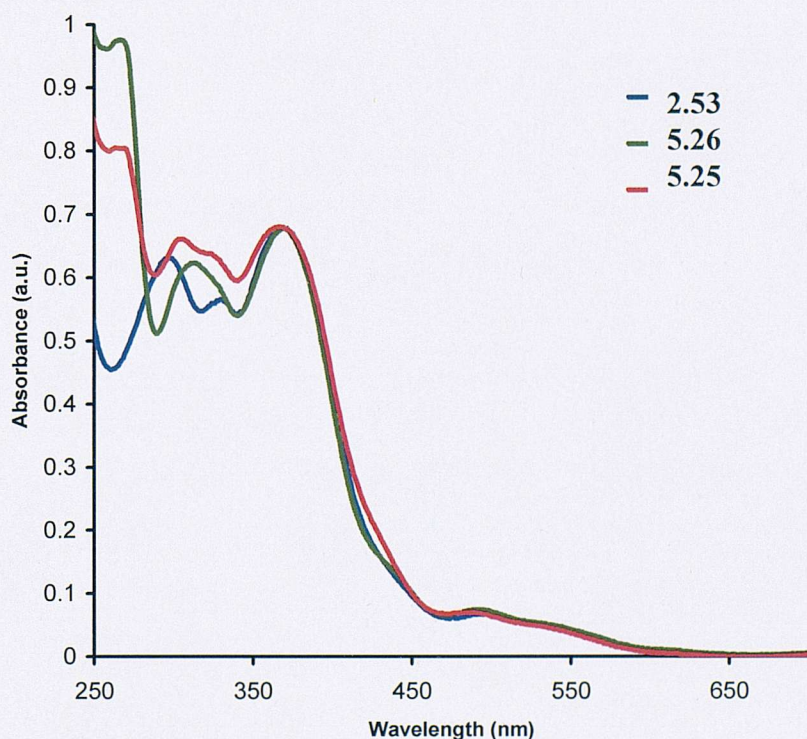


Figure 5.15: Solution UV-Vis absorption spectra of iridium complexes (DCM, $\sim 10^{-5}\text{M}$)

Figure 5.15 shows the UV-Vis absorption spectra of the difluorenyl **2.53**, dicarbazole **5.26** and asymmetric complex **5.25**. The main features correspond to π - π^* ligand based transitions. It can clearly be seen that the asymmetric complex possesses features present in both the symmetric compounds. The features at around 450 – 620 nm correspond to the MLCT absorptions which are very similar for all three complexes.

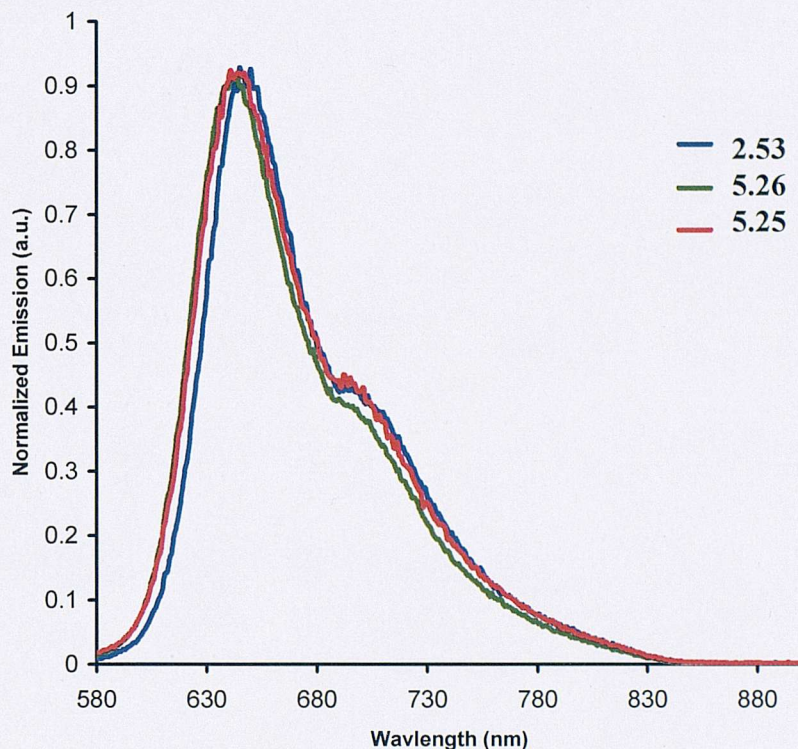


Figure 5.16: Solution photoluminescence of iridium complexes (DCM, Max. Abs. \sim 0.1, Ex. 350 nm)

Figure 5.16 shows the solution photoluminescence spectra of the three complexes. The emission maximum of the difluorenyl substituted complex **2.53** is slightly red-shifted compared to the dicarbazole complex **5.26**. The emission maximum of the asymmetric complex **5.25** is exactly in between that of the two symmetric complexes. Furthermore, the higher energy portion of the emission spectrum of the symmetric carbazole complex **5.26** and the asymmetric complex **5.25** are very similar. However, the lower energy portion of the emission spectra of the symmetric fluorenyl substituted complex **2.53** and the asymmetric complex **5.25** are extremely similar. This implies that both ligands are involved in the excited state and in the emission processes, and is likely to be due to the similarity in energy of the two ligands.

5.3 Asymmetric polymeric iridium complexes

Having demonstrated the synthesis of well defined asymmetric multifunctional iridium complexes it was hoped that polymeric analogues would be accessible through the use of similar chemistry, and/or the employment of protecting group chemistry that has recently been developed.

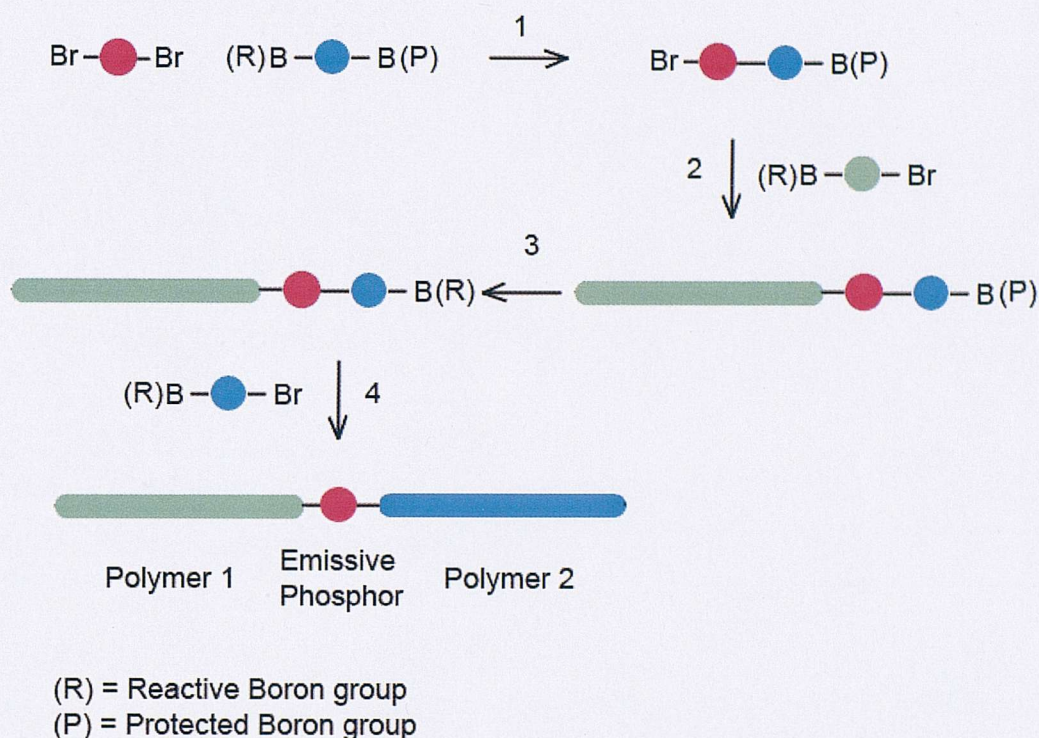


Figure 5.17: Proposed synthetic strategy for polymeric asymmetric iridium complexes

The steps involved in the planned synthesis are as follows:

1. Attachment of one monomer unit bearing a protected boron group creating an asymmetric iridium complex with only one remaining reactive functional group (aromatic bromine atom)
2. Growth of AB type polymer 1 on remaining bromine atom of asymmetric iridium complex
3. Deprotection of boron group providing a reactive functional group
4. Growth of polymer 2 from reactive boron group

5.3.1 Boronic acid protecting groups

There have been two main reports in the literature of boron protecting groups which would be suitable for the preparation of the asymmetric precursor shown in fig 5.17.^{190,191}

5.3.1.1 Acid labile boronic acid protecting group

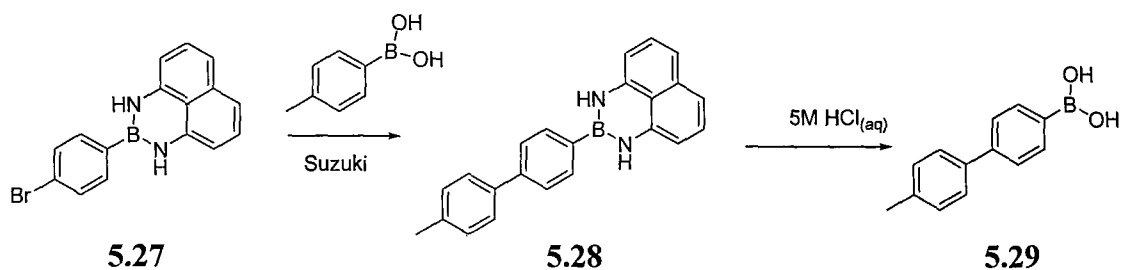


Figure 5.18: Acid labile boronic acid protecting group

Workers in the Suginome group developed a boronic acid masking strategy utilizing a 1,8-diaminonaphthalene protecting group.¹⁹¹ The protected boronic acid **5.28** was able to tolerate aqueous basic conditions, but could be removed in quantitative yields, under acidic conditions. It was suggested that the lone pair of electrons on the nitrogen atoms decreased the Lewis acidity of the boron atom, thus decreasing its susceptibility towards Suzuki coupling.¹⁹¹

5.3.1.2 Base labile boronic acid protecting group

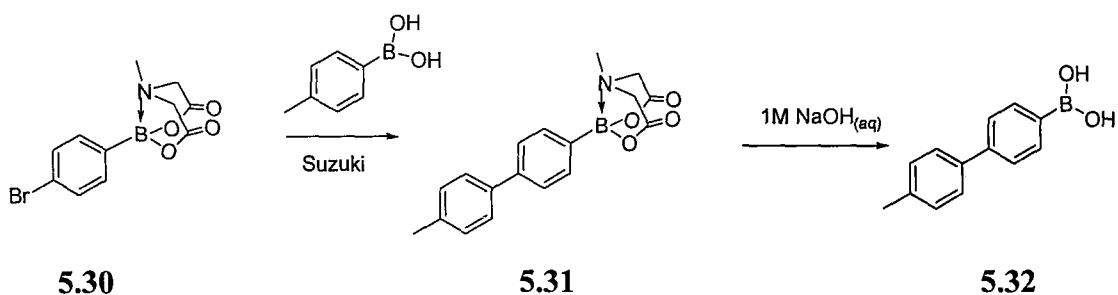


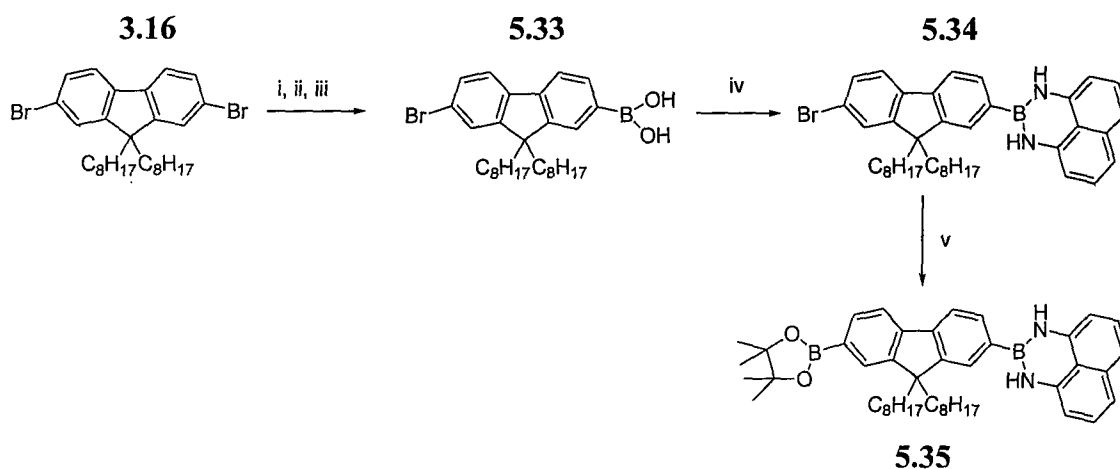
Figure 5.19: Base labile boronic acid protecting group

Workers in the Burke group reported the protection of boronic acid groups using *N*-methyliminodiacetic acid.^{190,192} This protected boronic acid group of **5.31** was stable towards anhydrous Suzuki coupling conditions as well as several other metal catalyzed reactions. Deprotection was achieved under mild basic conditions.^{190,192}

5.3.1.3 Strategy

Initially it was decided to utilize the acid labile protecting group as this would enable growth and attachment of the first polymer under conditions that have been used throughout this work (aqueous basic Suzuki coupling reactions). Deprotection under acidic conditions would then allow growth and attachment of the second polymer. Prior to the following synthesis, the stability of the iridium complex was tested under the conditions required for deprotection. It was found that the complex formed a chloro-bridged dimer, which could then be quantitatively reconverted to a monomeric complex under the conditions required to cleave chloro bridged dimers (i.e. by reaction with acetyl acetone under basic conditions).

5.3.2 Synthesis of protected fluorene units

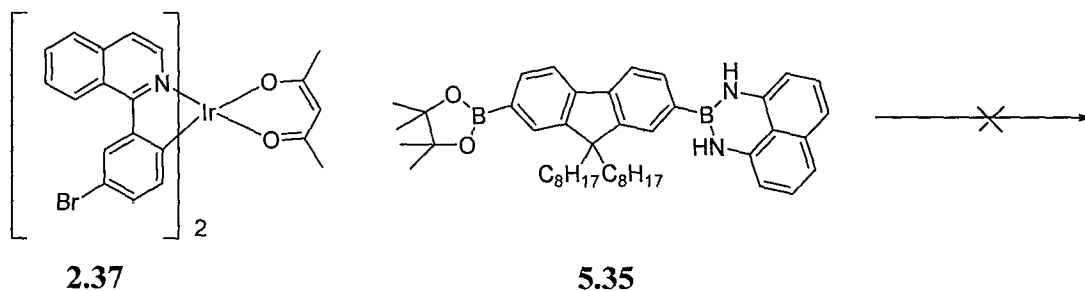


Reagents and conditions: i) *n*-BuLi, THF, -78 °C, ii) triisopropoxy borane, -78 °C → room temperature; iii) 1M HCl, 62%; iv) 1,8-diaminonaphthalene, Tol, Reflux, Dean-Stark, 100%; v) PdCl₂(dppf), Bis(pinacolato)diboron, KOAc, DMF, 74%

Figure 5.20: Synthesis of diaminonaphthalene protected fluorene unit

The synthesis of boronic acid substituted fluorene **5.33** was achieved via a metal halogen exchange, followed by the addition of tri-isopropoxy borane. Hydrolysis of the synthesized boronic ester was achieved by stirring it in aqueous 1M hydrochloric acid and afforded the desired compound **5.33**, in good yield (62%). The introduction of

the boron acid protecting group was achieved in quantitative yield through the use of a Dean-Stark condenser to drive the equilibrium. The remaining bromine group was converted into a boronic ester via a Miyaura borylation to yield **5.35** in high yield. Both fluorene units bearing the boron protecting group displayed light sensitivity and showed decomposition to an unidentified product, unless stored in the dark.

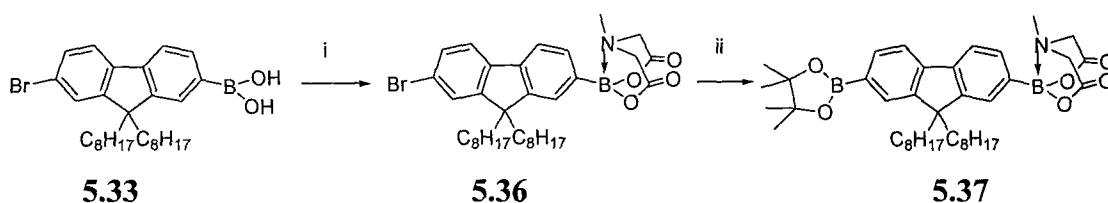


Reagents and conditions: Pd(OAc)₂, SPhos, Tol, TEAOH_(aq), 90 °C

Figure 5.21: Attempted synthesis of protected asymmetric iridium complex

Attempted coupling of protected fluorene moiety **5.35** with complex **2.37** under previously used Suzuki coupling conditions was unsuccessful, despite multiple attempts. ¹H NMR analysis of the crude product indicated the formation of multiple products. Attempted purification of the reaction mixture via column chromatography was not successful due to what appeared to be severe decomposition on the silica gel due to the colour of the main products changing from red to uncharacterisable black residues.

It was decided to abandon the use of the acid labile protecting group and attempt the same reaction with the other reported boron protecting group.



Reagents and conditions: i) N-methyliminodiacetic acid, Tol, DMSO, Reflux, Dean-Stark, 100%; ii) PdCl₂(dppf), Bis(pinacolato)diboron, KOAc, DMF, 69%

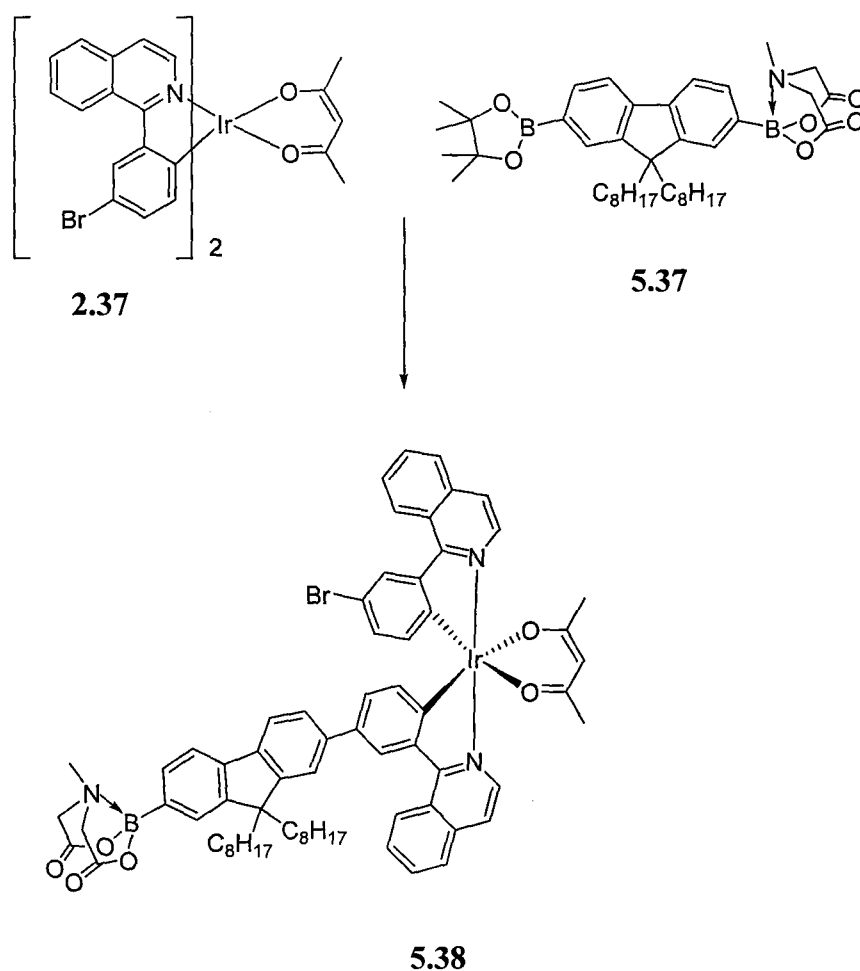
Figure 5.22: Synthesis of N-methyliminodiacetic acid protected fluorene unit

Synthesis of the alternative protect boron acid fluorene unit **5.37** was achieved under similar conditions to those mentioned above. A Dean-Stark condenser allowed quantitative isolation of **5.36**. Subsequent Miyaura borylation and purification via

column chromatography afforded di-boron compound **5.37** in good yields. Neither of the novel boron protected fluorene moieties displayed light sensitivity, and showed good stability towards ambient conditions and were fully characterized by ^1H and ^{13}C NMR, mass spectrometry and elemental analysis.

Due to the reported instability of the protecting group towards aqueous basic conditions, the subsequent Suzuki couplings must be performed anhydrously, of which there are several examples.^{193,194} The conditions employed for the following reaction are those reported by Barder *et al* which have been demonstrated as high yielding and very efficient.¹⁵⁴

5.3.3 Attempted synthesis of protected asymmetric iridium complex



Reagents and conditions: $\text{Pd}(\text{OAc})_2$, PCy_3 , K_3PO_4 , Tol, <5%

Figure 5.23: Synthesis of protected asymmetric iridium

Despite multiple attempts, under a variety of conditions, almost all compounds isolated from the reaction were starting materials. However, a small amount of what is believed to be the desired mono substituted protected boron fluorenyl moiety **5.38** was isolated

by preparative thin layer chromatography. It is believed that the absence of water prevents the partial hydrolysis of the boronic ester which is required for Suzuki coupling. This requirement is predominantly anecdotal and there is no firm literature basis for this assumption.¹⁵⁴ There is only one example of a successful Suzuki coupling of a boronic ester under anhydrous conditions.¹⁹² The author finds it likely that the success of this reported reaction is likely to be due to the presence of residual water in the DMSO which was used as the solvent as it is notoriously difficult to dry.

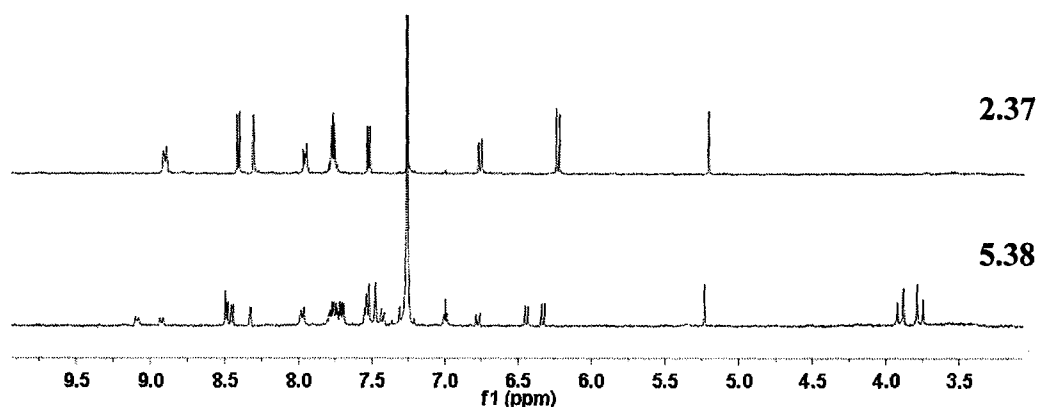
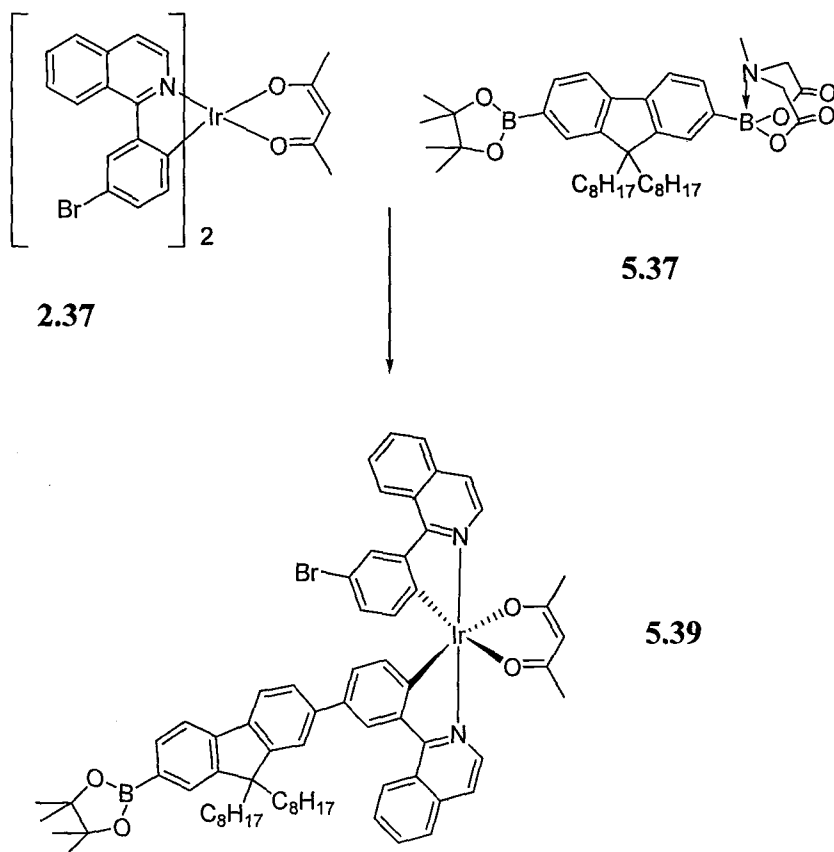


Figure 5.24: ^1H NMR spectrum of protected asymmetric iridium complex

Figure 5.24 shows the ^1H NMR of the material isolated by preparative TLC. The presence of two aromatic signals at ~ 9 , 7 and 6.5 ppm indicate the formation of an asymmetric product. The peaks present at ~ 3 ppm originate from the protons on the protecting group indicating that it is intact, and that the desired product **5.38** has been formed. Unfortunately, due to the extremely small amount of isolated material it was not possible to characterize this complex fully.



Reagents and conditions: $\text{Pd}(\text{OAc})_2$, SPhos, K_3PO_4 , Tol, ~20%

Figure 5.25: Attempted optimisation of Suzuki coupling

After exceedingly long (5 days) and forcing reaction conditions (reflux) a new product was observed and isolated via preparative thin layer chromatography. The ^1H NMR spectrum was consistent with the formation of the mono boronic ester fluorenyl substituted iridium complex **5.39**. It is likely that either the presence of residual water partially hydrolyzed the boronic acid protecting group or the extreme reaction conditions removed the ester functionality allowing Suzuki coupling to occur with the bromine atoms on the iridium complex.

5.3.4 Modification of synthetic route

The unreactive nature of the boronic ester compared to a boronic acid under anhydrous conditions inspired the development of a novel strategy where this difference in reactivity could be exploited.

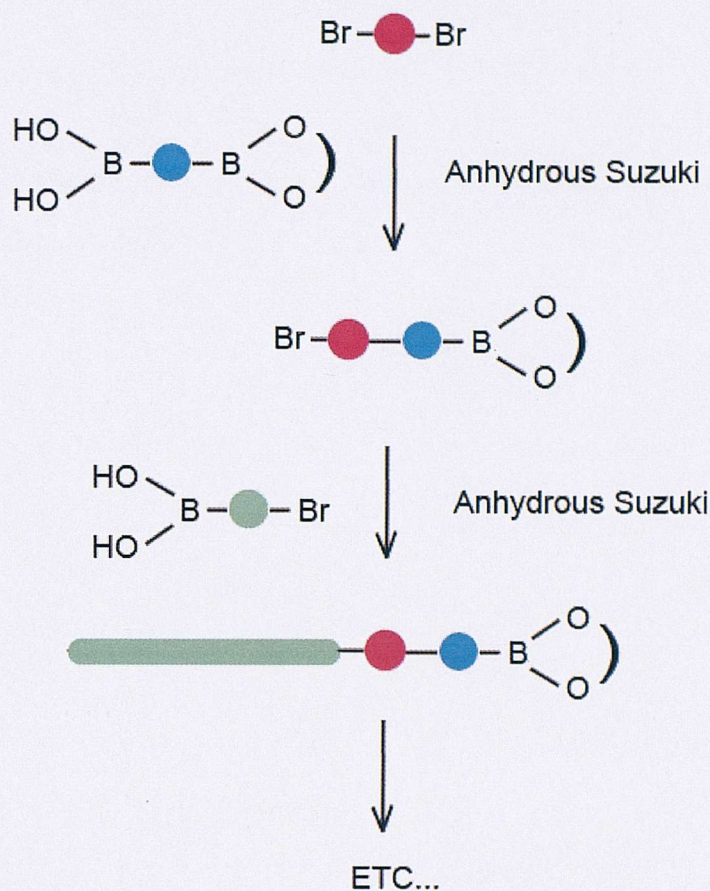


Figure 5.26: Modification of proposed synthetic route

By varying the reaction conditions it should be possible to either allow (aqueous) or suppress (anhydrous) the reactivity of the boronic ester functionality.

5.3.5 Synthesis of functionalized asymmetric iridium complex



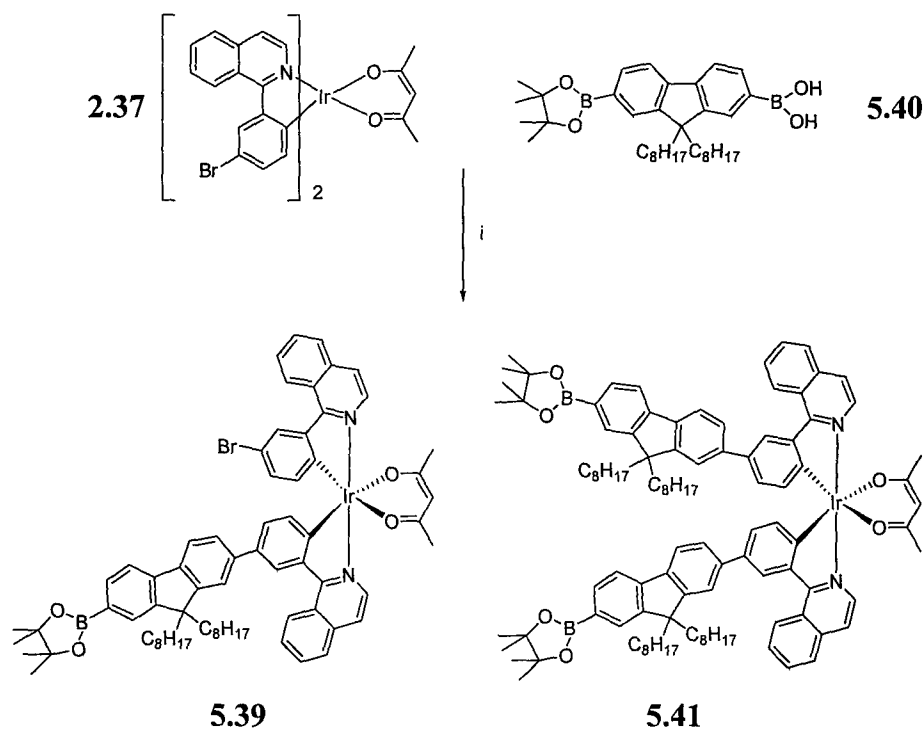
Reagents and conditions: i) Lithium isopropoxide, THF, room temperature; ii) *t*-BuLi, THF, $-78\text{ }^\circ\text{C}$, iii) 2-Isopropoxy-4,4,5,5-tetramethyl-1,3,2-dioxaborolane, $-78\text{ }^\circ\text{C} \rightarrow$ room temperature, 89%

Figure 5.27: Synthesis of fluorene unit bearing 2 different boron groups

The synthesis of the fluorene unit containing both a boronic ester and a boronic acid group was achieved by stirring **3.17** with lithium isopropoxide to create a temporary protecting “ate” complex.¹⁹⁵ Subsequent addition of *t*-butyllithium allows a metal-

halogen exchange to occur with the bromine atom, with no observable reaction occurring on the boronic ester functionality. Addition and hydrolysis of an excess of boron tri isopropoxide allowed isolation of the desired novel fluorene unit **5.40**.

The following reaction was performed using 1.5 equivalents of the novel di boron functionalized fluorene unit **5.40**.



Reagents and conditions: *i*) Pd(OAc)₂, SPhos, K₃PO₄, Tol, 90 °C; **5.39** (21%), **5.41** (15%)

Figure 5.28: Synthesis of boronic ester, fluorenyl substituted iridium complexes

Two products, **5.39** (21%) and **5.41** (15%) were isolated, the ¹H NMR spectra of which are shown below (Fig. 5.29). As was observed in previous reactions, both the symmetrical (disubstituted) **5.41** and unsymmetrical (mono substituted) **5.39** were observed.

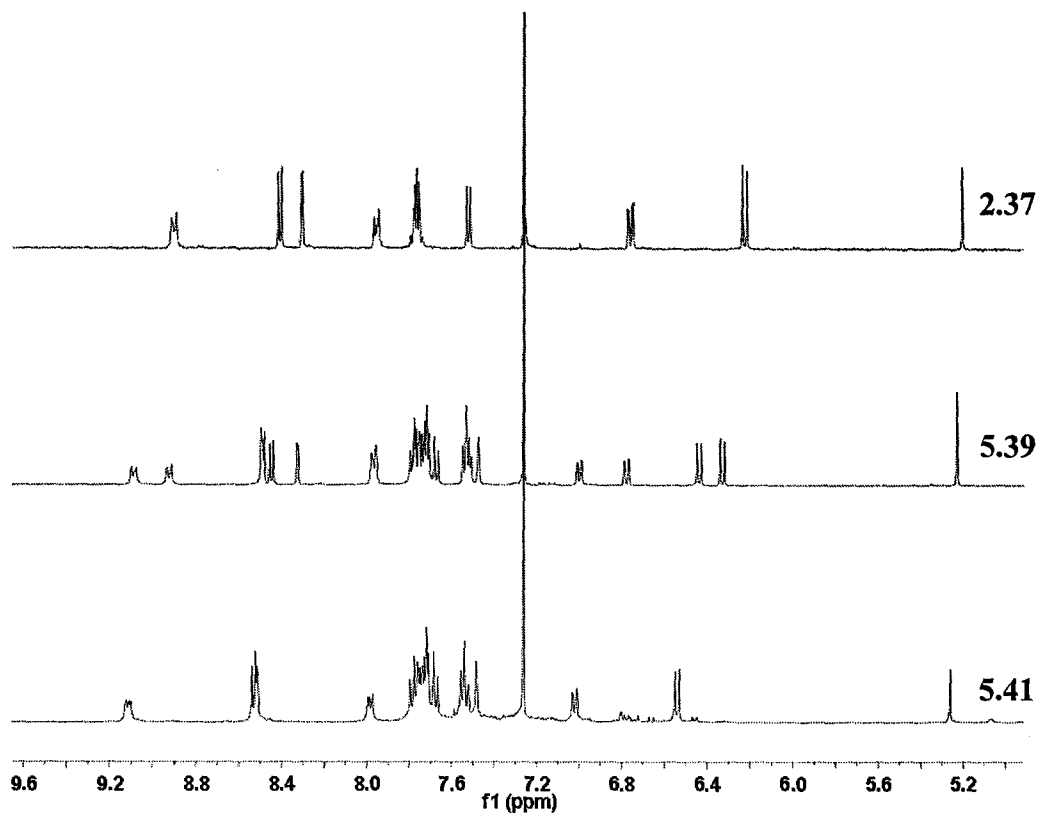


Figure 5.29: NMR spectra of boronic ester, fluorenyl substituted iridium complexes

The NMR spectrum of complex **5.39** demonstrates the typical two sets of peaks for the different ligands. Integration of the peaks is consistent with the proposed structures although impurities can be seen in both samples. Both compounds displayed decomposition on silica gel during purification, where it is believed the boronic ester groups are hydrolyzed.

The low yields can be explained by the equilibrium between the boronic acid **5.40** and the boroxine **5.42** shown below (Fig 5.30). As reagent **5.40** is dried under vacuum in preparation for the reaction, which is performed under anhydrous conditions, the equilibrium is shifted towards the right. In typical Suzuki couplings the boroxine is hydrolyzed in situ and reacts. Boroxines, however, are typically not capable of participating in the coupling reaction.¹⁹⁶ Consequently, the more anhydrous the reaction conditions required for the suppression of coupling involving the boronic ester, the lower the yield of the product due to the lower availability of free boronic acid.

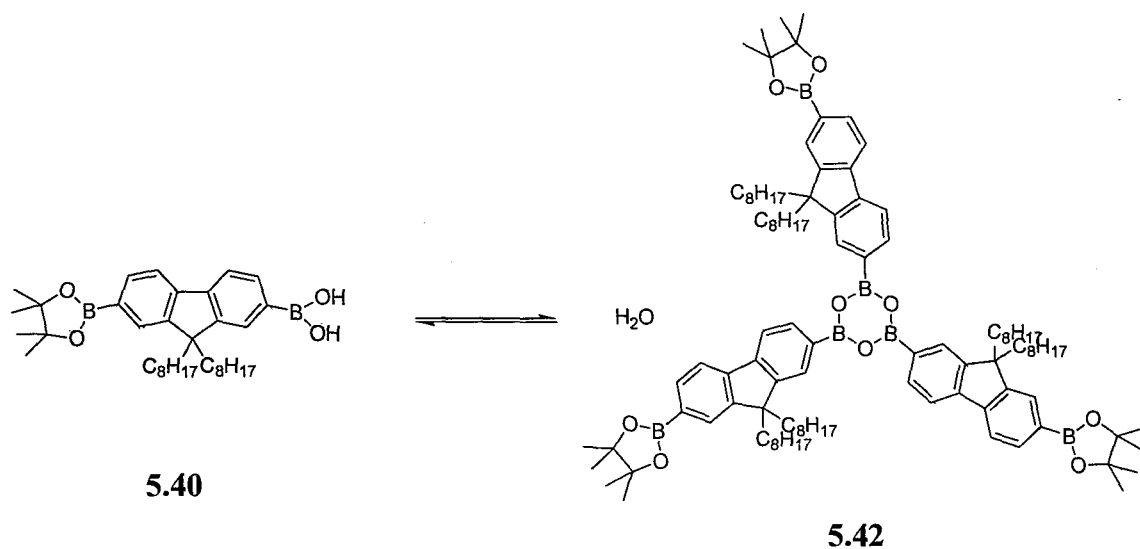


Figure 5.30: Boronic acid-boroxine equilibrium

Unfortunately, despite the moderate success of this novel methodology, both the symmetric and unsymmetrical boronic ester functionalized iridium complexes showed significant decomposition during attempts to isolate analytically pure samples and it was not possible to continue with this synthetic route.

5.3.6 Alternative strategy for synthesis of asymmetric polymeric iridium complexes

An alternative strategy to synthesize an asymmetric polymeric iridium complex was also attempted which will be outlined below.

The lack of selectivity in the Suzuki coupling necessary to attach a substituent does not enable direct introduction of a single polymer chain under stoichiometric conditions. However, by vastly increasing the number of equivalents present of the iridium complex it should be possible to make it unlikely that a disubstituted complex is produced.

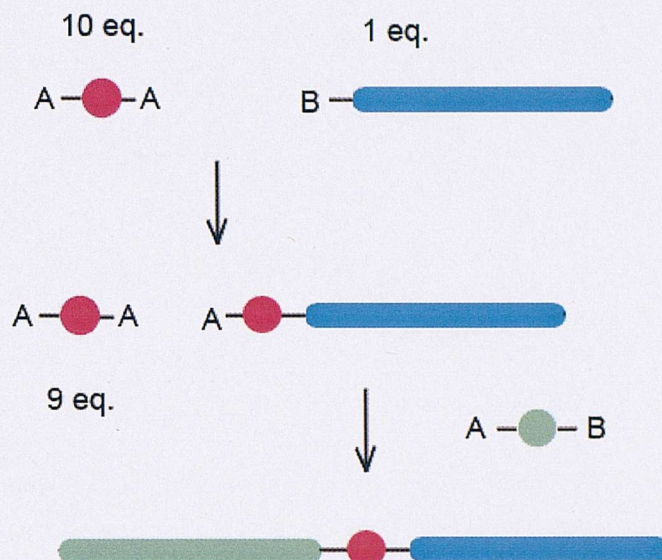
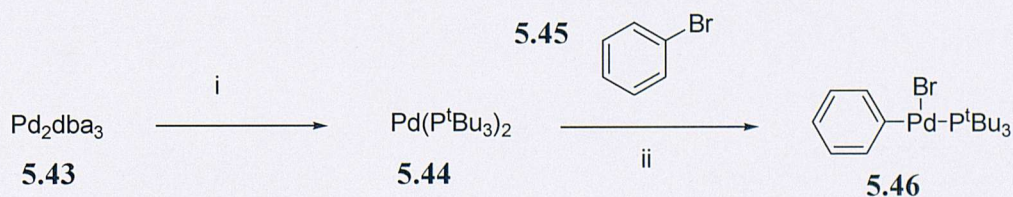


Figure 5.31: Alternative synthetic route

The success of this method depends on the ability to remove the large excess of unreacted starting material, and for the polymeric starting material to be completely consumed with little or no side reactions.

5.3.7 Synthesis

It was decided to first attach the oligofluorene chain as the chemistry of this oligomer is significantly more established, and it is a highly soluble polymer. A recent publication has reported the synthesis of mono bromine terminated oligofluorene chains from an externally added initiator unit. Furthermore, narrow polydispersities and quick reaction times were observed, consistent with a controlled polymerization mechanism.¹⁹⁷ It was decided to employ this methodology to synthesize the required polymeric moiety.



Reagents and conditions: i) P^tBu_3 , DMF, 58%; ii) PhBr, 80 °C, 67%

Figure 5.32: Synthesis of T-shaped palladium initiator

Synthesis of the tricoordinate palladium complex was achieved in two steps by reaction of palladium dibenzylidene with tris(*tert*-butyl)phosphine, followed by the oxidative addition of phenyl bromide. The isolated yields were similar to those reported by other groups.¹⁹⁷

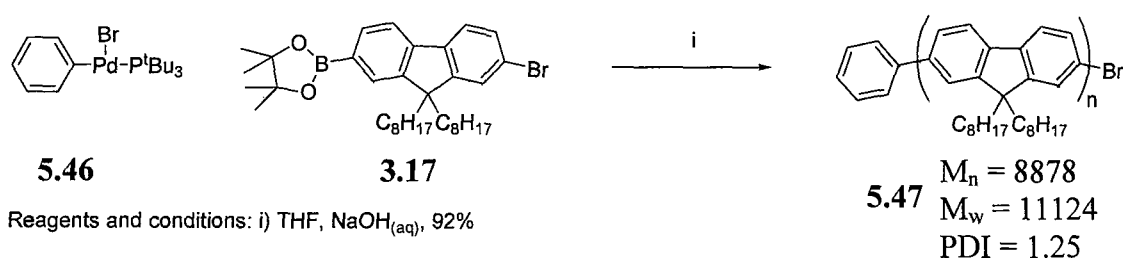
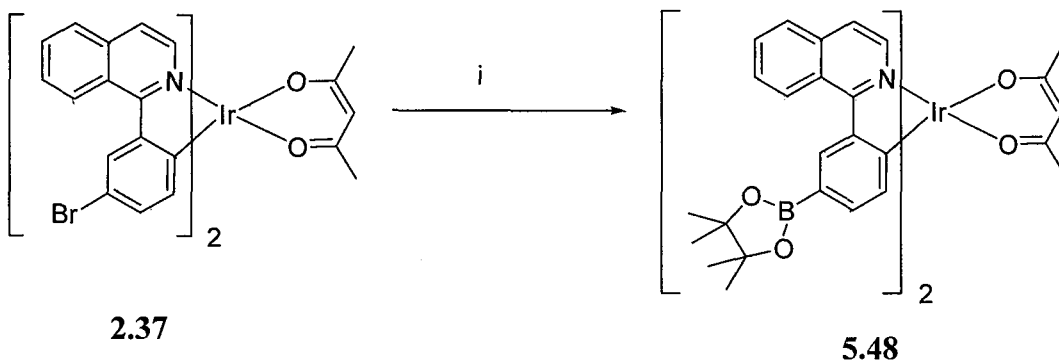


Figure 5.33: Chain transfer polymerization of polyfluorene (n=15)

The reaction was carried out as described in the literature with 1 equivalent of **5.46** added to 15 equivalents of the AB fluorene monomer **3.17**. Precipitation of the reaction mixture into methanol afforded the oligomer in good yield. ¹H NMR analysis (Fig. 5.38) indicates that the product is approximately 15 units long from integration of the end-capping phenyl unit protons relative to the alkyl chain protons.

The GPC chromatogram is shown in Fig. 5.39 and demonstrates that very low polydispersity index polymers (PDI = 1.25) can be achieved through this methodology. These are attributed to the polymerization occurring through a chain transfer mechanism. However, the obtained results were extremely dependent on the purity of the starting monomer, and the scale on which it was performed. Repeating the reaction on a larger scale resulted in a sample with a larger weight distribution and a bimodal distribution. The reason for this is not known, although it must be noted that precipitation of oligomeric products was observed during the reaction in this case.

Due to the presence of a bromine terminus on the oligomer chain, it is necessary to have complementary boron functionality on the iridium complex. A variety of methods for introducing a boronic ester onto the iridium complex were investigated, the best of which is shown below. A Miyaura borylation was performed, using recently described conditions, which afforded the boronic ester functionalized iridium complex **5.48** in excellent yield.¹⁹⁸



Reagents and conditions: i) $\text{PdCl}_2(\text{CH}_3\text{CN})_2$, SPhos, pinacol borane, NEt_3 , Dioxane, 110°C , 93%

Figure 5.34: Synthesis of boronic ester substituted iridium complex

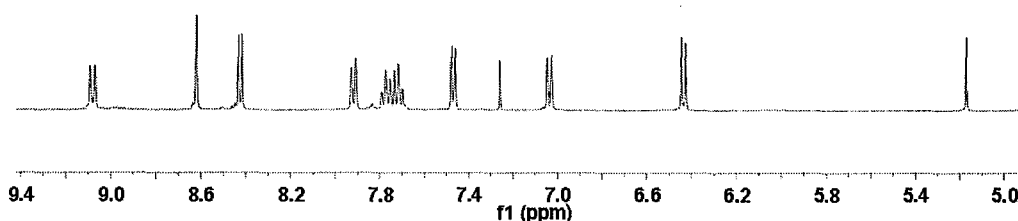
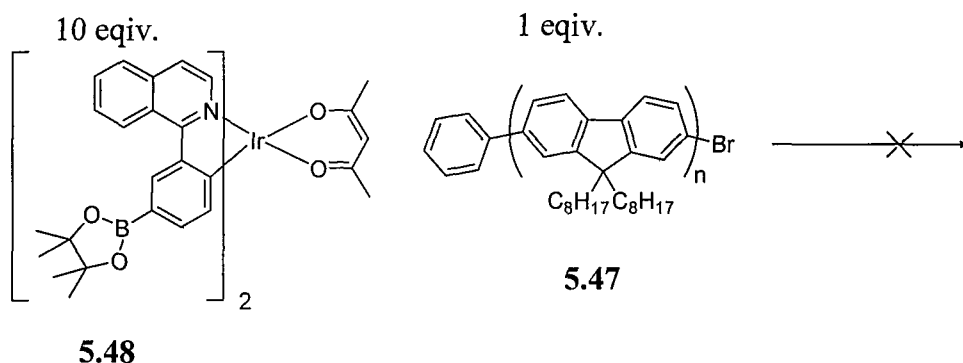


Figure 5.35: ^1H NMR spectrum of boronic ester substituted iridium complex

Unfortunately, despite multiple attempts with many different conditions, coupling of the bromo terminated polymer **5.47** and complex **5.48** was not possible. There was no evidence of any reaction, in contrast to the relatively high reactivity of the bromo complex towards Suzuki coupling (Chapters 3 and 4).



Reagents and conditions: $\text{Pd}(\text{OAc})_2$, SPhos, Tol, $\text{TEAOH}_{(\text{aq})}$, 90°C

Figure 5.36: Attempted synthesis of asymmetric polymeric iridium complex

Due to the failure of the above coupling reaction (Fig. 5.36), it was decided to change the functionality of the polymer chain to a boronic ester which would then be able to react with a bromo substituted complex, as has been demonstrated throughout this work.

This was necessary as the nature of the polymerization means it is not possible to have a boron terminus.

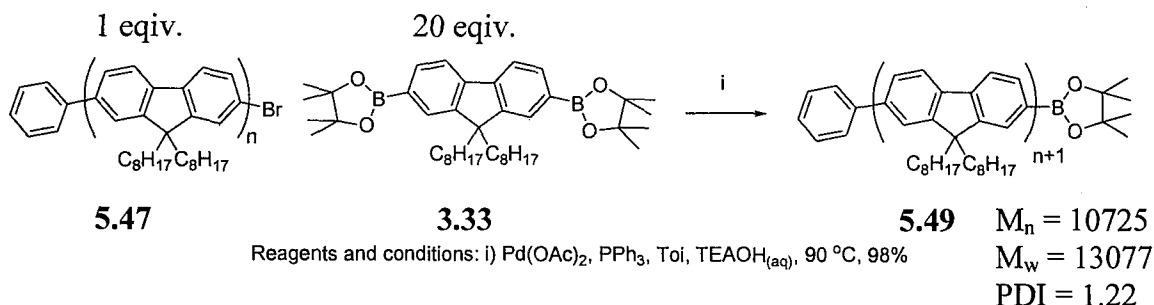


Figure 5.37: Synthesis of boronic ester terminated polyfluorene (n=15)

A variety of methods were investigated for the change of functional groups including Miyaura borylation and metal-halogen exchanges all of which displayed moderate success. Due to the extreme difficulties in purifying these reactions which did not proceed quantitatively these procedures were not used. However, it was found that reacting polymer **5.47** with a large excess of di-boronic ester fluorene unit **3.33** afforded the novel polymer **5.49** which had been chain extended by one monomer unit and possessed a boronic ester end group.

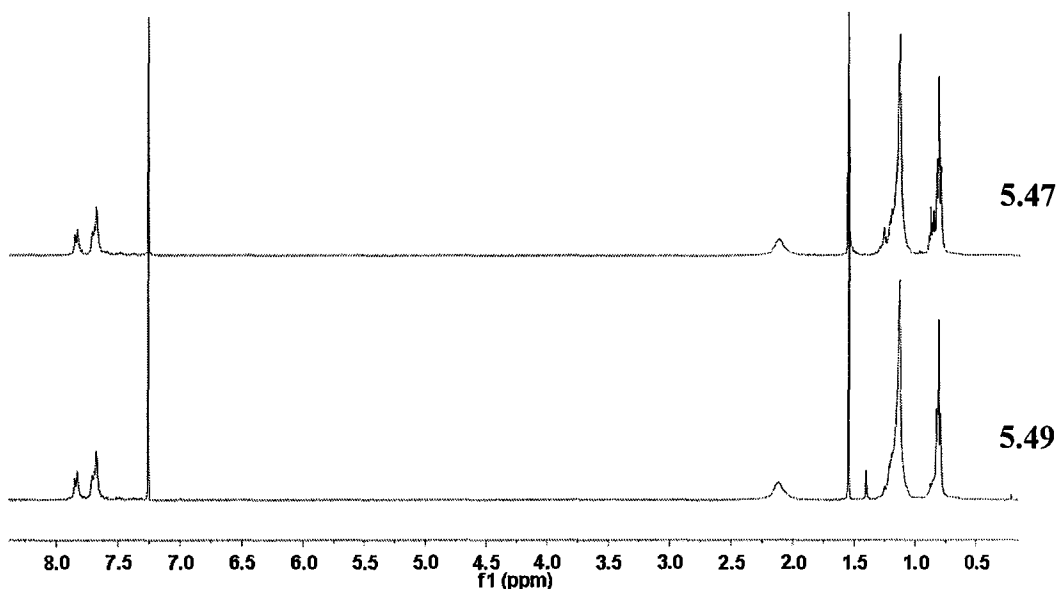


Figure 5.38: ¹H NMR spectra of polyfluorenes

Figure 5.38 shows the NMR spectra of the bromo terminated and boronic ester terminated oligofluorenes. The new peak at ~1.4 ppm originates from the methyl groups of the boronic ester. Integration of this peak relative to the signals originating from the alkyl chain protons (0.6 – 1.3 ppm) indicated a chain length of approximately 16 monomer units.

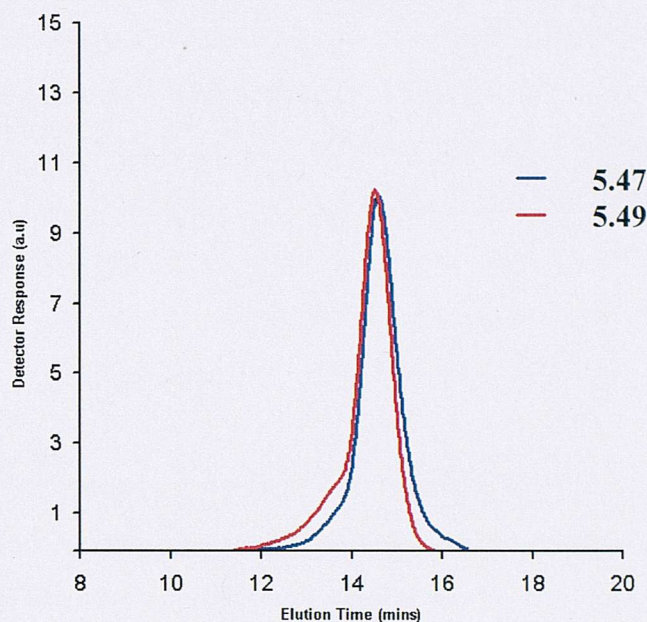


Figure 5.39: GPC chromatograms of polyfluorenes (PS standards, THF eluent)

The GPC chromatogram of the two polymers is shown above (Fig. 5.39). The narrow polydispersity indices of both samples (**5.47** PDI = 1.25; **5.49** PDI = 1.22) can clearly be seen. The M_n of the starting polymer is ~ 9000 compared to that of ~ 11000 for the boronic ester terminated polymer. The small shoulder that is observed at ~ 13 mins is thought to originate from a symmetrical diphenyl terminated oligofluorene that is a result of two bromo terminated chains reacting with the di-boronic fluorene moiety.

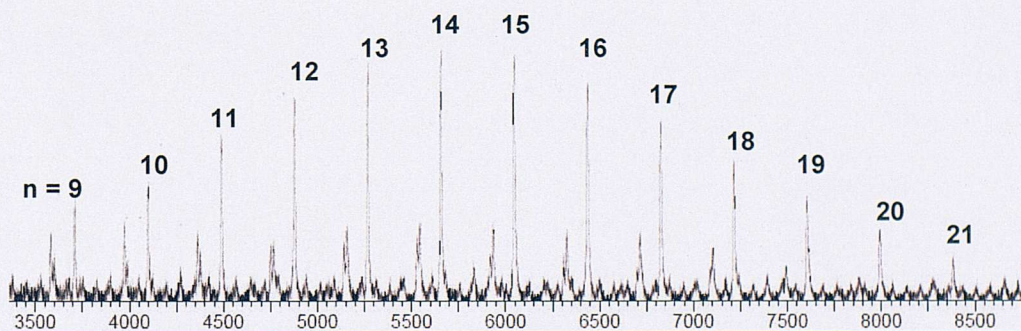


Figure 5.40: MALDI-TOF (dithranol) spectrum of boronic ester terminated polyfluorene

The synthesized polymer **5.49** was subjected to end group analysis by MALDI-TOF as shown above. The major peaks correspond to the desired boronic ester terminated

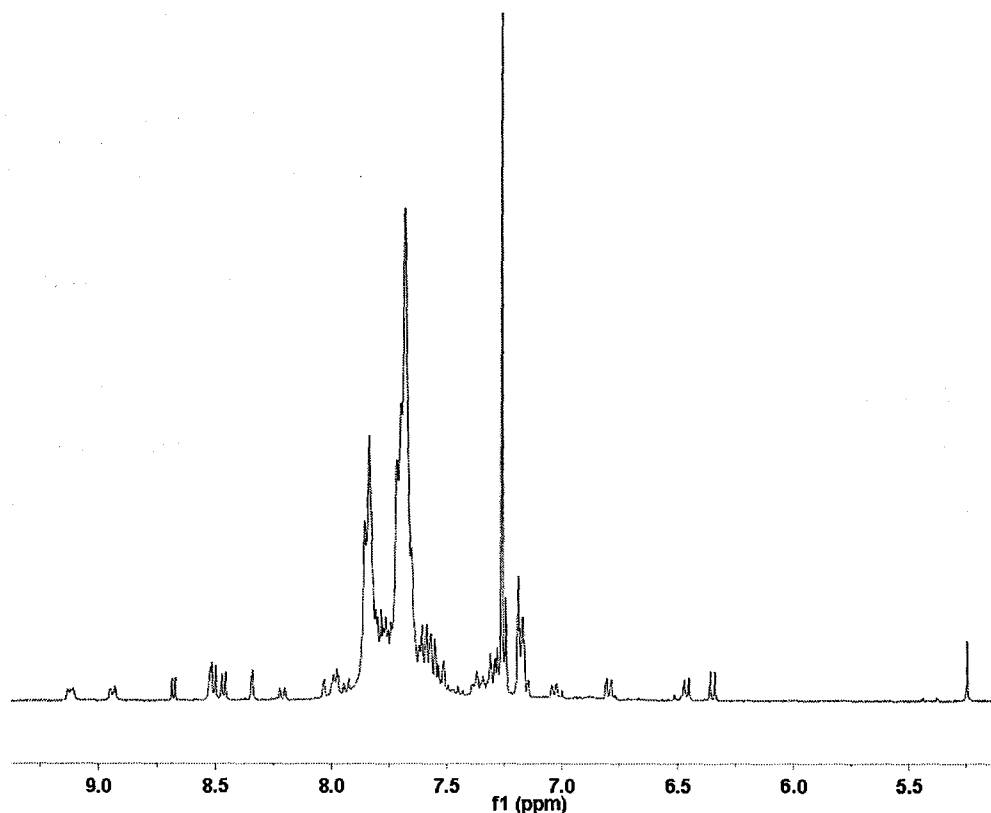


Figure 5.42: ^1H NMR spectra of the isolated polymeric material

The ^1H NMR spectrum of the isolated polymeric material (Fig. 5.42) indicates that the iridium complex is attached to the oligofluorene through only one ligand. This can be seen by the presence of the differing proton environments for the two ligands as has been observed in the cases of the well defined analogues of this material. This demonstrates that by using this methodology it is possible to synthesize an asymmetric polymeric iridium complex. Unfortunately, integration of the iridium complex protons relative to the oligofluorene alkyl chain protons indicates that a much lower amount of complex has been incorporated than desired. Furthermore, peaks corresponding to the boronic ester termini of the oligofluorene chain can still be seen (~ 1.4 ppm) indicating that the reaction has not gone to completion. Longer reaction times (48 hours) resulted in a disappearance of this peak but no increase in the amount of iridium incorporation indicating that the boronic ester groups are being hydrodeboronated instead of undergoing Suzuki coupling. Extensive attempts at optimizing the reaction conditions were undertaken but it was not possible to obtain the desired level of iridium incorporation. Attempts at separating either the unreacted or hydrolyzed oligofluorene from the asymmetric polymeric iridium complex by chromatography were undertaken but due to similarities in polarity and the chain length distributions of all species, these

were unsuccessful. It is estimated that approximately 20-30% of the boronic ester functionalized oligofluorene undergoes the desired Suzuki coupling reaction with 70%-80% either remaining unreacted or undergoing hydrolysis. Due to the extremely high amount of undesired inseparable oligomeric material in the sample it was decided to abandon the synthesis.

5.4 Conclusions

The synthesis of novel well defined asymmetric multifunctional iridium complexes has been demonstrated, allowing the isolation of bis-cyclometallated iridium complexes with two different cyclometallating ligands. To the best of our knowledge this is the first example of such complexes.

The emissive properties of the novel complexes have been probed and compared to their two symmetric counterparts, and the emission appears to include participation from both cyclometallating ligands, due to the common spectral features with both symmetric complexes.

Multiple attempts at synthesizing asymmetric polymeric analogues have been attempted. The use of boronic acid protecting groups has been investigated, including the synthesis of a novel fluorene moiety bearing a boronic acid and a boronic ester group. The difference in reactivity of the two functionalities has been exploited to allow selective coupling reactions to be performed depending on the reaction conditions.

Instability of the synthesized asymmetric precursors prevented the success of this route. It is believed for this to be successful, more robust functional groups must be employed.

Another attempted route at synthesizing polymeric asymmetric iridium complexes employed the use of a pre-synthesized oligofluorene chain which was reacted with a large excess of an iridium complex in an attempt to prevent multiple substitutions on a single complex. Suzuki coupling reactions with the bromine group on the iridium complex and the boronic ester group on the oligofluorene and vice-versa were attempted but neither was successful. It is believed that this methodology could be successful as promising results were obtained, although extensive optimization of the reaction conditions are needed.

Chapter 6: Experimental Procedures

6.1 Materials

All reactions were conducted under a nitrogen atmosphere, using either standard anaerobic techniques or in a nitrogen-filled glovebox. All solvents and reagents were obtained from commercial sources (Aldrich and Merck). Toluene, THF and diethyl ether were dried by distillation from Na-benzophenone. CHCl_3 and DCM were dried by distillation from CaH_2 . $\text{IrCl}_3 \cdot x\text{H}_2\text{O}$ was loaned by Johnson Matthey Plc. Column chromatography was performed using Merck silica gel 60, and thin layer chromatography was performed on Merck TLC F₂₅₄ silica gel 60 plates, observed under 254 or 336 nm ultraviolet light.

6.2 Measurements

^1H , $^{13}\text{C}\{^1\text{H}\}$ and $^{31}\text{P}\{^1\text{H}\}$ NMR spectra were performed on a Bruker Av-400 instrument. Elemental analyses were determined by Mr. Stephen Boyer at London Metropolitan University, North Campus, Holloway Road, London, N7. GPC (SEC) data were collected using a Polymer Laboratories PL GPC-50 instrument with THF as the eluent, at a flow rate of 1 mL/min. Two Polymer Laboratories mixed D columns were used in series, and the M_n values were calibrated against narrow M_n polystyrene standards (Easy-Cal standards A and B).

Chemical ionization (CI) and fast atom bombardment (FAB) mass spectra were recorded on a Micromass Autospec Premier instrument. Matrix assisted laser desorption ionization - time of flight (MALDI-TOF) was recorded on a Micromass MALDI micro MX instrument. NOTE: When assigning MALDI-TOF spectra the symbol (-B) refers to a boronic ester end group.

X-ray crystallographic analysis was performed by Dr. Andrew White (see Appendix A).

6.2.1 Absorption and Emission Spectroscopy

UV-visible spectra were recorded, at room temperature, on a Thermo Unicam UV500 spectrometer, in DCM solutions at concentrations of $\sim 10^{-5}$ M. Thin films of polymers

were spin coated from DCM solutions of 10 mg/mL on a Laurell spin coater at 2000 rpm for 30 s.

Optically induced phosphorescence spectra were collected using a CaryEclipse fluorescence spectrophotometer. Solution phosphorescence measurements were done on DCM solutions. The excitation wavelength was 350 nm, and the spectra were recorded at room temperature.

Solution quantum yields were determined in degassed DCM solutions with maximum absorbance of 0.1 and an excitation wavelength of 350 nm using the Parker-Rees¹⁹⁹ method. Compound **2.34** was used as the standard ($\Phi_{\text{Ph}} = 0.2$).²⁷

Thin film quantum yields were determined using an integrating sphere with an excitation wavelength of 325 nm using the method developed by de Mello *et al.*²⁰⁰

All spectra are uncorrected

6.2.2 Theoretical Methods

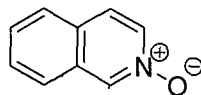
Density functional theory (DFT) and time dependent (TD) DFT using the B3LYP hybrid functional was applied for all calculations. Geometry optimizations were performed without any constraint. All calculations were performed using the 6-31G(d) basis set for the ligands and the LANL2DZ basis set for Ir(III), as implemented by Gaussian 03.²⁰¹ Mulliken population analysis was performed using QMForge, Version 2.1.²⁰²

6.2.3 Cyclic Voltammetry

Cyclic voltammetry measurements were recorded in degassed, anhydrous DCM, with 0.1 M tetrabutylammonium hexafluorophosphate as the supporting electrolyte (at a scan rate of 100 mV/s). The working electrode was platinum, with a platinum wire counter electrode and a silver pseudoreference electrode. Ferrocene was used as an internal standard.

6.3 Experimental For Chapter 2

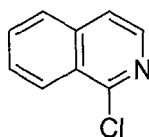
Isoquinoline-N-oxide⁶³ 2.14



Isoquinoline (3.01 g, 23.2 mmol) was dissolved in DCM (60 mL) and cooled to 0 °C. *m*-Chloroperbenzoic acid (77%, 8 g, 35.7 mmol) was added, portionwise, and the reaction mixture stirred for 4 h. The reaction was quenched by slow addition of Na₂CO₃ (20 mL of a saturated aqueous solution) and allowed to warm to room temperature. The layers were separated and the aqueous fraction washed with DCM (6 x 25 mL). The combined organic fractions were dried (MgSO₄), filtered and concentrated *in vacuo*. Purification by column chromatography (Silica gel, EtOH) enabled isolation of the product as an off white solid (2.26 g, 67%).

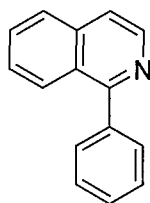
m.p. 103 - 104 °C; [Lit. 105 - 106 °C]²⁰³; ¹H NMR (270 MHz, CDCl₃, ppm) δ: 8.76 (s, 1H, ArH), 8.12 (dd, *J* = 1.69, 7.11, 1H, ArH), 7.81 - 7.55 (m, 5H, ArH); *m/z* (CI) 146 [M+H]⁺; The data is in agreement with the literature values.

1-Chloroisoquinoline⁶³ 2.15



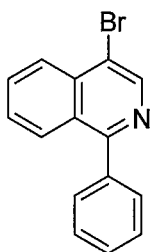
To a stirring solution of isoquinoline-*N*-oxide **2.14** (1.2 g, 8.3 mmol) in DCM (30 mL) was added POCl₃ (2.4 mL, 23.6 mmol). The solution was refluxed for 2 h and then cooled to room temperature after which it was cautiously poured onto ice and aqueous NH₃ (35% solution) was added until pH = 11 was attained. The layers were separated and the organic fraction dried (MgSO₄), filtered and concentrated *in vacuo*. Purification via Kugelrohr distillation under vacuum at 105 °C afforded the product as light yellow crystals (0.98 g, 73%).

m.p. 37 - 38 °C; [Lit. 36 - 37 °C]²⁰⁴; ¹H NMR (270 MHz, CDCl₃, ppm) δ: 8.36 (d, *J* = 8.1 Hz, 1H, ArH), 8.30 (dd, *J* = 1.1, 5.7 Hz, 1H, ArH), 7.86 (d, *J* = 7.9 Hz, 1H, ArH), 7.80 - 7.68 (m, 2H, ArH), 7.75 (d, *J* = 5.7 Hz, 1H, ArH); *m/z* (CI) 165 [M+H]⁺; The data is in agreement with the literature values.

1-Phenylisoquinoline⁴³ 2.17

1-Chloroisoquinoline **2.15** (2.1 g, 16.4 mmol), bromophenylboronic acid (2.4 g, 20.0 mmol), Pd(PPh₃)₄ (150 mg, 0.16 mmol) and Na₂CO₃ (1.9 g, 60 mmol) were suspended in a mixture of DME, H₂O and EtOH (40 mL, 3:1:1). The suspension was refluxed for 18 h and then allowed to cool to room temperature. The solution was extracted with DCM (50 mL) and washed with H₂O (3 x 50 mL), dried and concentrated *in vacuo*. Recrystallization from hexane afforded the product (2.34 g, 89%) as white crystals.

m.p. 94 - 95 °C; [Lit. 94 - 96 °C];²⁰⁵ ¹H NMR (400 MHz, CDCl₃, ppm) δ: 8.62 (d, *J* = 5.7 Hz, 1H, *ArH*), 8.10 (d, *J* = 8.8 Hz, 1H, *ArH*), 7.88 (d, *J* = 8.2 Hz, 1H, *ArH*), 7.69 (m, 4H, *ArH*), 7.54 (m, 4H, *ArH*); *m/z* (CI): 206 [M+H]⁺; The data is in agreement with the literature values.

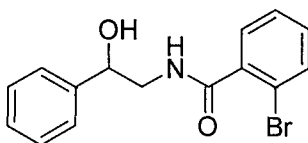
4-Bromo-1-phenylisoquinoline²⁰⁶ 2.18

1-Phenylisoquinoline **2.17** (1.0 g, 4.89 mmol), Br₂ (1.2 mL, 23 mmol) and I₂ (0.1 g, 0.39 mmol) were dissolved in nitrobenzene (50 mL) and the solution heated to reflux. After 3 h, the reaction mixture was allowed to cool to room temperature and concentrated *in vacuo*. The residue was taken up into CHCl₃ (50 mL) and washed with aqueous NaOH (50 mL of a 50% w/v solution), H₂O (2 x 100 mL), dried (MgSO₄) and concentrated *in vacuo*. Column chromatography (Silica gel, CHCl₃) afforded the product as a white solid. (1.16 g, 84%)

m.p. 128 - 133 °C; [Lit. 141 - 144 °C]²⁰⁶; ¹H NMR (400 MHz, CDCl₃, ppm) δ: 8.80 (s, 1H, *ArH*), 8.22 (d, *J* = 8.4 Hz, 1H, *ArH*), 8.07 (d, *J* = 8.5 Hz, 1H, *ArH*), 7.78 (t, *J* = 8.0 Hz, 1H, *ArH*), 7.65 (m, 2H, *ArH*), 7.53 (m, 4H, *ArH*); ¹³C{¹H} NMR (125 MHz, CDCl₃, ppm) δ: 160.3, 143.9, 138.8, 135.5, 131.3, 129.9, 128.9, 128.5, 128.2, 128.1,

128.0, 126.4, 118.7; m/z (CI) 284 $[M+H]^+$; The data is in agreement with the literature values.

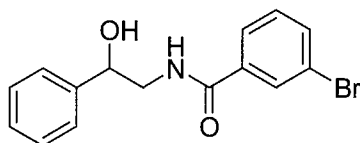
2-Bromo-*N*-(2-hydroxy-2-phenylethyl)-benzamide⁶⁵ 2.23



To a stirred solution of (\pm)-2-amino-1-phenylethanol (3.14 g, 22.8 mmol) and Et₃N (3.14 mL, 22.9 mmol) in DCM (50 mL) at 0 °C was added 2-bromobenzoyl chloride (5.00 g, 22.8 mmol), dropwise. Stirring was continued for 2 h after which time a white precipitate was observed. Filtration afforded the desired product in quantitative yield (7.28 g, 100%).

¹H NMR (400 MHz, CDCl₃, ppm) δ : 7.60 – 7.20 (m, 9H, ArH), 6.47 (br s, 1H, NH), 4.99 (m, 1H, (OH)CH), 3.91 (ddd, $J = 3.5, 7.0, 14.0$ Hz, 1H, CHH), 3.51 (m, 1H, CHH), 3.16 (br s, 1H, OH); m/z (CI) 285 $[M+H]^+$; The data is in agreement with the literature values.

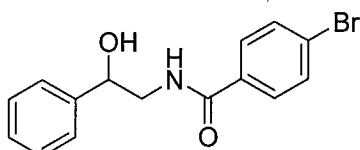
3-Bromo-*N*-(2-hydroxy-2-phenylethyl)-benzamide 2.24



Synthesized using the same procedure as 2-bromo-*N*-(2-hydroxy-2-phenylethyl)-benzamide using 3-bromobenzoyl chloride (5.00 g, 22.8 mmol). The product was isolated as a colourless solid (7.28 g, 100%).

¹H NMR (400 MHz, CDCl₃, ppm) δ : 7.60 – 7.20 (m, 9H, ArH), 6.43 (br s, 1H, NH), 4.96 (m, 1H, (OH)CH), 3.91 (ddd, $J = 3.4, 7.0, 13.8$ Hz, 1H, CHH), 3.50 (m, 1H, CHH), 3.16 (br s, 1H, OH); m/z (CI) 285 ($[M+H]^+$ 100%).

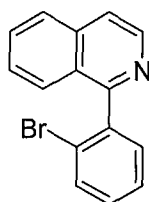
4-Bromo-*N*-(2-hydroxy-2-phenylethyl)-benzamide 2.25



Synthesized using the same procedure as 2-bromo-*N*-(2-hydroxy-2-phenylethyl)-benzamide using 4-bromobenzoyl chloride (5.00 g, 22.8 mmol). The product was isolated as a white solid (7.28 g, 100%).

^1H NMR (400 MHz, CDCl_3 , ppm) δ : 7.65 (dd, $J = 8.6, 24.2$ Hz, 4H, $\text{C}_6\text{H}_4\text{Br}$), 7.40 (m, 5H, C_6H_5), 6.59 (br s, 1H, NH), 5.00 (m, 1H, (OH)CH), 3.95 (ddd, $J = 3.4, 7.1, 14.1$ Hz, 1H, CHH), 3.53 (m, 1H, CHH), 3.08 (br s, 1H, OH); m/z (CI) 285 $[\text{M}+\text{H}]^+$

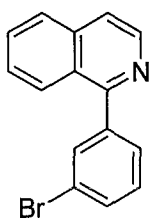
1-(2-Bromophenyl)-isoquinoline⁶⁵ 2.26



2-Bromo-*N*-(2-hydroxy-2-phenylethyl)-benzamide **2.23** (7.28 g, 22.75 mmol) was heated to reflux overnight in a 1:1 mixture of toluene and xylene (200 mL) with P_2O_5 (18 g, 64 mmol) and POCl_3 (25 mL, 273 mmol). The reaction mixture was cooled to room temperature and quenched by addition of MeOH. Addition of NaOH pellets until pH = 11 was obtained, followed by extraction with EtOAc, gave the crude title compound. Column chromatography (silica, petroleum ether: EtOAc 6:1) afforded the product as a colourless oil (4.51 g, 70%).

^1H NMR (270 MHz, CDCl_3 , ppm) δ : 8.62 (d, $J = 5.7$ Hz, 1H, ArH), 7.89 (d, $J = 8.2$ Hz, 1H, ArH), 7.75 - 7.35 (m, 8H, ArH); m/z (CI) 284 $[\text{M}+\text{H}]^+$; The data is in agreement with the literature values.

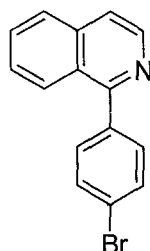
1-(3-Bromophenyl)-isoquinoline 2.27



Synthesized using the same procedure as for 1-(2-bromophenyl)-isoquinoline **2.26** using 3-bromo-*N*-(2-hydroxy-2-phenylethyl)-benzamide **2.24**. The compound was isolated as a white solid (4.88 g, 75%).

m.p. 52 - 53 °C; ^1H NMR (400 MHz, CDCl_3 , ppm) δ : 8.58 (d, $J = 5.6$ Hz, 1H, ArH), 8.02 (d, $J = 8.5$ Hz, 1H, ArH), 7.83 (m, 2H, ArH), 7.68 - 7.57 (m, 4H, ArH), 7.48 (t, $J = 7.3$ Hz, 1H, ArH), 7.37 (t, $J = 7.7$ Hz, 1H, ArH); $^{13}\text{C}\{^1\text{H}\}$ NMR (125 MHz, CDCl_3 , ppm) δ : 159.0, 142.2, 141.6, 136.9, 132.9, 131.7, 130.2, 129.9, 128.7, 127.6, 127.1, 126.6, 122.5, 120.4; m/z (CI) 284 $[\text{M}+\text{H}]^+$; Anal. Calcd. for $\text{C}_{15}\text{H}_{10}\text{BrN}$: C 64.40%, H 3.55%, N 4.93%; Found C 64.40%, H 3.57%, N 4.91%.

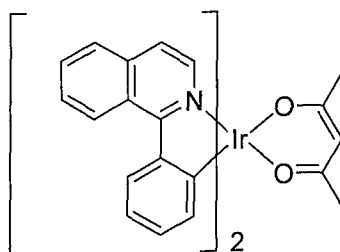
1-(4-Bromophenyl)-isoquinoline 2.28



Synthesised using the same procedure as for 1-(2-bromophenyl)-isoquinoline **2.26**, using 4-bromo-*N*-(2-hydroxy-2-phenylethyl)-benzamide **2.25**. The compound was isolated as a white solid (3.97 g, 61%).

m.p. 67 - 69 °C; ^1H NMR (400 MHz, CDCl_3 , ppm) δ : 8.62 (d, $J = 5.7$ Hz, 1H, ArH), 8.08 (d, $J = 8.5$ Hz, 1H, ArH), 7.01 (d, $J = 8.0$ Hz, 1H, ArH), 7.80 (m, 4H, ArH), 7.58 (m, 3H, ArH); $^{13}\text{C}\{^1\text{H}\}$ NMR (125 MHz, CDCl_3 , ppm) δ : 142.3, 142.2, 132.0, 131.6, 130.6, 130.2, 128.8, 127.5, 127.1, 126.9, 120.2, 120.0; m/z (CI): 284 $[\text{M}+\text{H}]^+$; Anal. Calcd. for $\text{C}_{15}\text{H}_{10}\text{BrN}$: C 64.40%, H 3.55%, N 4.93%; Found C 64.39%, H 3.63%, N 4.90%.

$[\text{Iridium(III)bis(1-phenylisoquinolinato-}N,C^2\text{)(acetylacetonate)}]^{27}$ 2.34

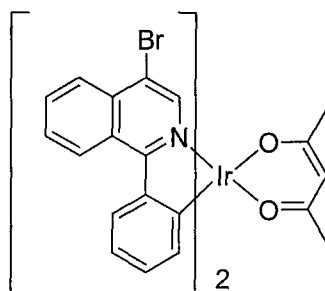


A mixture of $\text{IrCl}_3 \cdot x\text{H}_2\text{O}$ (0.08 g, 0.23 mmol) and 1-phenylisoquinoline **2.17** (0.14 g, 0.69 mmol) in 2-ethoxyethanol (7.5 mL) and H_2O (2.25 mL) was heated to 110 °C for 18 h. After the mixture cooled to room temperature, the precipitate was filtered and washed with $\text{EtOH}:\text{H}_2\text{O}$ (95:5, 30 mL) to yield crude $[\text{bis-iridium(III)di-}\mu\text{-chlorotetrakis(1-phenylisoquinolinato-}N,C^2\text{)}]$ as a red solid (0.14 g). The red solid was

added to 2-ethoxyethanol (10 mL) in the presence of acetyl acetone (0.10 mL, 0.61 mmol) and Na_2CO_3 (0.13 g, 1.3 mmol). The resulting suspension was stirred at 110 °C for 12 h. The reaction mixture was allowed to cool to room temperature and H_2O (10 mL) was added. The resulting red precipitate was filtered, washed with H_2O (30 mL) and then dissolved in DCM (30 mL), dried (MgSO_4), filtered and concentrated *in vacuo*. Purification by column chromatography (silica gel, DCM:Hexane, 5:1) afforded the product as a red solid (0.11 g, 68%).

^1H NMR (400 MHz, CDCl_3 , ppm) δ : 9.00 (m, 2H, ArH), 8.46 (d, $J = 6.4$ Hz, 2H, ArH), 8.21 (d, $J = 7.9$ Hz, 2H, ArH), 7.92 (m, 2H, ArH), 7.72 (m, 2H, ArH), 7.48 (d, $J = 6.4$ Hz, 2H, ArH), 6.89 (t, $J = 8.2$ Hz, 2H, ArH), 6.65 (t, $J = 7.7$ Hz, 2H, ArH), 6.39 (d, $J = 7.5$ Hz, 2H, ArH), 5.20 (s, 1H, $\text{OC}(\text{CH}_3)\text{CH}$), 1.75 (s, 6H, $\text{OC}(\text{CH}_3)\text{CH}$).; m/z (FAB): 700 $[\text{M}+\text{H}]^+$; The data is in agreement with the literature values.

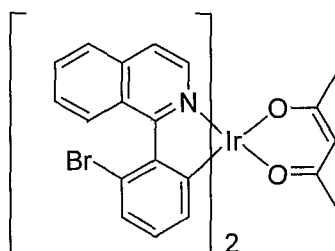
[Iridium(III)bis(4-bromo-1-phenylisoquinolinato-*N,C*)(acetylacetonate)] 2.35



A mixture of $\text{IrCl}_3 \cdot x\text{H}_2\text{O}$ (0.08 g, 0.23 mmol) and 4-bromo-1-phenylisoquinoline **2.18** (0.14 g, 0.51 mmol) in 2-ethoxyethanol (7.5 mL) and H_2O (2.25 mL) was heated to 110 °C for 18 h. After the mixture cooled to room temperature, the precipitate was filtered and washed with $\text{EtOH}:\text{H}_2\text{O}$ (95:5, 30 mL) to yield crude [bis-iridium(III)di- μ -chloro-tetrakis(4-bromo-1-phenylisoquinolinato)-*N,C*] as a red solid (0.14 g). Crude [bis-iridium(III)di- μ -chloro-tetrakis(4-bromo-1-phenylisoquinolinato)-*N,C*] (0.14 g, 0.143 mmol) was added to 2-ethoxyethanol (10 mL) in the presence of acetyl acetone (0.10 mL, 0.61 mmol) and Na_2CO_3 (0.13 g, 1.3 mmol). The resulting suspension was stirred at 110 °C for 12 h. The reaction mixture was allowed to cool to room temperature and H_2O (10 mL) was added. The resulting red precipitate isolated by filtration and washed with H_2O (2 x 30 mL). Purification via column chromatography (silica gel, DCM:Hexane, 5:1) afforded the product as a red solid (0.18 g, 92%).

^1H NMR (400 MHz, CDCl_3 , ppm) δ : 8.99 (d, $J = 8.4$ Hz, 2H, ArH), 8.63 (s, 2H, ArH), 8.32 (d, $J = 8.9$ Hz, 2H, ArH), 8.15 (d, $J = 7.9$ Hz, 2H, ArH), 7.84 (t, $J = 7.8$ Hz, 2H, ArH), 7.77 (t, $J = 7.1$ Hz, 2H, ArH), 6.91 (t, $J = 7.2$ Hz, 2H, ArH), 6.70 (t, $J = 6.5$ Hz, 2H, ArH), 6.41 (d, $J = 8.5$ Hz, 2H, ArH), 5.25 (s, 1H, $\text{OC}(\text{CH}_3)\text{CH}$), 1.81 (s, 6H, $\text{OC}(\text{CH}_3)\text{CH}$); $^{13}\text{C}\{^1\text{H}\}$ NMR (125 MHz, CDCl_3 , ppm) δ : 185.2, 151.4, 145.5, 141.8, 133.8, 131.9, 130.2, 129.5, 128.4, 127.5, 126.8, 126.5, 120.8, 115.8, 100.9, 28.8; m/z (FAB): 857 $[\text{M}+\text{H}]^+$; Anal. Calcd. for $\text{C}_{35}\text{H}_{25}\text{Br}_2\text{IrN}_2\text{O}_2$: C 49.02%, H 2.94%, N 3.27%; Found C 48.98%, H 2.97%, N 3.27%.

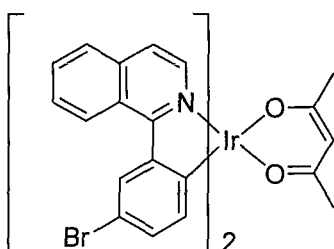
[Iridium(III)bis(1-(2-bromophenyl)isoquinolinato-*N,C*)(acetylacetonate)] 2.36



This compound was synthesized according to the method used to prepare compound **2.35** using 1-(2-(bromophenyl)isoquinoline **2.26**. It was isolated as a red solid (0.11 g, 57%).

^1H NMR (400 MHz, CDCl_3 , ppm) δ : 8.42 (d, $J = 8.3$ Hz, 2H, ArH), 8.32 (d, $J = 6.3$ Hz, 2H, ArH), 7.90 (d, $J = 8.1$ Hz, 2H, ArH), 7.71 (t, $J = 7.7$ Hz, 2H, ArH), 7.60 (t, $J = 7.6$ Hz, 4H, ArH), 7.11 (d, $J = 7.1$ Hz, 2H, ArH), 6.47 (br, 2H, ArH), 5.24 (br s, 1H, $\text{OC}(\text{CH}_3)\text{CH}$), 1.77 (br s, 6H, $\text{OC}(\text{CH}_3)\text{CH}$); $^{13}\text{C}\{^1\text{H}\}$ NMR (125 MHz, CDCl_3 , ppm) δ : 140.3, 140.0, 137.2, 131.3, 131.0, 130.7, 130.2, 129.7, 129.1, 127.7, 127.2, 127.0, 126.8, 125.9, 120.6, 119.9, 100.6, 28.6; m/z (FAB): 857 $[\text{M}+\text{H}]^+$; Anal. Calcd. for $\text{C}_{35}\text{H}_{25}\text{Br}_2\text{IrN}_2\text{O}_2$: C 49.02%, H 2.94%, N 3.27%; Found C 48.99%, H 2.95%, N 3.25%.

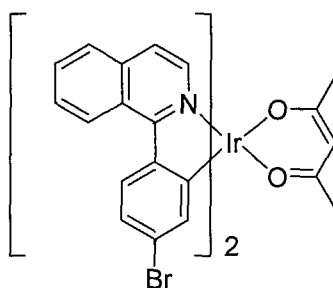
[Iridium(III)bis(1-(3-bromophenyl)isoquinolinato-*N,C*)(acetylacetonate)] 2.37



This compound was synthesized according to the method used to prepare compound **2.35** using 1-(3-(bromophenyl)isoquinoline **2.27**. It was isolated as a red solid (0.17 g, 63%).

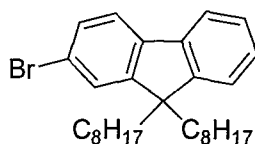
^1H NMR (400 MHz, CDCl_3 , ppm) δ : 8.91 (m, 2H, ArH), 8.41(d, $J = 6.4$ Hz, 2H, ArH), 8.30 (d, $J = 1.9$ Hz, 2H, ArH), 7.96 (m, 2H, ArH), 7.76 (m, 4H, ArH), 7.53 (d, $J = 6.3$ Hz, 2H, ArH), 6.77 (d, $J = 8.1$ Hz, 2H, ArH), 6.23 (d, $J = 8.2$ Hz, 2H, ArH), 5.21 (s, 1H, $\text{OC}(\text{CH}_3)\text{CH}$), 1.76 (s, 6H, $\text{OC}(\text{CH}_3)\text{CH}$); $^{13}\text{C}\{^1\text{H}\}$ NMR (125 MHz, CDCl_3 ppm) δ : 149.5, 148.6, 140.3, 137.2, 135.1, 132.0, 131.7, 131.0, 128.3, 127.4, 126.4, 120.7, 114.1; m/z (FAB): 857 $[\text{M}+\text{H}]^+$; Anal. Calcd. for $\text{C}_{35}\text{H}_{25}\text{Br}_2\text{IrN}_2\text{O}_2$: C 49.02%, H 2.94%, N 3.27%; Found C 48.95%, H 2.94%, N 3.23%.

[Iridium(III)bis(1-(4-bromophenyl)isoquinolino-*N,C*)(acetylacetonate)] **2.38**



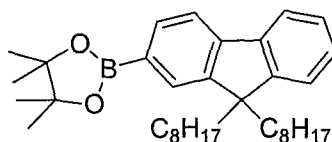
This compound was synthesized according to the method used to prepare compound **2.35**, using 1-(4-(bromophenyl)isoquinoline **2.28**. It was isolated as a red solid (0.18 g, 69%).

^1H NMR (400 MHz, CDCl_3 , ppm) δ : 9.03 (d, $J = 4.6$ Hz, 2H, ArH), 8.51 (d, $J = 6.3$ Hz, 2H, ArH), 8.26 (d, $J = 8.3$ Hz, 2H, ArH), 7.98 (d, $J = 4.6$ Hz, 2H, ArH), 7.77 (m, 4H, ArH), 7.55 (d, $J = 6.0$ Hz, 2H, ArH), 7.11 (d, $J = 8.0$ Hz, 2H, ArH), 6.56 (s, 2H, ArH), 5.26 (s, 1H, $\text{OC}(\text{CH}_3)\text{CH}$), 1.81 (s, 6H, $\text{OC}(\text{CH}_3)\text{CH}$); $^{13}\text{C}\{^1\text{H}\}$ NMR (125 MHz, CDCl_3 ppm) δ : 184.8, 169.0, 168.8, 151.9, 146.3, 140.6, 137.1, 131.5, 131.3, 130.7, 129.9, 128.7, 127.8, 127.4, 126.7, 126.4, 120.0, 119.5; m/z (FAB): 857 $[\text{M}+\text{H}]^+$; Anal. Calcd. for $\text{C}_{35}\text{H}_{25}\text{Br}_2\text{IrN}_2\text{O}_2$: C 49.02%, H 2.94%, N 3.27%; Found C 48.97%, H 2.93%, N 3.19%.

2-Bromo-9,9'-dioctyl-9H-fluorene³⁹ 2.40

2-Bromo-9H-fluorene (2.5 g, 10 mmol), 1-bromooctane (4 mL, 23 mmol) and tetrabutyl ammonium bromide (0.19 g, 0.01 mmol) were added to toluene (23 mL) and aqueous NaOH (23 mL of a 13 M solution) and the resulting suspension heated to reflux. After 6 h the reaction mixture was allowed cool to room temperature and the layers separated. The aqueous layer was extracted with DCM (3 x 50 mL) and the combined organic fractions were dried (MgSO₄), filtered and concentrated *in vacuo* to afford the crude title product. Excess 1-bromooctane was removed by Kugerohl distillation at 100 °C under vacuum to yield the product as a yellow oil (3.35 g, 70%).

¹H NMR (270 MHz, CDCl₃, ppm) δ: 7.71 - 7.63 (m, 1H, ArH), 7.57 - 7.54 (d, *J* = 8.7 Hz, 1H, ArH), 7.47 - 7.43 (m, 2H, ArH), 7.35 - 7.31 (m, 3H, ArH), 1.97 - 1.90 (m, 4H, CH₂), 1.22 - 1.04 (m, 20H, CH₂), 0.83 (t, *J* = 7.6 Hz, 6H, CH₃), 0.59 (m, 4H, CH₂); *m/z* (CI) 470 [M+H]⁺; The data is in agreement with the literature values.

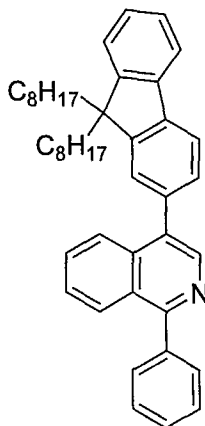
2-(9,9'-Dioctyl-9H-fluoren-2-yl)-4,4',5,5'-tetramethyl-1,3,2-dioxaborolane³⁸ 2.41

2-Bromo-9,9'-dioctyl-9H-fluorene **2.40** (5.0 g, 10.7 mmol) was dissolved in Et₂O (50 mL), at -78 °C, and *n*-butyllithium (8 mL of a 1.6 M solution in hexanes, 12.8 mmol) was added dropwise. The resulting milky suspension was stirred for 2 h after which it formed a pale yellow solution. 2-Isopropoxy-4,4',5,5'-tetramethyl-1,3,2-dioxaborolane (3.1 mL, 15 mmol) was added rapidly causing formation of a white suspension. After a further 2 h, the reaction was warmed to room temperature and stirred for 18 h. H₂O (10 mL) was added and the layers separated, the organic layer was dried (MgSO₄), filtered, and concentrated *in vacuo*. Column chromatography (silica gel, hexane:DCM, 5:1) enabled isolation of the product as a white crystalline solid (4.9 g, 89%).

m.p. 59 - 61 °C; [Lit. 50 - 53 °C]³⁸; ¹H NMR (270 MHz, CDCl₃, ppm) δ: 7.80 (d, *J* = 7.3 Hz, 1H, ArH), 7.72 (m, 3H, ArH), 7.32 (m, 3H, ArH), 1.97 (m, 4H, CH₂), 1.38 (s, 12H,

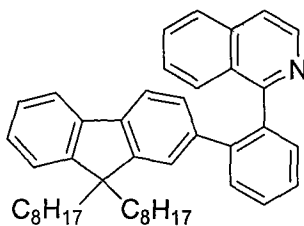
OCCH₃), 1.25 - 1.09 (m, 20H, CH₂), 0.81 (t, *J* = 6.6 Hz, 6H, CH₃), 0.59 (m, 4H, CH₂); *m/z* (CI) 518 [M+H]⁺; The data is in agreement with the literature values.

4-(9,9'-dioctyl-9H-fluoren-2-yl)-1-phenylisoquinoline 2.42



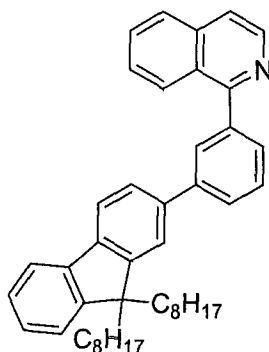
A solution of 2-(9,9'-dioctyl-9H-fluoren-2-yl)-4,4',5,5'-tetramethyl-1,3,2-dioxaborolane **2.41** (1.6 g, 3.1 mmol.), 4-bromo-1-phenylisoquinoline **2.18** (800 mg, 2.81 mmol), Pd(OAc)₂ (5 mg, 0.022 mmol) and PPh₃ (12 mg, 0.044 mmol) in toluene (75 mL) was heated to 90 °C. To this, aqueous Et₄NOH (7.50 mL of a 20 % solution) was added and the solution stirred at 110 °C. After 24 h, the reaction mixture was allowed to cool to room temperature and the layers separated. The organic layer was washed with H₂O (3 x 50 ml), dried (MgSO₄), filtered and concentrated *in vacuo*. Purification by column chromatography (silica gel, CHCl₃:Hexane; 2:1) afforded the title product as a colourless oil (1.53 g, 92%)

¹H NMR (400 MHz, CDCl₃, ppm) δ: 8.65 (s, 1H, ArH), 8.18 (d, *J* = 8.3 Hz, 1H, ArH), 8.01(d, *J* = 8.4 Hz, 1H, ArH), 7.86 (d, *J* = 7.7 Hz, 1H, ArH), 7.76 (m, 3H, ArH), 7.65 (t, *J* = 6.9 Hz, 1H, ArH), 7.54 (m, 6H, ArH), 7.38 (m, 3H, ArH), 1.98 (m, 4H, CH₂), 1.25 - 1.05 (m, 20H, CH₂), 0.82 - 0.70 (m, 10H, CH₂ and CH₃); ¹³C{¹H} NMR (125 MHz, CDCl₃ ppm) δ: 160.0, 151.1, 142.1, 140.9, 140.6, 139.7, 135.7, 135.4, 133.0, 130.0, 128.8, 128.6, 128.4, 127.9, 127.3, 126.9, 126.5, 125.3, 124.9, 123.0, 119.8, 55.2, 40.3, 31.8, 30.1, 29.2, 23.9, 22.6, 14.1; *m/z* (CI): 594 [M+H]⁺; Anal. Calcd. for C₄₄H₅₁N: C 88.99%, H 8.66%, N 2.36%; Found C 89.03%, H 8.69%, N 2.35%.

1-(2-(9,9'-Dioctyl-9H-fluoren-2-yl)phenyl)isoquinoline 2.43

1-(2-Bromophenyl)isoquinoline **2.26** (0.50 g, 1.77 mmol), 2-(9,9'-dioctyl-9H-fluoren-2-yl)-4,4',5,5'-tetramethyl-1,3,2-dioxaborolane **2.41** (1.01 g, 1.95 mmol) and Pd(PPh₃)₄ (10 mg, 0.01 mmol) were suspended in toluene (10 mL) and aqueous Et₄NOH (2 mL of a 20 % solution) and the reaction mixture was stirred at 90 °C for 18 h. After cooling to room temperature, the layers were separated and the organic layer was washed with H₂O (3 x 50 mL), dried (MgSO₄) and concentrated *in vacuo*. Column chromatography (silica gel, petroleum ether:EtOAc, 6:1) afforded the product as a colourless oil (0.75 g, 72%).

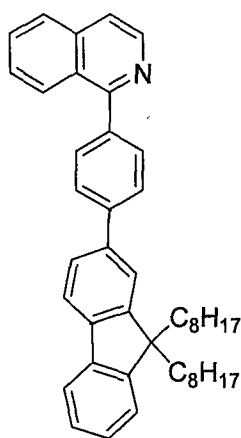
¹H NMR (400 MHz, CDCl₃, ppm) δ: 8.61 (d, *J* = 5.8 Hz, 1H, ArH), 7.63 (m, 9H, ArH), 7.44 (m, 2H, ArH), 7.23 (m, 4H, ArH), 6.96 (s, 1H, ArH), 1.64 (m, 6H, CH₃), 1.2 (m, 14H, CH₂), 0.90 (m, 14H, CH₂); ¹³C{¹H} NMR (125 MHz, CDCl₃ ppm) δ: 161.6, 150.7, 150.0, 142.0, 141.9, 140.6, 139.9, 139.4, 138.2, 135.9, 130.7, 130.1, 129.7, 128.7, 127.6, 127.5, 126.7, 126.5, 123.7, 122.7, 119.9, 119.4, 119.2, 54.6, 40.3, 40.0, 31.9, 31.8, 30.0, 29.3, 29.2, 23.4, 23.3, 22.6, 14.1; *m/z* (CI): 594 [M+H]⁺; Anal. Calcd. for C₄₄H₅₁N: C 88.99%, H 8.66%, N 2.36%; Found C 88.97%, H 8.63%, N 2.30%.

1-(3-(9,9'-Dioctyl-9H-fluoren-2-yl)phenyl)isoquinoline 2.44

Prepared according to the same procedure used for 1-(2-(9,9'-dioctyl-9H-fluoren-2-yl)phenyl)isoquinoline **2.43**, using 1-(3-bromophenyl)isoquinoline **2.27**. The title compound was isolated as a colourless oil (0.79 g, 80%).

^1H NMR (400 MHz, CDCl_3 , ppm) δ : 8.64 (d, $J = 5.7$ Hz, 1H, ArH), 8.17 (d, $J = 8.5$ Hz, 1H, ArH), 7.74 (m, 12H, ArH), 7.33 (m, 3H, ArH), 2.04 (m, 6H, CH_3), 1.03 (m, 28H, CH_2); $^{13}\text{C}\{^1\text{H}\}$ NMR (125 MHz, CDCl_3 ppm) δ : 161.8, 150.4, 159.6, 142.1, 141.9, 140.6, 134.0, 139.4, 138.2, 135.6, 130.7, 130.1, 129.7, 128.7, 127.6, 127.5, 126.7, 126.5, 123.7, 122.7, 119.8, 119.4, 119.2, 54.6, 40.3, 40.0, 31.8, 30.0, 29.4, 29.1, 23.4, 23.1, 22.8, 14.0; m/z (CI): 594 $[\text{M}+\text{H}]^+$; Anal. Calcd. for $\text{C}_{44}\text{H}_{51}\text{N}$: C 88.99%, H 8.66%, N 2.36%; Found C 88.98%, H 8.65%, N 2.31%

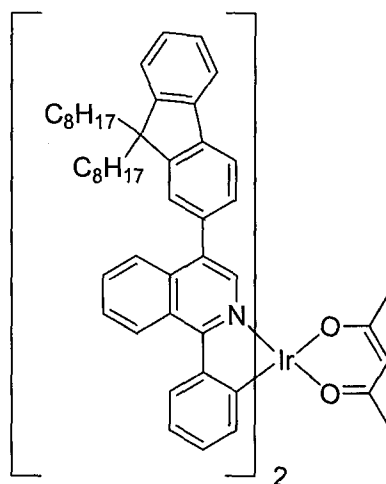
1-(4-(9,9'-dioctyl-9H-fluoren-2-yl)phenyl)isoquinoline 2.45



Prepared according to the same procedure used for 1-(2-(9,9'-dioctyl-9H-fluoren-2-yl)phenyl)isoquinoline **2.43**, using 1-(4-bromophenyl)isoquinoline **2.28**. The title compound was isolated as a colourless oil (0.68 g, 70%).

^1H NMR (400 MHz, CDCl_3 , ppm) δ : 8.67 (d, $J = 5.7$ Hz, 1H, ArH), 8.24 (d, $J = 8.5$ Hz, 1H, ArH), 7.95 (d, $J = 8.1$ Hz, 1H, ArH), 7.75 (m, 10H, ArH), 7.60 (t, $J = 7.7$ Hz, 1H, ArH), 7.38 (m, 3H, ArH), 2.06 (m, 4H, CH_2), 1.09 (m, 20H, CH_2), 0.83 (m, 6H, CH_3), 0.74 (m, 4H, CH_2); $^{13}\text{C}\{^1\text{H}\}$ NMR (125 MHz, CDCl_3 ppm) δ : 151.5, 151.0, 142.3, 141.9, 140.7, 139.4, 136.9, 130.4, 130.0, 127.6, 127.2, 127.1, 126.8, 126.0, 122.9, 121.5, 120.0, 119.9, 119.8, 61.0, 55.2, 40.4, 31.7, 30.0, 29.2, 23.8, 22.6, 14.0; m/z (CI): 594 $[\text{M}+\text{H}]^+$; Anal. Calcd. for $\text{C}_{44}\text{H}_{51}\text{N}$: C 88.99%, H 8.66%, N 2.36%; Found C 89.01%, H 8.67%, N 2.31%;

[Iridium(III)bis(4-(9,9'-dioctyl-9H-fluoren-2-yl)-1-phenylisoquinolinato-*N,C*) (acetylacetonate)] 2.50

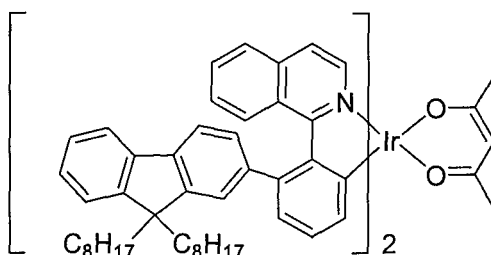


A mixture of $\text{IrCl}_3 \cdot x\text{H}_2\text{O}$ (0.114 g, 0.32 mmol) and 4-(2-(9,9'-dioctylfluorene))-1-phenylisoquinoline **2.42** (0.5 g, 0.84 mmol) in 2-ethoxyethanol (15 mL) and H_2O (5 mL) was heated to 110 °C for 18 h. After the mixture cooled to room temperature, the precipitate was filtered and washed with $\text{EtOH}:\text{H}_2\text{O}$ (95:5, 30 mL). The precipitate was then dissolved in DCM (50 mL), dried (MgSO_4) and concentrated *in vacuo* to yield crude [bis-iridium(III)di- μ -chlorotetrakis(4-(2-9,9'-dioctyl-9H-fluoren-2-yl)-1-phenylisoquinolinato-*N,C*)] as a dark red solid (312 mg). Crude [bis-iridium(III)di- μ -chlorotetrakis(4-(2-9,9'-dioctyl-9H-fluoren-2-yl)-1-phenylisoquinolinato-*N,C*)] (0.312 g, 0.11 mmol) was dissolved in 2-ethoxyethanol (10 mL) in the presence of acetyl acetone (0.10 mL, 0.61 mmol) and Na_2CO_3 (0.13 g, 1.3 mmol). The resulting suspension was stirred at 110 °C for 12 h. The reaction mixture was allowed to cool to room temperature and H_2O (10 mL) was added. The resulting red precipitate was filtered, washed with H_2O (30 mL) and then dissolved in DCM (30 mL), dried (MgSO_4), filtered and concentrated *in vacuo*. Purification by flash column chromatography (silica gel, DCM:Hexane, 5:1) afforded the title product as a red amorphous solid (0.26 g, 56%)

^1H NMR (400 MHz, CDCl_3 , ppm) δ : 9.08 (d, $J = 8.5$ Hz, 2H, ArH), 8.60 (s, 2H, ArH), 8.23(d, $J = 7.9$ Hz, 2H, ArH), 8.10 (d, $J = 8.8$ Hz, 2H, ArH), 7.85 (d, $J = 8.2$ Hz, 2H, ArH), 7.78 (d, $J = 7.3$ Hz, 2H, ArH), 7.74 (t, $J = 8.1$ Hz, 2H), 7.67 (t, $J = 7.3$ Hz, 2H), 7.55 (m, 4H, ArH), 7.39 (m, 6H, ArH), 6.95 (t, $J = 8.1$ Hz, 2H), 6.73 (t, $J = 8.1$ Hz, 2H), 6.60(d, $J = 7.4$ Hz, 2H, ArH), 5.28 (s, 1H, $\text{OC}(\text{CH}_3)\text{CH}$), 2.10 - 2.00, (m, 8H, CH_2), 1.77 (s, 6H, $\text{OC}(\text{CH}_3)\text{CH}$), 1.25 - 1.05 (s, 40H, CH_2), 0.85 - 0.60 (m, 20H, CH_2 and CH_3); $^{13}\text{C}\{^1\text{H}\}$ NMR (125 MHz, CDCl_3 , ppm) δ : 184.8, 169.1, 152.1, 150.8, 150.6,

145.8, 140.8, 140.1, 139.4, 137.1, 131.1, 130.6, 129.9, 127.7, 127.4, 126.7, 126.5, 126.4, 125.6, 122.6, 121.1, 120.9, 119.5, 119.3, 100.6, 99.9, 54.7, 40.5, 40.3, 31.8, 30.1, 30.0, 29.3, 29.2, 28.8, 23.6, 22.6, 14.1; m/z (FAB): 1477 $[M+H]^+$; Anal. Calcd. for $C_{93}H_{107}IrN_2O_2$: C 75.62%, H 7.30%, N 1.90%; Found C 75.58%, H 7.30%, N 1.96%;

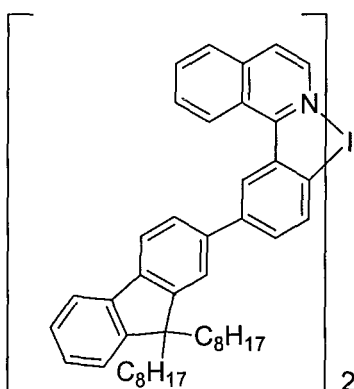
[Iridium(III)bis(1-(2-(9,9'-dioctyl-9H-fluoren-2-yl)phenyl)isoquinolinato-*N,C*)(acetylacetonate)] 2.51



This complex was synthesised according to the method used to prepare compound **2.50**, using 1-(2-(9,9'-dioctyl-9H-fluoren-2-yl)phenyl)isoquinoline **2.43**. It was isolated as a red solid (0.36 g, 44%).

1H NMR (400 MHz, $CDCl_3$, ppm) δ : 8.48 (d, $J = 6.3$ Hz, 2H, ArH), 8.07 (br, m, 2H, ArH), 7.62 (br m, 6H, ArH), 7.46 (br m, 4H, ArH), 7.24 (m, 10H, ArH), 7.01 (br m, 6H, ArH), 6.75 (br m, 2H, ArH), 5.39 (br s, 1H, OC(CH₃)CH), 1.92 (br m, 12H, CH₂ and CH₃), 1.28 (br m, 48H, OC(CH₃)CH and CH₃ and CH₂), 0.42 (br m, 8H, CH₂); $^{13}C\{^1H\}$ NMR (125 MHz, $CDCl_3$, ppm) δ : 185.1, 185.1, 171.6, 150.8, 143.1, 143.1, 140.7, 140.3, 138.9, 136.1, 131.7, 129.9, 129.7, 128.8, 128.7, 126.5, 125.6, 125.1, 124.8, 122.9, 120.0, 119.5, 107.9, 100.6, 54.6, 54.5, 39.9, 31.9, 31.7, 30.3, 30.0, 29.7, 29.5, 29.2, 28.7, 23.5, 22.7, 22.6, 14.1; m/z (FAB): 1477 $[M+H]^+$; Anal. Calcd. for $C_{93}H_{107}IrN_2O_2$: C 75.62%, H 7.30%, N 1.90%; Found C 75.63%, H 7.35%, N 1.92%.

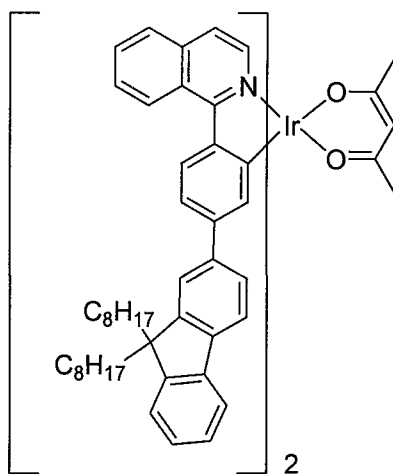
[Iridium(III)bis(1-(3-(9,9'-dioctyl-9H-fluoren-2-yl)phenyl)isoquinolinato-*N,C*)(acetylacetonate)] 2.52



This complex was synthesised according to the method used to prepare compound **2.50**, using 1-(3-(9,9'-dioctyl-9*H*-fluoren-2-yl)phenyl)isoquinoline **2.44**. It was isolated as a red solid (0.27 g, 47%).

^1H NMR (400 MHz, CDCl_3 , ppm) δ : 9.18 (m, 2H, Ar*H*), 8.59 (d, $J = 8.6$ Hz, 2H, Ar*H*), 8.57 (s, 2H, Ar*H*), 8.01 (m, 2H, Ar*H*), 7.75 (m, 8H, Ar*H*), 7.59 (m, 4H, Ar*H*), 7.53 (s, 2H, Ar*H*), 7.32 (m, 6H, Ar*H*), 7.08 (d, $J = 7.9$ Hz, 2H, Ar*H*), 6.61 (d, $J = 6.6$ Hz, 2H, Ar*H*), 5.31 (s, 1H, OC(CH₃)CH), 1.97 (m, 8H, CH₂), 1.86 (s, 6H, OC(CH₃)CH), 1.11 (m, 40H, CH₂), 0.81 (m, 12H, CH₃), 0.70 (m, 8H, CH₂); $^{13}\text{C}\{^1\text{H}\}$ NMR (125 MHz, CDCl_3 , ppm) δ : 184.9, 169.2, 151.3, 151.2, 150.9, 147.2, 141.4, 141.0, 140.6, 139.3, 137.3, 134.1, 133.9, 130.7, 128.6, 128.3, 127.7, 127.4, 126.8, 126.7, 126.5, 125.3, 122.8, 121.2, 120.0, 119.8, 119.5, 100.6, 54.9, 40.4, 31.7, 30.1, 29.2, 28.8, 23.8, 22.6, 14.0; m/z (FAB): 1477 [M+H]⁺; Anal. Calcd. for C₉₃H₁₀₇IrN₂O₂: C 75.62%, H 7.30%, N 1.90%; Found C 75.6%, H 7.18%, N 1.91%.

[Iridium(III)bis(1-(4-(9,9'-dioctyl-9*H*-fluoren-2-yl)phenyl)isoquinolinato-*N,C*(acetylacetonate)] 2.53

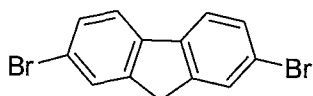


This complex was synthesised according to the method used to prepare compound **2.50**, using 1-(4-(9,9'-dioctyl-9*H*-fluoren-2-yl)phenyl)isoquinoline **2.45**. It was isolated as a red solid (0.21 g, 57%).

^1H NMR (400 MHz, CDCl_3 , ppm) δ : 9.09 (m, 2H, Ar*H*), 8.59 (d, $J = 6.2$ Hz, 2H, Ar*H*), 8.33 (d, $J = 8.5$ Hz, 2H, Ar*H*), 7.99 (m, 2H, Ar*H*), 7.81 (m, 4H, Ar*H*), 7.61 (d, $J = 7.1$ Hz, 2H, Ar*H*), 7.55 (d, $J = 6.3$ Hz, 2H, Ar*H*), 7.51 (d, $J = 7.9$ Hz, 2H, Ar*H*), 7.29 (m, 16H, Ar*H*), 7.12 (d, $J = 1.2$ Hz, 2H, Ar*H*), 6.76 (d, $J = 1.9$ Hz, 2H, Ar*H*), 5.32 (s, 1H, OC(CH₃)CH), 1.86 (s, 6H, OC(CH₃)CH), 1.80 (m, 4H, CH₂), 1.61 (m, 4H, CH₂), 0.7-

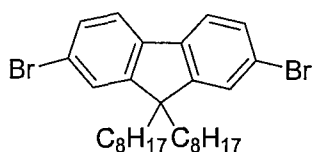
1.7 (m, 52H, CH_2 and CH_3), 0.46 (m, 8H, CH_2); $^{13}C\{^1H\}$ NMR (125 MHz, $CDCl_3$, ppm) δ : 184.8, 169.1, 152.1, 150.8, 150.6, 145.8, 140.8, 140.1, 139.4, 137.1, 131.1, 130.6, 129.9, 127.7, 127.4, 126.7, 126.5, 126.4, 125.6, 122.6, 121.1, 120.9, 119.5, 119.3, 100.6, 99.9, 54.7, 40.5, 40.3, 31.8, 30.1, 30.0, 29.3, 29.2, 28.8, 23.6, 22.6, 14.1; m/z (FAB): 1477 $[M+H]^+$; Anal. Calcd. for $C_{93}H_{107}IrN_2O_2$: C 75.62%, H 7.30%, N 1.90%; Found C 75.58%, H 7.15%, N 1.88%.

6.4 Experimental for Chapter 3

2,7-Dibromo-9*H*-fluorene³⁹ 3.15

9*H*-Fluorene (6.25 g, 37.6 mmol) and I₂ (0.75 g, 3.0 mmol) were dissolved in DCM (60 mL) and cooled to 0 °C, to give a deep red solution. Br₂ (4 mL, 77.5 mmol) in DCM (10 mL) was added dropwise, over a one hour period, to give a suspension. The reaction vessel was allowed to warm to room temperature and then stirred for a further four hours. Aqueous Na₂S₂O₃ (50 mL of a 1 M solution) was added slowly, causing the mixture to change from a deep red to a pale yellow suspension. The layers were separated and the aqueous fraction was extracted with DCM (2 x 50 mL). The combined organic fractions were dried (MgSO₄) and concentrated *in vacuo* to give an off-white solid which was recrystallized from EtOAc (100 mL) to give the product as white crystals (10.1 g, 83%).

m.p. (EtOAc) 162 - 163 °C; [Lit. (EtOAc) 164 - 166 °C]³⁹; ¹H NMR (270 MHz, CDCl₃, ppm) δ: 7.66 (m, 2H, Ar*H*), 7.61 - 7.59 (m, 2H, Ar*H*), 7.52 - 7.49 (m, 2H, Ar*H*), 3.87 (s, 2H, CH₂); *m/z* (CI) 325 [M+H]⁺; The data is in agreement with the literature values.

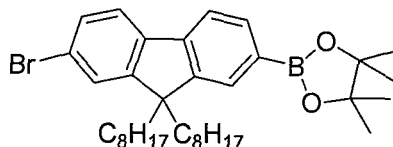
2,7-Dibromo-9,9'-dioctyl-9*H*-fluorene³⁹ 3.16

2,7-Dibromo-9*H*-fluorene **3.15** (10 g, 31 mmol), 1-bromooctane (16 mL, 93 mmol) and tetrabutylammoniumbromide (0.81 g, 0.05 mmol) were added to a round bottom flask containing aqueous NaOH (100 mL of a 13 M solution) and the resulting suspension heated to reflux. After 24 h the reaction mixture was allowed cool to room temperature and the layers separated. The aqueous layer was extracted with DCM (3 x 50 mL) and the combined organic fractions were washed with H₂O (3 x 50 mL), dried (MgSO₄), filtered and concentrated *in vacuo* to afford yellow crystals. Excess 1-bromooctane was removed by Kugerohl distillation, at 100 °C, under vacuum, and recrystallization from ethanol yielded the product as white crystals (14.4 g, 87%).

m.p. (EtOH) 53-59 °C; [Lit. (EtOH) 59 - 63 °C]³⁹; ¹H NMR (270 MHz, CDCl₃, ppm) δ: 7.53 - 7.51 (m, 2H, Ar*H*) 7.46 - 7.42 (m, 4H, Ar*H*), 1.93 - 1.89 (m, 4H, CH₂), 1.24 -

0.95 (m, 20H, CH_2), 0.83 (t, $J = 7.1$ Hz, 6H, CH_3), 0.56 (m, 4H, CH_2); m/z (CI) 549 $[\text{M}+\text{H}]^+$; The data is in agreement with the literature values.

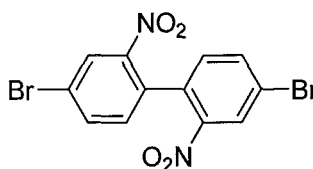
2-(7-Bromo-9,9'-dioctyl-9H-fluoren-2-yl)-4,4',5,5'-tetramethyl-1,3,2-dioxaborolane³⁹ 3.17



2,7-Dibromo-9,9'-dioctyl-9H-fluorene **3.16** (5.0 g, 9.25 mmol) was dissolved in THF (50 mL) at -78 °C and *n*-butyllithium (6 mL of a 1.6 M solution in hexanes) was added dropwise. The resulting suspension was stirred for 2 h after which point 2-isopropoxy-4,4',5,5'-tetramethyl-1,3,2-dioxaborolane (2.3 mL, 10 mmol) was added rapidly. After a further 2 h, the reaction was warmed to room temperature and stirred for a further 18 h. H_2O (10 mL) was added and the layers separated, the organic fraction was dried (MgSO_4), filtered, and concentrated *in vacuo*. Column chromatography (silica gel, hexane:DCM, 5:1, R_f 0.3) afforded a white solid which was recrystallized twice from propan-2-ol to afford the product as white crystals (2.87 g, 52%).

m.p. (propan-2-ol) $63\text{--}65$ °C; [Lit. $58 - 60$ °C]³⁹; ^1H NMR (270 MHz, CDCl_3 , ppm): 7.80 (d, $J = 7.5$ Hz, 1H, ArH), 7.72 (s, 1H, ArH), 7.65 (d, $J = 7.6$ Hz, 1H, ArH), 7.57 (d, $J = 7.5$ Hz, 1H, ArH), 7.47 (s, 1H, ArH), 7.45 (d, $J = 7.6$ Hz, 1H, ArH), 1.93 - 1.89 (m, 4H, CH_2), 1.37 (s, 12H, OCCH_3), 1.18-1.02 (m, 20H, CH_2), 0.83 (t, $J = 7.1$ Hz, 6H, CH_3), 0.56 (m, 4H, CH_2); m/z (CI) 595 $[\text{M}+\text{H}]^+$; The data is in agreement with the literature values.

4,4'-Dibromo-2,2'-dinitrophenyl²⁰⁷ 3.19

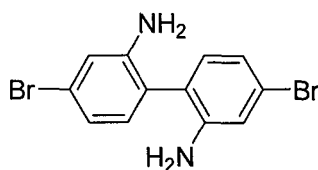


To a stirring solution of 2,5-dibromonitrobenzene (24.0 g, 85.4 mmol) in DMF (110 mL) was added Cu powder (12.0 g, 188.9 mmol), and the reaction mixture was heated to 125 °C. After 3 h, the mixture was allowed to cool to room temperature and concentrated *in vacuo*. The resulting solid was dissolved in toluene (400 mL) and filtered through Celite. The filtrate was washed with H_2O (2 x 50 mL) and aqueous

NaHCO₃ (50 mL of a 10% solution) and evaporated to dryness to yield the crude product as yellow crystals. The crude product was recrystallized from propan-2-ol to afford the product as white crystals (16.8 g, 98% yield).

m.p. (propan-2-ol) 148 - 150 °C; [Lit. 146 - 148 °C (Ethanol)]²⁰⁷; ¹H NMR (400 MHz, CDCl₃, ppm) δ: 7.17 (d, *J* = 8.0, 2H, ArH), 7.84 (dd, *J* = 8.0, 2.0, 2H, ArH), 8.39 (d, *J* = 2.0, 2H, ArH); *m/z* (Cl) 402 [M+H]⁺; The data is in agreement with the literature values.

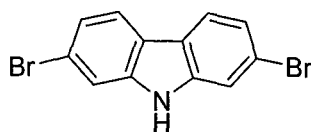
4,4'-Dibromobiphenyl-2,2'-diamine²⁰⁷ 3.20



To a solution of 4,4'-dibromo-2,2'-dinitrobiphenyl **3.19** (11.0 g, 27.4 mmol) in EtOH (135 mL) was added aqueous HCl (78.0 mL of a w/w 32% solution)). Sn powder (13.0 g, 108.5 mmol) was then added portionwise over 10 min, and the reaction mixture was heated to reflux for 2 h. After cooling, the mixture was poured into ice (400 mL) and then aqueous NaOH (20% w/w solution) was added until the solution was pH 9.0. The product was extracted with Et₂O and the organic layer was washed with H₂O (2 x 100 mL), dried (MgSO₄), filtered, and concentrated *in vacuo* to give the product as light-brown crystals (8.6 g, 92%).

m.p. 99 - 101 °C; [Lit. 99 - 105 °C (Ethanol)]²⁰⁷; ¹H NMR (400 MHz, CDCl₃, ppm) δ: 6.92 (s, 6H, ArH), 3.78 (br s, 2H, NH₂); *m/z* (Cl) 342 [M+H]⁺; The data is in agreement with the literature values.

2,7-Dibromo-9H-carbazole²⁰⁷ 3.21

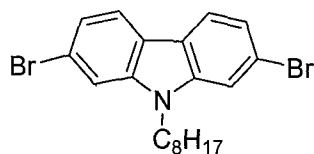


A solution of 2,2'-diamino-4,4'-dibromobiphenyl **3.20** (8.6 g, 26 mmol) in aqueous H₃PO₄, (90 mL of a 85% solution) was stirred at 200 °C for 48 h. The precipitate which had formed was filtered off, washed with H₂O (100 mL), dissolved in toluene (100 mL) and then filtered through Celite 545. The filtrate was concentrated to approximately 20

mL and hexane (100 mL) was added to precipitate the product as beige crystals (6.9 g, 85%).

m.p. 202 - 206 °C; [Lit. 198 - 203 °C]²⁰⁷; ¹H NMR (400 MHz, CDCl₃, ppm) δ: 8.05 (br s, 1H, NH), 7.89 (d, *J* = 8.3 Hz, 2H, ArH), 7.59 (d, *J* = 1.7 Hz, 2H, ArH), 7.37 (dd, *J* = 8.3, 1.7 Hz, 2H, ArH); *m/z* (CI) 326 [M+H]⁺; The data is in agreement with the literature values.

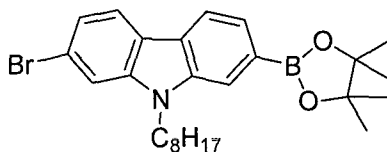
2,7-Dibromo-9-octyl-9H-carbazole²⁰⁸ 3.22



2,7-dibromo-9H-carbazole **3.21** (3 g, 9.23 mmol), K₂CO₃ (2.5 g, 18.1 mmol), and 1-bromooctane (2.5 mL, 15 mmol) were added to DMF (100 mL). The resulting mixture was stirred at 80 °C for 12 h. The solution was allowed to cool to room temperature and H₂O (150 mL) was added, the layers separated and aqueous layer was extracted twice with CHCl₃ (2 x 100 mL). The combined organic layers were washed with H₂O (5 x 50 mL), dried (MgSO₄), and then concentrated *in vacuo*. Recrystallization from MeOH afforded the product as white crystals (3.3 g, 82% yield).

m.p. (MeOH) 71 - 72 °C; [Lit. 66 - 67 °C (MeOH)]²⁰⁸; ¹H NMR (400 MHz, CDCl₃, ppm) δ: 7.86 (d, *J* = 8.3 Hz, 2H, ArH), 7.51 (d, *J* = 1.6 Hz, 2H, ArH), 7.33 (dd, *J* = 8.3, 1.6 Hz, 2H, ArH), 4.16 (t, *J* = 7.4 Hz, 2H, NCH₂), 1.82 (m, 2H, CH₂), 1.30 (m, 10H, CH₂), 0.89 (t, *J* = 6.9 Hz, 3H, CH₃); *m/z* (CI) 438 [M+H]⁺; The data is in agreement with the literature values.

2-Bromo-9-octyl-7-(4,4',5,5'-tetramethyl-1,3,2-dioxaborolan-2-yl)-9H-carbazole 3.23

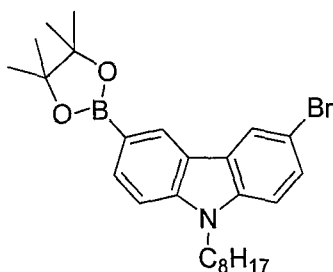


2,7-Dibromo-9-octyl-9H-carbazole **3.22** (5.0 g, 11.4 mmol) was dissolved in THF (50 mL), at -78 °C, and *n*-butyllithium (7.75 mL of a 1.6 M solution in hexanes, 12.5 mmol) was added dropwise. The resulting suspension was stirred for 2 h after which point 2-isopropoxy-4,4,5,5-tetramethyl-1,3,2-dioxaborolane (3.1 mL, 15 mmol) was added

rapidly. After a further 2 h, the reaction was warmed to room temperature and stirred for a further 18 h. H₂O (10 mL) was added and the layers separated, the organic fraction was dried (MgSO₄), filtered, and concentrated *in vacuo*. Column chromatography (silica gel, hexane:DCM:Et₃N 5:1:0.01,) enabled isolation of the pure product as a colourless oil (4.25 g, 77%).

¹H NMR (400 MHz, CDCl₃, ppm) δ: 7.80 (d, *J* = 7.5 Hz, 1H, ArH), 7.72 (s, 1H, ArH), 7.65 (d, *J* = 7.6 Hz, 1H, ArH), 7.57 (d, *J* = 7.5 Hz, 1H, ArH), 7.47 (s, 1H, ArH), 7.45 (d, *J* = 7.6 Hz, 1H, ArH), 4.16 (t, *J* = 7.4 Hz, 2H, NCH₂), 1.82 (m, 2H, CH₂), 1.37 (s, 12H, OCCH₃) 1.30 (m, 10H, CH₂), 0.89 (t, *J* = 6.9 Hz, 3H, CH₃); ¹³C{¹H} NMR (125 MHz, CDCl₃, ppm) δ: 141.7, 125.5, 124.8, 121.9, 121.5, 119.9, 119.6, 115.2, 111.9, 83.9, 43.1, 31.8, 29.3, 29.2, 29.0, 27.1, 24.9, 22.6, 14.1; *m/z* (CI) 595 [M+H]⁺; Anal. Calcd. for C₂₆H₃₅BBrNO₂: C 64.48%, H 7.28%, N 2.89%; Found C 64.48%, H 7.25%, N 2.88%.

3-Bromo-9-octyl-6-(4,4',5,5'-tetramethyl-1,3,2-dioxaborolan-2-yl)-9H-carbazole 3.25

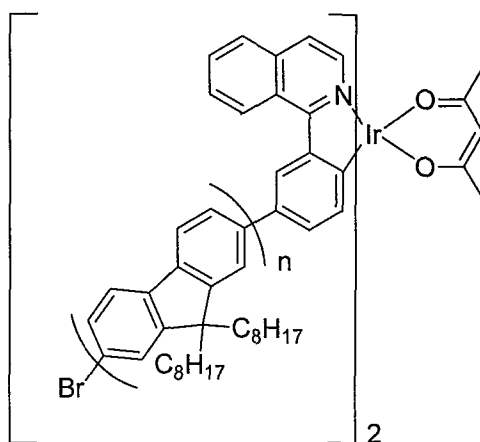


3,6-Dibromo-9-octyl-9H-carbazole (5.0 g, 11.4 mmol) was dissolved in THF (50 mL), at -78 °C, and *n*-butyllithium (7.75 mL of a 1.6 M solution in hexanes, 12.5 mmol) was added, dropwise. The resulting suspension was stirred for 2 h, after which point 2-isopropoxy-4,4',5,5'-tetramethyl-1,3,2-dioxaborolane (3.1 mL, 15 mmol) was added rapidly. After a further 2 h, the reaction was warmed to room temperature and stirred for a further 18 hr. H₂O (10 mL) was added and the layers separated, the organic fraction was dried (MgSO₄), filtered, and concentrated *in vacuo*. Column chromatography (silica gel, hexane:DCM:Et₃N 5:1:0.01,) enabled isolation of the pure product as a colourless oil (3.42 g, 62%).

¹H NMR (400 MHz, CDCl₃) δ: 8.55 (s, 1H, ArH), 8.24 (d, *J* = 1.9 Hz, 1H, ArH), 7.92 (dd, *J* = 0.8, 8.3 Hz, 1H, ArH), 7.53 (dd, *J* = 1.9, 8.7 Hz, 1H, ArH), 7.38 (d, *J* = 8.3 Hz, 1H, ArH), 7.27 (d, *J* = 8.3 Hz, 1H, ArH), 4.27 (t, *J* = 7.2, 2H, NCH₂), 1.91 – 1.77 (m,

2H, CH₂), 1.39 (s, 12H, OCCH₃), 1.37 – 1.10 (m, 12H, CH₂), 0.91 – 0.82 (m, 3H, CH₃); ¹³C{¹H} NMR (125 MHz, CDCl₃, ppm) δ: 142.8, 139.2, 132.7, 128.2, 128.0, 124.8, 123.3, 121.6, 112.0, 110.2, 108.3, 83.7, 43.2, 31.8, 29.3, 29.1, 28.9, 27.2, 24.9, 22.6, 14.1; *m/z* (CI) 595 [M+H]⁺; Anal. Calcd. for C₂₆H₃₅BBrNO₂: C 64.48%, H 7.28%, N 2.89%; Found C 64.51%, H 7.36%, N 2.85%.

[Iridium(III)bis(1-(3-(ω-bromo-oligo(9,9'-dioctyl-9*H*-fluorene-2,7-diyl))phenyl)isoquinolinato-*N,C*(acetylacetonate)] 3.26

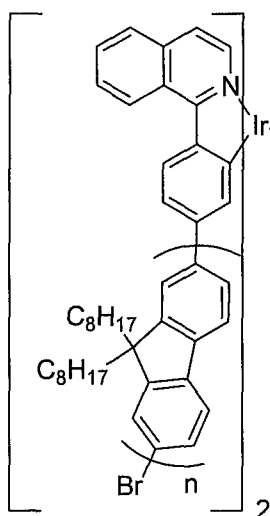


A solution of 2-(7-bromo-9,9'-dioctyl-9*H*-fluorene-2-yl)-4,4',5,5'-tetramethyl-1,3,2-dioxaborolane **3.17** (1.04 g, 1.74 mmol), Ir(III)bis(1-(3-bromophenyl)isoquinolinato-*N,C*(acetylacetonate) **2.37** (83 mg, 0.097 mmol, 1 eq.), Pd(OAc)₂ (5 mg, 0.022 mmol) and PCy₃ (12 mg, 0.044 mmol) in toluene (75 mL) was heated to 90 °C. To this, aqueous Et₄NOH (7.50 mL of a 20 % solution) was added and the solution stirred at 110 °C for 48 h. The reaction mixture was cooled to room temperature and subsequently poured into a large excess of MeOH (200 mL), which resulted in the precipitation of the polymer. The precipitate was isolated by filtration, washed with H₂O (40 mL), MeOH (40 mL) and acetone (30 mL) and filtered through celite using toluene as the eluent. The resulting solution was concentrated (to 20 mL) and Na₂CO₃ (0.20 g), acetyl acetone (2.00 mL) and 2-ethoxyethanol (10 mL) were added. The reaction mixture was stirred for 2 h at 110 °C and subsequently cooled to room temperature. The solution was again poured into an excess of MeOH (100 mL) and the precipitate filtered, washed with H₂O (40 mL) and MeOH (40 mL) and dried *in vacuo*. The pure product was isolated as a red powder (0.42 g, 55%).

¹H NMR (400 MHz, CDCl₃, ppm) δ: 9.14 (br m, Piq*H*), 8.54 (br m, Piq*H*), 7.90 - 7.60 (br m, 6H, Ar*H*), 7.04 (br m, Piq*H*), 6.56 (br m, Piq*H*), 5.27 (br s, OC(CH₃)CH), 2.30-

2.00 (br m, 4H, CH_2), 1.83 (br s, $OC(CH_3)CH$), 1.30-1.00 (br m, 20H, CH_2), 0.90-0.70 (br m, 10H, CH_3 and CH_2); $^{13}C\{^1H\}$ NMR (125 MHz, $CDCl_3$, ppm) δ : 151.8, 140.5, 140.0, 126.2, 121.5, 119.9, 55.3, 40.5, 40.4, 31.8, 30.1, 29.2, 23.9, 22.6, 14.1; GPC (PS): $M_n = 11555$, $M_w = 21439$, PDI = 1.85; m/z MALDI-TOF: 1558 (H-F₄-H), 1636 (H-F₄-Br), 1946 (H-F₅-H), 2022 (H-F₅-Br), 2335 (H-F₆-H), 2413 (H-F₆-Br), 2724 (H-F₇-H), 3112 (H-F₈-H), 3501 (H-F₉-H), 3889 (H-F₁₀-H), 4278 (H-F₁₁-H), 4667 (H-F₁₂-H); Anal. Calcd. for $C_{905}H_{1225}Br_2IrN_2O_2$: C 86.84%, H 9.86%, N 0.22%; Found C 83.42%, H 9.68%, N 0.26%;

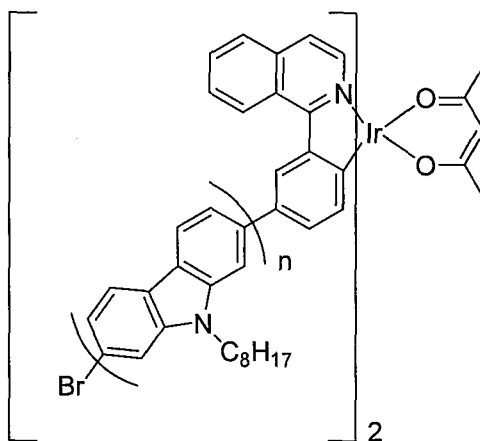
[Iridium(III)bis(1-(4-(ω -bromo-oligo(9,9'-dioctyl-9H-fluorene-2,7-diyl))phenyl)isoquinolinato-*N,C*(acetylacetonate)] 3.27



This complex was synthesised according to the same procedure used to produce **3.26**, using [Ir(III)bis(1-(4-bromophenyl)isoquinolinato-*N,C*(acetylacetonate)] **2.38** and isolated as a red powder (0.44 g, 58%).

1H NMR (400 MHz, $CDCl_3$, ppm) δ : 9.10 (br m, $PiqH$), 8.59 (br m, $PiqH$), 8.32 (br m, $PiqH$), 7.90-7.60 (br m, 6H, ArH), 7.15 (br m, $PiqH$), 6.78 (br m, $PiqH$), 5.32 (br s, $OC(CH_3)CH$), 2.30-2.00 (br m, 4H, CH_2), 1.86 (br s, $OC(CH_3)CH$), 1.30-1.00 (br m, 20H, CH_2), 0.90-0.70 (br m, 10H, CH_3 and CH_2); $^{13}C\{^1H\}$ NMR (125 MHz, $CDCl_3$, ppm) δ : 151.8, 140.5, 140.0, 126.2, 121.5, 119.9, 55.4, 40.4, 31.8, 30.1, 29.2, 23.9, 22.6, 14.1; GPC (PS): $M_n = 12112$, $M_w = 21266$, PDI = 1.7; m/z MALDI-TOF : 1558 (H-F₄-H), 1638 (H-F₄-Br), 1947 (H-F₅-H), 2022 (H-F₅-Br), 2335 (H-F₆-H), 2413 (H-F₆-Br), 2724 (H-F₇-H), 3112 (H-F₈-H), 3501 (H-F₉-H); Anal. Calcd. for $C_{557}H_{745}Br_2IrN_2O_2$: C 85.19%, H 9.56%, N 0.36%; Found C 83.42%, H 9.36%, N 0.23%.

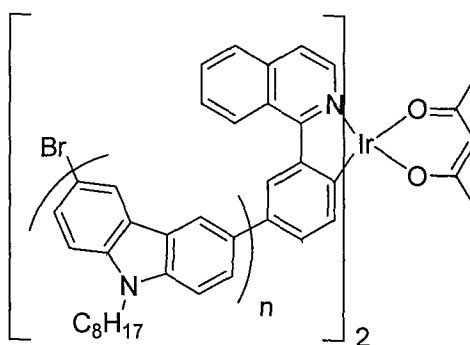
[Iridium(III)bis(1-(3-(ω -bromo-oligo(9-octyl-9*H*-carbazole-2,7-diyI))phenyl)isoquinolino-*N,C*(acetylacetonate))] 3.28



This complex was synthesised according to the same procedure used to produce **3.26**, using 2-bromo-9-octyl-7-(4,4',5,5'-tetramethyl-1,3,2-dioxaborolan-2-yl)-9*H*-carbazole **3.23** and isolated as a red powder (0.28 g, 40%).

^1H NMR (400 MHz, CDCl_3) δ : 9.16 (br m, PiqH), 8.93 (br m, PiqH), 8.57 (br m, PiqH), 8.40 - 7.30 (br m, 6H, ArH), 7.08 (br m, PiqH), 6.81 (br m, PiqH), 6.60 (br m, PiqH), 6.48 (br m, PiqH), 6.37 (br m, PiqH), 5.30 (br s, $\text{OC}(\text{CH}_3)\text{CH}$), 5.25 (br s, $\text{OC}(\text{CH}_3)\text{CH}$), 4.61 - 4.19 (br m, 2H, CH_2), 2.03 (br m, 2H, CH_2), 1.85 (br s, $\text{OC}(\text{CH}_3)\text{CH}$), 1.80 (br s, $\text{OC}(\text{CH}_3)\text{CH}$), 1.60 - 1.10 (br m, 10H, CH_2), 0.85 (br m, 3H, CH_3); $^{13}\text{C}\{^1\text{H}\}$ NMR (125 MHz, CDCl_3) δ : 143.2, 142.1, 141.7, 140.3, 121.9, 120.7, 120.5, 119.2, 107.9, 107.8, 31.9, 29.5, 29.2, 29.1, 28.9, 27.5, 22.6, 14.2, 14.0, 1.0; GPC(PS): $M_n = 2902$, $M_w = 3944$, $\text{PDI} = 1.4$; m/z MALDI-TOF : 1236 (B-C $_4$ -H), 1314 (B-C $_4$ -Br), 1513 (B-C $_5$ -H), 1592 (B-C $_5$ -Br), 1790 (B-C $_6$ -H), 1870 (B-C $_6$ -Br), 2068 (B-C $_7$ -H), 2148 (B-C $_7$ -Br), 2346 (B-C $_8$ -H), 2425 (B-C $_8$ -Br), 2622 (B-C $_9$ -H), 2702 (B-C $_9$ -Br), 2901 (B-C $_{10}$ -H), 2979 (B-C $_{10}$ -Br), 3178 (B-C $_{11}$ -H), 3257 (B-C $_{11}$ -Br), 3453 (B-C $_{12}$ -H), 3533 (B-C $_{12}$ -Br), 3731 (B-C $_{13}$ -H), 3810 (B-C $_{13}$ -Br); Anal. Calcd. for $\text{C}_{315}\text{H}_{347}\text{Br}_2\text{IrN}_{16}\text{O}_2$: C 79.80%, H 7.38%, N 4.73%; Found C 78.24%, H 7.30%, N 4.48%.

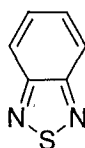
[Iridium(III)bis(1-(3-(ω -bromo-oligo[9-octyl-9H-carbazole-3,6-diyl])phenyl)isoquinolino-*N,C*(acetylacetonate))] 3.29



This complex was synthesised according to the same procedure used to produce **3.26**, using 3-bromo-9-octyl-6-(4,4',5,5'-tetramethyl-1,3,2-dioxaborolan-2-yl)-9H-carbazole **3.25** and isolated as a red powder (0.48 g, 46%).

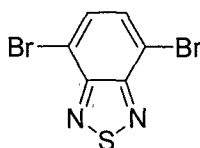
^1H NMR (400 MHz, CDCl_3) δ : 9.14 (br m, *PiqH*), 8.90 (br m, *ArH*), 8.73 - 7.30 (br m, *ArH*), 7.09 (br m, *PiqH*), 6.58 (br m, *PiqH*), 5.23 (br s, $\text{OC}(\text{CH}_3)\text{CH}$), 4.41 - 3.82 (br m, 2H, CH_2), 2.10 - 1.70 (br m, 2H, $\text{OC}(\text{CH}_3)\text{CH}$ and CH_2), 1.60 - 1.10 (br m, 10H, CH_2), 0.85 (br m, 3H, CH_3); $^{13}\text{C}\{^1\text{H}\}$ NMR (125 MHz, CDCl_3) δ : 139.9, 133.2, 125.6, 125.4, 123.7, 123.4, 119.0, 118.8, 109.1, 108.9, 108.7, 43.3, 43.3, 31.8, 29.4, 29.2, 29.1, 28.9, 28.8, 27.4, 22.6, 14.2, 14.1, 13.9; GPC (PS): $M_n = 2306$, $M_w = 3613$, PDI = 1.6; m/z MALDI-TOF : 1111 (H-C z_4 -H), 1389 (H-C z_5 -H), 2222 (H-C z_8 -H); Anal. Calcd. for $\text{C}_{555}\text{H}_{623}\text{Br}_2\text{IrN}_{28}\text{O}_2$: C 82.60%, H 7.78%, N 4.86%; Found C 79.83%, H 7.51%, N 4.75%.

Benzo-2,1,3-thiadiazole⁹⁷ 3.31



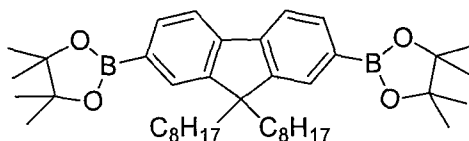
o-Phenylenediamine (5.4 g, 50 mmol) was added to a solution of SOCl_2 (17.5 mL, 243.4 mmol) and conc. Sulphuric acid (1 mL, 19 mmol). The mixture was refluxed for 1 h, cooled and cautiously poured into 500 mL of ice. The resulting precipitate was filtered and then washed with H_2O until pH = 7 was attained to afford pure benzo-2,1,3-thiadiazole (6.5 g, 95%).

m.p. 44 - 45 $^\circ\text{C}$ [Lit. 42 - 44 $^\circ\text{C}$]⁹⁷; ^1H NMR (400 MHz, CDCl_3 , ppm) δ : 7.96 (m, 2H, *ArH*), 7.52 (m, 2H, *ArH*); m/z (CI) 137 [$\text{M}+\text{H}$]⁺; The data is in agreement with the literature values.

4,7-Dibromobenzo-2,1,3-thiadiazole⁹⁶ 3.32

A mixture of benzo-2,1,3-thiadiazole **3.31** (5.0 g, 36.8 mmol) in aqueous HBr (48%, 100 mL) was heated to reflux with stirring, while Br₂ (6 mL, 117 mmol) was added dropwise over a 1 h period. The resulting suspension was then heated to reflux for a further 2 h after which point it was filtered whilst hot, cooled and filtered again. The residue was washed with H₂O (2 x 100 mL) and then recrystallized from MeOH to afford the product as white crystals (6.9 g, 64%).

m.p. (MeOH) 189 - 190 °C [Lit. (CHCl₃) 187 - 188 °C]⁹⁶; ¹H NMR (400 MHz, CDCl₃, ppm) δ: 7.71 (s, 2H, ArH); *m/z* (CI): 295 [M+H]⁺; The data is in agreement with the literature values.

9,9'-Dioctyl-2,7-bis(4,4',5,5'-tetramethyl-1,3,2-dioxaborolan-2-yl)-9H-fluorene³⁸ 3.33

n-Butyllithium (14 mL of a 1.6 M solution in hexane, 22.5 mmol) was added dropwise into a stirring solution of 2,7-dibromo-9,9'-dioctyl-9H-fluorene **3.16** (5.6 g, 10.2 mmol) in THF (130 mL) at -78 °C. The mixture was stirred at -78 °C for 2 h after which 2-isopropoxy-4,4',5,5'-tetramethyl-1,3,2-dioxaborolane (6.3 mL, 30.8 mmol) was added rapidly. The solution was stirred for a further 2 h and then allowed to warm to room temperature and stirred for a further 18 h. The resulting suspension was poured into H₂O (100 mL) and extracted with ether (100 mL). The organic layer was separated and washed with brine (100 mL of a saturated aqueous solution), dried (MgSO₄) and concentrated *in vacuo*. The residue was recrystallized twice from hexane to afford the product as a white crystalline solid (5.4 g, 81%).

m.p. (hexane) 130 - 132 °C [Lit. (acetone) 128 - 131 °C]³⁸; ¹H NMR (400 MHz, CDCl₃, ppm) δ: 7.81 (d, *J* = 7.3 Hz, 2H, ArH), 7.74 (s, 2H, ArH), 7.71 (d, *J* = 7.6 Hz, 2H, ArH), 1.99 (m, 4H, CH₂), 1.39 (s, 24H, OCCH₃), 1.22-1.00 (m, 20H, CH₂ and CH₃), 0.81 (m,

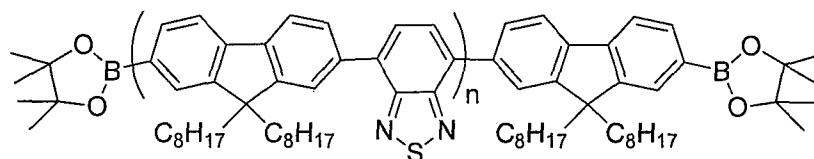
6H, CH₃), 0.56 (m, 4H, CH₂); *m/z* (CI) 643 [M+H]⁺; The data is in agreement with the literature values.

Bis-tetraethylammonium carbonate 3.35

Solid CO₂ (approx. 50 g) was added to aqueous tetraethylammonium hydroxide (10 mL of a 20% solution) with stirring and then allowed to warm to room temperature. The solution was then evaporated to dryness to afford the product as a white hygroscopic powder (1.1 g)

IR (Thin Film) 1650 br C=O stretch.

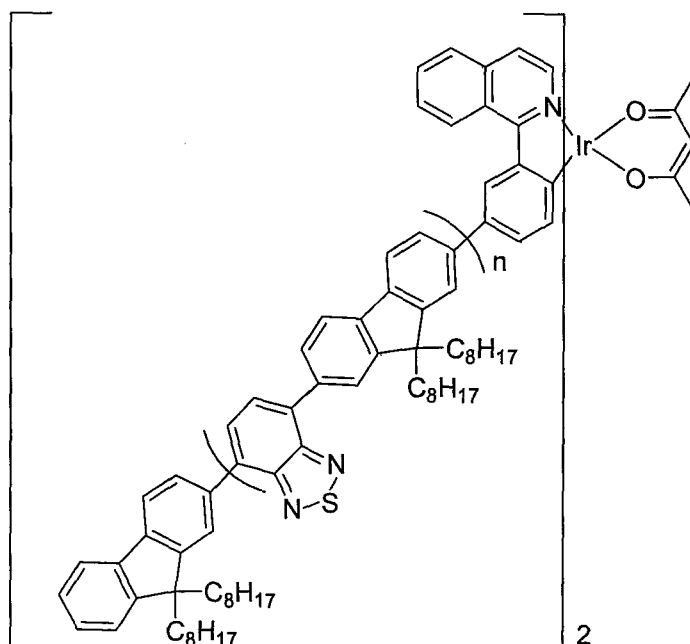
α,ω -Bis(4,4',5,5'-tetramethyl-1,3,2-dioxaborolan-2-yl)poly(9,9'-dioctylfluorene-alt-benzothiadiazole) (F8BT)⁹⁸ 3.36



4,7-Dibromobenzo-1,2,5-thiadiazole **3.32** (0.15 g, 0.51 mmol), 9,9'-dioctyl-2,7-bis(4,4',5,5'-tetramethyl-1,3,2-dioxaborolan-2-yl)-9*H*-fluorene **3.33** (0.39 g, 0.61 mmol), bis-tetraethylammonium carbonate (1.0 g, 3 mol) and Pd(OAc)₂ (3 mg, 0.004 mmol) were suspended in a mixture of THF (3 mL), H₂O (2 mL) and toluene (3 mL). The resulting suspension was then heated to reflux (90 °C) for 18 h. The reaction vessel was allowed to cool to room temperature after which the suspension was poured into MeOH (300 mL). The precipitated polymer was filtered to afford a yellow fibrous product which was subsequently purified by dissolution in toluene and re-precipitation with MeOH to give the product as a yellow powder (0.2 g, 66%).

¹H NMR (400 MHz, CDCl₃, ppm) δ : 8.10 – 7.97 (m, 66H, ArH), 2.18 – 2.10 (m, 30H, CH₂), 1.44 (s, 24H, OCCH₃), 1.25 – 0.96 (m, 280H, CH₂ and CH₃); GPC (PS): M_n = 5641, M_w = 9596, PD = 1.99; *m/z* MALDI-TOF : 1167 (B-F8BT₁-B), 1690 (B-F8BT₂-B), 2213 (B-F8BT₃-B), 2736 (B-F8BT₄-B), 3259 (B-F8BT₅-B), 3783 (B-F8BT₆-B), 4306 (B-F8BT₇-B); Anal. Calcd. for C₃₂₁H₄₀₀B₂N₁₆O₄S₈: C 79.91%, H 8.36%, N 4.64%; Found C 79.82%, H 8.35%, N 4.49%. The data is in agreement with the literature values.

[Iridium(III)bis(1-(3-(oligo(9,9'-dioctylfluorene-alt-benzothiadiazole)phenyl)isoquinolinato-*N,C*)(acetylacetonate)] 3.37

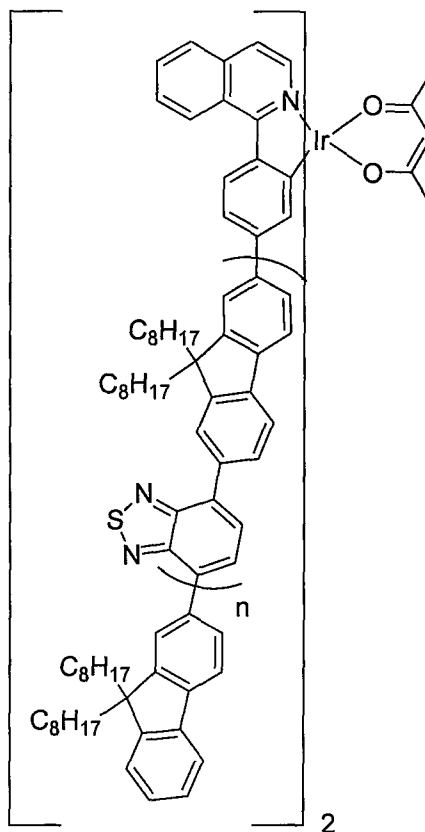


A solution of F8BT **3.36** (0.63 g, 0.132 mmol, 2.5 eq.), iridium(III) bis(1-(3-bromophenyl)isoquinolinato-*N,C*)(acetylacetonate) **2.37** (45 mg, 0.053 mmol, 1 eq.), Pd(OAc)₂ (5 mg, 0.022 mmol) and PCy₃ (12 mg, 0.044 mmol) in toluene (50 mL) was heated to 90 °C. To this, aqueous Et₄NOH (6.5 mL of a 20 % solution) was added and the solution stirred at 110 °C for 20 h. The reaction mixture was allowed to cool to room temperature and subsequently poured into a large excess of MeOH, which resulted in the precipitation of the polymer. The precipitate was filtered, washed with H₂O (40 mL), MeOH (40 mL) and acetone (30 mL) and filtered through celite using toluene as the eluent. The resulting solution was concentrated (to 20 mL) and Na₂CO₃ (0.20 g), acetyl acetone (2.00 mL) and 2-ethoxyethanol (10 mL) were added. The reaction mixture was stirred for 2 h at 110 °C and subsequently cooled down to room temperature. The solution was again poured into an excess of MeOH and the precipitate filtered, washed with H₂O (40 mL) and MeOH (40 mL) and dried *in vacuo*. The pure product was isolated as an orange powder (0.34 g, 72%).

¹H NMR (400 MHz, CDCl₃, ppm) δ: 9.17 (br m, PiqH), 8.59 (br m, PiqH), 8.2 – 7.6 (m, 8H, ArH), 7.08 (br m, PiqH), 6.59 (br m, PiqH), 5.30 (s, OC(CH₃)CH), 1.86 (s, OC(CH₃)CH), (2.3 – 2.0 (m, 4H, CH₂), 1.2 – 0.7 (m, 30H, CH₃ and CH₂); ¹³C{¹H} NMR (125 MHz, CDCl₃ ppm) δ: 154.4, 151.8, 140.9, 136.5, 133.6, 128.3, 128.1, 124.0, 120.1, 55.6, 40.3, 31.9, 30.2, 29.3, 24.1, 22.6, 14.1; GPC (PS): Mn = 12205, Mw =

27175, PD = 2.22; m/z MALDI-TOF : 1438 (H-F8BT₂-H), 1961 (H-F8BT₃-H), 2485 (H-F8BT₄-H), 3005 (H-F8BT₅-H); Anal. Calcd. for C₉₀₄H₁₀₇₅IrN₅₀O₂S₂₄ : C 79.63%, H 7.95%, N 5.14%; Found C 77.01%, H 7.89%, N 4.14%.

[Iridium(III)bis(1-(4-(oligo(9,9'-dioctylfluorene-alt-benzothiadiazole)phenyl)isoquinolinato-N,C)(acetylacetonate)] 3.38

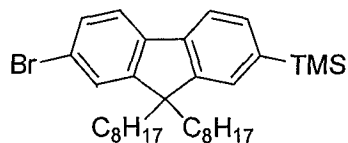


This complex was synthesised according to the same procedure used to produce **3.37** using [Ir(III)bis(1-(4-bromophenyl)isoquinolinato-N,C)(acetylacetonate)] **2.38** and isolated as a yellow powder (0.32 g, 69%).

¹H NMR (400 MHz, CDCl₃, ppm) δ: 9.11 (br m, PiqH), 8.59 (br m, PiqH), 8.2 - 7.6 (m, 8H, ArH), 8.03 (br m, PiqH), 7.17 (br m, PiqH), 6.78 (br m, PiqH), 5.32 (s, OC(CH₃)CH), 1.85 (s, OC(CH₃)CH), (2.3 - 2.0 (m, 4H, CH₂), 1.2 - 0.7 (m, 30H, CH₃ and CH₂); ¹³C{¹H} NMR (125 MHz, CDCl₃ ppm) δ: 154.4, 151.8, 140.9, 136.5, 133.6, 128.3, 128.0, 124.0, 123.9, 120.1, 112.0, 55.5, 40.3, 31.9, 30.1, 29.3, 24.1, 22.6, 14.1; GPC (PS): Mn = 12975, Mw = 28499, PD = 2.20; m/z MALDI-TOF : 1437 (H-F8BT₂-H), 1960 (H-F8BT₃-H), 2482 (H-F8BT₄-H), 3005 (H-F8BT₅-H); Anal. Calcd. for

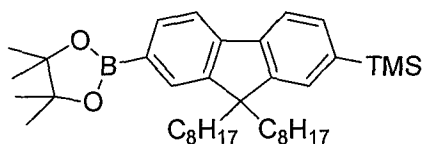
$C_{904}H_{1075}IrN_{50}O_2S_{24}$: C 79.63%, H 7.95%, N 5.14%; Found C 77.26%, H 7.88%, N 4.14%.

6.5 Experimental for Chapter 4

(7-Bromo-9,9'-dioctyl-9H-fluoren-2-yl)trimethylsilane²⁰⁹ 4.6

2,7-Dibromo-9,9'-dioctyl-9H-fluorene **3.16** (5.0 g, 9.13 mmol) was dissolved in THF (50 mL) at $-78\text{ }^{\circ}\text{C}$ and *n*-butyllithium (6 mL of a 1.6 M solution in hexanes, 9.1 mmol) was added dropwise. The resulting suspension was stirred for 2 h after which point trimethylsilylchloride (2.3 mL, 10 mmol) was added rapidly. After a further 2 h, the reaction was warmed to room temperature and stirred for a further 18 h. H₂O (20 mL) and Et₂O (20 mL) were added and the layers separated, the organic fraction was dried (MgSO₄), filtered, and concentrated *in vacuo*. Column chromatography (silica gel, hexane) afforded a mixture of the product and some unidentified impurities as a colourless oil (4.8 g, 98%).

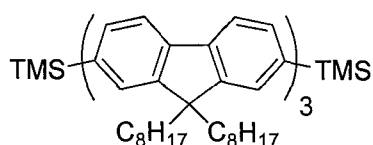
¹H NMR (400 MHz, CDCl₃, ppm) δ : 7.62 (d, $J = 7.4$ Hz, 1H, ArH), 7.54 (d, $J = 7.9$ Hz, 1H, ArH), 7.44 (m, 4H, ArH), 2.00 - 1.84 (m, 4H, CH₂), 1.20 - 1.00 (m, 20H, CH₂), 0.86 - 0.80 (m, 6H, CH₃), 0.70 - 0.56 (m, 4H, CH₂), 0.30 (s, 9H, Si(CH₃)₃); m/z (CI): 542 [M+H]⁺; The data is in agreement with the literature values.

(9,9'-Dioctyl-7-(4,4',5,5'-tetramethyl-1,3,2-dioxaborolan-2-yl)-9H-fluoren-2-yl)trimethylsilane²⁰⁹ 4.7

(7-Bromo-9,9'-dioctyl-9H-fluoren-2-yl)trimethylsilane **4.6** (4.0 g, 7.4 mmol) was dissolved in THF (50 mL) at $-78\text{ }^{\circ}\text{C}$ and *n*-butyl lithium (9 mL of a 1.6 M solution in hexanes, 9 mmol) was added, dropwise. The resulting suspension was stirred for 2 h after which point 2-isopropoxy-4,4',5,5'-tetramethyl-1,3,2-dioxaborolane (2 mL, 10 mmol) was added rapidly. After a further 2 h, the reaction was warmed to room temperature and stirred for a further 18 h. H₂O (10 mL) and Et₂O were added and the layers separated, the organic fraction was dried (MgSO₄), filtered, and concentrated *in vacuo*. Column chromatography (silica gel, hexane:DCM, 5:1) enabled isolation of the pure product as a white crystalline solid (2.66 g, 61%).

m.p. 92 - 94 °C [Lit. 72 - 73 °C (ethanol, methanol)]²⁰⁹; ¹H NMR (400 MHz, CDCl₃, ppm) δ: 7.78 (d, *J* = 7.6 Hz, 1H, ArH), 7.74 (s, 1H, ArH), 7.70 (d, *J* = 7.5 Hz, 2H, ArH), 7.46 (m, 2H, ArH), 1.96 (t, *J* = 8.2 Hz, 4H, CH₂), 1.38 (s, 12H, OCCH₃), 1.20 – 1.00 (m, 20H, CH₂), 0.86 – 0.80 (t, *J* = 7.3 Hz, 6H, CH₃), 0.70 – 0.56 (m, 4H, CH₂), 0.30 (s, 9H, Si(CH₃)₃); *m/z* (CI): 589 [M+H]⁺; The data is in agreement with the literature values.

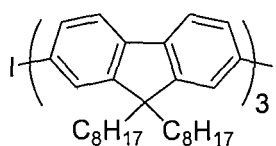
2-(7-(9,9'-Dioctyl-7-(trimethylsilyl)-9H-fluoren-2-yl)-9,9'-dioctyl-9H-fluoren-2-yl)-9,9'-dioctyl-7-(trimethylsilyl)-9H-fluorene 4.8



A solution of (9,9'-dioctyl-7-(4,4',5,5'-tetramethyl-1,3,2-dioxaborolan-2-yl)-9H-fluoren-2-yl)trimethylsilane **4.7** (1.8 g, 3.1 mmol.), 2,7-dibromo-9,9'-dioctyl-9H-fluorene **3.16** (0.77 g, 1.4 mmol), Pd(OAc)₂ (5 mg, 0.022 mmol) and PPh₃ (12 mg, 0.044 mmol) in toluene (75 mL) was heated to 90 °C. To this, aqueous Et₄NOH (7.50 mL of a 20 % solution) was added and the solution stirred at 110 °C. After 24h, the reaction mixture was allowed to cool to room temperature and the layers separated. The organic layer was washed with H₂O (3 x 50 ml), dried (MgSO₄), filtered and concentrated *in vacuo*. Purification by flash column chromatography (silica gel, hexane) afforded the title product as a colourless oil (1.56 g, 85%).

¹H NMR (400 MHz, CDCl₃, ppm) δ: 7.92 - 7.50 (m, 18H, ArH), 2.26 - 2.06 (m, 12H, CH₂), 1.44 - 1.10 (m, 60H, CH₂), 1.00 - 0.76 (m, 30H, CH₂ and CH₃), 0.42 (s, 18H, Si(CH₃)₃); ¹³C{¹H} NMR (400 MHz, CDCl₃, ppm) δ: 151.9, 150.1, 141.6, 140.7, 140.6, 140.4, 140.1, 139.0, 131.9, 127.7, 126.2, 126.1, 121.5, 120.0, 119.1, 55.4, 55.2, 40.5, 40.23, 31.9, 30.1, 30.0, 29.4, 24.0, 23.9, 22.7, 14.1, -0.8; *m/z* MALDI-TOF : 1312; Anal. Calcd. for C₉₃H₁₃₈Si₂ : C 85.12%, H 10.60%; Found C 85.21%, H 10.67%.

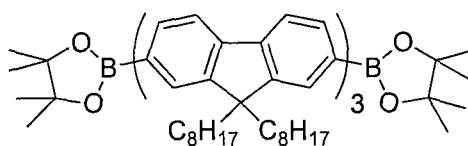
2-Iodo-7-(7-(7-iodo-9,9'-dioctyl-9*H*-fluoren-2-yl)-9,9'-dioctyl-9*H*-fluoren-2-yl)-9,9'-dioctyl-9*H*-fluorene 4.9



ICl (1.50 mL of a 1.0 M solution in DCM) was slowly added to a stirring solution of 2-(7-(9,9'-dioctyl-7-(trimethylsilyl)-9*H*-fluoren-2-yl)-9,9'-dioctyl-9*H*-fluoren-2-yl)-9,9'-dioctyl-7-(trimethylsilyl)-9*H*-fluorene **4.8** (0.50 g, 0.38 mmol) in DCM (5 mL) at 0 °C. The resulting dark red solution was stirred for a further 2 h and then warmed to room temperature and quenched by addition of a large excess of aqueous Na₂S₂O₃ solution. The layers were separated and the organic fraction was washed with H₂O (2 x 20 mL), dried (MgSO₄) filtered and concentrated *in vacuo*. Column chromatography (silica gel, hexane:DCM; 4:1) enabled isolation of the product as a white solid (0.54 g, 100%).

m.p. 95 - 99 °C; ¹H NMR (400 MHz, CDCl₃, ppm) δ: 7.82 (d, *J* = 7.6 Hz, 2H, Ar*H*), 7.76 (d, *J* = 7.6 Hz, 2H, Ar*H*), 7.69, 7.51 (d, *J* = 7.6 Hz, 2H, Ar*H*), 2.20 - 1.95 (m, 12H, CH₂), 1.30 - 1.10 (m, 60H, CH₂), 0.95 - 0.65 (m, 30H, CH₂ and CH₃); ¹³C{¹H} NMR (125 MHz, CDCl₃, ppm) δ: 153.5, 151.9, 151.0, 141.2, 140.6, 140.5, 140.3, 140.2, 140.1, 140.0, 139.3, 135.9, 132.2, 126.2, 121.5, 121.4, 120.0, 92.5, 55.5, 55.4, 40.4, 40.3, 31.8, 30.1, 30.0, 29.3, 24.0, 23.8, 22.7, 14.1; *m/z* MALDI-TOF : 1419; Anal. Calcd. for C₈₇H₁₂₀I₂ : C 76.60%, H 8.52%; Found C 76.48%, H 8.53%.

2-(7-(7-(9,9'-Dioctyl-7-(4,4',5,5'-tetramethyl-1,3,2-dioxaborolan-2-yl)-9*H*-fluoren-2-yl)-9,9'-dioctyl-9*H*-fluoren-2-yl)-9,9'-dioctyl-9*H*-fluoren-2-yl)-4,4',5,5'-tetramethyl-1,3,2-dioxaborolane 4.10

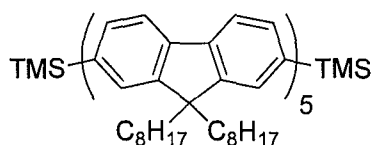


2-Iodo-7-(7-(7-iodo-9,9'-dioctyl-9*H*-fluoren-2-yl)-9,9'-dioctyl-9*H*-fluoren-2-yl)-9,9'-dioctyl-9*H*-fluorene **4.9** (0.5 g, 0.35 mmol) was dissolved in THF (10 mL) at -78 °C and *n*-butyllithium (0.5 mL of a 1.6 M solution in hexanes, 0.78 mmol) was added dropwise. The resulting suspension was stirred for 2 h after which point 2-isopropoxy-4,4',5,5'-tetramethyl-1,3,2-dioxaborolane (0.2 mL, 1 mmol) was added rapidly. After a further 2 h, the reaction was warmed to room temperature and stirred for a further 18 h. H₂O (10 mL) and Et₂O were added and the layers separated, the organic fraction was dried

(MgSO₄), filtered, and concentrated *in vacuo*. Column chromatography (silica gel, hexane:DCM, 5:1) enabled isolation of the pure product as a colourless oil (0.29 g, 58%).

¹H NMR (400 MHz, CDCl₃, ppm) δ: 7.88 - 7.80 (m, 8H, ArH), 7.77 (d, *J* = 7.8 Hz, 2H, ArH), 7.71 - 7.64 (m, 8H, ArH), 2.20 - 1.95 (m, 12H, CH₂), 1.41 (s, 24H, OCCCH₃), 1.30 - 1.10 (m, 60H, CH₂), 0.95 - 0.65 (m, 30H, CH₂ and CH₃); ¹³C{¹H} NMR (125 MHz, CDCl₃, ppm) δ: 152.1, 151.8, 150.2, 143.8, 141.0, 140.5, 140.2, 140.0, 133.8, 128.9, 126.2, 126.1, 121.5, 120.4, 120.0, 119.1, 83.7, 55.3, 40.4, 40.3, 31.8, 31.6, 30.1, 29.2, 25.0, 23.9, 23.8, 22.6, 14.1; *m/z* MALDI-TOF: 1420; Anal. Calcd. for C₉₉H₁₄₄B₂O₄ : C 83.75%, H 10.22%; Found C 83.65%, H 10.26%.

2-(7-(7-(7-(9,9'-Dioctyl-7-(trimethylsilyl)-9H-fluoren-2-yl)-9,9'-dioctyl-9H-fluoren-2-yl)-9,9'-dioctyl-9H-fluoren-2-yl)-9,9'-dioctyl-9H-fluoren-2-yl)-9,9'-dioctyl-9H-fluorene 4.11

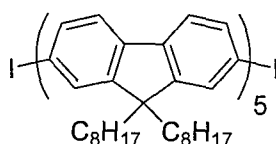


A solution of (9,9'-dioctyl-7-(4,4',5,5'-tetramethyl-1,3,2-dioxaborolan-2-yl)-9H-fluoren-2-yl)trimethylsilane **4.7** (830 mg, 1.4 mmol.), 2-iodo-7-(7-(7-iodo-9,9'-dioctyl-9H-fluoren-2-yl)-9,9'-dioctyl-9H-fluoren-2-yl)-9,9'-dioctyl-9H-fluorene **4.9** (800 mg, 0.56 mmol), Pd(OAc)₂ (5 mg, 0.022 mmol) and PPh₃ (12 mg, 0.044 mmol) in toluene (15 mL) was heated to 90 °C. To this, aqueous Et₄NOH (5 mL of a 20 % solution) was added and the solution stirred at 90 °C. After 24hr the reaction mixture was allowed to cool to room temperature and the layers separated. The organic layer was washed with H₂O (3 x 50 ml), dried (MgSO₄), filtered and concentrated *in vacuo*. Purification by flash column chromatography (silica gel, hexane) afforded the title product as a colourless oil (0.89 g, 76%).

¹H NMR (400 MHz, CDCl₃, ppm) δ: 7.93 - 7.84 (m, 8H, ArH), 7.82 - 7.68 (m, 18H, ArH), 7.61 - 7.56 (m, 4H, ArH), 2.28 - 2.03 (m, 20H, CH₂), 1.38 - 1.08 (m, 100H, CH₂), 1.00 - 0.74 (m, 50H, CH₂ and CH₃), 0.39 (s, 18H, Si(CH₃)₃); ¹³C{¹H} NMR (125 MHz, CDCl₃, ppm) δ: 151.9, 150.2, 141.5, 140.7, 140.6, 140.4, 140.1, 139.0, 131.9, 127.7, 126.2, 126.1, 121.5, 120.0, 119.1, 55.4, 55.2, 40.5, 40.23, 31.9, 30.1, 30.0, 29.3, 24.0,

23.9, 22.7, 14.1, -0.8; m/z MALDI-TOF : 2089; Anal. Calcd. for $C_{151}H_{218}Si_2$: C 86.80%, H 10.52%; Found C 86.72%, H 10.43%.

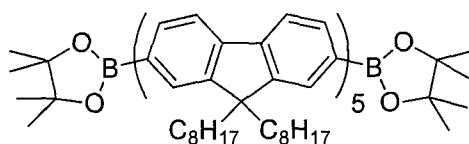
2-Iodo-7-(7-(7-(7-(7-iodo-9,9'-dioctyl-9H-fluoren-2-yl)-9,9'-dioctyl-9H-fluoren-2-yl)-9,9'-dioctyl-9H-fluoren-2-yl)-9,9'-dioctyl-9H-fluoren-2-yl)-9,9'-dioctyl-9H-fluorene 4.12



ICI (1.50 mL of a 1.0 M solution in DCM) was slowly added to a stirring solution of 2-(7-(7-(7-(9,9'-dioctyl-7-(trimethylsilyl)-9H-fluoren-2-yl)-9,9'-dioctyl-9H-fluoren-2-yl)-9,9'-dioctyl-9H-fluoren-2-yl)-9,9'-dioctyl-9H-fluoren-2-yl)-9,9'-dioctyl-7-(trimethylsilyl)-9H-fluorene **4.11** (0.50 g, 0.24 mmol) in DCM (5 mL) at 0 °C. The resulting dark red solution was stirred for a further 2 h and then warmed to room temperature and quenched by addition of a large excess of aqueous $Na_2S_2O_3$ solution. The layers were separated and the organic fraction was washed with H_2O (2 x 20 mL), dried ($MgSO_4$) filtered and concentrated *in vacuo*. Column chromatography (silica gel, hexane:DCM; 4:1) enabled isolation of the product as a colourless oil (0.53 g, 100%).

1H NMR (400 MHz, $CDCl_3$, ppm) δ : 7.84 (m, 6H, ArH), 7.76 (d, $J = 7.9$ Hz, 2H, ArH), 7.72 - 7.63 (m, 20H, ArH), 7.51 (d, $J = 7.9$ Hz, 2H, ArH), 2.20 - 1.95 (m, 20H, CH_2), 1.30 - 1.10 (m, 100H, CH_2), 0.95 - 0.65 (m, 50H, CH_2 and CH_3); $^{13}C\{^1H\}$ NMR (125 MHz, $CDCl_3$, ppm) δ : 153.5, 151.9, 151.0, 141.2, 140.6, 140.5, 140.3, 140.2, 140.1, 140.0, 139.3, 135.9, 132.2, 126.2, 121.5, 121.4, 120.0, 92.5, 55.5, 55.4, 40.4, 40.3, 31.8, 30.1, 30.0, 29.3, 24.0, 23.8, 22.7, 14.1; m/z MALDI-TOF : 2197; Anal. Calcd. for $C_{145}H_{200}I_2$: C 79.27%, H 9.18%; Found C 79.28%, H 9.21%.

2-(7-(7-(7-(7-(9,9'-Dioctyl-7-(4,4',5,5'-tetramethyl-1,3,2-dioxaborolan-2-yl)-9H-fluoren-2-yl)-9,9'-dioctyl-9H-fluoren-2-yl)-9,9'-dioctyl-9H-fluoren-2-yl)-9,9'-dioctyl-9H-fluoren-2-yl)-9,9'-dioctyl-9H-fluorene-2-yl)-4,4',5,5'-tetramethyl-1,3,2-dioxaborolane 4.13



4.14**m = 11**

2,7-Dibromo-9,9'-dioctyl-9*H*-fluorene **3.16** (547 mg, 0.85 mmol), 9,9'-dioctyl-2,7-bis(4,4',5,5'-tetramethyl-1,3,2-dioxaborolan-2-yl)-9*H*-fluorene **3.33** (388 mg, 0.71 mmol), Pd(OAc)₂ (3 mg, 0.013 mmol), PPh₃ (18 mg, 0.069 mmol), toluene (5 mL), Aqueous Et₄NOH (5 mL of a 20% solution).

Yield (560 mg, 92%); ¹H NMR (400 MHz, CDCl₃, ppm) δ: 8.20 – 7.35 (br m, 66H, Ar*H*), 2.12 (br m, 44H, CH₂), 1.41 (s, 24H, OCCH₃), 1.14 - 0.80 (br m, 330H, CH₂ and CH₃); GPC (PS): M_n = 3572, M_w = 5586, PDI = 1.6; *m/z* MALDI-TOF : 2974 (B-F₇-B), 3751 (B-F₉-B), 4524 (B-F₁₁-B), 5287 (B-F₁₃-B); Anal. Calcd. for C₃₃₁H₄₆₄B₂O₄ : C 87.78%, H 10.33%; Found C 86.22%, H 10.30%.

4.15**m = 23**

2,7-Dibromo-9,9'-dioctyl-9*H*-fluorene **3.16** (500 mg, 0.78 mmol), 9,9'-dioctyl-2,7-bis(4,4',5,5'-tetramethyl-1,3,2-dioxaborolan-2-yl)-9*H*-fluorene **3.33** (388 mg, 0.71 mmol), Pd(OAc)₂ (3 mg, 0.013 mmol), PPh₃ (18 mg, 0.069 mmol), toluene (5 mL), Aqueous Et₄NOH (5 mL of a 20% solution).

Yield (550 mg, 95%); ¹H NMR (400 MHz, CDCl₃, ppm) δ: 8.20 – 7.35 (br m, 138H, Ar*H*), 2.12 (br m, 92H, CH₂), 1.41 (s, 24H, OC(CH₃)), 1.14 - 0.80 (br m, 690H, CH₂ and CH₃); GPC (PS): M_n = 11632, M_w = 26775, PDI = 2.3; *m/z* MALDI-TOF : 1419 (B-F₃-B), 2198 (B-F₅-B), 2977 (B-F₇-B), 3756 (B-F₉-B), 4535 (B-F₁₁-B), 5315 (B-F₁₃-B), 6091 (B-F₁₅-B); Anal. Calcd. for C₆₇₉H₉₄₄B₂O₄ : C 88.72%, H 10.35%; Found C 88.61%, H 10.37%.

4.16**m = 38**

2,7-Dibromo-9,9'-dioctyl-9*H*-fluorene **3.16** (479 mg, 0.75 mmol), 9,9'-dioctyl-2,7-bis(4,4',5,5'-tetramethyl-1,3,2-dioxaborolan-2-yl)-9*H*-fluorene **3.33** (388 mg, 0.71

mmol), Pd(OAc)₂ (3 mg, 0.013 mmol), PPh₃ (18 mg, 0.069 mmol), toluene (5 mL), Aqueous Et₄NOH (5 mL of a 20% solution).

Yield (498 mg, 88%); ¹H NMR (400 MHz, CDCl₃, ppm) δ: 8.20 – 7.35 (br m, 228H, ArH), 2.12 (br m, 152H, CH₂), 1.41 (s, 24H, OC(CH₃)), 1.14 - 0.80 (br m, 1140H, CH₂ and CH₃); GPC (PS): M_n = 24197, M_w = 58661, PDI = 2.4; *m/z* MALDI-TOF : 3629 (B-F₉-H), 3755 (B-F₉-B), 4408 (B-F₁₁-H), 4534 (B-F₁₁-B), 5186 (B-F₁₃-H), 5313 (B-F₁₃-B), 5964 (B-F₁₅-H), 6096 (B-F₁₅-B); Anal. Calcd. for C₁₁₁₄H₁₅₄₄B₂O₄ : C 89.07%, H 10.36%; Found C 88.80%, H 10.29%.

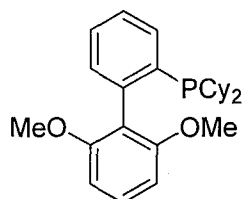
4.17

m = 76

2,7-Dibromo-9,9'-dioctyl-9*H*-fluorene **3.16** (467 mg, 0.73 mmol), 9,9'-dioctyl-2,7-bis(4,4',5,5'-tetramethyl-1,3,2-dioxaborolan-2-yl)-9*H*-fluorene **3.33** (388 mg, 0.71 mmol), Pd(OAc)₂ (3 mg, 0.013 mmol), PPh₃ (18 mg, 0.069 mmol), toluene (15 mL), Aqueous Et₄NOH (10 mL of a 20% solution)

Yield (530 mg, 95%); ¹H NMR (400 MHz, CDCl₃, ppm) δ: 8.20 – 7.35 (br m, 456H, ArH), 2.12 (br m, 304H, CH₂), 1.41 (s, 24H, OC(CH₃)), 1.14 - 0.80 (br m, 2280H, CH₂ and CH₃); *m/z* MALDI-TOF : 2926, 3390, 3655, 3705, 4167, 4433; GPC (PS): M_n = 36971, M_w = 102490, PDI = 2.8; Anal. Calcd. for C₂₂₁₆H₃₀₆₄B₂O₄ : C 89.35%, H 10.37%; Found C 89.35%, H 10.41%.

2-Dicyclohexylphosphino-2,6-dimethoxybiphenyl¹⁵⁴ SPhos 4.22



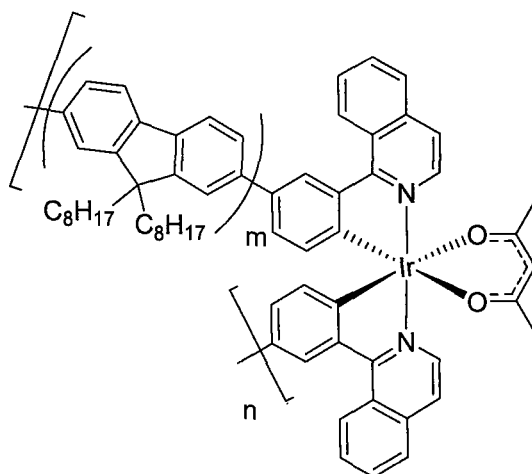
To a cold (0 °C), stirred solution of 1,3-dimethoxybenzene (2.00 mL, 15.3 mmol) in THF (35 mL) was added *n*-Butyllithium (6.20 mL, 2.5 M solution in hexanes, 15.5 mmol) dropwise via syringe over 5 min. The reaction mixture was allowed to warm to room temperature and then stirred for 3.5 h. The mixture was re-cooled to 0 °C and neat 2-bromochlorobenzene (1.60 mL, 13.7 mmol) was added dropwise via syringe over 15 min with vigorous stirring and stirred for an additional 15 min. The reaction mixture

was cooled to $-78\text{ }^{\circ}\text{C}$ and *n*-Butyllithium (6.20 mL, 2.5 M solution in hexanes, 15.5 mmol) was added dropwise. The resulting mixture was stirred at $-78\text{ }^{\circ}\text{C}$ for 30 min. Chlorodicyclohexylphosphine (3.03 mL, 13.7 mmol, 1.0 equiv) was then added via syringe. The reaction mixture was stirred at $-78\text{ }^{\circ}\text{C}$ for 1 h and then allowed to slowly warm to room temperature. The resulting mixture was filtered through a pad of silica gel topped with a layer of celite, eluting with EtOAc (400 mL). The filtrate was concentrated under reduced pressure to provide a yellow solid. Recrystallization twice from acetone afforded the product as a white solid (3.2 g, 51%).

m.p. (acetone) $162 - 164\text{ }^{\circ}\text{C}$ [Lit. $162 - 162.5\text{ }^{\circ}\text{C}$ (acetone)]²⁰⁹; ^1H NMR (400 MHz, C_6D_6 , ppm) δ : 7.59 (d, $J = 7.2\text{ Hz}$, 1H, ArH), 7.39 - 7.42 (m, 1H, ArH), 7.15 - 7.25 (m, 3H, ArH), 6.43 (d, $J = 8.5\text{ Hz}$, 2H, ArH), 3.33 (s, 6H, OCH_3), 1.60 - 1.94 (m, 12H, alkylH), 1.06 - 1.36 (m, 10 H, alkylH); $^{31}\text{P}\{^1\text{H}\}$ NMR (121 MHz, C_6D_6 , ppm) δ : 8.6; The data is in agreement with the literature values

Alternating Copolymers 4.23 – 4.28

Poly[Iridium(III)bis(1-(3-*alt*-oligo(9,9'-dioctyl-9*H*-fluorene-2,7-diyl)-phenyl)isoquinolinato-*N,C*)(acetylacetonate)]



Aqueous Et_4NOH (see below) was added to a stirred solution of [Ir(III)bis(1-(3-bromophenyl)isoquinolinato-*N,C*)(acetylacetonate)] **2.37** (see below), bis(4,4',5,5'-tetramethyl-1,3,2-dioxaborolan-2-yl)poly(9,9'-dioctyl-9*H*-fluorene-2,7-diyl) (see below), $\text{Pd}(\text{OAc})_2$ (see below) and SPhos (see below) in toluene (see below) at RT. The mixture was stirred vigorously for 18 h at $90\text{ }^{\circ}\text{C}$. The mixture was cooled to RT and added to stirring methanol (100 mL). The resultant precipitate was isolated, washed with methanol (100 mL) and dried under vacuum. The crude polymer was then added to a vessel containing Na_2CO_3 (0.10 g), acetyl acetone (1.00 mL), toluene (10 mL) and 2-

ethoxyethanol (10 mL). The reaction mixture was stirred for 4 h at 110 °C and subsequently cooled down to room temperature and added dropwise to stirring methanol (100 mL). The resultant precipitate was isolated, washed with H₂O (100 mL) and methanol (100 mL), dissolved in a minimum amount of toluene and added dropwise to stirring methanol. The precipitate was isolated, washed with H₂O (100 mL) and methanol (100 mL) and dried under vacuum.

4.23

Ir% 20 (m = 3, n = 13)

[Ir(III)bis(1-(3-bromophenyl)isoquinolinato-*N,C*)(acetylacetonate)] **2.37** (46 mg, 0.053 mmol), bis(4,4',5,5'-tetramethyl-1,3,2-dioxaborolan-2-yl)poly(9,9'-dioctyl-9*H*-fluorene-2,7-diyl) **4.10** (76 mg, 0.053 mmol), Pd(OAc)₂ (5 mg, 0.02 mmol), Sphos (17 mg, 0.04 mmol), toluene (5 mL), aqueous Et₄NOH (2.5 mL of a 20% solution).

Yield (92 mg, 75%); ¹H NMR (400 MHz, CDCl₃, ppm) δ: 9.14 (br m, H, P*iqH*), 8.55 (br m, 2aH, P*iqH*), 7.99 (br m, aH, P*iqH*), 7.90 - 7.35 (br m, (6+3a)H, Ar*H*), 7.04 (br m, aH, P*iqH*), 6.56 (br m, aH, P*iqH*), 5.27 (br s, 0.5aH OC(CH₃)CH), 2.12 (br m, 4H, CH₂), 1.83 (br s, 3aH, OC(CH₃)CH), 1.14 - 0.82 (br m, 30H, CH₂ and CH₃), a = 0.4; ¹³C{¹H} NMR (125 MHz, CDCl₃, ppm) δ: 151.8, 140.5, 140.0, 126.2, 121.5, 120.0, 55.4, 40.4, 31.8, 31.0, 30.0, 29.2, 23.9, 22.6, 14.1; GPC (PS): M_n = 12608, M_w = 26097, PDI = 2.1; *m/z* MALDI-TOF : 1169 (H-F₃-H); Anal. Calcd. for Ir:F₄ : C 80.45%, H 8.36%, N 1.24%; Found C 74.07%, H 7.47% N 1.29%.

4.24

Ir% 14.3 (m = 5, n = 14)

[Ir(III)bis(1-(3-bromophenyl)isoquinolinato-*N,C*)(acetylacetonate)] **2.37** (37 mg, 0.043 mmol), bis(4,4',5,5'-tetramethyl-1,3,2-dioxaborolan-2-yl)poly(9,9'-dioctyl-9*H*-fluorene-2,7-diyl) **4.13** (94 mg, 0.053 mmol), Pd(OAc)₂ (5 mg, 0.02 mmol), Sphos (17 mg, 0.04 mmol), toluene (7.5 mL), aqueous Et₄NOH (5 mL of a 20% solution).

Yield (112 mg, 85%); ¹H NMR (400 MHz, CDCl₃, ppm) δ: 9.14 (br m, aH, P*iqH*), 8.55 (br m, 2aH, P*iqH*), 7.99 (br m, aH, P*iqH*), 7.90 - 7.35 (br m, (6+3a)H, Ar*H*), 7.04 (br m, aH, P*iqH*), 6.56 (br m, aH, P*iqH*), 5.27 (br s, 0.5aH OC(CH₃)CH), 2.12 (br m, 4H,

CH_2), 1.83 (br s, 3aH, OC(CH₃)CH), 1.14 - 0.82 (br m, 30H, CH₂ and CH₃), $a = 0.287$; ¹³C{¹H} NMR (125 MHz, CDCl₃, ppm) δ : 151.8, 140.5, 140.0, 126.2, 121.5, 120.0, 55.4, 40.4, 31.8, 31.0, 30.0, 29.2, 23.9, 22.6, 14.1; GPC (PS): $M_n = 29623$, $M_w = 61194$, PDI = 2.1; m/z MALDI-TOF : 1946 (H-F₅-H); Anal. Calcd. for Ir:F₆ : C 82.80%, H 8.88%, N 0.92%; Found C 78.22%, H 8.37% N 0.94%.

4.25

Ir% 6.7 ($m = 11$, $n = 9$)

[Ir(III)bis(1-(3-bromophenyl)isoquinolinato-*N,C*)(acetylacetonate)] **2.37** (66 mg, 0.077 mmol), bis(4,4',5,5'-tetramethyl-1,3,2-dioxaborolan-2-yl)poly(9,9'-dioctyl-9*H*-fluorene-2,7-diyl) **4.14** (350 mg, 0.077 mmol), Pd(OAc)₂ (5 mg, 0.02 mmol), Sphos (17 mg, 0.04 mmol), toluene (20 mL), aqueous Et₄NOH (10 mL of a 20% solution).

Yield (376 mg, 91%); ¹H NMR (400 MHz, CDCl₃, ppm) δ : 9.14 (br m, aH, P*iqH*), 8.55 (br m, 2aH, P*iqH*), 8.20 - 7.35 (br m, (6+4a)H, Ar*H*), 7.04 (br m, aH, P*iqH*), 6.56 (br m, aH, P*iqH*), 5.27 (br s, 0.5aH OC(CH₃)CH), 2.12 (br m, 4H, CH₂), 1.83 (br s, 3aH OC(CH₃)CH), 1.14 - 0.82 (br m, 30H, CH₂ and CH₃), $a = 0.134$; ¹³C{¹H} NMR (125 MHz, CDCl₃, ppm) δ : 151.8, 140.5, 140.0, 126.2, 121.5, 120.0, 55.4, 40.4, 31.8, 30.1, 29.2, 23.9, 22.6, 14.1; GPC (PS): $M_n = 31265$, $M_w = 72605$, PDI = 2.3; m/z MALDI-TOF : 1168 (H-F₃-H), 1946 (H-F₅-H); Anal. Calcd. for Ir:F₁₄ : C 86.26%, H 9.64%, N 0.46%; Found C 83.01%, H 9.31% N 0.55%.

4.26

Ir% 3.3 ($m = 23$, $n = 4$)

[Ir(III)bis(1-(3-bromophenyl)isoquinolinato-*N,C*)(acetylacetonate)] **2.37** (32 mg, 0.038 mmol), bis(4,4',5,5'-tetramethyl-1,3,2-dioxaborolan-2-yl)poly(9,9'-dioctyl-9*H*-fluorene-2,7-diyl) **4.15** (350 mg, 0.038 mmol), Pd(OAc)₂ (5 mg, 0.02 mmol), Sphos (17 mg, 0.04 mmol), toluene (22 mL), aqueous Et₄NOH (11 mL of a 20% solution).

Yield (340 mg, 89%); ¹H NMR (400 MHz, CDCl₃, ppm) δ : 9.14 (br m, aH, P*iqH*), 8.55 (br m, 2aH, P*iqH*), 8.20 - 7.35 (br m, (6+4a)H, Ar*H*), 7.04 (br m, aH, P*iqH*), 6.56 (br m, aH, P*iqH*), 5.27 (br s, 0.5aH OC(CH₃)CH), 2.12 (br m, 4H, CH₂), 1.83 (br s, 3aH OC(CH₃)CH), 1.14 - 0.82 (br m, 30H, CH₂ and CH₃), $a = 0.066$; ¹³C{¹H} NMR (125

MHz, CDCl₃, ppm) δ : 151.8, 140.5, 140.0, 126.2, 121.5, 120.0, 55.4, 40.4, 31.8, 30.1, 29.2, 23.9, 22.6, 14.1; GPC (PS): $M_n = 42290$, $M_w = 103993$, PDI = 2.4; m/z MALDI-TOF : 1946 (H-F₅-H); Anal. Calcd. for Ir:F₂₉ : C 87.90%, H 10.00%, N 0.23%; Found C 85.83%, H 9.88% N 0.22%.

4.27

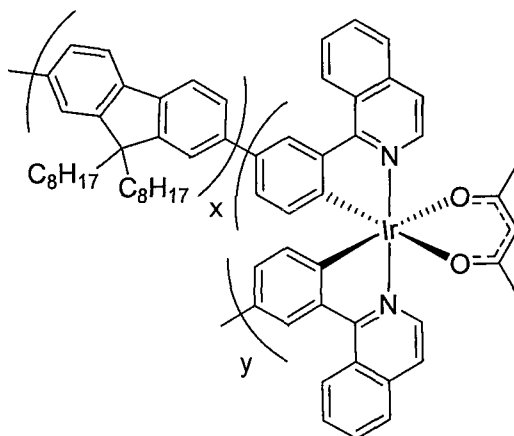
Ir% 1.8 ($m = 38$, $n = 3$)

[Ir(III)bis(1-(3-bromophenyl)isoquinolinato-*N,C*)(acetylacetonate)] **2.37** (14 mg, 0.016 mmol), bis(4,4',5,5'-tetramethyl-1,3,2-dioxaborolan-2-yl)poly(9,9'-dioctyl-9*H*-fluorene-2,7-diyl) **4.16** (250 mg, 0.016 mmol), Pd(OAc)₂ (2 mg, 0.01 mmol), Sphos (7 mg, 0.02 mmol), toluene (10 mL), aqueous Et₄NOH (5 mL of a 20% solution),

Yield (231 mg, 88%); ¹H NMR (400 MHz, CDCl₃, ppm) δ : 9.14 (br m, aH, PiqH), 8.55 (br m, 2aH, PiqH), 8.20 - 7.35 (br m, (6+4a)H, ArH), 7.04 (br m, aH, PiqH), 6.56 (br m, aH, PiqH), 5.27 (br s, 0.5aH OC(CH₃)CH), 2.12 (br m, 4H, CH₂), 1.83 (br s, 3aH OC(CH₃)CH), 1.14 - 0.82 (br m, 30H, CH₂ and CH₃), $a = 0.036$; ¹³C{¹H} NMR (125 MHz, CDCl₃, ppm) δ : 151.8, 140.5, 140.0, 126.2, 121.5, 120.0, 55.4, 40.4, 31.8, 30.1, 29.2, 23.9, 22.6, 14.1; GPC (PS): $M_n = 71305$, $M_w = 157900$, PDI = 2.2; MALDI-TOF : 1168 (H-F₃-H), 1947 (H-F₅-H); Anal. Calcd. for Ir:F₅₅ : C 88.69%, H 10.17%, N 0.14%; Found C 87.52%, H 10.12% N 0.15%.

Random co-polymers 4.29 – 4.32

Poly[Iridium(III)bis(1-(3-co-oligo(9,9'-dioctyl-9*H*-fluorene-2,7-diyl)-phenyl)isoquinolinato-*N,C*)(acetylacetonate)]



Aqueous Et_4NOH (see below) was added to a stirred solution of [Ir(III)bis(1-(3-bromophenyl)isoquinolinato-*N,C*)(acetylacetonate)] **2.37** (see below), 2,7-dibromo-9,9'-dioctyl-9*H*-fluorene **3.16** (see below), 9,9'-dioctyl-2,7-bis(4,4',5,5'-tetramethyl-1,3,2-dioxaborolan-2-yl)-9*H*-fluorene **3.33** (see below), $\text{Pd}(\text{OAc})_2$ (see below) and PPh_3 (see below) in toluene (see below) at RT. The mixture was stirred vigorously for 18 h at 90 °C. The mixture was cooled to RT and added to stirring methanol (100 mL). The resultant precipitate was isolated, washed with methanol (100 mL) and dried under vacuum. The crude polymer was then added to a vessel containing Na_2CO_3 (0.10 g), acetyl acetone (1.00 mL), toluene (10 mL) and 2-ethoxyethanol (10 mL). The reaction mixture was stirred for 4 h at 110 °C and subsequently cooled down to room temperature and added dropwise to stirring methanol (100 mL). The resultant precipitate was isolated, washed with H_2O (100 mL) and methanol (100 mL), dissolved in a minimum amount of toluene and added dropwise to stirring methanol. The precipitate was isolated, washed with H_2O (100 mL) and methanol (100 mL) and dried under vacuum.

4.29

Ir 12.8% ($x = 0.872$, $y = 0.128$)

[Ir(III)bis(1-(3-bromophenyl)isoquinolinato-*N,C*)(acetylacetonate)] **2.37** (38 mg, 0.044 mmol), 2,7-dibromo-9,9'-dioctyl-9*H*-fluorene **3.16** (61 mg, 0.111 mmol), 9,9'-dioctyl-2,7-bis(4,4',5,5'-tetramethyl-1,3,2-dioxaborolan-2-yl)-9*H*-fluorene **3.33** (100 mg, 0.156 mmol), $\text{Pd}(\text{OAc})_2$ (2 mg, 0.01 mmol), PPh_3 (12 mg, 0.05 mmol), toluene (5 mL), aqueous Et_4NOH (5 mL of a 20% solution).

Yield (91 mg, 70%); ^1H NMR (400 MHz, CDCl_3 , ppm) δ : 9.14 (br m, aH, *PiqH*), 8.55 (br m, 2aH, *PiqH*), 7.99 (br m, aH, *PiqH*), 7.90 – 7.35 (br m, (6+3a)H, *ArH*), 7.04 (br m, aH, *PiqH*), 6.56 (br m, aH, *PiqH*), 5.27 (br s, 0.5aH $\text{OC}(\text{CH}_3)\text{CH}$), 2.12 (br m, 4H, CH_2), 1.83 (br s, 3aH, $\text{OC}(\text{CH}_3)\text{CH}$), 1.14 - 0.82 (br m, 30H, CH_2 and CH_3), $a = 0.256$; $^{13}\text{C}\{^1\text{H}\}$ NMR (125 MHz, CDCl_3 , ppm) δ : 151.8, 140.5, 140.0, 126.2, 121.5, 120.0, 55.4, 40.4, 31.8, 31.0, 30.0, 29.2, 23.9, 22.6, 14.1; GPC (PS): $M_n = 9916$, $M_w = 27555$, PDI = 2.8; m/z MALDI-TOF : 1245 (Br- F_3 -H), 1321 (Br- F_3 -Br), 2023 (Br- F_5 -H), 2099 (Br- F_5 -Br); Anal. Calcd. for Ir: F_7 : C 83.63%, H 8.99%, N 0.82%; Found C 80.35%, H 8.61% N 0.98%

4.30**Ir 6.1%** ($x = 0.939$, $y = 0.061$)

[Ir(III)bis(1-(3-bromophenyl)isoquinolinato-*N,C*)(acetylacetonate)] **2.37** (18 mg, 0.021 mmol), 2,7-dibromo-9,9'-dioctyl-9*H*-fluorene **3.16** (74 mg, 0.135 mmol), 9,9'-dioctyl-2,7-bis(4,4',5,5'-tetramethyl-1,3,2-dioxaborolan-2-yl)-9*H*-fluorene **3.33** (100 mg, 0.156 mmol), Pd(OAc)₂ (2 mg, 0.01 mmol), PPh₃ (12 mg, 0.05 mmol), toluene (5 mL), aqueous Et₄NOH (5 mL of a 20% solution).

Yield (103 mg, 82%); ¹H NMR (400 MHz, CDCl₃, ppm) δ: 9.14 (br m, aH, Piq*H*), 8.55 (br m, 2aH, Piq*H*), 8.20 - 7.35 (br m, (6+4a)H, Ar*H*), 7.04 (br m, aH, Piq*H*), 6.56 (br m, aH, Piq*H*), 5.27 (br s, 0.5aH OC(CH₃)CH), 2.12 (br m, 4H, CH₂), 1.83 (br s, 3aH OC(CH₃)CH), 1.14 - 0.82 (br m, 30H, CH₂ and CH₃), $a = 0.122$; ¹³C{¹H} NMR (125 MHz, CDCl₃, ppm) δ: 151.8, 140.5, 140.0, 126.2, 121.5, 120.0, 55.4, 40.4, 31.8, 30.1, 29.2, 23.9, 22.6, 14.1; GPC (PS): M_n = 43913, M_w = 98744, PDI = 2.2; *m/z* MALDI-TOF : 1245 (Br-F₃-H), 1321 (Br-F₃-Br), 2023 (Br-F₅-H), 2099 (Br-F₅-Br); Anal. Calcd. for Ir:F₁₅ : C 86.46%, H 9.68%, N 0.43%; Found C 84.62%, H 9.39% N 0.57%.

4.31**Ir 3.1%** ($x = 0.969$, $y = 0.031$)

[Ir(III)bis(1-(3-bromophenyl)isoquinolinato-*N,C*)(acetylacetonate)] **2.37** (9 mg, 0.010 mmol), 2,7-dibromo-9,9'-dioctyl-9*H*-fluorene **3.16** (80 mg, 0.146 mmol), 9,9'-dioctyl-2,7-bis(4,4',5,5'-tetramethyl-1,3,2-dioxaborolan-2-yl)-9*H*-fluorene **3.33** (100 mg, 0.156 mmol), Pd(OAc)₂ (2 mg, 0.01 mmol), PPh₃ (12 mg, 0.05 mmol), toluene (5 mL), aqueous Et₄NOH (5 mL of a 20% solution).

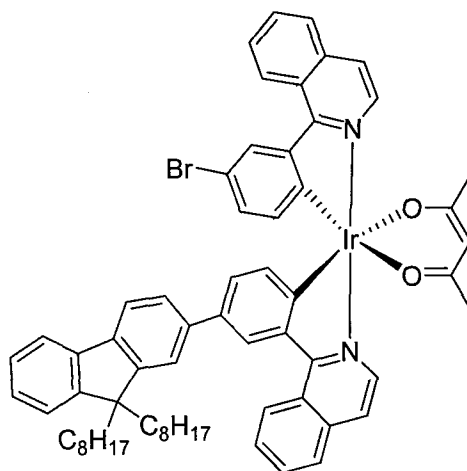
Yield (114 mg, 93%); ¹H NMR (400 MHz, CDCl₃, ppm) δ: 9.14 (br m, aH, Piq*H*), 8.55 (br m, 2aH, Piq*H*), 8.20 - 7.35 (br m, (6+4a)H, Ar*H*), 7.04 (br m, aH, Piq*H*), 6.56 (br m, aH, Piq*H*), 5.27 (br s, 0.5aH OC(CH₃)CH), 2.12 (br m, 4H, CH₂), 1.83 (br s, 3aH OC(CH₃)CH), 1.14 - 0.82 (br m, 30H, CH₂ and CH₃), $a = 0.062$; ¹³C{¹H} NMR (125 MHz, CDCl₃, ppm) δ: 151.8, 140.5, 140.0, 126.2, 121.5, 120.0, 55.4, 40.4, 31.8, 30.1, 29.2, 23.9, 22.6, 14.1; GPC (PS): M_n = 72233, M_w = 195545, PDI = 2.7; *m/z* MALDI-TOF : 2022 (Br-F₅-H), 2099 (Br-F₅-Br); Anal. Calcd. for Ir:F₃₁ : C 88.00%, H 10.02%, N 0.22%; Found C 86.51%, H 9.92% N 0.19%.

4.32**Ir 1.1%** ($x = 0.989$, $y = 0.011$)

[Ir(III)bis(1-(3-bromophenyl)isoquinolinato-*N,C*)(acetylacetonate)] **2.37** (5 mg, 0.006 mmol), 2,7-dibromo-9,9'-dioctyl-9*H*-fluorene **3.16** (82 mg, 0.150 mmol), 9,9'-dioctyl-2,7-bis(4,4',5,5'-tetramethyl-1,3,2-dioxaborolan-2-yl)-9*H*-fluorene **3.33** (100 mg, 0.156 mmol), Pd(OAc)₂ (2 mg, 0.01 mmol), PPh₃ (12 mg, 0.05 mmol), toluene (5 mL), aqueous Et₄NOH (5 mL of a 20% solution).

Yield (107 mg, 88%); ¹H NMR (400 MHz, CDCl₃, ppm) δ: 9.14 (br m, aH, Piq*H*), 8.55 (br m, 2aH, Piq*H*), 8.20 - 7.35 (br m, (6+4a)H, Ar*H*), 7.04 (br m, aH, Piq*H*), 6.56 (br m, aH, Piq*H*), 5.27 (br s, 0.5aH OC(CH₃)CH), 2.12 (br m, 4H, CH₂), 1.83 (br s, 3aH OC(CH₃)CH), 1.14 - 0.82 (br m, 30H, CH₂ and CH₃), $a = 0.022$; ¹³C{¹H} NMR (125 MHz, CDCl₃, ppm) δ: 151.8, 140.5, 140.0, 126.2, 121.5, 120.0, 55.4, 40.4, 31.8, 30.1, 29.2, 23.9, 22.6, 14.1; GPC (PS): M_n = 49034, M_w = 108419, PDI = 2.2; *m/z* MALDI-TOF : 1321 (Br-F₃-Br), 1633 (Br-F₄-H), 2098 (Br-F₅-Br), 2411 (Br-F₆-H); Anal. Calcd. for Ir:F₈₉ : C 89.04%, H 10.25%, N 0.08%; Found C 87.39%, H 10.10% N 0.11%.

6.6 Experimental For Chapter 5

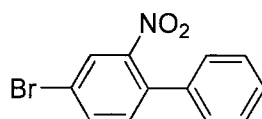
[Iridium(III)(1-(3-bromophenyl)isoquinoline-*N,C*)-(1-(3-(9,9'-dioctyl-9*H*-fluoren-2-yl)phenyl)isoquinoline-*N,C*)(acetylacetonate)] 5.16

A solution of 2-(9,9'-dioctyl-9*H*-fluoren-2-yl)-4,4',5,5'-tetramethyl-1,3,2-dioxaborolane **2.41** (136 mg, 0.26 mmol), [Ir(III)bis(1-(3-bromophenyl)isoquinolinato-*N,C*)(acetylacetonate)] **2.37** (150 mg, 0.175 mmol), Pd(OAc)₂ (2 mg, 0.009 mmol) and PPh₃ (10 mg, 0.004 mmol) and aqueous Et₄NOH (5 mL of a 20 % solution) in toluene (10 mL) was heated to 110 °C. After 6 h the reaction mixture was allowed to cool to room temperature and the layers separated. The organic layer was washed with H₂O (3 x 50 ml), dried (MgSO₄), filtered and concentrated *in vacuo*. The resulting red solid, Na₂CO₃ (0.10 g), acetyl acetone (1.00 mL) were added to a round bottom flask containing 2-ethoxyethanol (10 mL) and the reaction mixture stirred for 2 h at 110 °C. The resulting red solution was allowed to cooled down to room temperature at which point H₂O (30 mL) was added forming a precipitate. Filtration followed by washing with H₂O (50 mL) afforded the crude title product. Purification by flash column chromatograph (silica gel, CHCl₃:hexane; 1:1) allowed isolation of [Ir(III)bis(1-(3-(9,9'-dioctyl-9*H*-fluoren-2-yl)phenyl)isoquinolinato-*N,C*)(acetylacetonate)] (109 mg, 42%) and [Ir(III)(1-(3-bromophenyl)isoquinoline-*N,C*)-(1-(3-(9,9'-dioctyl-9*H*-fluoren-2-yl)phenyl)isoquinoline-*N,C*)(acetylacetonate)] (92 mg, 45%) as red solids.

¹H NMR (400 MHz, CDCl₃, ppm) δ: 9.08 (m, 1H, ArH), 8.91 (m, 1H, ArH), 8.48 (m, 2H, ArH), 8.44 (d, *J* = 6.4 Hz, 1H, ArH), 8.32 (s, 1H, ArH), 7.95 (m, 2H, ArH), 7.75 (m, 4H, ArH), 7.68 (m, 2H, ArH), 7.53 (m, 3H, ArH), 7.47 (s, 1H, ArH), 7.30 (m, 3H, ArH), 6.99 (dd, *J* = 1.8, 7.9 Hz, 1H, ArH), 6.76 (dd, *J* = 1.9, 8.2 Hz, 1H, ArH), 6.43 (d, *J* = 7.9 Hz, 1H, ArH), 6.32 (d, *J* = 8.2 Hz, 1H, ArH), 5.23 (s, 1H, OC(CH₃)CH), 1.90 (m, 4H, CH₂), 1.79 (s, 3H, OC(CH₃)CH), 1.78 (s, 3H, OC(CH₃)CH), 1.20 - 1.00 (m, 20H,

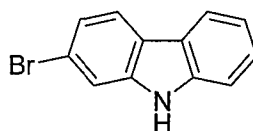
CH_2), 0.76 (m, 6H, CH_3), 0.64 (m, 4H, CH_2); $^{13}\text{C}\{^1\text{H}\}$ NMR (125 MHz, CDCl_3 , ppm) δ : 185.0, 169.0, 167.8, 151.2, 151.0, 150.7, 150.2, 148.7, 147.1, 141.3, 141.0, 140.6, 140.4, 139.4, 137.3, 137.2, 135.3, 134.3, 133.8, 132.0, 131.7, 130.9, 128.6, 128.3, 128.2, 127.8, 127.4, 126.8, 126.7, 126.5, 126.4, 125.3, 122.8, 121.1, 120.6, 120.2, 119.8, 119.5, 114.0, 100.7, 55.0, 40.4, 31.8, 30.1, 29.3, 28.8, 23.8, 22.6, 14.1; m/z (FAB): 1166 $[\text{M}+\text{H}]^+$; Anal. Calcd. for $\text{C}_{64}\text{H}_{66}\text{BrIrN}_2\text{O}_2$: C 65.85%, H 5.70%, N 2.40%; Found C 65.69%, H 5.77% N 2.32%.

4-Bromo-2-nitrobiphenyl¹⁸⁹ 5.19



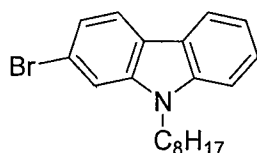
Phenylboronic acid (2.0 g, 16.4 mmol), 2,5-dibromonitrobenzene (4.6 g, 16.4 mmol) and $\text{Pd}(\text{PPh}_3)_4$ (0.5 g, 0.5 mmol) were dissolved in a mixture of toluene (25 mL) and aqueous Na_2CO_3 (15 mL of a 2M solution). The resulting mixture was heated to 90 °C for 6 h after which point it was allowed to cool to room temperature. The layers were separated and the organic phase washed with H_2O (2 x 50 mL). The combined organic fraction were dried (MgSO_4), filtered and concentrated *in vacuo* to afford the crude product as a brown solid which was used without any further purification (4.4 g)

2-Bromo-9H-carbazole¹⁸⁹ 5.20



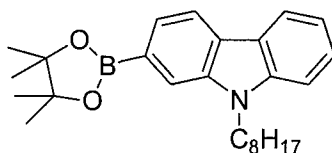
Crude 4-bromo-2-nitrobiphenyl **5.19** (2.9 g) and PPh_3 (4 g, 14.9 mmol) were dissolved in *o*-dichlorobenzene (25 mL) and heated to reflux. After 24 h, the reaction mixture was allowed to cool to room temperature and concentrated *in vacuo*. Purification by flash column chromatography (silica gel, DCM) afforded the product as a white crystals (0.81 g, 20% overall).

m.p. 245 - 249 °C [Lit. (ethanol) 249 - 250 °C]²¹⁰; ^1H NMR (400 MHz, DMSO, ppm) δ : 11.39 (s, 1H, NH), 8.12 (d, $J = 7.8$ Hz, 1H, ArH), 8.06 (d, $J = 8.3$ Hz, 1H, ArH), 7.66 (d, $J = 1.6$ Hz, 1H, ArH), 7.49 (d, $J = 8.1$ Hz, 1H, ArH), 7.41 (t, $J = 7.4$ Hz, 1H, ArH), 7.28 (d, $J = 8.3$ Hz, 1H, ArH), 7.18 (t, $J = 7.2$ Hz, 1H, ArH); m/z (CI): 244 $[\text{M}+\text{H}]^+$; The data is in agreement with the literature values.

2-Bromo-9-octyl-9H-carbazole 5.21

To a stirred solution of 2-bromo-9H-carbazole **5.20** (0.32 g, 1.29 mmol) and K_2CO_3 (0.36 g, 2.58 mmol) in DMF (30 mL) at 80 °C was added 1-bromooctane (0.34 mL, 1.94 mmol). The reaction mixture was heating was continued for 24 h, after which point it was allowed to cool to room temperature. The product was extracted with Et_2O (50 mL) and washed with H_2O (4 x 150 mL). The organic layer was dried ($MgSO_4$), filtered and concentrated *in vacuo*. Purification by flash column chromatography (silica gel, hexane: Et_3N , 98:2) afforded the product as white crystals (0.27 g, 59%).

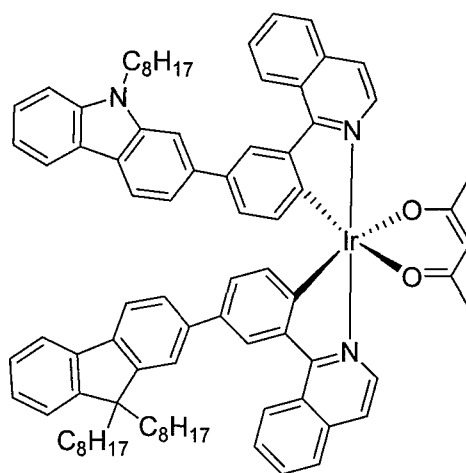
m.p. 104 - 107 °C; 1H NMR (400 MHz, $CDCl_3$, ppm) δ : 8.04 (d, $J = 7.8$ Hz, 1H, ArH), 7.92 (d, $J = 8.2$ Hz, 1H, ArH), 7.53 (d, $J = 1.6$ Hz, 1H, ArH), 7.48 (t, $J = 8.1$ Hz, 1H, ArH), 7.40 (d, $J = 8.2$ Hz, 1H, ArH), 7.31 (dd, $J = 8.3$ Hz, $J = 1.7$ Hz, 1H, ArH), 7.23 (d, $J = 7.1$ Hz, 1H, ArH), 4.24 (t, $J = 7.3$ Hz, 2H, NCH_2), 1.85 (m, 2H, CH_2), 1.42 - 1.20 (m, 10H, CH_2), 0.87 (t, $J = 6.7$ Hz, 3H, CH_3); $^{13}C\{^1H\}$ NMR (125 MHz, $CDCl_3$, ppm) δ : 141.3, 140.6, 126.0, 122.4, 121.9, 121.8, 121.5, 120.3, 119.3, 119.2, 111.8, 108.9, 43.2, 31.6, 29.3, 29.1, 28.9, 27.2, 24.9, 22.6, 14.1; m/z (CI): 358 $[M+H]^+$; Anal. Calcd. for $C_{20}H_{24}BrN$: C 67.04%, H 6.75%, N 3.91%; Found C 67.04%, H 6.77% N 3.94%.

9-Octyl-2-(4,4',5,5'-tetramethyl-1,3,2-dioxaborolan-2-yl)-9H-carbazole²¹¹ 5.22

2-Bromo-9-octyl-9H-carbazole **5.21** (0.27 g, 0.74 mmol) was dissolved in THF (25 mL) at -78 °C and *n*-butyllithium (0.7 mL of a 1.6 M solution in hexanes, 1.1 mmol) was added dropwise. The resulting milky solution was stirred for 1 h, after which point 2-isopropoxy-4,4,5,5-tetramethyl-1,3,2-dioxaborolane (0.46 mL, 2.24 mmol) was added rapidly. After a further 1 h, the reaction was allowed to warm to room temperature and stirred for 18 h. The reaction mixture was extracted with Et_2O (50 mL) and washed with H_2O (2 x 50 mL). The organic layer was dried ($MgSO_4$), filtered, and concentrated *in vacuo*. Column chromatography (silica gel, hexane:DCM: Et_3N 2:1:0.02) enabled isolation of the product as a colourless oil (0.25 g, 83%).

^1H NMR (400 MHz, CDCl_3 , ppm) δ : 8.11 (m, 2H, ArH), 7.87 (s, 1H, ArH), 7.69 (d, $J = 7.8$ Hz, 1H, ArH), 7.47 (t, $J = 7.9$ Hz, 1H, ArH), 7.42 (d, $J = 8.1$ Hz, 1H, ArH), 7.21 (t, $J = 7.3$ Hz, 1H, ArH), 4.33 (d, $J = 7.3$ Hz, 2H, NCH_2), 1.87 (m, 2H, CH_2), 1.40 (s, 12H, OCCH_3) 1.38 - 1.20 (m, 10H, CH_2), 1.03 (t, $J = 7.2$ Hz, 3H, CH_3); m/z (CI): 406 $[\text{M}+\text{H}]^+$; The data is in agreement with the literature values.

[Iridium(III)(1-(3-(9-octyl-9H-carbazol-2-yl)phenyl)isoquinoline-N,C)-(1-(3-(9,9'-dioctyl-9H-fluoren-2-yl)phenyl)isoquinoline-N,C)(acetylacetonate)] 5.23

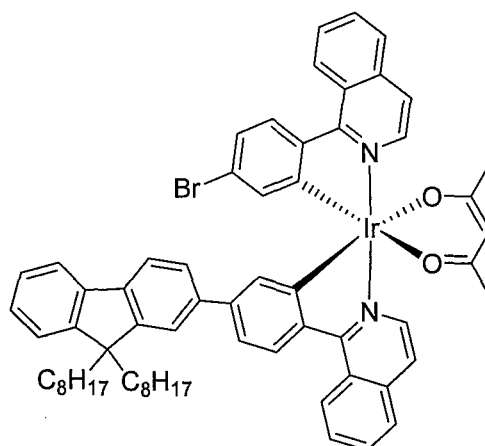


A degassed solution of 9-octyl-2-(4,4',5,5'-tetramethyl-1,3,2-dioxaborolan-2-yl)-9H-carbazole **5.22** (21 mg, 0.05 mmol, $[\text{Ir}(\text{III})(1-(3\text{-bromophenyl})\text{isoquinoline-}N,C)-(1-(3-(9,9'\text{-dioctyl-9H-fluoren-2-yl})\text{phenyl})\text{isoquinoline-}N,C)(\text{acetylacetonate})]$ **5.16** (50 mg, 0.043 mmol), $\text{Pd}(\text{OAc})_2$ (1 mg, 0.004 mmol) and PPh_3 (5 mg, 0.002 mmol) and aqueous Et_4NOH (2 mL of a 20 % solution) in toluene (10 mL) was heated to 110 °C. After 24 h, the reaction mixture was allowed to cool to room temperature and the layers separated. The organic layer was washed with H_2O (3 x 20 mL), dried (MgSO_4), filtered and concentrated *in vacuo*. The resulting red solid, Na_2CO_3 (0.10 g), acetyl acetone (1.00 mL) were added to a round bottom flask containing a 2:1 mixture of toluene and 2-ethoxyethanol (30 mL) and the reaction mixture stirred for 2 h at 110 °C. The resulting red solution was cooled to room temperature and extracted with toluene (30 mL) and washed with H_2O (3 x 50 mL). The organic layer was dried (MgSO_4), filtered and concentrated *in vacuo*. Purification by column chromatograph (silica gel, CHCl_3 :hexane: Et_3N , 2:1:0.01) allowed isolation of the product as a red solid (59 mg, 65%).

^1H NMR (400 MHz, CDCl_3 , ppm) δ : 9.13 (m, 2H, ArH), 8.52 (m, 4H, ArH), 8.07 (t, $J = 7.9$ Hz, 2H, ArH), 7.97 (m, 2H, ArH), 7.75 (m, 4H, ArH), 7.68 (t, $J = 8.0$ Hz, 2H, ArH),

7.54 (t, $J = 8.5$ Hz, 4H, ArH), 7.49 (d, $J = 7.1$ Hz, 2H, ArH), 7.42 (t, $J = 8.0$ Hz, 2H, ArH), 7.37 (d, $J = 8.1$ Hz, 1H, ArH), 7.29 (m, 2H, ArH), 7.19 (t, $J = 7.4$ Hz, 1H, ArH), 7.08 (dd, $J = 8.0$ Hz, $J = 1.7$ Hz, 2H, ArH), 6.55 (t, $J = 7.9$ Hz, 2H, ArH), 5.26 (s, 1H, OC(CH₃)CH), 4.19 (m, 2H, NCH₂), 1.91 (m, 4H, CH₂), 1.81 (s, 3H, OC(CH₃)CH), 1.80 (s, 3H, OC(CH₃)CH), 1.40 - 0.56 (m, 45H, CH₂ and CH₃); ¹³C{¹H} NMR (125 MHz, CDCl₃, ppm) δ : 184.9, 169.2, 169.1, 150.9, 147.2, 141.0, 140.8, 140.6, 139.3, 137.3, 134.2, 133.9, 130.9, 130.7, 129.1, 128.9, 128.6, 128.3, 127.8, 127.7, 127.6, 127.4, 126.8, 126.7, 126.6, 126.5, 125.2, 124.5, 122.8, 121.4, 121.2, 121.1, 120.4, 120.2, 119.8, 119.7, 119.5, 118.3, 106.7, 100.7, 54.9, 43.1, 40.4, 31.8, 30.1, 29.7, 29.4, 29.2, 28.9, 28.8, 27.4, 23.8, 22.6, 14.1; m/z (FAB): 1365 [M+H]⁺; Anal. Calcd. for C₈₄H₉₀BrIrN₃O₂: C 73.87%, H 6.64%, N 3.08%; Found C 73.86%, H 6.64% N 3.01%.

[Iridium(III)(1-(4-bromophenyl)isoquinoline-*N,C*)-(1-(4-(9,9'-dioctyl-9*H*-fluoren-2-yl)phenyl)isoquinoline-*N,C*)(acetylacetonate)] 5.24

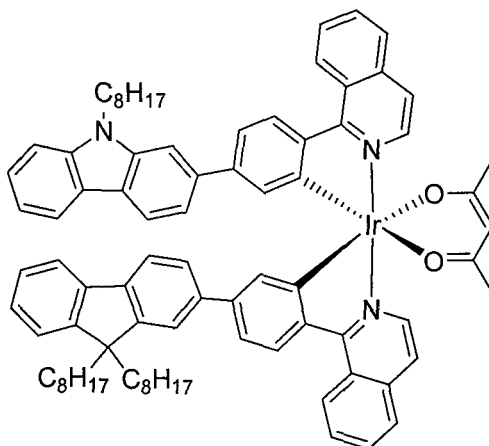


This complex was synthesised according to the method used to prepare compound **5.16** using [Ir(III)bis(1-(4-bromophenyl)isoquinolinato-*N,C*)(acetylacetonate)] **2.38**. It was isolated as a red solid (56 mg, 43%).

¹H NMR (400 MHz, CDCl₃, ppm) δ : 9.04 (m, 1H, ArH), 8.96 (m, 1H, ArH), 8.50 (d, $J = 6.4$ Hz, 1H, ArH), 8.44 (d, $J = 6.4$ Hz, 1H, ArH), 8.31 (d, $J = 8.5$ Hz, 1H, ArH), 8.09 (d, $J = 8.6$ Hz, 1H, ArH), 7.95 (m, 2H, ArH), 7.75 (m, 5H, ArH), 7.58 (m, 1H, ArH), 7.54 (m, 2H, ArH), 7.48 (d, $J = 7.9$ Hz, 1H, ArH), 7.27 (m, 4H, ArH), 7.14 (s, 1H, ArH), 7.08 (d, $J = 8.5$ Hz, $J = 2.1$ Hz, 1H, ArH), 6.64 (d, $J = 1.8$ Hz, 1H, ArH), 6.61 (d, $J = 2.0$ Hz, 1H, ArH), 5.25 (s, 1H, OC(CH₃)CH), 1.82 (s, 3H, OC(CH₃)CH), 1.78 (s, 3H, OC(CH₃)CH), 1.70 - 1.50 (m, 4H, CH₂), 1.30 - 0.73 (m, 26H, CH₂ and CH₃), 0.50 - 0.35 (m, 4H, CH₂); ¹³C{¹H} NMR (125 MHz, CDCl₃, ppm) δ : 184.9, 168.6, 168.6, 154.7, 150.9, 150.7, 145.7, 140.9, 140.7, 140.4, 140.2, 139.3, 137.3, 137.1, 136.1,

131.1, 130.9, 130.7, 130.6, 130.1, 129.9, 128.2, 128.1, 127.8, 127.5, 127.4, 126.9, 126.8, 126.6, 126.4, 126.3, 126.2, 125.7, 124.5, 123.6, 122.7, 121.1, 120.9, 120.8, 120.1, 119.9, 119.8, 119.6, 119.4, 100.7, 54.8, 40.4, 40.3, 31.8, 30.1, 30.1, 29.3, 29.2, 28.8, 28.7, 23.6, 22.6, 14.1; m/z (FAB): 1166 $[M+H]^+$; Anal. Calcd. for $C_{64}H_{66}BrIrN_2O_2$: C 65.85%, H 5.70%, N 2.40%; Found C 66.21%, H 5.88% N 2.20%.

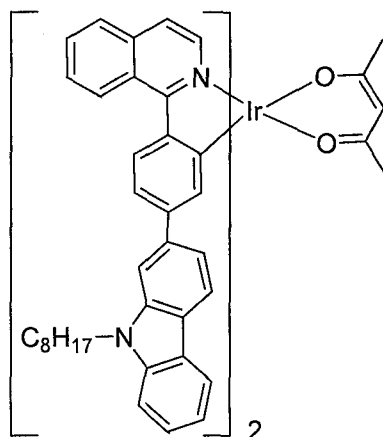
[Iridium(III)(1-(4-(9-octyl-9H-carbazol-2-yl)phenyl)isoquinoline-N,C)-(1-(4-(9,9'-dioctyl-9H-fluoren-2-yl)phenyl)isoquinoline-N,C)(acetylacetonate)] 5.25



This complex was synthesised according to the method used to prepare compound **5.23** using [Ir(III)(1-(4-bromophenyl)isoquinoline-N,C)-(1-(4-(9,9'-dioctyl-9H-fluoren-2-yl)phenyl)isoquinoline-N,C)(acetylacetonate)] **5.24**. It was isolated as a red solid (25 mg, 86%).

1H NMR (400 MHz, $CDCl_3$, ppm) δ : 9.08 (m, 2H, ArH), 8.57 (d, $J = 6.3$ Hz, 2H, ArH), 8.34 (d, $J = 8.4$ Hz, 1H, ArH), 8.30 (d, $J = 8.5$ Hz, 1H, ArH), 7.98 (m, 3H, ArH), 7.89 (d, $J = 8.1$ Hz, 1H, ArH), 7.75 (m, 4H, ArH), 7.58 (m, 1H, ArH), 7.51 (m, 3H, ArH), 7.39 (t, $J = 7.9$ Hz, 1H, ArH), 7.29 (m, 8H, ArH), 7.16 (m, 3H, ArH), 6.77 (d, $J = 1.7$ Hz, 2H, ArH), 5.28 (s, 1H, OC(CH₃)CH), 4.04 (m, 2H, NCH₂), 1.83 (s, 3H, OC(CH₃)CH), 1.82 (s, 3H, OC(CH₃)CH), 1.70 - 0.56 (m, 49H, CH₂ and CH₃); $^{13}C\{^1H\}$ NMR (125 MHz, $CDCl_3$, ppm) δ : 184.9, 169.2, 169.1, 152.2, 152.1, 150.9, 150.7, 145.8, 141.8, 140.9, 140.8, 140.6, 140.1, 139.5, 139.0, 137.1, 132.2, 131.3, 130.9, 130.7, 130.6, 129.9, 127.8, 127.6, 127.4, 127.3, 126.8, 126.6, 126.4, 125.7, 125.3, 122.7, 122.6, 121.8, 121.1, 120.2, 119.9, 119.8, 119.7, 119.6, 119.5, 119.4, 119.3, 118.6, 108.5, 107.3, 100.6, 54.8, 53.4, 42.8, 40.5, 40.3, 31.8, 31.6, 30.2, 30.1, 29.4, 29.3, 29.2, 28.9, 28.8, 27.3, 23.6, 22.2, 14.1; m/z (FAB): 1365 $[M+H]^+$; Anal. Calcd. for $C_{84}H_{90}BrIrN_3O_2$: C 73.87%, H 6.64%, N 3.08%; Found C 73.85%, H 6.64% N 3.08%.

[Iridium(III)bis(1-(4-(9-octyl-9*H*-carbazol-2-yl)phenyl)isoquinolinato-*N,C*)(acetylacetonate)] 5.26

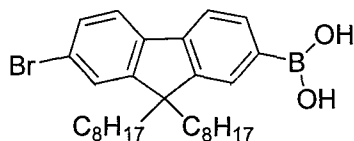


A solution of 9-octyl-2-(4,4',5,5'-tetramethyl-1,3,2-dioxaborolan-2-yl)-9*H*-carbazole **5.22** (120 mg, 0.29 mmol), [Ir(III)bis(1-(4-bromophenyl)isoquinolinato-*N,C*)(acetylacetonate)] **2.38** (100 mg, 0.12 mmol), Pd(OAc)₂ (1 mg, 0.004 mmol), PPh₃ (5 mg, 0.002 mmol) and aqueous Et₄NOH (2 mL of a 20 % solution) in toluene (10 mL) was heated to 110 °C. After 24 h the reaction mixture was allowed to cool to room temperature and the layers separated. The organic layer was washed with H₂O (3 x 50 mL), dried (MgSO₄), filtered and concentrated *in vacuo*. The resulting red solid, Na₂CO₃ (0.10 g), acetyl acetone (1.00 mL) were added to a round bottom flask containing a 2:1 mixture of toluene and 2-ethoxyethanol (30 mL) and the reaction mixture stirred for 2 h at 110 °C. The resulting red solution was cooled to room temperature and extracted with toluene (30 mL) and washed with H₂O (3 x 50 mL). The organic layer was dried (MgSO₄), filtered and concentrated *in vacuo*. Purification by flash column chromatograph (silica gel, CHCl₃:hexane:Et₃N; 2:1:0.01) allowed isolation of the product as a red solid (141 mg, 86%).

¹H NMR (400 MHz, CDCl₃, ppm) δ: 9.09 (m, 2H, Ar*H*), 8.56 (d, *J* = 6.4 Hz, 2H, Ar*H*), 8.30 (d, *J* = 8.4 Hz, 2H, Ar*H*), 7.99 (d, *J* = 7.6 Hz, 2H, Ar*H*), 7.93 (m, 2H, Ar*H*), 7.87 (d, *J* = 8.1 Hz, 2H, Ar*H*), 7.75 (m, 4H, Ar*H*), 7.51 (d, *J* = 6.4 Hz, 2H, Ar*H*), 7.39 (t, *J* = 8.1 Hz, 2H, Ar*H*), 7.30 (m, 6H, Ar*H*), 7.15 (m, 4H, Ar*H*), 6.79 (d, *J* = 1.8 Hz, 2H, Ar*H*), 5.25 (s, 1H, OC(CH₃)CH), 4.04 (m, 4H, NCH₂), 1.81 (s, 6H, OC(CH₃)CH), 1.21 - 0.8 (m, 30H, CH₂ and CH₃); ¹³C{¹H} NMR (125 MHz, CDCl₃, ppm) δ: 184.9, 169.1, 152.1, 145.7, 141.8, 140.9, 140.8, 140.6, 139.0, 137.2, 132.2, 130.6, 130.1, 129.9, 127.7, 127.5, 127.3, 126.8, 126.5, 125.4, 122.6, 121.8, 120.5, 120.2, 112.0, 119.6,

118.7, 118.6, 118.4, 108.5, 107.3, 107.1, 100.7, 42.8, 31.9, 29.5, 29.3, 28.9, 28.8, 27.3, 22.7, 14.1; m/z (FAB): 1255 $[M+H]^+$; Anal. Calcd. for $C_{75}H_{73}BrIrN_4O_2$: C 71.80%, H 5.86%, N 4.47%; Found C 71.65%, H 5.85% N 4.32%.

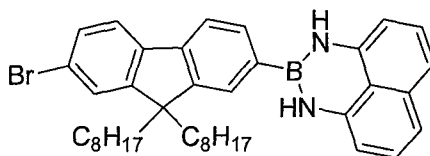
7-Bromo-9,9'-dioctyl-9H-fluoren-2-ylboronic acid⁹² 5.33



2,7-Dibromo-9,9'-dioctyl-9H-fluorene **3.16** (5.0 g, 9.13 mmol) was dissolved in THF (50 mL) at -78 °C and *n*-butyllithium (5.7 mL of a 1.6 M solution in hexanes, 9.1 mmol) was added dropwise. The resulting suspension was stirred for 2 h after which point triisopropyl borate (4.2 mL, 18.26 mmol) was added rapidly. After a further 2 h, the reaction was warmed to room temperature and stirred for a further 18 h. The reaction mixture was poured into aqueous HCl (100 mL of a 1M solution) and vigorously stirred for 1 h. Et₂O (50 mL) was added and the layers separated. The aqueous fraction was extracted with Et₂O (2 x 25 mL) and the combined organic fractions were dried (MgSO₄), filtered and concentrated *in vacuo*. Column chromatography (Silica gel; Toluene → EtOAc) allowed isolation of the product as a colourless oil (2.9 g, 62%).

¹H NMR (400 MHz, CDCl₃, ppm) δ : 8.30 (d, $J = 7.8$, 0.25H, *ArH*), 8.18 (s, 0.25H, *ArH*), 7.85 (d, $J = 7.5$, 0.25H, *ArH*), 7.72 - 7.38 (m, 5.25H, *ArH*), 2.23 - 1.75 (m, 4H, CH₂), 1.32 - 0.90 (m, 20H, CH₂), 0.87 - 0.40 (m, 10H, CH₂ and CH₃); m/z (CI): 513 $[M+H]^+$; The data is in agreement with the literature values

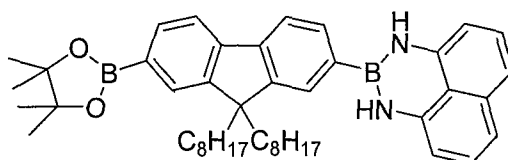
2-(7-Bromo-9,9'-dioctyl-9H-fluoren-2-yl)-2,3-dihydro-1H-naphtho[1,8-de][1,3,2]diazaborinine 5.34



A mixture of 7-bromo-9,9'-dioctyl-9H-fluoren-2-ylboronic acid **5.33** (1.0 g, 1.95 mmol), 1,8-diaminonaphthalene (0.32 g, 2.0 mmol), in toluene was heated for 2 h under reflux with azeotropic removal of H₂O. The reaction mixture was allowed to cool to room temperature and concentrated *in vacuo*. Column chromatography (Silica gel, hexane:DCM; 2:1) allowed isolation of the product as a colourless oil (1.24 g, 100%).

^1H NMR (400 MHz, CDCl_3 , ppm) δ : 7.73 (d, $J = 7.5$, 1H, ArH), 7.65 - 7.54 (m, 3H, ArH), 7.50 - 7.44 (m, 2H, ArH), 7.16 (t, $J = 7.6$, 2H, ArH), 7.07 (d, $J = 8.2$, 2H, ArH), 6.47 (d, $J = 7.3$, 2H, ArH), 6.08 (s, 2H, NH), 2.09 - 1.89 (m, 4H, CH_2), 1.29 - 0.99 (m, 20H, CH_2), 0.81 (t, $J = 7.1$, 6H, CH_3), 0.69 - 0.53 (m, 4H, CH_2); m/z (CI): 636 $[\text{M}+\text{H}]^+$; Anal. Calcd. for $\text{C}_{39}\text{H}_{48}\text{BBrN}_2$: C 73.71%, H 7.61%, N 4.41%; Found C 74.68%, H 7.66% N 4.95%.

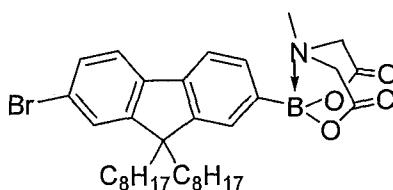
2-(9,9'-Dioctyl-7-(4,4',5,5'-tetramethyl-1,3,2-dioxaborolan-2-yl)-9H-fluoren-2-yl)-2,3-dihydro-1H-naphtho[1,8-de][1,3,2]diazaborinine 5.35



A solution of 2-(7-bromo-9,9'-dioctyl-9H-fluoren-2-yl)-2,3-dihydro-1H-naphtho[1,8-de][1,3,2]diazaborinine **5.34** (1.0 g, 1.47 mmol), $\text{PdCl}_2(\text{dppf})$ (67 mg, 0.08 mmol), KOAc (0.46 g, 4.71 mmol) and bis(pinacolato)diboron (0.64 g, 2.52 mmol) were in DMF (20 mL) was heated to 80 °C for 24 h. The reaction mixture was allowed to cool to room temperature and Et_2O (50 mL) and H_2O (50 mL) were added. The layers were separated and the organic layer was washed with H_2O (4 x 50 mL) and Brine (2 x 50 mL of a sat. aqueous solution). The organic fraction was dried (MgSO_4), filtered, and concentrate *in vacuo*. Column chromatography (Silica gel; hexane:DCM; 1:1) afforded the product as a white crystalline solid (0.79 g, 74%).

m.p. 92 °C Decomposition; ^1H NMR (400 MHz, CDCl_3 , ppm) δ : 7.85 - 7.72 (m, 4H, ArH), 7.63 (d, $J = 7.6$, 1H, ArH), 7.58 (s, 1H, ArH), 7.16 (t, $J = 7.8$, 2H, ArH), 7.07 (d, $J = 8.2$, 2H, ArH), 6.47 (d, $J = 7.2$, 2H, ArH), 6.10 (s, 2H, NH), 2.11 - 1.96 (m, 4H, CH_2), 1.40 (s, 12H, OCCH_3), 1.23 - 0.96 (m, 20H, CH_2), 0.80 (t, $J = 7.1$, 6H, CH_3), 0.59 (m, 4H, CH_2); $^{13}\text{C}\{^1\text{H}\}$ NMR (125 MHz, CDCl_3 , ppm) δ : 151.1, 150.2, 143.7, 143.2, 141.2, 136.4, 133.8, 130.1, 128.9, 127.6, 125.6, 112.0, 119.8, 119.3, 117.8, 106.0, 83.8, 55.2, 40.3, 31.8, 30.0, 29.2, 24.9, 23.7, 22.6, 14.1; m/z (CI): 684 $[\text{M}+\text{H}]^+$; Anal. Calcd. for $\text{C}_{45}\text{H}_{60}\text{B}_2\text{N}_2\text{O}_2$: C 79.18%, H 8.86%, N 4.10%; Found C 80.05%, H 8.99% N 4.91%.

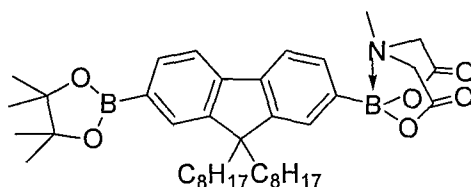
2-(7-Bromo-9,9'-dioctyl-9*H*-fluoren-2-yl)-6-methyl-1,3,6,2-dioxazaborocane-4,8-dione 5.36



A mixture of 7-bromo-9,9'-dioctyl-9*H*-fluoren-2-ylboronic acid **5.33** (1.0 g, 1.95 mmol), *N*-methyliminodiacetic acid (0.29 g, 2 mmol), in toluene (50 mL) and DMSO (5 mL) was heated for 24 h under reflux with azeotropic removal of H₂O. The reaction mixture was allowed to cool to room temperature and concentrated *in vacuo*. Column chromatography (Silica gel, EtOAc) allowed isolation of the product as a colourless oil (1.2 g, 100%).

¹H NMR (400 MHz, CDCl₃, ppm) δ: 7.68 (d, *J* = 7.5, 1H, Ar*H*), 7.56 (2, *J* = 9.0, 1H, Ar*H*), 7.50 (s, 1H, Ar*H*), 7.47 - 7.43 (m, 3H, Ar*H*), 3.98 (d, *J* = 16.4, 2H, NCH₂), 3.79 (d, *J* = 16.4, 2H, NCH₂), 2.52 (s, 3H, NCH₃), 2.00 - 1.87 (m, 4H, CH₂), 1.29 - 0.93 (m, 20H, CH₂), 0.81 (t, *J* = 7.1, 6H, CH₃), 0.62 - 0.41 (m, 4H, CH₂); ¹³C{¹H} NMR (125 MHz, CDCl₃, ppm) δ: 167.3, 153.1, 150.4, 142.0, 139.7, 130.8, 130.0, 126.5, 126.2, 121.6, 121.3, 119.8, 61.8, 60.4, 55.5, 47.3, 40.2, 31.8, 29.9, 29.3, 29.2, 23.8, 22.6, 14.2, 14.1; *m/z* (CI): 625 [M+H]⁺; Anal. Calcd. for C₃₄H₄₇BBrNO₄ : C 65.40%, H 7.59%, N 2.24%; Found C 65.24%, H 7.57% N 2.53%.

2-(9,9'-Dioctyl-7-(4,4',5,5'-tetramethyl-1,3,2-dioxaborolan-2-yl)-9*H*-fluoren-2-yl)-6-methyl-1,3,6,2-dioxazaborocane-4,8-dione 5.37

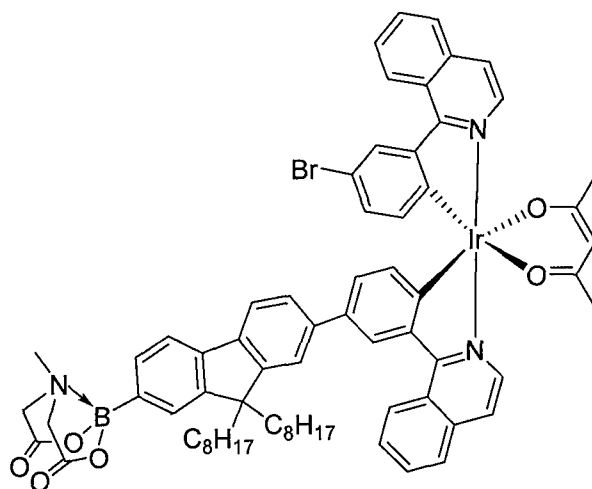


A solution of 2-(7-bromo-9,9'-dioctyl-9*H*-fluoren-2-yl)-6-methyl-1,3,6,2-dioxazaborocane-4,8-dione **5.36** (1.0 g, 1.6 mmol), PdCl₂(dppf) (68 mg, 0.08 mmol), KOAc (0.47 g, 4.8 mmol) and bis(pinacolato)diboron (0.65 g, 2.56 mmol) in DMF (10 mL) was heated to 80 °C for 24 h. The reaction mixture was allowed to cool to room temperature and Et₂O (50 mL) and H₂O (50 mL) were added. The layers were separated and the organic layer was washed with H₂O (4 x 50 mL) and brine (2 x 50 mL of a sat.

aqueous solution). The organic fraction was dried (MgSO_4), filtered, and concentrate *in vacuo*. Column chromatography (Silica gel; EtOAc) afforded the product as a white crystalline solid (0.74 g, 69%).

m.p. 84 - 87 °C; ^1H NMR (400 MHz, CDCl_3 , ppm) δ : 7.82 (d, 1H, $J = 7.2$ Hz, ArH), 7.74 (d, 2H, $J = 7.5$ Hz, ArH), 7.72 (d, 2H, $J = 8.0$ Hz, ArH), 7.51 (s, 1H, ArH), 7.46 (d, 2H, $J = 7.1$ Hz, ArH), 3.97 (d, 2H, $J = 16.3$ Hz, NCH_2), 3.80 (d, 2H, $J = 16.3$ Hz, NCH_2), 2.51 (s, 3H, NCH_3), 2.10 - 1.85 (m, 4H, CH_2), 1.39 (s, 12H, OCCH_3), 1.22 - 0.90 (m, 20H, CH_2), 0.80 (t, $J = 7.0$ Hz, 6H, CH_3), 0.60 - 0.35 (m, 4H, CH_2); $^{13}\text{C}\{^1\text{H}\}$ NMR (125 MHz, CDCl_3 , ppm) δ : 167.1, 151.3, 133.7, 130.5, 128.9, 126.5, 119.2, 83.7, 61.7, 60.4, 55.1, 47.2, 40.2, 31.7, 29.9, 29.3, 29.2, 24.9, 23.8, 22.6, 14.2, 14.1; m/z (CI): 673 $[\text{M}+\text{H}]^+$; Anal. Calcd. for $\text{C}_{40}\text{H}_{59}\text{B}_2\text{NO}_6$: C 71.54%, H 8.86%, N 2.09%; Found C 71.55%, H 8.88% N 2.02%.

[Ir(III)(1-(3-bromophenyl)isoquinoline-*N,C*)-(1-(3-(9,9'-dioctyl-7-(6-methyl-1,3,6,2-dioxaborocane-4,8-dione)-9H-fluoren-2-yl)phenyl)isoquinoline-*N,C*(acetylacetonate))] 5.38

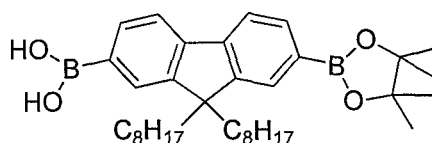


A solution of 2-(9,9'-dioctyl-7-(4,4',5,5'-tetramethyl-1,3,2-dioxaborolan-2-yl)-9H-fluoren-2-yl)-6-methyl-1,3,6,2-dioxaborocane-4,8-dione **5.37** (120 mg, 0.17 mmol), [Ir(III)bis(1-(3-bromophenyl)isoquinolinato-*N,C*)(acetylacetonate)] **2.37** (100 mg, 0.12 mmol), $\text{Pd}(\text{OAc})_2$ (1 mg, 0.004 mmol), PCy_3 (5 mg, 0.02 mmol) and K_3PO_4 (76 mg, 0.36 mmol) in toluene (10 mL) was heated to 90 °C. After 24 h, the reaction mixture was allowed to cool to room temperature and concentrated *in vacuo*. Preparative thin layer chromatography (silica, EtOAc) allowed isolation of a sample of the product. Crude ^1H NMR indicates the product is formed in approximately 5% yield.

^1H NMR (400 MHz, CDCl_3 , ppm) δ : 9.14 - 9.03 (m, 1H, ArH), 8.96 - 8.89 (m, 1H, ArH), 8.47 (m, 3H, ArH), 8.33 (s, 1H, ArH), 7.96 (m, 2H, ArH), 7.82 - 7.67 (m, 6H, ArH), 7.53 (m, 3H, ArH), 7.48 (s, 2H, ArH), 7.44 (d, $J = 7.1$ Hz, 1H, ArH), 7.00 (dd, $J = 7.7, 1.6$ Hz, 1H, ArH), 6.76 (dd, $J = 8.3, 1.9$ Hz, 1H, ArH), 6.44 (d, $J = 7.9$, 1H, ArH), 6.33 (d, $J = 8.2$, 1H, ArH), 5.23 (s, 1H, OC(CH₃)CH), 3.90 (d, $J = 16.4$, 2H, NCH₂), 3.77 (d, $J = 16.3$, 2H, NCH₂), 2.51 (s, 3H, NCH₃), 1.93 (m, 4H, CH₂), 1.78 (2 x s, 2 x 3H, 2x OC(CH₃)CH), 1.18 - 0.47 (m, 30H, CH₂ and CH₃).

Insufficient material was isolated to allow complete characterization.

9,9'-Dioctyl-7-(4,4',5,5'-tetramethyl-1,3,2-dioxaborolan-2-yl)-9H-fluoren-2-ylboronic acid 5.40

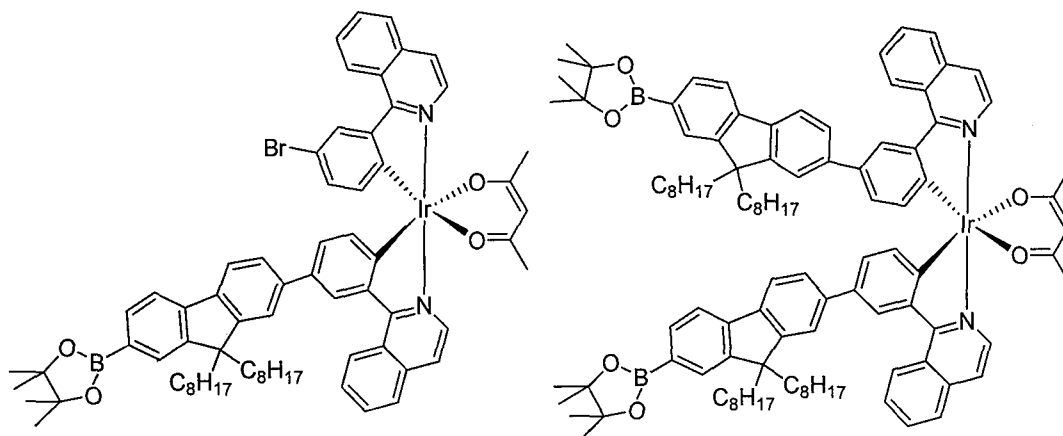


To a solution of 7-bromo-9,9'-dioctyl-9H-fluoren-2-ylboronic acid **3.17** (1 g, 1.7 mmol) in THF (20 mL) was added Li*o*-Pr (0.85 mL, 2 M in THF, 1.7 mmol) at room temperature. After 2 h the reaction the mixture was cooled to -78 °C and *t*-butyllithium (2.2 mL, 1.7 M in hexane, 3.75 mmol) was added dropwise, and the reaction was stirred for 30 min. At this point, 2-isopropoxy-4,4',5,5'-tetramethyl-1,3,2-dioxaborolane (0.4 mL, 2 mmol) was added rapidly. After a further 1 h, the reaction was allowed to warm to room temperature and stirred for 18 h. The reaction was quenched with aqueous NH_4Cl (20 mL of a sat. solution) and extracted with Et_2O (3 x 25 mL). The combined organic fractions were dried (MgSO_4), filtered, and concentrated *in vacuo*. Column chromatography (silica gel, Toluene \rightarrow EtOAc) enabled isolation of the product as a colourless oil (0.85 g, 89%).

^1H NMR (400 MHz, CDCl_3 , ppm) δ : 8.30 (d, $J = 7.5$, 0.25H, ArH), 8.22 (s, 0.25H, ArH), 7.91 (d, $J = 7.6$, 0.25H, ArH), 7.88 - 7.63 (m, 5.25H, ArH), 2.20 - 1.90 (m, 4H, CH₂), 1.43 - 1.34 (m, 12H, OCCH₃), 1.27 - 0.96 (m, 20H, CH₂), 0.85 - 0.49 (m, 10H, CH₂ and CH₃); $^{13}\text{C}\{^1\text{H}\}$ NMR (125 MHz, CDCl_3 , ppm) δ : 119.7, 119.4, 83.8, 58.9, 58.5, 55.1, 40.2, 31.8, 29.9, 29.2, 24.9, 23.7, 23.6, 22.6, 18.4, 17.2, 14.1.

[Ir(III)(1-(3-bromophenyl)isoquinoline-*N,C*)-(1-(3-(9,9'-dioctyl-7-(4,4',5,5'-tetramethyl-1,3,2-dioxaborolan-2-yl)-9*H*-fluoren-2-yl)phenyl)isoquinoline-*N,C*)(acetylacetonate)] 5.39

[Ir(III)bis(1-(3-(9,9'-dioctyl-7-(4,4',5,5'-tetramethyl-1,3,2-dioxaborolan-2-yl)-9*H*-fluoren-2-yl)phenyl)isoquinoline-*N,C*)(acetylacetonate)] 5.41



A solution of 9,9'-dioctyl-7-(4,4',5,5'-tetramethyl-1,3,2-dioxaborolan-2-yl)-9*H*-fluoren-2-ylboronic acid **5.40** (98 mg, 0.17 mmol), [Ir(III)bis(1-(3-bromophenyl)isoquinolinato-*N,C*)(acetylacetonate)] **2.37** (100 mg, 0.12 mmol), Pd(OAc)₂ (1 mg, 0.005 mmol), SPhos (4 mg, 0.01 mmol) and K₃PO₄ (76 mg, 0.36 mmol), in toluene (20 mL) was heated to 90 °C. After 6 h the reaction mixture was allowed to cool to room temperature and concentrated *in vacuo*. Column chromatography (Silica gel, DCM:hexane 1:1) allowed isolation of [Ir(III)(1-(3-bromophenyl)isoquinoline-*N,C*)-(1-(3-(9,9'-dioctyl-7-(4,4',5,5'-tetramethyl-1,3,2-dioxaborolan-2-yl)-9*H*-fluoren-2-yl)phenyl)isoquinoline-*N,C*)(acetylacetonate)] (31 mg, 21%) and [Ir(III)bis(1-(3-(9,9'-dioctyl-7-(4,4',5,5'-tetramethyl-1,3,2-dioxaborolan-2-yl)-9*H*-fluoren-2-yl)phenyl)isoquinoline-*N,C*)(acetylacetonate)] (30 mg, 15%) as red solids.

[Ir(III)(1-(3-bromophenyl)isoquinoline-*N,C*)-(1-(3-(9,9'-dioctyl-7-(4,4',5,5'-tetramethyl-1,3,2-dioxaborolan-2-yl)-9*H*-fluoren-2-yl)phenyl)isoquinoline-*N,C*)(acetylacetonate)] 5.39

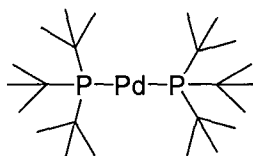
¹H NMR (400 MHz, CDCl₃, ppm) δ: 9.12 - 9.06 (m, 1H, Ar*H*), 8.96 - 8.89 (m, 1H, Ar*H*), 8.52 - 8.47 (m, 2H, Ar*H*), 8.45 (d, *J* = 6.4, 1H, Ar*H*), 8.33 (d, *J* = 1.8, 1H, Ar*H*),

8.00 - 7.93 (m, 2H, ArH), 7.82 - 7.65 (m, 8H, ArH), 7.56 - 7.49 (m, 3H, ArH), 7.47 (s, 1H, ArH), 7.00 (dd, $J = 1.6, 7.9$, 1H, ArH), 6.78 (dd, $J = 1.9, 8.2$, 1H, ArH), 6.44 (d, $J = 7.9$, 1H, ArH), 6.33 (d, $J = 8.2$, 1H, ArH), 5.23 (s, 1H, OC(CH₃)CH), 2.01 - 1.86 (m, 4H, CH₂), 1.78 (2 x s, 2 x 3H, 2 x OC(CH₃)CH), 1.38 (s, 12H, OCCH₃), 1.19 - 0.93 (m, 20H, CH₂), 0.75 (m, 6H, CH₃), 0.61 (m, 4H, CH₂); ¹³C{¹H} NMR (125 MHz, CDCl₃, ppm) δ : 185.0, 169.0, 167.5, 151.2, 151.0, 150.7, 150.6, 148.7, 147.1, 141.3, 141.0, 140.4, 139.4, 137.3, 137.2, 134.3, 133.8, 132.4, 131.7, 130.9, 128.6, 128.3, 128.1, 127.8, 127.4, 126.8, 126.7, 126.5, 126.4, 125.3, 122.8, 121.1, 120.6, 120.2, 119.8, 119.2, 114.0, 100.7, 84.3, 55.0, 40.4, 30.1, 29.3, 28.8, 23.8, 22.6, 21.2, 14.1; m/z (FAB) 1374 [M+H]⁺.

[Ir(III)bis(1-(3-(9,9'-dioctyl-7-(4,4',5,5'-tetramethyl-1,3,2-dioxaborolan-2-yl)-9H-fluoren-2-yl)phenyl)isoquinoline-*N,C*)(acetylacetonate)] **5.41**

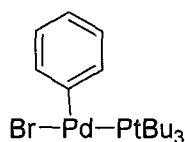
¹H NMR (400 MHz, CDCl₃, ppm) δ : 9.18 - 9.06 (m, 2H, ArH), 8.58 - 8.47 (m, 4H, ArH), 7.98 (d, $J = 5.2$, 2H, ArH), 7.84 - 7.65 (m, 14H, ArH), 7.52 (dd, $J = 10.2, 18.6$, 4H, ArH), 7.02 (d, $J = 8.0$, 2H, ArH), 6.54 (d, $J = 7.9$, 2H, ArH), 5.26 (s, 1H, OC(CH₃)CH), 2.03 - 1.85 (m, 8H, CH₂), 1.81 (s, 6H, OC(CH₃)CH), 1.38 (s, 24H, OCCH₃), 1.21 - 0.93 (m, 20H, CH₂), 0.79 - 0.70 (m, 12H, CH₃), 0.70 - 0.53 (m, 8H, CH₂).

Bis(tri-*tert*-butylphosphine)palladium(0)¹⁹⁷ 5.44



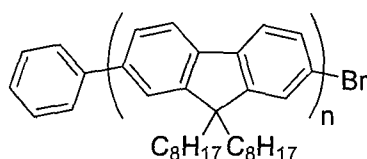
A solution of Pd₂(dba)₃ (0.46 g, 0.50 mmol) and P(*t*-Bu)₃ (0.42 g, 2.1 mmol), in DMF (10 mL) was stirred for 3 h at room temperature. The resulting precipitate was collected by filtration, washed with DMF (3 x 15 mL), and then dissolved in hexane (20 mL). The hexane solution was filtered and concentrated *in vacuo*, affording the product as white crystals (0.31 g, 60%).

¹H NMR (400 MHz, C₆D₆, ppm) δ : 1.52 (t, $J = 5.7$ Hz, 54H, CH₃); ³¹P{¹H} NMR (121 MHz, C₆D₆, ppm) δ : 85.2; The data is in agreement with the literature values.

${}^t\text{Bu}_3\text{PPd}(\text{Ph})\text{Br}^{197}$ 5.46

Bis(tri-*tert*-butylphosphine)palladium(0) **5.44** (293 mg, 0.574 mmol) and 2.8 mL of phenyl bromide (26 mmol) were heated at 70 °C for 3 h. After the reaction mixture had cooled to room temperature pentane (30 mL) was added forming an orange precipitate. Stirring was continued for a further 10 min. At this time, the precipitate was isolated by filtration and washed with pentane (5 x 10 mL) to afford the product as an orange solid (143 mg, 0.37 mmol, 64%).

${}^1\text{H}$ NMR (400 MHz, C_6D_6 , ppm) δ : 1.00 (d, $J = 12.8$ Hz, 27H, CH_3), 6.74 (t, $J = 7.2$ Hz, 1H, ArH), 6.82 (t, $J = 7.2$ Hz, 2H, ArH), 7.43 (m, 2H, ArH), ${}^{31}\text{P}\{{}^1\text{H}\}$ NMR (121 MHz, C_6D_6 , ppm) δ : 63.0; The data is in agreement with the literature values.

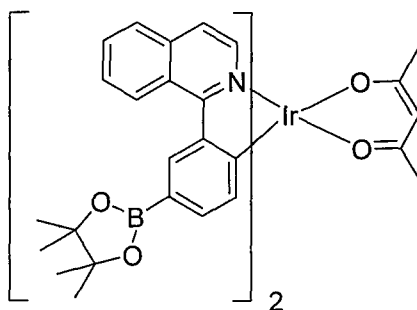
 α -Phenyl- ω -bromo(poly(9,9'-dioctyl-9*H*-fluorene-2,7-diyl))¹⁹⁷ (n = 15) 5.47

2-(7-Bromo-9,9'-dioctyl-9*H*-fluorene-2-yl)-4,4',5,5'-tetramethyl-1,3,2-dioxaborolane **3.17** (148 mg, 0.248 mmol), THF (8 mL) and aqueous Na_2CO_3 (5 mL of a 2M solution) were stirred vigorously at room temperature. The polymerization was initiated by adding a solution of $\text{PtBu}_3\text{Pd}(\text{Ph})\text{Br}$ **5.46** (7.4 mg, 0.016 mmol, 6.7 mol % based on fluorene monomer) in THF (2 mL). After 30 min, the organic phase was separated and poured into a mixture of aqueous HCl (5 mL of a 2M solution) and MeOH (40 mL) with stirring. The precipitate was collected by filtration, washed with H_2O (50 mL) and MeOH (50 mL) to afford the product as a yellow powder (92 mg, 94%).

${}^1\text{H}$ NMR (400 MHz, CDCl_3 , ppm) δ : 7.95 - 7.54 (m, 98H, ArH), 7.52 - 7.46 (m, 2H, PhH), 7.40 - 7.35 (m, 1H, PhH), 2.31 - 1.89 (m, 54H, CH_2), 1.35 - 0.61 (m, 581H, CH_2 and CH_3); ${}^{13}\text{C}\{{}^1\text{H}\}$ NMR (125 MHz, CDCl_3 , ppm) δ : 151.8, 140.5, 140.0, 128.8, 127.2, 126.1, 121.5, 120.0, 55.3, 40.4, 31.8, 30.0, 29.2, 23.9, 22.6, 14.1; GPC (PS): $M_n = 8878$, $M_w = 11124$, PDI = 1.25; m/z MALDI-TOF : 2415 (Ph- F_6 -H), 2496 (Ph- F_6 -Br), 2804 (Ph- F_6 -H), 2888 (Ph- F_6 -Br), 3192 (Ph- F_6 -H), 3272 (Ph- F_6 -Br), 3583 (Ph- F_6 -H), 3663

(Ph-F₆-Br), 3973 (Ph-F₆-H), 4052 (Ph-F₆-Br), 4362 (Ph-F₆-H), 4441 (Ph-F₆-Br), 4752 (Ph-F₆-H), 4831 (Ph-F₆-Br), 5141 (Ph-F₆-H), 5219 (Ph-F₆-Br), 5530 (Ph-F₆-H), 5610 (Ph-F₆-Br), 5920 (Ph-F₆-H), 6002 (Ph-F₆-Br), 6309 (Ph-F₆-H), 6390 (Ph-F₆-Br), 6698 (Ph-F₆-H), 6778 (Ph-F₆-Br), 7086 (Ph-F₆-H), 7166 (Ph-F₆-Br), 7474 (Ph-F₆-H), 7554 (Ph-F₆-Br); Anal. Calcd. for C₄₄₁H₆₀₅Br: C 88.48%, H 10.19%; Found C 88.32%, H 10.12%; The data is in agreement with the literature values.

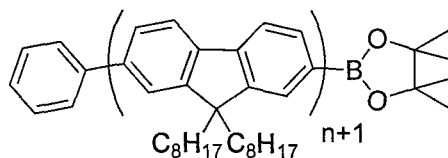
[Iridium(III)bis(1-(3-(4,4',5,5'-tetramethyl-1,3,2-dioxaborolan-2-yl)phenyl)isoquinolino-*N,C*)(acetylacetonate)] 5.48



A solution of [Ir(III)bis(1-(3-bromophenyl)isoquinolino-*N,C*)(acetylacetonate)] **2.37** (100 mg, 0.12 mmol), PdCl₂(CH₃CN)₂ (1 mg, 0.004 mmol), SPhos (8 mg, 0.02 mmol), Et₃N (0.1 mL, 0.72 mmol) and pinacol borane (0.05 mL, 0.36 mmol) in 1,4 Dioxane (10 mL) was heated to 110 °C for 24 h. The reaction mixture was allowed to cool to room temperature and concentrate *in vacuo*. Column chromatography (Silica gel; hexane:DCM; 1:1) afforded the product as a red solid (103 mg, 93%).

¹H NMR (400 MHz, CDCl₃, ppm) δ: 9.08 (d, *J* = 8.5, 2H, ArH), 8.63 (d, *J* = 6.6, 2H, ArH), 8.43 (d, *J* = 6.4, 2H, ArH), 7.92 (d, *J* = 7.8, 2H, ArH), 7.81 - 7.68 (m, 4H, ArH), 7.47 (d, *J* = 6.4, 2H, ArH), 7.04 (d, *J* = 7.7, 2H, ArH), 6.44 (d, *J* = 7.6, 2H, ArH), 5.17 (s, 1H, OC(CH₃)CH), 1.73 (s, 6H, OC(CH₃)CH), 1.27 (s, 24H, OCCH₃); ¹³C{¹H} NMR (125 MHz, CDCl₃, ppm) δ: 149.8, 148.5, 140.3, 137.2, 134.1, 132.0, 131.7, 131.0, 128.1, 127.4, 120.8, 114.1, 84.2, 21.2; *m/z* (FAB): 952 [M+H]⁺; Anal. Calcd. for C₄₇H₄₉B₂IrN₂O₆: C 59.31%, H 5.19%, N 2.94%; Found C 59.53%, H 5.26%, N 3.02%.

α -Phenyl- ω -(4,4',5,5'-tetramethyl-1,3,2-dioxaborolan-2-yl)(poly(9,9'-dioctyl-9H-fluorene-2,7-diyl)) (n = 15) 5.49



Aqueous Et_4NOH (5 mL of a 20% solution) was added to a stirred solution of α -Phenyl- ω -bromo(poly(9,9'-dioctyl-9H-fluorene-2,7-diyl)) **5.47** (80 mg, 0.013 mmol), 9,9'-dioctyl-2,7-bis(4,4',5,5'-tetramethyl-1,3,2-dioxaborolan-2-yl)-9H-fluorene **3.33** (167 mg, 0.26 mmol), $\text{Pd}(\text{OAc})_2$ (2 mg, 0.009 mmol) and PPh_3 (10 mg, 0.004 mmol) in toluene (10 mL) at room temperature. The mixture was stirred vigorously for 18 h at 90 °C. The mixture was cooled to RT and added to stirring methanol (100 mL). The resultant precipitate was isolated, washed with MeOH (100 mL), dissolved in a minimum amount of toluene and added dropwise to stirring MeOH (100 mL). The precipitate was isolated, washed with methanol (100 mL) and dried under vacuum (81 mg, 98%).

^1H NMR (400 MHz, CDCl_3 , ppm) δ : 7.95 - 7.56 (m, 107H, ArH), 7.52 - 7.46 (m, 2H, PhH), 7.40 - 7.34 (m, 1H, PhH), 2.34 - 1.81 (m, 68H, CH_2), 1.41 (s, 12H, OCCH_3), 1.33 - 0.53 (m, 600H, CH_2 and CH_3); $^{13}\text{C}\{^1\text{H}\}$ NMR (125 MHz, CDCl_3 , ppm) δ : 151.8, 140.5, 140.0, 128.8, 127.2, 126.1, 121.5, 120.0, 83.8, 55.3, 40.4, 31.8, 30.0, 29.2, 23.9, 22.6, 21.4, 14.1; GPC (PS): $M_n = 10725$, $M_w = 13077$, PDI = 1.22; m/z MALDI-TOF : 3581 (Ph-F₉-H), 3709 (Ph-F₉-B), 3972 (Ph-F₁₀-H), 4098 (Ph-F₁₀-B), 4361 (Ph-F₁₁-H), 4486 (Ph-F₁₁-B), 4765 (Ph-F₁₂-H), 4875 (Ph-F₁₂-B), 5157 (Ph-F₁₃-H), 5266 (Ph-F₁₃-B), 5545 (Ph-F₁₄-H), 5656 (Ph-F₁₄-B), 5933 (Ph-F₁₅-H), 6045 (Ph-F₁₅-B), 6324 (Ph-F₁₆-H), 6433 (Ph-F₁₆-B), 6712 (Ph-F₁₇-H), 6825 (Ph-F₁₇-B), 7102 (Ph-F₁₈-H), 7214 (Ph-F₁₈-B), 7492 (Ph-F₁₉-H), 7603 (Ph-F₁₉-B), 7991 (Ph-F₂₀-H), 8382 (Ph-F₂₁-B), 8770 (Ph-F₂₂-H), 9170 (Ph-F₂₃-B); Anal. Calcd. for $\text{C}_{476}\text{H}_{657}\text{BO}_2$: C 89.02%, H 10.31%; Found C 88.89%, H 10.21%.

Chapter 7: References

- (1) Tang, C. W.; Vanslyke, S. A. *Appl. Phys. Lett.* **1987**, *51*, 913.
- (2) Burroughes, J. H.; Bradley, D. D. C.; Brown, A. R.; Marks, R. N.; Mackay, K.; Friend, R. H.; Burns, P. L.; Holmes, A. B. *Nature* **1990**, *347*, 539.
- (3) Hung, L. S.; Chen, C. H. *Mat. Sci. Eng.* **2002**, *39*, 143.
- (4) van Dijken, A.; Perro, A.; Meulenkamp, E. A.; Brunner, K. *Org. Electron.* **2003**, *4*, 131.
- (5) Santerre, F.; Bedja, I.; Dodelet, J. P.; Sun, Y.; Lu, J.; Hay, A. S.; D'Iorio, M. *Chem. Mater.* **2001**, *13*, 1739.
- (6) Kulkarni, A. P.; Tonzola, C. J.; Babel, A.; Jenekhe, S. A. *Chem. Mater.* **2004**, *16*, 4556.
- (7) Adachi, C.; Baldo, M. A.; Thompson, M. E.; Forrest, S. R. *J. Appl. Phys.* **2001**, *90*, 5048.
- (8) Segal, M.; Baldo, M. A.; Holmes, R. J.; Forrest, S. R.; Soos, Z. G. *Phys. Rev. B: Condens. Matter* **2003**, *68*, 075211
- (9) Yersin, H. *Transition Metal and Rare Earth Compounds III* **2004**; Vol. 241.
- (10) Greenham, N. C.; Friend, R. H.; Bradley, D. D. C. *Adv. Mater.* **1994**, *6*, 491.
- (11) Ho, P. K. H.; Kim, J. S.; Burroughes, J. H.; Becker, H.; Li, S. F. Y.; Brown, T. M.; Cacialli, F.; Friend, R. H. *Nature* **2000**, *404*, 481.
- (12) Cao, Y.; Parker, I. D.; Yu, G.; Zhang, C.; Heeger, A. J. *Nature* **1999**, *397*, 414.
- (13) Baldo, M. A.; Thompson, M. E.; Forrest, S. R. *Pure Appl. Chem.* **1999**, *71*, 2095.
- (14) Chou, P. T.; Chi, Y. *Eur. J. Inorg. Chem.* **2006**, 3319.
- (15) Evans, R. C.; Douglas, P.; Winscom, C. J. *Coordin. Chem. Rev.* **2006**, *250*, 2093.
- (16) Holder, E.; Langeveld, B. M. W.; Schubert, U. S. *Adv. Mater.* **2005**, *17*, 1109.
- (17) Baldo, M. A.; O'Brien, D. F.; You, Y.; Shoustikov, A.; Sibley, S.; Thompson, M. E.; Forrest, S. R. *Nature* **1998**, *395*, 151.
- (18) Baldo, M. A.; Lamansky, S.; Burrows, P. E.; Thompson, M. E.; Forrest, S. R. *Appl. Phys. Lett.* **1999**, *75*, 4.
- (19) Lamansky, S.; Djurovich, P.; Murphy, D.; Abdel-Razzaq, F.; Kwong, R.; Tsyba, I.; Bortz, M.; Mui, B.; Bau, R.; Thompson, M. E. *Inorg. Chem.* **2001**, *40*, 1704.
- (20) Lamansky, S.; Djurovich, P.; Murphy, D.; Abdel-Razzaq, F.; Lee, H. E.; Adachi, C.; Burrows, P. E.; Forrest, S. R.; Thompson, M. E. *J. Am. Chem. Soc.* **2001**, *123*, 4304.

-
- (21) Adachi, C.; Baldo, M. A.; Forrest, S. R.; Thompson, M. E. *Appl. Phys. Lett.* **2000**, *77*, 904.
- (22) Kawamura, Y.; Goushi, K.; Brooks, J.; Brown, J. J.; Sasabe, H.; Adachi, C. *Appl. Phys. Lett.* **2005**, *86*, 071104.
- (23) Gong, X.; Ostrowski, J. C.; Bazan, G. C.; Moses, D.; Heeger, A. J.; Liu, M. S.; Jen, A. K. Y. *Adv. Mater.* **2003**, *15*, 45.
- (24) Balzani, V.; Bergamini, G.; Campagna, S.; Puntoriero, F. *Photochemistry and Photophysics of Coordination Compounds I* **2007**; Vol. 280.
- (25) Gong, X.; Ostrowski, J. C.; Moses, D.; Bazan, G. C.; Heeger, A. J. *Adv. Funct. Mat* **2003**, *13*, 439.
- (26) Holmes, R. J.; D'Andrade, B. W.; Forrest, S. R.; Ren, X.; Li, J.; Thompson, M. E. *Appl. Phys. Lett.* **2003**, *83*, 3818.
- (27) Su, Y. J.; Huang, H. L.; Li, C. L.; Chien, C. H.; Tao, Y. T.; Chou, P. T.; Datta, S.; Liu, R. S. *Adv. Mater.* **2003**, *15*, 884.
- (28) De Angelis, F.; Fantacci, S.; Evans, N.; Klein, C.; Zakeeruddin, S. M.; Moser, J. E.; Kalyanasundaram, K.; Bolink, H. J.; Gratzel, M.; Nazeeruddin, M. K. *Inorg. Chem.* **2007**, *46*, 5989.
- (29) Hwang, F. M.; Chen, H. Y.; Chen, P. S.; Liu, C. S.; Chi, Y.; Shu, C. F.; Wu, F. L.; Chou, P. T.; Peng, S. M.; Lee, G. H. *Inorg. Chem.* **2005**, *44*, 1344.
- (30) Kwon, T. H.; Cho, H. S.; Kim, M. K.; Kim, J. W.; Kim, J. J.; Lee, K. H.; Park, S. J.; Shin, I. S.; Kim, H.; Shin, D. M.; Chung, Y. K.; Hong, J. I. *Organometallics* **2005**, *24*, 1578.
- (31) You, Y. M.; Park, S. Y. *J. Am. Chem. Soc.* **2005**, *127*, 12438.
- (32) Jansson, E.; Minaev, B.; Schrader, S.; Agren, H. *Chem. Phys.* **2007**, *333*, 157.
- (33) Avilov, I.; Minoofar, P.; Cornil, J.; De Cola, L. *J. Am. Chem. Soc.* **2007**, *129*, 8247.
- (34) Noh, Y. Y.; Lee, C. L.; Kim, J. J.; Yase, K. *J. Chem. Phys.* **2003**, *118*, 2853.
- (35) Ostrowski, J. C.; Robinson, M. R.; Heeger, A. J.; Bazan, G. C. *Chem. Commun.* **2002**, 784.
- (36) Ding, J. Q.; Lu, J. H.; Cheng, Y. X.; Xie, Z. Y.; Wang, L. X.; Jing, X. B.; Wang, F. S. *Adv. Funct. Mat* **2008**, *18*, 2754.
- (37) Burn, P. L.; Lo, S. C.; Samuel, I. D. W. *Adv. Mater.* **2007**, *19*, 1675.
- (38) Evans, N. R.; Devi, L. S.; Mak, C. S. K.; Watkins, S. E.; Pascu, S. I.; Kohler, A.; Friend, R. H.; Williams, C. K.; Holmes, A. B. *J. Am. Chem. Soc.* **2006**, *128*, 6647.
-

-
- (39) Sandee, A. J.; Williams, C. K.; Evans, N. R.; Davies, J. E.; Boothby, C. E.; Kohler, A.; Friend, R. H.; Holmes, A. B. *J. Am. Chem. Soc.* **2004**, *126*, 7041.
- (40) Lo, S. C.; Anthopoulos, T. D.; Namdas, E. B.; Burn, P. L.; Samuel, I. D. W. *Adv. Mater.* **2005**, *17*, 1945.
- (41) Chien, C. H.; Liao, S. F.; Wu, C. H.; Shu, C. F.; Chang, S. Y.; Chi, Y.; Chou, P. T.; Lai, C. H. *Adv. Funct. Mat* **2008**, *18*, 1430.
- (42) Wilson, J. S.; Chawdhury, N.; Al-Mandhary, M. R. A.; Younus, M.; Khan, M. S.; Raithby, P. R.; Kohler, A.; Friend, R. H. *J. Am. Chem. Soc.* **2001**, *123*, 9412.
- (43) Tsuboyama, A.; Iwawaki, H.; Furugori, M.; Mukaide, T.; Kamatani, J.; Igawa, S.; Moriyama, T.; Miura, S.; Takiguchi, T.; Okada, S.; Hoshino, M.; Ueno, K. *J. Am. Chem. Soc.* **2003**, *125*, 12971.
- (44) Duan, J. P.; Sun, P. P.; Cheng, C. H. *Adv. Mater.* **2003**, *15*, 224.
- (45) Wu, F. I.; Su, H. J.; Shu, C. F.; Luo, L. Y.; Diau, W. G.; Cheng, C. H.; Duan, J. P.; Lee, G. H. *J. Mater. Chem.* **2005**, *15*, 1035.
- (46) Ho, C. L.; Wong, W. Y.; Gao, Z. Q.; Chen, C. H.; Cheah, K. W.; Yao, B.; Xie, Z. Y.; Wang, Q.; Ma, D. G.; Wang, L. A.; Yu, X. M.; Kwok, H. S.; Lin, Z. Y. *Adv. Funct. Mat* **2008**, *18*, 319.
- (47) Liang, B.; Jiang, C. Y.; Chen, Z.; Zhang, X. J.; Shi, H. H.; Cao, Y. *J. Mater. Chem.* **2006**, *16*, 1281.
- (48) Rho, H. H.; Park, Y. H.; Lee, Y. H.; Park, N. G.; Ha, Y.; Kim, Y. S. *Mol. Cryst. Liq. Cryst.* **2006**, *444*, 145.
- (49) Li, C. L.; Su, Y. J.; Tao, Y. T.; Chou, P. T.; Chien, C. H.; Cheng, C. C.; Liu, R. S. *Adv. Funct. Mat* **2005**, *15*, 387.
- (50) Fang, K. H.; Wu, L. L.; Huang, Y. T.; Yang, C. H.; Sun, I. W. *Inorg. Chim. Acta* **2006**, *359*, 441.
- (51) Huang, Y. T.; Chuang, T. H.; Shu, Y. L.; Kuo, Y. C.; Wu, P. L.; Yang, C. H.; Sun, I. W. *Organometallics* **2005**, *24*, 6230.
- (52) Okada, S.; Okinaka, K.; Iwawaki, H.; Furugori, M.; Hashimoto, M.; Mukaide, T.; Kamatani, J.; Igawa, S.; Tsuboyama, A.; Takiguchi, T.; Ueno, K. *Dalton Trans.* **2005**, 1583.
- (53) Zhao, Q.; Liu, S. J.; Shi, M.; Wang, C. M.; Yu, M. X.; Li, L.; Li, F. Y.; Yi, T.; Huang, C. H. *Inorg. Chem.* **2006**, *45*, 6152.
- (54) Liang, B.; Wang, L.; Xu, Y.; Shi, H.; Cao, Y. *Adv. Funct. Mat* **2007**, *17*, 3580.
- (55) Hu, Z. Y.; Luo, C. P.; Wang, L.; Huang, F. L.; Zhu, K. L.; Wang, Y. F.; Zhu, M. X.; Zhu, W. G.; Cao, Y. *Chem. Phys. Lett.* **2007**, *441*, 277.
-

-
- (56) Du, B.; Wang, L.; Wu, H. B.; Yang, W.; Zhang, Y.; Liu, R. S.; Sun, M. L.; Peng, J. B.; Cao, Y. *Chem. Eur. J.* **2007**, *13*, 7432.
- (57) Liu, S. J.; Zhao, Q.; Chen, R. F.; Deng, Y.; Fan, Q. L.; Li, F. Y.; Wang, L. H.; Huang, C. H.; Huang, W. *Chem. Eur. J.* **2006**, *12*, 4351.
- (58) Zhen, H. Y.; Jiang, C. Y.; Yang, W.; Jiang, J. X.; Huang, F.; Cao, Y. *Chem. Eur. J.* **2005**, *11*, 5007.
- (59) Zhang, K.; Chen, Z.; Yang, C. L.; Gong, S. L.; Qin, J. G.; Cao, Y. *Macromol. Rapid Comm.* **2006**, *27*, 1926.
- (60) Zhang, K.; Chen, Z.; Zou, Y.; Yang, C. L.; Qin, J. G.; Cao, Y. *Organometallics* **2007**, *26*, 3699.
- (61) Deng, Y.; Liu, S. J.; Fan, Q. L.; Fang, C.; Zhu, R.; Pu, K. Y.; Yuwen, L. H.; Wang, L. H.; Huang, W. *Synth. Met.* **2007**, *157*, 813.
- (62) Zhen, H. Y.; Luo, C.; Yang, W.; Song, W. Y.; Du, B.; Jiang, J. X.; Jiang, C. Y.; Zhang, Y.; Cao, Y. *Macromolecules* **2006**, *39*, 1693.
- (63) Cortright, S. B.; Johnston, J. N. *Angew. Chem. Int. Edit.* **2002**, *41*, 345.
- (64) Ramage, J. K. G. R. *J. Chem. Soc.* **1954**, 936
- (65) Funabashi, K.; Ratni, H.; Kanai, M.; Shibasaki, M. *J. Am. Chem. Soc.* **2001**, *123*, 10784.
- (66) Yang, C. H.; Su, W. L.; Fang, K. H.; Wang, S. P.; Sun, I. W. *Organometallics* **2006**, *25*, 4514.
- (67) Chen, X. W.; Liao, J. L.; Liang, Y. M.; Ahmed, M. O.; Tseng, H. E.; Chen, S. A. *J. Am. Chem. Soc.* **2003**, *125*, 636.
- (68) Jiang, J. X.; Jiang, C. Y.; Yang, W.; Zhen, H. G.; Huang, F.; Cao, Y. *Macromolecules* **2005**, *38*, 4072.
- (69) Hayer, A.; Khan, A. L. T.; Friend, R. H.; Kohler, A. *Phys. Rev. B: Condens. Matter* **2005**, *71*, 241302.
- (70) Blondin, P.; Bouchard, J.; Beaupre, S.; Belletete, M.; Durocher, G.; Leclerc, M. *Macromolecules* **2000**, *33*, 5874.
- (71) Ranger, M.; Leclere, M. *Can. J. Chem.* **1998**, *76*, 1571.
- (72) D'Andrade, B. W.; Datta, S.; Forrest, S. R.; Djurovich, P.; Polikarpov, E.; Thompson, M. E. *Org. Electron.* **2005**, *6*, 11.
- (73) Di Censo, D.; Fantacci, S.; De Angelis, F.; Klein, C.; Evans, N.; Kalyanasundaram, K.; Bolink, H. J.; Gratzel, M.; Nazeeruddin, M. K. *Inorg. Chem.* **2008**, *47*, 980.
-

-
- (74) Ho, C. L.; Wong, W. Y.; Wang, Q.; Ma, D. G.; Wang, L. X.; Lin, Z. Y. *Adv. Funct. Mat* **2008**, *18*, 928.
- (75) Yang, L.; Okuda, F.; Kobayashi, K.; Nozaki, K.; Tanabe, Y.; Ishii, Y.; Haga, M. A. *Inorg. Chem.* **2008**, *47*, 7154.
- (76) Byun, Y.; Jeon, W. S.; Lee, T. W.; Lyu, Y. Y.; Chang, S.; Kwon, O.; Han, E.; Kim, H.; Kim, M.; Lee, H. J.; Das, R. R. *Dalton Trans.* **2008**, 4732.
- (77) Nie, D. B.; Liu, Z. W.; Bian, Z. Q.; Huang, C. H. *J. Mol. Struct.* **2008**, *861*, 97.
- (78) Bronstein, H. A.; Finlayson, C. E.; Kirov, K. R.; Friend, R. H.; Williams, C. K. *Organometallics* **2008**, *27*, 2980.
- (79) Baranoff, E.; Suarez, S.; Bugnon, P.; Barolo, C.; Buscaino, R.; Scopelliti, R.; Zuppiroli, L.; Graetzel, M.; Nazeeruddin, M. K. *Inorg. Chem.* **2008**, *47*, 6575.
- (80) Tao, Y. T.; Wang, Q.; Yang, C. L.; Zhang, K.; Wang, Q.; Zou, T. T.; Qin, J. G.; Ma, D. G. *J. Mater. Chem.* **2008**, *18*, 4091.
- (81) Tsuzuki, T.; Tokito, S. *Appl. Phys. Express* **2008**, *1*, 021805.
- (82) Zhou, G. J.; Wong, W. Y.; Yao, B.; Xie, Z.; Wang, L. *J. Mater. Chem.* **2008**, *18*, 1799.
- (83) Tokito, S.; Suzuki, M.; Sato, F.; Kamachi, M.; Shirane, K. *Org. Electron.* **2003**, *4*, 105.
- (84) Haldi, A.; Kimyonok, A.; Domercq, B.; Hayden, L. E.; Jones, S. C.; Marder, S. R.; Weck, M.; Kippelen, B. *Adv. Funct. Mat* **2008**, *18*, 3056.
- (85) Zhang, Y.; Xiong, Y.; Li, C.; Peng, J. B.; Cao, Y. *Chem. Lett.* **2008**, *37*, 742.
- (86) Zhen, H. Y.; Luo, J.; Yang, W.; Chen, Q. L.; Ying, L.; Zou, J. H.; Wu, H. B.; Cao, Y. *J. Mater. Chem.* **2007**, *17*, 2824.
- (87) Schulz, G. L.; Chen, X. W.; Chen, S. A.; Holdcroft, S. *Macromolecules* **2006**, *39*, 9157.
- (88) Blouin, N.; Leclerc, M. *Accounts Chem. Res.* **2008**, *41*, 1110.
- (89) Morin, J. F.; Leclerc, M.; Ades, D.; Siove, A. *Macromol. Rapid Comm.* **2005**, *26*, 761.
- (90) Brunner, K.; van Dijken, A.; Borner, H.; Bastiaansen, J.; Kiggen, N. M. M.; Langeveld, B. M. W. *J. Am. Chem. Soc.* **2004**, *126*, 6035.
- (91) Bernius, M. T.; Inbasekaran, M.; O'Brien, J.; Wu, W. S. *Adv. Mater.* **2000**, *12*, 1737.
- (92) Zhang, X. J.; Tian, H. K.; Liu, Q.; Wang, L. X.; Geng, Y. H.; Wang, F. S. *J. Org. Chem.* **2006**, *71*, 4332.
- (93) Suzuki, A. *J. Organomet. Chem.* **1999**, *576*, 147.
-

-
- (94) Tour, J. M. *Chem. Rev.* **1996**, *96*, 537.
- (95) Kappaun, S.; Zelzer, M.; Bartl, K.; Saf, R.; Stelzer, F.; Slugovc, C. *J. Polym. Sci., Part A: Polym. Chem.* **2006**, *44*, 2130.
- (96) Yang, R. Q.; Tian, R. Y.; Yan, J. G.; Zhang, Y.; Yang, J.; Hou, Q.; Yang, W.; Zhang, C.; Cao, Y. *Macromolecules* **2005**, *38*, 244.
- (97) Shulla, I. A. B. T. A. *Chemistry of Heterocyclic Compounds* **1989**, *25*, 1303.
- (98) Yan, H.; Lee, P.; Armstrong, N. R.; Graham, A.; Evmenenko, G. A.; Dutta, P.; Marks, T. J. *J. Am. Chem. Soc.* **2005**, *127*, 3172.
- (99) Akasaka, K.; Suzuki, T.; Ohrui, H.; Meguro, H.; Shindo, Y.; Takahashi, H. *Anal. Lett.* **1987**, *20*, 1581.
- (100) Kappaun, S.; Scheiber, H.; Trattnig, R.; Zojer, E.; List, E. J. W.; Slugovc, C. *Chem. Commun.* **2008**, 5170.
- (101) Murage, J.; Eddy, J. W.; Zimbalist, J. R.; McIntyre, T. B.; Wagner, Z. R.; Goodson, F. E. *Macromolecules* **2008**, *41*, 7330.
- (102) Grell, M.; Bradley, D. D. C.; Long, X.; Chamberlain, T.; Inbasekaran, M.; Woo, E. P.; Soliman, M. *Acta Polym.* **1998**, *49*, 439.
- (103) Gupta, D.; Singh, S.; Katiyar, M.; Deepak; Hazra, T.; Verma, A.; Manoharan, S. *S. Mater. Manuf. Process.* **2006**, *21*, 285.
- (104) Micaroni, L.; Nart, F. C.; Hummelgen, I. A. *J. Solid State Electrochem.* **2002**, *7*, 55.
- (105) Zade, S. S.; Bendikov, M. *Chem. Eur. J.* **2007**, *13*, 3688.
- (106) Thomas, C. A.; Zong, K. W.; Abboud, K. A.; Steel, P. J.; Reynolds, J. R. *J. Am. Chem. Soc.* **2004**, *126*, 16440.
- (107) Mondal, R.; Wex, B.; Shah, B. K.; Kaafarani, B. R.; Danilov, E. O.; Jabbour, G. E.; Neckers, D. C. *Org. Electron.* **2008**, *9*, 227.
- (108) Huang, W. S.; Lin, J. T.; Lin, H. C. *Org. Electron.* **2008**, *9*, 557.
- (109) Westenhoff, S.; Howard, I. A.; Hodgkiss, J. M.; Kirov, K. R.; Bronstein, H. A.; Williams, C. K.; Greenham, N. C.; Friend, R. H. *J. Am. Chem. Soc.* **2008**, *130*, 13653.
- (110) Monkman, A. P.; Burrows, H. D.; Hartwell, L. J.; Horsburgh, L. E.; Hamblett, I.; Navaratnam, S. *Phys. Rev. Lett.* **2001**, *86*, 1358.
- (111) Sudhakar, M.; Djurovich, P. I.; Hogen-Esch, T. E.; Thompson, M. E. *J. Am. Chem. Soc.* **2003**, *125*, 7796.
- (112) Cook, S.; Ohkita, H.; Durrant, J. R.; Kim, Y.; Benson-Smith, J. J.; Nelson, J.; Bradley, D. D. C. *Appl. Phys. Lett.* **2006**, *89*, 101128.
-

-
- (113) Ribierre, J. C.; Ruseckas, A.; Knights, K.; Staton, S. V.; Cumpstey, N.; Burn, P. L.; Samuel, I. D. W. *Phys Rev Lett* **2008**, *100*, 017402.
- (114) Gong, X.; Robinson, M. R.; Ostrowski, J. C.; Moses, D.; Bazan, G. C.; Heeger, A. J. *Adv. Mater.* **2002**, *14*, 581.
- (115) Gong, X.; Lim, S. H.; Ostrowski, J. C.; Moses, D.; Bardeen, C. J.; Bazan, G. C. *J. Appl. Phys.* **2004**, *95*, 948.
- (116) Jiang, C. Y.; Yang, W.; Peng, J. B.; Xiao, S.; Cao, Y. *Adv. Mater.* **2004**, *16*, 537.
- (117) Reineke, S.; Walzer, K.; Leo, K. *Phys. Rev. B: Condens. Matter* **2007**, *75*, 125328.
- (118) Chen, F. C.; Yang, Y.; Thompson, M. E.; Kido, J. *Appl. Phys. Lett.* **2002**, *80*, 2308.
- (119) Kalinowski, J.; Stampor, W.; Mezyk, J.; Cocchi, M.; Virgili, D.; Fattori, V.; Di Marco, P. *Phys. Rev. B: Condens. Matter* **2002**, *66*, 235321.
- (120) Ribierre, J. C.; Ruseckas, A.; Samuel, I. D. W.; Staton, S. V.; Burn, P. L. *Phys. Rev. B: Condens. Matter* **2008**, *77*, 085211.
- (121) Fishchuk, II; Kadashchuk, A.; Devi, L. S.; Heremans, P.; Bassler, H.; Kohler, A. *Phys. Rev. B: Condens. Matter* **2008**, *78*, 045211.
- (122) Kalinowski, J.; Stampor, W.; Szmytkowski, J.; Virgili, D.; Cocchi, M.; Fattori, V.; Sabatini, C. *Phys. Rev. B: Condens. Matter* **2006**, *74*, 085316.
- (123) Baldo, M. A.; Adachi, C.; Forrest, S. R. *Phys. Rev. B: Condens. Matter* **2000**, *62*, 10967.
- (124) Bera, R. N.; Cumpstey, N.; Burn, P. L.; Samuel, I. D. W. *Adv. Funct. Mat* **2007**, *17*, 1149.
- (125) Kwon, T. H.; Kim, M. K.; Kwon, J.; Shin, D. Y.; Park, S. J.; Lee, C. L.; Kim, J. J.; Hong, J. I. *Chem. Mater.* **2007**, *19*, 3673.
- (126) Pu, Y. J.; Harding, R. E.; Stevenson, S. G.; Namdas, E. B.; Tedeschi, C.; Markham, J. P. J.; Rummings, R. J.; Burn, P. L.; Samuel, I. D. W. *J. Mater. Chem.* **2007**, *17*, 4255.
- (127) Ding, J. Q.; Gao, J.; Cheng, Y. X.; Xie, Z. Y.; Wang, L. X.; Ma, D. G.; Jing, X. B.; Wang, F. S. *Adv. Funct. Mat* **2006**, *16*, 575.
- (128) Lo, S. C.; Namdas, E. B.; Shipley, C. P.; Markham, J. P. J.; Anthopolous, T. D.; Burn, P. L.; Samuel, I. D. W. *Org. Electron.* **2006**, *7*, 85.
- (129) Cumpstey, N.; Bera, R. N.; Burn, P. L.; Samuel, I. D. W. *Macromolecules* **2005**, *38*, 9564.

-
- (130) Anthopoulos, T. D.; Frampton, M. J.; Namdas, E. B.; Burn, P. L.; Samuel, I. D. W. *Adv. Mater.* **2004**, *16*, 557.
- (131) Frampton, M. J.; Namdas, E. B.; Lo, S. C.; Burn, P. L.; Samuel, I. D. W. *J. Mater. Chem.* **2004**, *14*, 2881.
- (132) Anthopoulos, T. D.; Markham, J. P. J.; Namdas, E. B.; Lawrence, J. R.; Samuel, I. D. W.; Lo, S. C.; Burn, P. L. *Org. Electron.* **2003**, *4*, 71.
- (133) Anthopoulos, T. D.; Markham, J. P. J.; Namdas, E. B.; Samuel, I. D. W.; Lo, S. C.; Burn, P. L. *Appl. Phys. Lett.* **2003**, *82*, 4824.
- (134) Lo, S. C.; Namdas, E. B.; Burn, P. L.; Samuel, I. D. W. *Macromolecules* **2003**, *36*, 9721.
- (135) Lo, S. C.; Male, N. A. H.; Markham, J. P. J.; Magennis, S. W.; Burn, P. L.; Salata, O. V.; Samuel, I. D. W. *Adv. Mater.* **2002**, *14*, 975.
- (136) Liu, S. J.; Zhao, Q.; Deng, Y.; Xia, Y. J.; Lin, J.; Fan, Q. L.; Wang, L. H.; Huang, W. *J. Phys. Chem. C* **2007**, *111*, 1166.
- (137) Cowie, J. M. G. *Polymers: Chemistry and Physics of Modern Materials*; Stanley Thornes: Cheltenham, UK, **1998**; 2nd ed.
- (138) Langecker, J.; Rehahn, M. *Macromol. Chem. Physic.* **2008**, *209*, 258.
- (139) Wang, X. Y.; Prabhu, R. N.; Schmehl, R. H.; Weck, M. *Macromolecules* **2006**, *39*, 3140.
- (140) Liu, F.; Lai, W. Y.; Tang, C.; Wu, H. B.; Chen, Q. Q.; Peng, B.; Wei, W.; Huang, W.; Cao, Y. *Macromol. Rapid Comm.* **2008**, *29*, 659.
- (141) Chi, C. Y.; Wegner, G. *Macromol. Rapid Comm.* **2005**, *26*, 1532.
- (142) Chi, C. Y.; Im, C.; Enkelmann, V.; Ziegler, A.; Lieser, G.; Wegner, G. *Chem. Eur. J.* **2005**, *11*, 6833.
- (143) Jo, J. H.; Chi, C. Y.; Hoger, S.; Wegner, G.; Yoon, D. Y. *Chem. Eur. J.* **2004**, *10*, 2681.
- (144) Kanibolotsky, A. L.; Berridge, R.; Skabara, P. J.; Perepichka, I. F.; Bradley, D. D. C.; Koeberg, M. *J. Am. Chem. Soc.* **2004**, *126*, 13695.
- (145) Anemian, R.; Mulatier, J. C.; Andraud, C.; Stephan, O.; Vial, J. C. *Chem. Commun.* **2002**, 1608.
- (146) Zhang, K.; Chen, Z.; Yang, C. L.; Tao, Y. T.; Zou, Y.; Qin, J. G.; Cao, Y. *J. Mater. Chem.* **2008**, *18*, 291.
- (147) Wu, F. I.; Yang, X. H.; Neher, D.; Dodda, R.; Tseng, Y. H.; Shu, C. F. *Adv. Funct. Mat* **2007**, *17*, 1085.
- (148) Yang, J. S.; Huang, H. H.; Ho, J. H. *J. Phys. Chem. B* **2008**, *112*, 8871.
-

-
- (149) Zhang, K.; Chen, Z.; Yang, C. L.; Zou, Y.; Gong, S. L.; Qin, J. G.; Cao, Y. J. *Phys. Chem. C* **2008**, *112*, 3907.
- (150) Zhang, K.; Chen, Z.; Yang, C. L.; Zou, Y.; Gong, S. L.; Tao, Y. T.; Qin, J. G.; Cao, Y. J. *Mater. Chem.* **2008**, *18*, 3366.
- (151) Li, B. S.; Li, J.; Fu, Y. Q.; Bo, Z. S. *J. Am. Chem. Soc.* **2004**, *126*, 3430.
- (152) Zhou, X. H.; Yan, J. C.; Pei, J. *Org. Lett.* **2003**, *5*, 3543.
- (153) Liu, Q.; Qu, Y.; Geng, Y. H.; Wang, F. S. *Macromolecules* **2008**, *41*, 5964.
- (154) Barder, T. E.; Walker, S. D.; Martinelli, J. R.; Buchwald, S. L. *J. Am. Chem. Soc.* **2005**, *127*, 4685.
- (155) Montes, V. A.; Zyryanov, G. V.; Danilov, E. O.; Agarwal, N.; Palacios, M. A.; Anzenbacher, P. *J. Am. Chem. Soc.* **2009**, DOI: 10.1021/ja805175w.
- (156) Giebeler, C.; Antoniadis, H.; Bradley, D. D. C.; Shirota, Y. *J. Appl. Phys.* **1999**, *85*, 608.
- (157) Meerheim, R.; Scholz, S.; Olthof, S.; Schwartz, G.; Reineke, S.; Walzer, K.; Leo, K. *J. Appl. Phys.* **2008**, *104*, 014510.
- (158) Scott, J. C.; Karg, S.; Carter, S. A. *J. Appl. Phys.* **1997**, *82*, 1454.
- (159) Yang, X. H.; Wu, F. I.; Neher, D.; Chien, C. H.; Shu, C. F. *Chem. Mater.* **2008**, *20*, 1629.
- (160) Zhao, D. W.; Song, S. F.; Zhang, F. J.; Xu, C.; Xu, Z.; Sun, X. W. *Displays* **2008**, *29*, 408.
- (161) Ho, C. L.; Wong, W. Y.; Zhou, G. H.; Yao, B.; Xie, Z. Y.; Wang, L. X. *Adv. Funct. Mat* **2007**, *17*, 2925.
- (162) He, Z.; Wong, W. Y.; Yu, X. M.; Kwok, H. S.; Lin, Z. Y. *Inorg. Chem.* **2006**, *45*, 10922.
- (163) Wong, W. Y.; Ho, C. L.; Gao, Z. Q.; Mi, B. X.; Chen, C. H.; Cheah, K. W.; Lin, Z. Y. *Angew. Chem. Int. Edit.* **2006**, *45*, 7800.
- (164) Furuta, P. T.; Deng, L.; Garon, S.; Thompson, M. E.; Frechet, J. M. J. *J. Am. Chem. Soc.* **2004**, *126*, 15388.
- (165) Sun, S. S.; Zhang, C.; Ledbetter, A.; Choi, S.; Seo, K.; Bonner, C. E.; Drees, M.; Sariciftci, N. S. *Appl. Phys. Lett.* **2007**, *90*, 043117.
- (166) Yang, X. N.; Loos, J.; Veenstra, S. C.; Verhees, W. J. H.; Wienk, M. M.; Kroon, J. M.; Michels, M. A. J.; Janssen, R. A. J. *Nano Lett.* **2005**, *5*, 579.
- (167) Spanggaard, H.; Krebs, F. C. *Sol. Energ. Mat. Sol.* **2004**, *83*, 125.
- (168) Sun, S. S. *Sol. Energ. Mat. Sol.* **2003**, *79*, 257.
-

-
- (169) Gu, X.; Fei, T.; Zhang, H. Y.; Xu, H.; Yang, B.; Ma, Y. G.; Liu, X. D. *J. Phys. Chem. A* **2008**, *112*, 8387.
- (170) Chen, T. R. *J. Organomet. Chem.* **2008**, *693*, 3117.
- (171) Stagni, S.; Colella, S.; Palazzi, A.; Valenti, G.; Zacchini, S.; Paolucci, F.; Marcaccio, M.; Albuquerque, R. O.; De Cola, L. *Inorg. Chem.* **2008**, *47*, 10509.
- (172) Chang, C. J.; Yang, C. H.; Chen, K.; Chi, Y.; Shu, C. F.; Ho, M. L.; Yeh, Y. S.; Chou, P. T. *Dalton Trans.* **2007**, 1881.
- (173) Polosan, S.; Chow, T. J.; Tsuboi, T. *J. Phys. Org. Chem.* **2008**, *21*, 315.
- (174) Arm, K. J.; Williams, J. A. G. *Dalton Trans.* **2006**, 2172.
- (175) Lee, J. Y. *Appl. Phys. Lett.* **2006**, *89*, 223517.
- (176) Huo, S. Q.; Deaton, J. C.; Rajeswaran, M.; Lenhart, W. C. *Inorg. Chem.* **2006**, *45*, 3155.
- (177) Dedeian, K.; Shi, J. M.; Shepherd, N.; Forsythe, E.; Morton, D. C. *Inorg. Chem.* **2005**, *44*, 4445.
- (178) McDonald, A. R.; Lutz, M.; von Chrzanowski, L. S.; van Klink, G. P. M.; Spek, A. L.; van Koten, G. *Inorg. Chem.* **2008**, *47*, 6681.
- (179) Karatsu, T.; Ito, E.; Yagai, S.; Kitamura, A. *Chem. Phys. Lett.* **2006**, *424*, 353.
- (180) Namdas, E. B.; Anthopoulos, T. D.; Samuel, I. D. W.; Frampton, M. J.; Lo, S. C.; Burn, P. L. *Appl. Phys. Lett.* **2005**, *86*, 161104.
- (181) Bottcher, H. C.; Graf, M.; Kruger, H.; Wagner, C. *Inorg. Chem. Commun.* **2005**, *8*, 278.
- (182) Williams, J. A. G.; Wilkinson, A. J.; Whittle, V. L. *Dalton Trans.* **2008**, 2081.
- (183) Whittle, V. L.; Williams, J. A. G. *Inorg. Chem.* **2008**, *47*, 6596.
- (184) Wilkinson, A. J.; Puschmann, H.; Howard, J. A. K.; Foster, C. E.; Williams, J. A. G. *Inorg. Chem.* **2006**, *45*, 8685.
- (185) Wilkinson, A. J.; Goeta, A. E.; Foster, C. E.; Williams, J. A. G. *Inorg. Chem.* **2004**, *43*, 6513.
- (186) Flamigni, L.; Baranoff, E.; Collin, J. P.; Sauvage, J. P. *Chem. Eur. J.* **2006**, *12*, 6592.
- (187) Weber, S. K.; Galbrecht, F.; Scherf, U. *Org. Lett.* **2006**, *8*, 4039.
- (188) Dong, C. G.; Hu, Q. S. *J. Am. Chem. Soc.* **2005**, *127*, 10006.
- (189) Tavasli, M.; Bettington, S.; Bryce, M. R.; Batsanov, A. S.; Monkman, A. P. *Synthesis* **2005**, 1619.
- (190) Gillis, E. P.; Burke, M. D. *J. Am. Chem. Soc.* **2007**, *129*, 6716.
- (191) Noguchi, H.; Hojo, K.; Suginome, M. *J. Am. Chem. Soc.* **2007**, *129*, 758.
-

- (192) Lee, S. J.; Gray, K. C.; Paek, J. S.; Burke, M. D. *J. Am. Chem. Soc.* **2008**, *130*, 466.
- (193) Littke, A. F.; Dai, C. Y.; Fu, G. C. *J. Am. Chem. Soc.* **2000**, *122*, 4020.
- (194) Wolfe, J. P.; Buchwald, S. L. *Angew. Chem. Int. Edit.* **1999**, *38*, 2413.
- (195) Jiang, Q.; Ryan, M.; Zhichkin, P. *J. Org. Chem.* **2007**, *72*, 6618.
- (196) Cioffi, C. L.; Spencer, W. T.; Richards, J. J.; Herr, R. J. *J. Org. Chem.* **2004**, *69*, 2210.
- (197) Yokoyama, A.; Suzuki, H.; Kubota, Y.; Ohuchi, K.; Higashimura, H.; Yokozawa, T. *J. Am. Chem. Soc.* **2007**, *129*, 7236.
- (198) Billingsley, K. L.; Buchwald, S. L. *J. Org. Chem.* **2008**, *73*, 5589.
- (199) Parker, C. A.; Rees, W. T. *Analyst* **1960**, *85*, 587.
- (200) deMello, J. C.; Wittmann, H. F.; Friend, R. H. *Adv. Mater.* **1997**, *9*, 230.
- (201) Gaussian 03, R. C., Frisch, M. J.; Trucks, G. W.; Schlegel, H. B.; Scuseria, G. E.; Robb, M. A.; Cheeseman, J. R.; Montgomery, Jr., J. A.; Vreven, T.; Kudin, K. N.; Burant, J. C.; Millam, J. M.; Iyengar, S. S.; Tomasi, J.; Barone, V.; Mennucci, B.; Cossi, M.; Scalmani, G.; Rega, N.; Petersson, G. A.; Nakatsuji, H.; Hada, M.; Ehara, M.; Toyota, K.; Fukuda, R.; Hasegawa, J.; Ishida, M.; Nakajima, T.; Honda, Y.; Kitao, O.; Nakai, H.; Klene, M.; Li, X.; Knox, J. E.; Hratchian, H. P.; Cross, J. B.; Bakken, V.; Adamo, C.; Jaramillo, J.; Gomperts, R.; Stratmann, R. E.; Yazyev, O.; Austin, A. J.; Cammi, R.; Pomelli, C.; Ochterski, J. W.; Ayala, P. Y.; Morokuma, K.; Voth, G. A.; Salvador, P.; Dannenberg, J. J.; Zakrzewski, V. G.; Dapprich, S.; Daniels, A. D.; Strain, M. C.; Farkas, O.; Malick, D. K.; Rabuck, A. D.; Raghavachari, K.; Foresman, J. B.; Ortiz, J. V.; Cui, Q.; Baboul, A. G.; Clifford, S.; Cioslowski, J.; Stefanov, B. B.; Liu, G.; Liashenko, A.; Piskorz, P.; Komaromi, I.; Martin, R. L.; Fox, D. J.; Keith, T.; Al-Laham, M. A.; Peng, C. Y.; Nanayakkara, A.; Challacombe, M.; Gill, P. M. W.; Johnson, B.; Chen, W.; Wong, M. W.; Gonzalez, C.; and Pople, J. A.; Gaussian, Inc., Wallingford CT, 2004.
- (202) Tenderholt, A. L. *QMForge, Version 2.1*, <http://qmforge.sourceforge.net>.
- (203) Robison, M. M.; Robison, B. L. *J. Org. Chem.* **1956**, *21*, 1337
- (204) Haworth, R. D.; Robinson, S. *J. Chem. Soc.* **1948**, 777.
- (205) Brodrick, C. I.; Short, W. F. *J. Chem. Soc.* **1949**, 2587.
- (206) Wommack, J. B.; Barbee, T. G.; Thoennes, D. J.; McDonald, M. A.; Pearson, D. E. *J. Heterocycl. Chem.* **1969**, *6*, 243.

-
- (207) Yamato, T.; Hideshima, C.; Prakash, G. K. S.; Olah, G. A. *J. Org. Chem.* **1991**, *56*, 3955.
- (208) Bouchard, J.; Wakim, S.; Leclerc, M. *J. Org. Chem.* **2004**, *69*, 5705.
- (209) Jeeva, S.; Moratti, S. C. *Synthesis* **2007**, 3323.
- (210) Percec, V.; Obata, M.; Rudic, J. G.; De B, B.; Glodde, M.; Bera, T. K.; Magonow, S. N.; Balagurusamy, V. S. K.; Heiney, P. A. *J. Polym. Sci., Part A: Polym. Chem.* **2002**, *40*, 3509.
- (211) Belletete, M.; Bedard, M.; Bouchard, J.; Leclerc, M.; Durocher, G. *Can. J. Chem.* **2004**, *82*, 1280.

Appendix A

X-Ray crystal structure data for 2.37

Formula	C35 H25 Br2 Ir N2 O2
Formula weight	857.59
Temperature	173(2) K
Diffractometer, wavelength	OD Xcalibur PX Ultra, 1.54184 Å
Crystal system, space group	Triclinic, P-1
Unit cell dimensions	a = 10.0058(3) Å α = 86.546(2)° b = 10.8536(3) Å β = 77.878(2)° c = 14.2610(3) Å γ = 70.441(3)°
Volume, Z	1426.74(7) Å ³ , 2
Density (calculated)	1.996 Mg/m ³
Absorption coefficient	12.633 mm ⁻¹
F(000)	824
Crystal colour / morphology	Orange/red prisms
Crystal size	0.13 x 0.08 x 0.05 mm ³
θ range for data collection	3.17 to 71.29°
Index ranges	-12 ≤ h ≤ 12, -13 ≤ k ≤ 13, -17 ≤ l ≤ 14
Reflns collected / unique	18636 / 5422 [R(int) = 0.0287]
Reflns observed [F > 4 σ (F)]	4855
Absorption correction	Semi-empirical from equivalents
Max. and min. transmission	1.00000 and 0.29207
Refinement method	Full-matrix least-squares on F ²
Data / restraints / parameters	5422 / 0 / 381
Goodness-of-fit on F ²	1.019
Final R indices [F > 4 σ (F)]	R1 = 0.0244, wR2 = 0.0612
R indices (all data)	R1 = 0.0282, wR2 = 0.0621
Largest diff. peak, hole	1.212, -1.123 eÅ ⁻³
Mean and maximum shift/error	0.000 and 0.001

Table 2. Bond lengths [Å] and angles [°] for CW0816.

Ir-C(16)	1.970(4)
Ir-C(36)	1.983(4)
Ir-N(1)	2.025(3)
Ir-N(21)	2.028(3)
Ir-O(40)	2.142(2)
Ir-O(42)	2.159(2)
Br(1)-C(13)	1.903(4)
Br(2)-C(33)	1.909(4)
N(1)-C(10)	1.355(5)
N(1)-C(2)	1.375(4)
C(2)-C(3)	1.350(5)
C(3)-C(4)	1.406(5)
C(4)-C(5)	1.408(5)
C(4)-C(9)	1.424(5)
C(5)-C(6)	1.361(6)
C(6)-C(7)	1.399(6)
C(7)-C(8)	1.367(5)
C(8)-C(9)	1.418(5)
C(9)-C(10)	1.440(5)
C(10)-C(11)	1.485(5)
C(11)-C(12)	1.405(5)
C(11)-C(16)	1.423(5)
C(12)-C(13)	1.382(5)
C(13)-C(14)	1.376(6)
C(14)-C(15)	1.379(5)
C(15)-C(16)	1.410(5)
N(21)-C(30)	1.351(5)
N(21)-C(22)	1.373(5)
C(22)-C(23)	1.342(5)
C(23)-C(24)	1.415(5)
C(24)-C(25)	1.414(5)
C(24)-C(29)	1.427(5)
C(25)-C(26)	1.362(6)
C(26)-C(27)	1.398(6)
C(27)-C(28)	1.368(6)
C(28)-C(29)	1.418(5)
C(29)-C(30)	1.440(5)
C(30)-C(31)	1.488(5)
C(31)-C(32)	1.399(5)
C(31)-C(36)	1.426(5)
C(32)-C(33)	1.378(5)
C(33)-C(34)	1.381(6)
C(34)-C(35)	1.378(5)
C(35)-C(36)	1.412(5)
O(40)-C(40)	1.270(4)
C(40)-C(41)	1.389(5)
C(40)-C(43)	1.502(5)
C(41)-C(42)	1.395(5)
C(42)-O(42)	1.276(4)
C(42)-C(44)	1.510(5)
C(16)-Ir-C(36)	89.35(14)
C(16)-Ir-N(1)	79.32(13)
C(36)-Ir-N(1)	97.09(13)
C(16)-Ir-N(21)	98.70(13)
C(36)-Ir-N(21)	79.44(13)
N(1)-Ir-N(21)	176.06(11)
C(16)-Ir-O(40)	89.02(12)
C(36)-Ir-O(40)	176.02(12)
N(1)-Ir-O(40)	86.18(10)
N(21)-Ir-O(40)	97.22(10)
C(16)-Ir-O(42)	175.48(12)
C(36)-Ir-O(42)	93.27(12)
N(1)-Ir-O(42)	96.69(10)
N(21)-Ir-O(42)	85.41(11)
O(40)-Ir-O(42)	88.59(9)
C(10)-N(1)-C(2)	121.4(3)
C(10)-N(1)-Ir	119.1(2)
C(2)-N(1)-Ir	119.5(2)
C(3)-C(2)-N(1)	122.0(3)
C(2)-C(3)-C(4)	119.8(3)

C(3) -C(4) -C(5)	120.4(3)
C(3) -C(4) -C(9)	119.1(3)
C(5) -C(4) -C(9)	120.5(4)
C(6) -C(5) -C(4)	121.2(4)
C(5) -C(6) -C(7)	119.4(4)
C(8) -C(7) -C(6)	120.4(4)
C(7) -C(8) -C(9)	122.5(4)
C(8) -C(9) -C(4)	115.9(3)
C(8) -C(9) -C(10)	125.5(3)
C(4) -C(9) -C(10)	118.6(3)
N(1) -C(10) -C(9)	118.9(3)
N(1) -C(10) -C(11)	111.1(3)
C(9) -C(10) -C(11)	130.0(3)
C(12) -C(11) -C(16)	119.1(3)
C(12) -C(11) -C(10)	127.0(3)
C(16) -C(11) -C(10)	113.9(3)
C(13) -C(12) -C(11)	119.9(4)
C(14) -C(13) -C(12)	122.2(3)
C(14) -C(13) -Br(1)	119.1(3)
C(12) -C(13) -Br(1)	118.6(3)
C(13) -C(14) -C(15)	118.3(3)
C(14) -C(15) -C(16)	122.4(4)
C(15) -C(16) -C(11)	118.0(3)
C(15) -C(16) -Ir	125.5(3)
C(11) -C(16) -Ir	116.6(3)
C(30) -N(21) -C(22)	120.9(3)
C(30) -N(21) -Ir	118.9(2)
C(22) -N(21) -Ir	120.1(2)
C(23) -C(22) -N(21)	122.5(4)
C(22) -C(23) -C(24)	119.8(3)
C(25) -C(24) -C(23)	120.8(4)
C(25) -C(24) -C(29)	120.5(4)
C(23) -C(24) -C(29)	118.7(3)
C(26) -C(25) -C(24)	120.6(4)
C(25) -C(26) -C(27)	119.6(4)
C(28) -C(27) -C(26)	121.0(4)
C(27) -C(28) -C(29)	121.7(4)
C(28) -C(29) -C(24)	116.2(3)
C(28) -C(29) -C(30)	125.7(3)
C(24) -C(29) -C(30)	118.1(3)
N(21) -C(30) -C(29)	119.6(3)
N(21) -C(30) -C(31)	111.6(3)
C(29) -C(30) -C(31)	128.8(3)
C(32) -C(31) -C(36)	119.2(3)
C(32) -C(31) -C(30)	126.9(3)
C(36) -C(31) -C(30)	113.9(3)
C(33) -C(32) -C(31)	120.1(4)
C(32) -C(33) -C(34)	121.9(3)
C(34) -C(33) -Br(2)	119.4(3)
C(34) -C(33) -Br(2)	118.7(3)
C(35) -C(34) -C(33)	118.7(3)
C(34) -C(35) -C(36)	121.9(4)
C(35) -C(36) -C(31)	117.9(3)
C(35) -C(36) -Ir	126.0(3)
C(31) -C(36) -Ir	116.1(3)
C(40) -O(40) -Ir	125.1(2)
O(40) -C(40) -C(41)	126.0(3)
O(40) -C(40) -C(43)	115.4(3)
C(41) -C(40) -C(43)	118.7(3)
C(40) -C(41) -C(42)	129.6(3)
O(42) -C(42) -C(41)	126.3(3)
O(42) -C(42) -C(44)	115.8(3)
C(41) -C(42) -C(44)	117.8(3)
C(42) -O(42) -Ir	124.0(2)

Appendix B

Investigation into the Phosphorescence of a Series of Regioisomeric Iridium(III) Complexes

Hugo A. Bronstein,[†] Chris E. Finlayson,[‡] Kiril R. Kirov,[‡] Richard H. Friend,[‡] and Charlotte K. Williams^{*,†}

Department of Chemistry, Imperial College London, London, SW7 2AZ, U.K., and Optoelectronics Group, Cavendish Laboratory, Cambridge University, JJ Thompson Avenue, Cambridge CB3 0HE, U.K.

Received January 7, 2008

A series of heteroleptic cyclometalated Ir(III) complexes with the general structure $[\text{Ir}(\text{piq-X})_2(\text{acac})]$ (where $\text{piq} = 1\text{-phenylisoquinolato}$, $\text{X} = \text{bromine, 9,9-dioctyl-2-fluorenyl, poly(9,9-dioctyl-2,7-fluorene)}$, $\text{acac} = \text{acetyl acetonate}$) have been prepared. The complexes are regioisomers where the X substituents occupy positions 2, 3, or 4 on the phenyl ring. The isomers all show red phosphorescence but have varying wavelengths and quantum yields. The nature and site of substitution influence the energy and localization of the frontier molecular orbitals, and this is investigated using electrochemistry, absorption and emission spectroscopy, and density functional theory calculations. Substitution in the 3-phenyl site leads to complexes with the highest quantum yields and results in an increase in the highest occupied molecular orbital (HOMO) energy. Conversely, substitution at the 4-phenyl position lowers the lowest unoccupied orbital energy (LUMO). Some of the complexes are applied in single-layer-polymer light-emitting devices (PLEDs), which show red electrophosphorescence.

Introduction

The discovery of electroluminescence (EL) from conjugated polymers in light-emitting devices (LEDs) has led to the rapid development of new electroactive polymers.¹ Small molecule (SMOLED) and polymer (PLED) devices have also attracted industrial interest, and some displays are already on the market.² The performance of SMOLEDs has been dramatically improved by using phosphorescent organometallic complexes or triplet emitters as dopants.^{2,3} Efficient phosphorescence requires a significant degree of metal participation in the triplet state, as this generally reduces the singlet–triplet gap, enhances intersystem crossing, and increases emission decay rates.⁴ Cyclometalated Ir(III) complexes have been widely applied as triplet emitters; they have high quantum yields and controllable emission color.^{5,6} Multilayer SMOLEDs have been fabricated using green-emitting Ir(III) complexes with outstanding external quantum efficiencies (EQE) of 19%.⁷ Efficient blends of phosphorescent Ir(III) complexes in conjugated polymer hosts have also been realized,^{8–11} but there can be problems with film stability, phase separation, triplet–triplet annihilation at large

current densities, and triplet back transfer from phosphor to conjugated polymer low-lying triplet states.^{12,13} An alternative approach involves covalent attachment of the phosphor to the conjugated polymer, thereby forming an Ir(III)–polymer complex. This prevents phase separation and provides fully characterized materials with controllable separations between the polymer and the phosphorescent complex. The covalent attachment has been accomplished using either a nonconjugated spacer, often an alkyl chain, or a conjugated bond.

Attaching Ir(III) phosphors via nonconjugated linkers has been explored by several groups. Chen et al. reported the attachment of a red phosphorescent Ir(III) complex, $[\text{Ir}(\text{btp})_2(\text{acac})]$, via an alkyl chain from the β -diketonate to a fluorene monomer.¹⁴ Jiang and co-workers obtained EQEs of up to 4.9% using copoly(fluorene-*alt*-carbazole) with red phosphorescent Ir(III) complexes attached via alkyl linkages between the β -diketonate and a carbazole unit.¹⁵ In a detailed study Evans et al. compared $[\text{Ir}(\text{btp})_2(\text{acac})]$ complexes attached via the β -diketonate group either directly or through an alkyl chain to the 9-position of a 9-octylfluorene host.¹⁶ The copolymers of the alkyl chain linked materials had efficiencies double those of the spacerless copolymers. This was attributed

* Corresponding author. E-mail: c.k.williams@imperial.ac.uk.

[†] Imperial College London.

[‡] Cambridge University.

(1) Burroughes, J. H.; Bradley, D. D. C.; Brown, A. R.; Marks, R. N.; Mackay, K.; Friend, R. H.; Burns, P. L.; Holmes, A. B. *Nature* **1990**, *347*, 539.

(2) Holder, E.; Langeveld, B. M. W.; Schubert, U. S. *Adv. Mater.* **2005**, *17*, 1109.

(3) Kohle, A.; Wilson, J. S.; Friend, R. H. *Adv. Mater.* **2002**, *14*, 701.

(4) Yersin, H. *Top. Curr. Chem.* **2004**, *241*, 1.

(5) Lamansky, S.; Djurovich, P.; Murphy, D.; Abdel-Razzaq, F.; Kwong, R.; Tsyba, I.; Bortz, M.; Mui, B.; Bau, R.; Thompson, M. E. *Inorg. Chem.* **2001**, *40*, 1704.

(6) Lamansky, S.; Djurovich, P.; Murphy, D.; Abdel-Razzaq, F.; Lee, H. E.; Adachi, C.; Burrows, P. E.; Forrest, S. R.; Thompson, M. E. *J. Am. Chem. Soc.* **2001**, *123*, 4304.

(7) Adachi, C.; Baldo, M. A.; Thompson, M. E.; Forrest, S. R. *J. Appl. Phys.* **2001**, *90*, 5048.

(8) Gong, X.; Robinson, M. R.; Ostrowski, J. C.; Moses, D.; Bazan, G. C.; Heeger, A. J. *Adv. Mater.* **2002**, *14*, 581.

(9) Gong, X.; Ostrowski, J. C.; Moses, D.; Bazan, G. C.; Heeger, A. J. *Adv. Funct. Mater.* **2003**, *13*, 439.

(10) Gong, X.; Ostrowski, J. C.; Bazan, G. C.; Moses, D.; Heeger, A. J.; Liu, M. S.; Jen, A. K. Y. *Adv. Mater.* **2003**, *15*, 45.

(11) van Dijken, A.; Bastiaansen, J.; Kikken, N. M. M.; Langeveld, B. M. W.; Rothe, C.; Monkman, A.; Bach, I.; Stossel, P.; Brunner, K. J. *Am. Chem. Soc.* **2004**, *126*, 7718.

(12) Noh, Y. Y.; Lee, C. L.; Kim, J. J.; Yase, K. *J. Chem. Phys.* **2003**, *118*, 2853.

(13) Sudhakar, M.; Djurovich, P. I.; Hogen-Esch, T. E.; Thompson, M. E. *J. Am. Chem. Soc.* **2003**, *125*, 7796.

(14) Chen, X. W.; Liao, J. L.; Liang, Y. M.; Ahmed, M. O.; Tseng, H. E.; Chen, S. A. *J. Am. Chem. Soc.* **2003**, *125*, 636.

(15) Jiang, J. X.; Jiang, C. Y.; Yang, W.; Zhen, H. G.; Huang, F.; Cao, Y. *Macromolecules* **2005**, *38*, 4072.

(16) Evans, N. R.; Devi, L. S.; Mak, C. S. K.; Watkins, S. E.; Pasqu, S. I.; Kohler, A.; Friend, R. H.; Williams, C. K.; Holmes, A. B. *J. Am. Chem. Soc.* **2006**, *128*, 6647.

to the suppression of back transfer of triplets from the Ir(III) to the copolyfluorenes in the tethered materials.

Attaching Ir(III) phosphors directly to and in conjugation with the polymer backbone has been accomplished by Suzuki condensation polymerization between bromine-substituted Ir(III) cyclometalates and boronic ester-substituted electroactive monomers.¹⁷ The first report from Sandee et al. involved green and red phosphorescent Ir(III) complexes conjugated to polyfluorenes; efficient energy transfer occurred only with the red emitters.¹⁷ PLEDs showed exclusive red emission regardless of the loading of Ir(III), indicating efficient charge trapping on the Ir(III) center. Furthermore, the PLEDs fabricated with the novel materials showed higher efficiencies than blends. Several related polymer complexes have subsequently been reported using copoly(flourene-*alt*-carbazole), copoly(flourene-*alt*-thiophene), polycarbazole, and polyphenylene in conjugation with Ir(III) complexes.^{18–26} Zhen et al. recently reported a bis(2(1-naphthalene)pyridine)iridium–polyfluorene complex that gave efficient red emission. When used in PLEDs, an external quantum efficiency of 5.3% was measured at 100 mA/cm².²³

1-Phenylisoquinolino Ir(III) cyclometalates were previously synthesized in high yields and showed good red color purity.^{27,28} The high quantum yields, obtained using [Ir(piq)₃], were rationalized by the emission occurring from a predominantly ³MLCT (metal-to-ligand charge transfer) state, which has a radiative decay rate an order of magnitude higher than complexes that emit from a predominantly ³LC (ligand centered) state.²⁷ Despite the availability of these studies, insight into the influence of the nature and site of substitution is needed.^{28–34} Here, we report a series of substituted [bis(1-phenylisoquinolino)iridium(acetyl acetonate)] complexes (Figure 1). The complexes are substituted with bromine or fluorenyl groups at 2-, 3-, or 4-positions on the phenyl ring of the cyclometalating ligand. These regioisomers are used to probe the influence of the substituents on the photophysical properties of the complexes

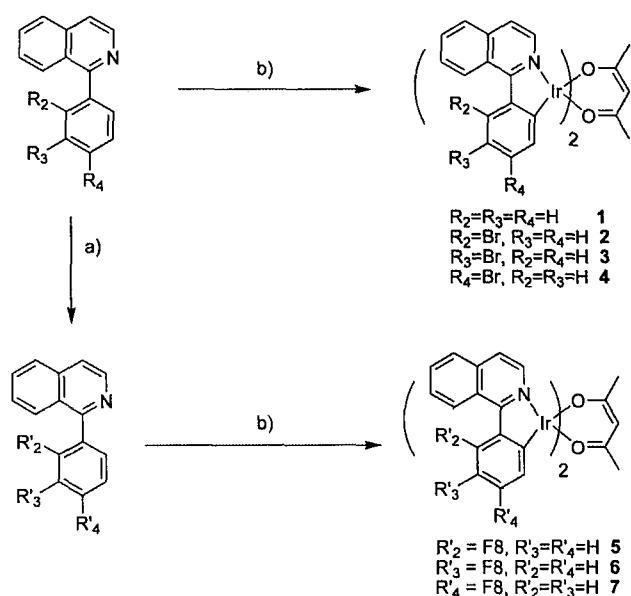


Figure 1. Synthesis of the well-defined iridium complexes 1–7. Reagents and conditions: (a) 2-(4',4',5',5'-tetramethyl-1',3',2'-dioxaborolan-2'-yl)-9,9-dioctylfluorene, Pd(PPh₃)₄ (1 mol %), Et₄NOH(aq), toluene, 90 °C, 18 h. 72% (R'₂ = fluorenyl), 80% (R'₃ = fluorenyl), 70% (R'₄ = fluorenyl). (b) (i) IrCl₃·xH₂O, 2-ethoxyethanol(aq), 110 °C, 18 h, (ii) acetyl acetone, 2-ethoxyethanol, Na₂CO₃, 110 °C, 12 h. 57% (2), 63% (3), 69% (4), 44% (5), 47% (6), 57% (7).

and as models for the polymer–iridium complexes. The new materials are characterized using optical absorption and emission spectroscopy and cyclic voltammetry. Density functional theory (DFT) using the B3LYP hybrid functional is used to model the frontier molecular orbitals in order to explain the changes in the phosphorescence. Regioisomeric polyfluorenyl–iridium complexes have also been prepared, characterized, and used as the active layer in PLEDs, where they yield red electrophosphorescence.

Results and Discussion

Well-Defined Ir(III) Complex Synthesis. The bromine-substituted 1-phenylisoquinoline ligands were prepared in excellent yields by reaction and subsequent cyclization of (±)-2-amino-1-phenylethanol with the corresponding bromine-substituted benzoyl chloride (Figure S1). The fluorenyl (F8)-substituted 1-phenylisoquinoline ligands were synthesized via a Suzuki coupling condensation between the appropriate bromine 1-phenylisoquinoline regioisomer and 2-(4',4',5',5'-diisopropylboronate)-9,9-dioctylfluorene. The bis(cyclometalated) Ir(III) complexes 1–7 were prepared in excellent yields using adaptations of literature procedures (Figure 1).^{5,6}

The new ligands were reacted with IrCl₃·xH₂O to yield chloro-bridged dimeric complexes, and these species were subsequently cleaved by reaction with acetyl acetone to give clean conversion to complexes 1–7. All the complexes were isolated as red powders in moderate to good yield (50–90%), relative to their ligand precursors. The purity and coordination geometries were confirmed by NMR spectroscopy, elemental analysis, and mass spectrometry. The ¹H NMR spectra confirmed the formation of C₂-symmetric complexes, consistent with the nitrogen atoms occupying *trans* axial coordination sites at the iridium center; such a geometry is common for heteroleptic bis(cyclometalated) Ir(III) complexes.^{5,6} It was noteworthy that both 2 and 5, which have 2-bromine and 2-fluorenyl

(17) Sandee, A. J.; Williams, C. K.; Evans, N. R.; Davies, J. E.; Boothby, C. E.; Kohler, A.; Friend, R. H.; Holmes, A. B. *J. Am. Chem. Soc.* **2004**, *126*, 7041.

(18) Zhen, H. Y.; Jiang, C. Y.; Yang, W.; Jiang, J. X.; Huang, F.; Cao, Y. *Chem.–Eur. J.* **2005**, *11*, 5007.

(19) Yang, W.; Zhen, H. Y.; Jiang, C. Y.; Su, L. J.; Jiang, J. X.; Shi, H. H.; Cao, Y. *Synth. Met.* **2005**, *153*, 189.

(20) Schulz, G. L.; Chen, X. W.; Chen, S. A.; Holdercroft, S. *Macromolecules* **2006**, *39*, 9157.

(21) Zhen, H. Y.; Luo, J.; Yang, W.; Chen, Q. L.; Ying, L.; Zou, J. H.; Wu, H. B.; Cao, Y. *J. Mater. Chem.* **2007**, *17*, 2824.

(22) Ito, T.; Suzuki, S.; Kido, J. *Polym. Adv. Tech.* **2005**, *16*, 480.

(23) Zhen, H. Y.; Luo, C.; Yang, W.; Song, W. Y.; Du, B.; Jiang, J. X.; Jiang, C. Y.; Zhang, Y.; Cao, Y. *Macromolecules* **2006**, *39*, 1693.

(24) Zhang, K.; Chen, Z.; Yang, C. L.; Gong, S. L.; Qin, J. G.; Cao, Y. *Macromol. Rapid Commun.* **2006**, *27*, 1926.

(25) Zhang, K.; Chen, Z.; Zou, Y.; Yang, C. L.; Qin, J. G.; Cao, Y. *Organometallics* **2007**, *26*, 3699.

(26) Jiang, J. X.; Yang, W.; Cao, Y. *J. Inorg. Organomet. Polym. Mater.* **2007**, *17*, 37.

(27) Tsuboyama, A.; Iwawaki, H.; Furugori, M.; Mukaide, T.; Kamatani, J.; Igawa, S.; Moriyama, T.; Miura, S.; Takiguchi, T.; Okada, S.; Hoshino, M.; Ueno, K. *J. Am. Chem. Soc.* **2003**, *125*, 12971.

(28) Su, Y. J.; Huang, H. L.; Li, C. L.; Chien, C. H.; Tao, Y. T.; Chou, P. T.; Datta, S.; Liu, R. S. *Adv. Mater.* **2003**, *15*, 884.

(29) Li, C. L.; Su, Y. J.; Tao, Y. T.; Chou, P. T.; Chien, C. H.; Cheng, C. C.; Liu, R. S. *Adv. Funct. Mater.* **2005**, *15*, 387.

(30) Yang, C. H.; Su, W. L.; Fang, K. H.; Wang, S. P.; Sun, I. W. *Organometallics* **2006**, *25*, 4514.

(31) Fang, K. H.; Wu, L. L.; Huang, Y. T.; Yang, C. H.; Sun, I. W. *Inorg. Chin. Acta* **2006**, *359*, 441.

(32) Huang, Y. T.; Chuang, T. H.; Shu, Y. L.; Kuo, Y. C.; Wu, P. L.; Yang, C. H.; Sun, I. W. *Organometallics* **2005**, *24*, 6230.

(33) Yang, C. H.; Tai, C. C.; Sun, I. W. *J. Mater. Chem.* **2004**, *14*, 947.

(34) Hu, Z. Y.; Luo, C. P.; Wang, L.; Huang, F. L.; Zhu, K. L.; Wang, Y. F.; Zhu, M. X.; Zhu, W. G.; Cao, Y. *Chem. Phys. Lett.* **2007**, *441*, 277.

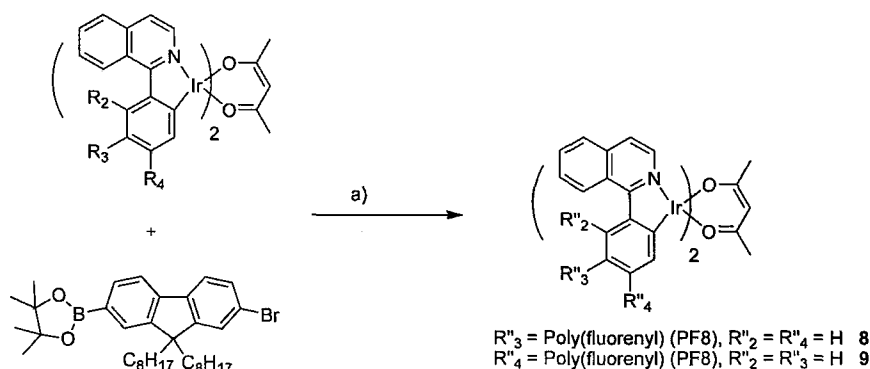


Figure 2. Chain extension polymerization to synthesize the $[\text{Ir}(\text{piq-PF8})_2(\text{acac})]$ regioisomers. Reagents and conditions: (a) 18 equiv of 2-(4',4',5',5'-tetramethyl-1',3',2'-dioxaborolan-2'-yl)-7-bromo-9,9-dioctylfluorene, 0.2 equiv of $\text{Pd}(\text{OAc})_2$ (20 mol %), 0.4 equiv of tricyclohexylphosphine, $\text{Et}_4\text{NOH}(\text{aq})$, toluene, 110 °C; 48 h; 55% (**8**), 58% (**9**).

substituents, respectively, exhibited a significant broadening in their NMR spectra, due to the increased steric demand of that particular substitution position inducing a degree of fluxionality to the complex. Additionally, a small amount of the geometric isomer in which the cyclometalating ligands are coordinated with the N atoms *cis* to one another (5%) was isolated alongside **2**. It was identified by NMR spectroscopy due to its reduced symmetry (C_1 vs C_2) leading to an increased number of signals being observed.

Conjugated Polymer-Ir(III) Complex Synthesis. The successful synthesis of the series of $[\text{Ir}(\text{piq-X})_2(\text{acac})]$ complexes enabled the preparation of the regioisomeric polyfluorene-Ir(III) complexes of the type $[\text{Ir}(\text{piq-PF8})_2(\text{acac})]$. The synthetic method was analogous to that reported by Sandee et al.¹⁷ and involved a Suzuki condensation polymerization between a fluorene AB monomer 2-(4',4',5',5'-tetramethyl-1',3',2'-dioxaborolan-2'-yl)-7-bromo-9,9-dioctylfluorene and the bromine-substituted iridium complex **3** or **4** (Figure 2).

A Suzuki polycondensation using 18 equiv of the fluorene AB monomer to 1 equiv of either **3** or **4** yielded polyfluorene-Ir(III) complexes **8** and **9** in 55% and 58% isolated yields, respectively. In both **8** and **9** the Ir(III) phosphor was bound to two polyfluorene chains; thus the metal complex acted as a chain extender. The iridium complex loadings were deduced from their ^1H NMR spectra by integration of the methine signals on the acetyl acetonate ligand against the aromatic signals on the polyfluorene backbone. The incorporation of the iridium complex was approximately 6% by weight in both **8** and **9**, which is slightly lower than the feed loading of 8%, but confirms findings by other groups making related Ir(III)-polymer complexes.^{21,23,25} The SEC data showed M_n of 11 600 and 12 100 for **8** and **9**, respectively. All attempts to isolate a polymer-Ir(III) complex substituted at the 2-phenyl position, by reaction of **2** with the AB monomer, led to the isolation of a polymer without iridium incorporation, probably due to the steric hindrance of **2**.

Absorption Spectroscopy. The solution absorption spectra were compared for the series of small-molecule regioisomers **1–7** (Figure 3a, X = Br; Figure 3b, X = F8) and for the polymer-Ir(III) complexes **8** and **9** (Figure 3c, X = PF8).

The spectra are all assigned by analogy to related literature bis(cyclometalated)Ir(III) complexes.^{5,6,27,28} The introduction of bromine substituents has little effect on the absorption spectra of complexes **2–4** compared to the unsubstituted analogue **1** (Figure 3a). The intense absorption bands between 250 and 350 nm (molar absorption coefficient, $\epsilon = 10\,000\text{--}60\,000\text{ M}^{-1}\text{ cm}^{-1}$) are attributed to $^1\pi\text{-}\pi^*$ transitions between 1-phenylisoquinolinato-centered states. The weaker absorption bands (ϵ

$= 1000\text{--}6000\text{ M}^{-1}\text{ cm}^{-1}$) in the range 350–440 nm are assigned to the spin-allowed metal-to-ligand charge transfer transitions, $^1\text{MLCT}$, and those at 450–500 nm to the spin-forbidden metal-to-ligand charge transfer transitions, $^3\text{MLCT}$, which gain intensity through the strong spin-orbit coupling.^{5,6,28,35,36} Substitution of the 1-phenylisoquinolinato ligands with fluorenyl groups, on the other hand, significantly alters the absorption spectra for **5–7** (Figure 3b). As for **1–4**, the intense absorption bands between 250 and 300 nm are attributed to $^1\pi\text{-}\pi^*$ transitions of 1-phenylisoquinolinato-centered states. The absorption bands between 320 and 400 nm are attributed to $^1\pi\text{-}\pi^*$ transitions of the fluorenyl substituents. Complexes **5** and **7** each display red-shifted fluorenyl absorption peaks. For **5** this peak is also of reduced intensity. The weaker MLCT absorption bands in the range 450–600 nm are also red-shifted compared to **1**. These red-shifts indicate extended conjugation, i.e., orbital overlap between the fluorenyl substituents and the iridium complex. Figure 3c shows the solution absorption spectra of the polyfluorene-Ir(III) complexes **8** and **9**. They display absorption maxima at approximately 380 nm, which are attributed to $\pi\text{-}\pi^*$ transitions of the polyfluorene. The maxima are red-shifted compared with the fluorenyl absorptions of **5–7** due to the extended conjugation along the polyfluorene backbone. Lower intensity absorptions are present at 430–440 nm, which are attributed to $\pi\text{-}\pi^*$ transitions of the polyfluorene in its β -phase. Their relative intensity is consistent with previously reported spectra.³⁷

Emission Spectroscopy. The optically excited phosphorescence spectra of **1–7** were measured in CH_2Cl_2 solutions at 298 K, using an excitation wavelength of 350 nm (Figure 4).

The unsubstituted complex **1** has an emission maxima at 623 nm, close to that reported previously for **1** (622 nm).²⁸ Complexes **2**, **3**, and **5–7** all display red-shifted emissions, while complex **4** displays a blue-shift. The influence of the site of substitution on the shift in the emission differs between the bromine- and fluorenyl-substituted complexes. For the bromine substituents, the λ_{max} varies in the order $2 > 3 > 1 > 4$, and for the fluorenyl substituents, the order is $7 > 6 > 5 \gg 1$. It is also worth noting that complexes **2** and **5** have identical emission maxima.

The optically induced emission spectra of the polymer complexes **8** and **9** differ according to the conditions of the measurements (Figure 5).

(35) Colombo, M. G.; Hauser, A.; Gudel, H. U. *Inorg. Chem.* **1993**, *32*, 3088.

(36) Schmid, B.; Garces, F. O.; Watts, R. J. *Inorg. Chem.* **1994**, *33*, 9.

(37) Hayer, A.; Khan, A. L. T.; Friend, R. H.; Kohler, A. *Phys. Rev. B* **2005**, *71*, 241302.

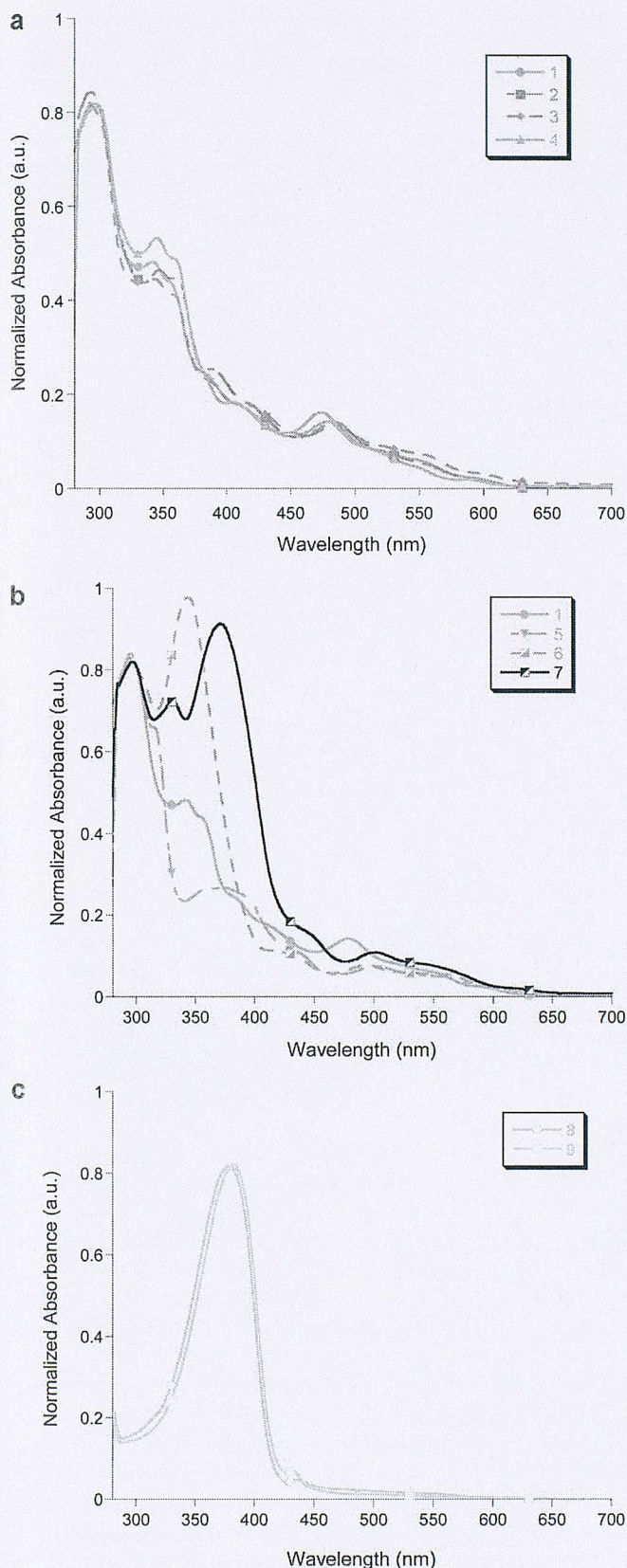


Figure 3. UV-vis absorption spectra of 1–4 (a), 1 and 5–7 (b), and 8 and 9 (c). The spectra were determined in 0.0001 M CH_2Cl_2 solutions at 298 K.

In solution, both **8** and **9** emit almost exclusively from their polyfluorene backbones, showing an intense blue fluorenyl fluorescence signal at 416 nm with only a low-intensity red phosphorescence signal. This is due to the lack of energy transfer from the polyfluorene chain to the central phosphor.¹³ In the

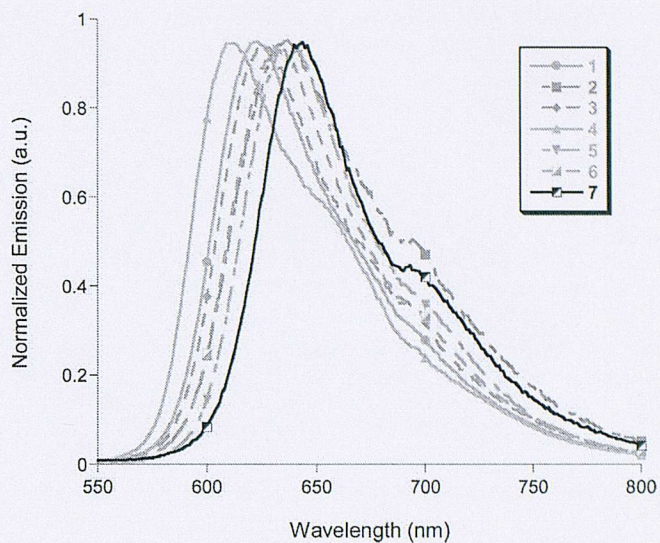


Figure 4. Solution phosphorescence spectra of compounds 1–7. The spectra were determined in degassed CH_2Cl_2 solutions at 298 K. All excitation energies were 350 nm.

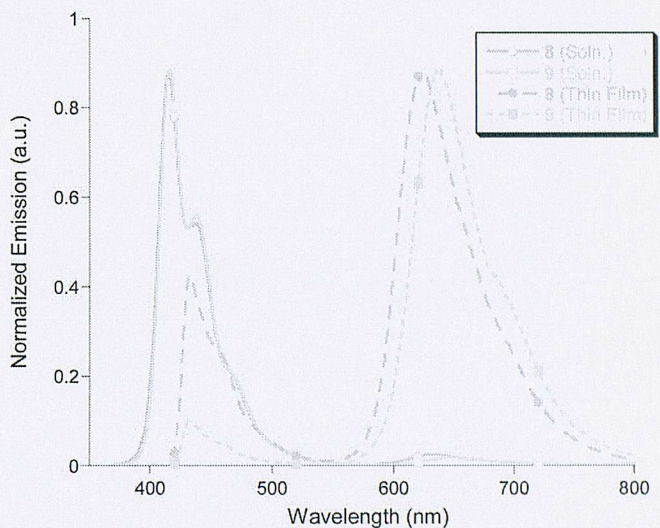


Figure 5. Thin film and solution phosphorescence spectra of compounds **8** and **9**. The solution spectra were determined in degassed CH_2Cl_2 solutions at 298 K. Thin films were spin coated from CH_2Cl_2 solutions of a 10 mg/mL dilution. All excitation energies were 350 nm.

solid state (thin films, spin coated from CH_2Cl_2 solutions), **8** and **9** display predominantly red phosphorescence, at 625 and 639 nm, respectively, and originating from their Ir(III) phosphors, with only low-intensity polyfluorene emission. This is due to the close proximity of molecules, which allows greater energy transfer from the polyfluorene chain to the central iridium phosphor.^{13,16} The residual thin film emissions originating from the polyfluorene chain are also red-shifted by approximately 15 nm compared to the solution spectra, due to aggregation effects.^{38,39} The phosphorescence spectra of **8** and **9** correspond well with those of their small-molecule analogues **6** and **7**, indicating that the well-defined Ir(III) complexes are viable models for the polymer–Ir(III) complexes.

Quantum Yields. The solution phosphorescence quantum yields, Φ , of **2**–**7** were measured in degassed methylene

(38) Grell, M.; Bradley, D. D. C.; Long, X.; Chamberlain, T.; Inbasekaran, M.; Woo, E. P.; Soliman, M. *Acta Polym.* **1998**, *49*, 439.

(39) Blondin, P.; Bouchard, J.; Beaupre, S.; Belletete, M.; Durocher, G.; Leclerc, M. *Macromolecules* **2000**, *33*, 5874.

Table 1. Solution Absorbance and Emission Wavelengths and Quantum Yields of Complexes 1–9 (absorption and emission spectra were determined in CH₂Cl₂ solutions at room temperature)

compound	absorbance wavelength (molar absorption coefficient, $\epsilon/M^{-1}cm^{-1}$) λ_{max}/nm		phosphorescence emission wavelength λ_{max}/nm		quantum yields, Φ^a
1	234 (32 054)		623		0.20
	291 (20 570)				
	351 (10 474)				
	477 (2524)				
2	248 (45 318)		637		0.07
	296 (30 816)				
	351 (16 919)				
	395 (9063)				
	490 (4834)				
3	235 (59 528)		626		0.14
	274 (37 487)				
	351 (16 249)				
	412 (6275)				
4	482 (2896)		612		0.10
	236 (48 521)				
	295 (33 518)				
	348 (18 675)				
	405 (6704)				
5	472 (4310)		637		0.03
	233 (47 144)				
	289 (33 447)				
	376 (8601)				
6	477 (1752)		634		0.15
	294 (23 423)				
	336 (24 187)				
	426 (2164)				
7	481 (1273)		644		0.06
	235 (36 132)				
	298 (26 083)				
	332 (22 021)				
	371 (2586)				
8	495 (2138)		416 (soln)		n/a
	382		625 (thin film)		0.22
9	441		416 (soln)		n/a
	385		639 (thin film)		0.10
	436				

^a Φ was determined in degassed CH₂Cl₂ solutions using **1** as the standard. Thin films were spin coated from CH₂Cl₂ solutions of a 10 mg/mL dilution. Thin film Φ 's were determined using an integrating sphere. All excitation energies were 350 nm.

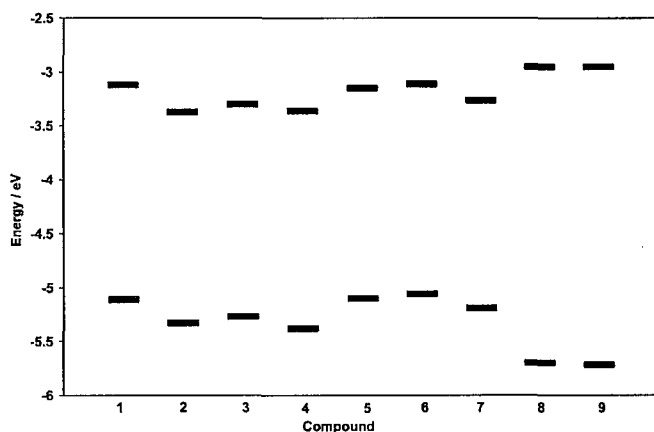
chloride solutions using **1** as the standard (Table 1). Complexes **2** and **5** have low quantum yields and display significant peak broadening in their ¹H NMR spectra, which are attributed to fluxional processes. It is believed that this is due to steric interactions between the substituent at the 2-phenyl position and the isoquinoline ring, which results in an increase in nonradiative relaxation pathways. Complexes **3**, **4**, **6**, and **7** all show moderate quantum yields ($\Phi = 0.06$ – 0.15). The quantum yields for the thin films of the polymer complexes **8** and **9** ($\Phi = 0.10$ – 0.22) are comparable to those of the fluorenyl-substituted model compounds. Substitution in the 3-phenyl position leads to the highest quantum yields for all the substituted complexes. The origin of this phenomenon is currently being explored.

Energy Levels. In order to understand the variation in optical properties of the regioisomers, it was important to establish the properties of the frontier molecular orbitals. The orbital energies were determined by cyclic voltammetry and absorption spectroscopy. Density functional theory (DFT) calculations, using the hybrid functional B3LYP, were used to model the linear combination of atomic orbitals (LCAO) and the pattern of the molecular orbitals. A measure for the HOMO energy, E_{HOMO} , is the ionization potential; here the ionization potential was calculated from the half-wave oxidation potential ($E_{1/2}$) as determined by cyclic voltammetry, conducted in methylene

Table 2. Molecular Orbital Energies (eV) and the Phenyl Isoquinoline C–C Bond Torsion Angles (deg) for Complexes 1–9

compound	ΔE^a /eV	E_{HOMO}^b /eV	E_{LUMO}^c /eV	torsion angle ^d /deg
1	1.99	-5.11	-3.12	16
2	1.96	-5.33	-3.37	32
3	1.97	-5.27	-3.3	16
4	2.02	-5.38	-3.36	16
5	1.95	-5.10	-3.15	29
6	1.95	-5.06	-3.11	18
7	1.93	-5.19	-3.26	17
8	2.75	-5.70	-2.95	n/a
9	2.77	-5.72	-2.95	n/a

^a Determined from the absorption onset wavelength in the UV–vis spectrum, in CH₂Cl₂, room temperature.⁴¹ ^b Determined from cyclic voltammetry, in CH₂Cl₂ solution.⁴⁰ ^c $E_{LUMO} = E_{HOMO} + \Delta E$. ^d Determined from the optimized geometries obtained by DFT calculations.

**Figure 6.** HOMO and LUMO energies for compounds 1–9. HOMO energies calculated from the $E_{1/2}$ obtained by cyclic voltammetry (in CH₂Cl₂ solutions)⁴⁰ and LUMO energies obtained from the optical energy gap,⁴¹ estimated from the absorption onset energy obtained by UV–vis spectroscopy (in CH₂Cl₂ solution).

chloride solution (Table 2, Figure 6).⁴⁰ Complexes **1**–**7** all showed cyclic voltammograms with a single, reversible one-electron oxidation peak. No reduction processes were detected within the solvent cathodic limit. Polymer complexes **8** and **9** displayed irreversible one-electron oxidations, but again no reduction waves were detected. Therefore, the optical energy gap of the complexes was estimated from the absorption onset in the absorption spectra, and this was used to obtain the LUMO energy, E_{LUMO} (Table 2, Figure 6).⁴¹ Both the nature of the substituents and their positions on the phenyl ring exert a significant influence over the orbitals' energies and therefore over the optical properties.

B3LYP calculations were performed on **1**–**7**. The frontier molecular orbital contour plots (Figure 7) were generated from geometry optimizations on the singlet ground state. Such an approach has previously been successful for modeling other phosphorescent Ir(III) complexes.^{31,42} For the entire series, the HOMOs are predominantly localized on the two phenyl rings but also have a significant contribution from the d-atomic orbitals of Ir(III). The lowest unoccupied molecular orbitals (LUMOs) are mostly localized on the isoquinoline rings; however, there are LCAO coefficients at the 2- and 4-phenyl positions and a node at the 3-phenyl site. The calculated trends

(40) D'Andrade, B. W.; Datta, S.; Forrest, S. R.; Djurovich, P.; Polikarpov, E.; Thompson, M. E. *Org. Electron.* **2005**, *6*, 11.

(41) Burrows, P. E.; Shen, Z.; Bulovic, V.; McCarty, D. M.; Forrest, S. R.; Cronin, J. A.; Thompson, M. E. *J. App. Phys.* **1996**, *79*, 7991.

(42) Hay, P. J. *J. Phys. Chem. A* **2002**, *106*, 1634.

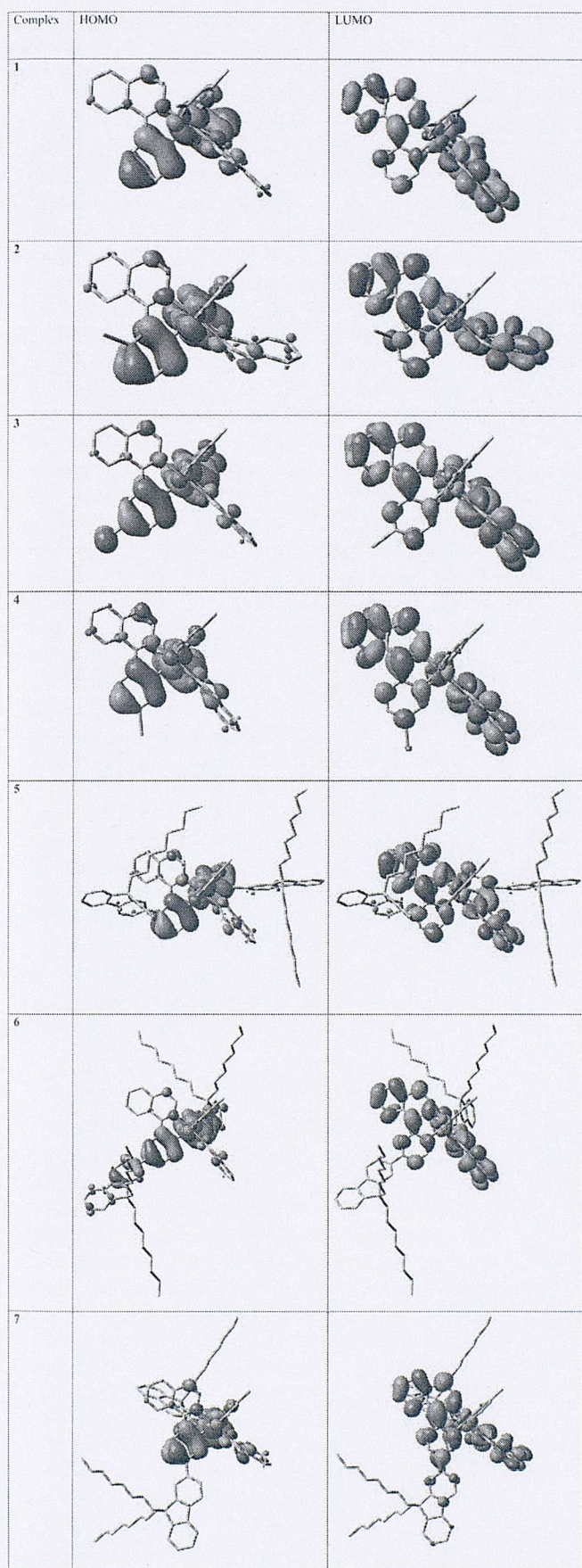


Figure 7. Contour plots of the HOMOs and LUMOs for complexes 1–7. The color and size of the lobes reflect the sign and amplitude of the linear combination of atomic orbital (LCAO) coefficients, respectively.

in the orbital energies (Figure S2) were in excellent agreement with those observed experimentally (Figure 6). Indeed, the

calculated E_{HOMO} values showed exactly the same variations as those in Figure 6, while the trend for the E_{LUMO} was in good agreement except for 3 and 6, which showed values that were lower than observed.

The bromine-substituted regioisomers 2 and 3 have significantly lower E_{HOMO} and E_{LUMO} than the unsubstituted complex 1. This is due to the inductive, electron-withdrawing effect of the bromine atom stabilizing the frontier orbitals, resulting in a net lowering of E_{HOMO} and E_{LUMO} . For complex 4, the Br substituent exerts predominantly an inductive effect, which affects the HOMO to a greater extent than the LUMO and results in a net separation of its frontier orbitals. This is supported by the DFT calculations, which show LCAO coefficients for both the HOMO and LUMO at the 4-phenyl position. The HOMO and LUMO levels of 3 are lowered less than 4. For 3, the Br substituent can exert both an inductive and mesomeric effect. The significant contribution of the Br 4p atomic orbitals to the HOMO can clearly be seen in 3 (Figure 7). The mesomeric effect leads to a destabilization of the HOMO. A similar destabilization was observed by Avilov et al., who carried out DFT calculations on fluorinated phenyl pyridine iridium cyclometallates.⁴³ Furthermore, for 3 the presence of a node in the LUMO at the 3-position means the LUMO is less affected by the inductive effect of the bromine than 2 and 4. The consequence is a smaller energy gap for 3; this is verified by a bathochromic shift in its emission.

E_{HOMO} and E_{LUMO} for the fluorenyl-substituted complexes 5–7 are similar to those of the substituted derivative 1. The DFT calculations show molecular orbitals with significant coefficients on the fluorenyl rings. Fluorenyl substituents in conjugation with the phenyl ring result in a stabilization of the LUMO energy level and a destabilization of the HOMO energy. Complex 6 has a raised HOMO energy, but its LUMO is unchanged from 1. DFT calculations show that the LUMO of 6 has the same distribution as 1 (i.e., predominantly localized on the isoquinoline ring but with a node at the 3-phenyl position). The fluorenyl substituent in 6 therefore cannot strongly influence the LUMO energy. However, DFT shows that its HOMO is significantly delocalized onto the fluorenyl substituent. This results in its higher HOMO energy and the bathochromic shift in the emission. Conversely, 7 has a HOMO that is isoelectronic with that of 1, but its LUMO energy is lower due to significant delocalization onto the fluorenyl substituents. Experimentally this is observed in the bathochromic shift in its emission. In general, the stabilizing effect on the LUMO by fluorenyl substituents has a greater magnitude than the destabilizing of the HOMO; therefore a greater bathochromic shift occurs in the emission of 7 relative to 6. Complexes 2 and 5 have identical emission maxima despite the significant difference in the energy levels of their frontier orbitals.

The torsion angles of the C–C bond that joins the phenyl and isoquinoline rings were measured from the optimized geometries obtained from the DFT calculation (Table 2). Complexes 1, 3, 4, 6, and 7 all have torsion angles of 16–18°, demonstrating that substitutions at the 3- and 4-phenyl positions do not impose any additional steric demands. Complexes 2 and 5 have significantly increased torsion angles (32°) due to the hindrance between substituents at the 2-phenyl position and the phenyl and isoquinoline rings. It is believed that this increased torsion leads to a reduction in the HOMO–LUMO energy gap and produces the observed red-shift. Similar bathochromic shifts have been observed by Fang et al.³¹ As mentioned previously,

(43) Avilov, I.; Minoofar, P.; Cornil, J.; De Cola, L. *J. Am. Chem. Soc.* **2007**, *129*, 8247.

it is also likely that the observed broadening of the NMR spectra and the reduced quantum yields for complexes **2** and **5** is a consequence of their large torsion angles.

Cyclic voltammetry indicates that complexes **8** and **9** have the same HOMO and LUMO energies as polyfluorene. Oxidation and reduction processes originating from the Ir(III) in these complexes are not observed due to their low loading levels. The measured orbitals are higher and lower in energy than the LUMO and HOMO of **1–7**, which implies that charge trapping will be a significant process in electrophosphorescence. The relative order of the emission energies of **8** and **9** mirrors those observed with the small molecule complexes; that is, the substitution at the 4-phenyl position results in a greater bathochromic shift in the emission wavelength (smaller energy gap) than the 3-phenyl position. Therefore, **9** emits at longer wavelength than **8**, as was observed for the small molecules with **7** emitting at longer wavelength than **6**. In the thin films, compound **8** displays significantly more fluorenyl singlet emission, but its quantum yield for phosphorescence is significantly greater than compound **9**. We propose that the lower LUMO energy of compound **9** (*vide supra*) facilitates energy transfer from the polyfluorene to the phosphor, leading to a reduction in the polyfluorene singlet emission. However, compound **9** shows a lower quantum yield, in an analogous manner to compound **7**.

Electrophosphorescence. The LEDs used for electrophosphorescence characterization consisted of a basic planar structure, as shown in the inset in Figure 8a.

Figure 8a also shows the electrophosphorescence spectra obtained for the homologous series of compounds **5–7**, while Figure 8b shows the spectra for compounds **8** and **9**. In both cases, the observed electrophosphorescence spectra closely matched the corresponding optically induced phosphorescent emission in the solid state. Thus, complexes **8** and **9** showed red electrophosphorescence with emission maxima at 636 and 648 nm, respectively. Further work is currently in progress in order to optimize the functional design of these prototypical LEDs, so that the maximum attainable luminances and quantum efficiencies can be quantitatively determined.

Conclusions

A series of regioisomeric $[\text{Ir}(\text{piq-X})_2(\text{acac})]$ complexes have been synthesized and their photophysical properties related to their chemical structures. The nature and site of the substituents exert a significant influence over the emission from the iridium complexes. The site of substitution was systematically varied around the phenyl ring of the 1-phenylisoquinolinato cyclometalating ligand. Substituents at the 3-position exerted a greater influence over the HOMO; electrochemistry and optical methods show its energy is raised by substitution at this site. DFT calculations showed a mesomeric effect, which results in 3-phenyl substituents influencing the electron density in the C–Ir bond. The 3-substitution site exerted a minimal influence on the LUMO energy. DFT calculations showed a node at this site. The 4-phenyl substitution site has a greater influence on the LUMO, reducing its energy with both a bromine and a fluorenyl substituent. The DFT calculations showed a LCAO coefficient at the 4-phenyl position; thus the bromine substituent reduces the LUMO energy by an inductive effect and the fluorenyl substituent by a mesomeric effect. The 2-phenyl substitution position shows severe steric hindrance, by both spectroscopic and theoretical methods. This results in a similarly reduced HOMO–LUMO energy gap for different substituents, which appears to be more dependent on the torsion angle than

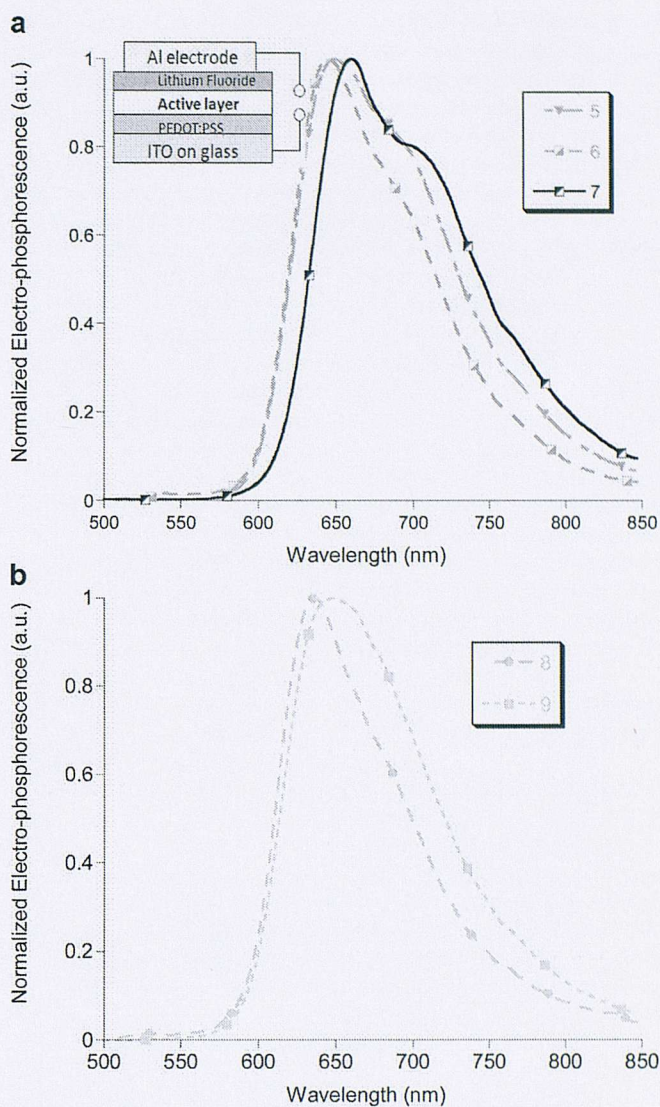


Figure 8. Electrophosphorescence spectra for compounds **5–7**, together with an inset showing the schematic structure of the planar LEDs (a). Electrophosphorescence spectra for compounds **8** and **9** (b), with the Commission Internationale de l’Eclairage (CIE) coordinates of ($x = 0.652$, $y = 0.323$) and ($x = 0.676$, $y = 0.325$), respectively.

its chemical nature. The emission quantum yields also depend on the site of substitution, with much better yields being observed for substituents in the 3-phenyl site than the 2-phenyl or 4-phenyl positions. The synthesis of polymeric–Ir(III) complexes of the type $[\text{Ir}(\text{piq-PF8})_2(\text{acac})]$ was achieved in good yield by Suzuki polycondensation between an AB monomer and a bromine-substituted Ir(III) regioisomer. The materials have efficient energy transfer from the polyfluorene to the phosphor, and they show red phosphorescence in the solid state. The emission energies of the regioisomeric polymer complexes mirror those observed with the small molecule complexes; that is, the substitution at the 4-phenyl position results in a greater bathochromic shift in the emission wavelength (smaller energy gap) than the 3-phenyl position. The electrophosphorescence spectra of compounds **5–9** show the same trends as the optically induced emission spectra.

Experimental Section

Materials. All reactions were conducted under a nitrogen atmosphere, using either standard anaerobic techniques or in a

nitrogen-filled glovebox. All solvents and reagents were obtained from commercial sources (Aldrich and Merck). Toluene was dried by distillation from sodium, and chloroform- d_3 was dried by distillation from calcium hydride. $\text{IrCl}_3 \cdot x\text{H}_2\text{O}$ was loaned by Johnson Matthey Plc. 2-(4',4',5',5'-Tetramethyl-1',3',2'-dioxaborolan-2'-yl)-9,9-dioctylfluorene,⁴⁴ 2-(4',4',5',5'-tetramethyl-1',3',2'-dioxaborolan-2'-yl)-7-bromo-9,9-dioctylfluorene,¹⁷ and [Ir(III) bis(1-(phenyl)isoquinolinato-*N,C'*)(acetylacetonate)] (**1**)²⁸ were prepared according to the literature methods. The preparations of 2-bromo-*N*-(2-hydroxy-2-phenylethyl)benzamide, 1-(2-bromophenyl)isoquinoline, 1-(3-bromophenyl)isoquinoline, and 1-(4-bromophenyl)isoquinoline are described in the Supporting Information.

Measurements. ^1H and ^{13}C (^1H) NMR spectra were performed on a Bruker Av-400 instrument. Elemental analyses were determined by Mr. Stephen Boyer at London Metropolitan University, North Campus, Holloway Road, London, N7. SEC data were collected using a Polymer Laboratories PL GPC-50 instrument with THF as the eluent, at a flow rate of 1 mL min^{-1} . Two Polymer Laboratories mixed D columns were used in series, and the M_n values were calibrated against narrow M_n polystyrene standards (Easy-Cal standards A and B). Chemical ionization (CI) and fast atom bombardment (FAB) mass spectra were recorded on a Micromass Autospec Premier instrument.

Absorption and Emission Spectroscopy. UV-visible spectra were recorded, at room temperature, on a Thermo Unicam UV500 spectrometer, in methylene chloride solutions at concentrations of 0.0001 M. Thin films of polymers **8** and **9** were spin coated from methylene chloride solutions of 10 mg/mL on a Laurell spin coater at 2000 rpm for 30 s.

Optically induced phosphorescence spectra were collected using a CaryEclipse fluorescence spectrophotometer. Solution phosphorescence measurements were done on methylene chloride solutions. The excitation wavelength was 350 nm, and the spectra were recorded at room temperature. Solution quantum yields were determined in degassed methylene chloride solutions with maximum absorbance of 0.2 using the Parker-Rees method.⁴⁵ Compound **1** was used as the standard ($\Phi_p = 0.2$ in methylene chloride).²⁸ Thin film quantum yields were determined using an integrating sphere with an excitation wavelength of 350 nm using the method developed by de Mello et al.⁴⁶ All spectra were corrected.

Theoretical Methods. Density functional theory (DFT) using the B3LYP hybrid functional was applied for all calculations. Geometry optimizations were performed without any constraint. All calculations were performed using the 6-31G basis set for the ligands and the LANL2DZ basis set for Ir(III),⁴² as implemented by Gaussian 03.⁴⁷

Cyclic Voltammetry. Cyclic voltammetry measurements were recorded in degassed, anhydrous methylene chloride, with 1 M tetrabutylammonium hexafluorophosphate as the supporting elec-

trolyte (at a scan rate of 100 mV/s). The working electrode was platinum, with a platinum wire counter electrode and a saturated Ag/AgCl pseudoreference electrode. Ferrocene was used as an internal standard. No reduction wave was observed from 0 to -2 V . Complexes **1**–**7** showed reversible oxidations, whereas complexes **8** and **9** displayed nonreversible oxidations. The oxidation potentials were converted into ionization potentials by relating the electrochemical energy scale to the vacuum energy scale, according to the method described by D'Andrade et al.⁴⁰ The LUMO energy level (E_{LUMO}) was calculated by adding the optical energy gap (ΔE) (calculated from the absorption edge) to the HOMO energy level.⁴¹

Electrophosphorescence. A 60 nm layer of poly(3,4-ethylene-dioxythiophene)/poly(styrene sulfonate) (PEDOT:PSS) was spin-coated onto ITO (indium-tin oxide)-coated glass, as a hole-injecting, semitransparent electrode. A thin film ($\sim 80 \text{ nm}$ thickness) of the compound under study was then spin-coated, from chlorobenzene solution, onto the PEDOT:PSS layer. The electron-injecting electrode was deposited by thermally evaporating approximately 1 nm of LiF, followed by 80 nm of aluminum. The prepared LED devices were encapsulated and tested under vacuum conditions at room temperature. The device testing was performed using a high-sensitivity parameter analyzer and a spectrally calibrated photodiode. Electrophosphorescence spectra were recorded using a fiber-coupled CCD spectrometer (ORIEL), with a spectral resolution of around 1 nm. All the devices were operated at similar driving biases of a few volts, and spectra were generally observed to be independent of driving bias.

Ligand Syntheses. 1-(2-(9',9'-Dioctylfluoren-2'-yl)phenyl)isoquinoline. 1-(2-Bromophenyl)isoquinoline (0.25 g, 1.77 mmol), 2-(4',4',5',5'-tetramethyl-1',3',2'-dioxaborolan-2'-yl)-9,9-dioctylfluorene (0.41 g, 1.77 mmol), and Pd(PPh₃)₄ (10 mg, 0.01 mmol) were suspended in toluene (10 mL) and Et₃NOH (2 mL of a 20% solution in water), and the reaction mixture was stirred at 90 °C for 18 h. The solution was extracted with CH₂Cl₂ (50 mL), washed with water (3 × 50 mL), dried (MgSO₄), and concentrated *in vacuo*. Column chromatography (silica gel, petroleum ether/EtOAc, 6:1) afforded the product as a colorless oil (0.75 g, 72%).

Anal. Calcd for C₄₄H₅₁N: C 88.99, H 8.66, N 2.36. Found: C 88.97, H 8.63, N 2.30. ^1H NMR (400 MHz, CDCl₃, ppm): δ 8.61 (d, $J = 5.8 \text{ Hz}$, 1H, ArH), 7.63 (m, 9H, ArH), 7.44 (m, 2H, ArH), 7.23 (m, 4H, ArH), 6.96 (s, 1H, ArH), 1.64 (m, 6H, CH₃), 1.2 (m, 14H, CH₂), 0.90 (m, 14H, CH₂). ^{13}C (^1H) NMR (125 MHz, CDCl₃, ppm): δ 161.6, 150.7, 150.0, 142.0, 141.9, 140.6, 139.9, 139.4, 138.2, 135.9, 130.7, 130.1, 129.7, 128.7, 127.6, 127.5, 126.7, 126.5, 123.7, 122.7, 119.9, 119.4, 119.2, 54.6, 40.3, 40.0, 31.9, 31.8, 30.0, 29.3, 29.2, 23.4, 23.3, 22.6, 14.1. *m/z* (CI): 594 [M + H]⁺.

1-(3-(9',9'-Dioctylfluoren-2'-yl)phenyl)isoquinoline. Prepared according to the same procedure used for 1-(2-(9',9'-dioctylfluoren-2'-yl)phenyl)isoquinoline. The title compound was a colorless oil (0.79 g, 80%).

Anal. Calcd for C₄₄H₅₁N: C 88.99, H 8.66, N 2.36. Found: C 88.99, H 8.65, N 2.31. ^1H NMR (400 MHz, CDCl₃, ppm): δ 8.64 (d, $J = 5.7 \text{ Hz}$, 1H, ArH), 8.17 (d, $J = 8.5 \text{ Hz}$, 1H, ArH), 7.74 (m, 12H, ArH), 7.33 (m, 3H, ArH), 2.04 (m, 6H, CH₃), 1.03 (m, 28H, CH₂). ^{13}C (^1H) NMR (125 MHz, CDCl₃, ppm): δ 161.8, 150.4, 159.6, 142.1, 141.9, 140.6, 134.0, 139.4, 138.2, 135.6, 130.7, 130.1, 129.7, 128.7, 127.6, 127.5, 126.7, 126.5, 123.7, 122.7, 119.8, 119.4, 119.2, 54.6, 40.3, 40.0, 31.8, 30.0, 29.4, 29.1, 23.4, 23.1, 22.8, 14.0. *m/z* (CI): 594 [M + H]⁺.

1-(4-(9',9'-Dioctylfluoren-2'-yl)phenyl)isoquinoline. This compound was prepared according to the same procedure used for 1-(2-(9',9'-dioctylfluoren-2'-yl)phenyl)isoquinoline. The title compound was isolated as a white crystalline solid (0.68 g, 70%).

Anal. Calcd for C₄₄H₅₁N: C 88.99, H 8.66, N 2.36. Found: C 89.01, H 8.67, N 2.31. ^1H NMR (400 MHz, CDCl₃, ppm): δ 8.67 (d, $J = 5.7 \text{ Hz}$, 1H, ArH), 8.24 (d, $J = 8.5 \text{ Hz}$, 1H, ArH), 7.95 (d, $J = 8.1 \text{ Hz}$, 1H, ArH), 7.75 (m, 10H, ArH), 7.60 (t, $J = 7.7 \text{ Hz}$,

(44) Ranger, M.; Leclere, M. *Can. J. Chem.* **1998**, *76*, 1571.

(45) Parker, C. A.; Rees, W. T. *Analyst* **1960**, *85*, 587.

(46) deMello, J. C.; Wittmann, H. F.; Friend, R. H. *Adv. Mater.* **1997**, *9*, 230.

(47) Frisch, M. J.; Trucks, G. W.; Schlegel, H. B.; Scuseria, G. E.; Robb, M. A.; Cheeseman, J. R.; Montgomery, Jr., J. A.; Vreven, T.; Kudin, K. N.; Burant, J. C.; Millam, J. M.; Iyengar, S. S.; Tomasi, J.; Barone, V.; Mennucci, B.; Cossi, M.; Scalmani, G.; Rega, N.; Petersson, G. A.; Nakatsuji, H.; Hada, M.; Ehara, M.; Toyota, K.; Fukuda, R.; Hasegawa, K.; Ishida, M.; Nakajima, T.; Honda, Y.; Kitao, O.; Nakai, H.; Klene, M.; Li, X.; Knox, J. E.; Hratchian, H. P.; Cross, J. B.; Bakken, V.; Adamo, C.; Jaramillo, J.; Gomperts, R.; Stratmann, R. E.; Yazyev, O.; Austin, A. J.; Cammi, R.; Pomelli, C.; Ochterski, J. W.; Ayala, P. Y.; Morokuma, K.; Voth, G. A.; Salvador, P.; Dannenberg, J. J.; Zakrzewski, V. G.; Dapprich, S.; Daniels, A. D.; Strain, M. C.; Farkas, O.; Malick, D. K.; Rabuck, A. D.; Raghavachari, K.; Foresman, J. B.; Ortiz, J. V.; Cui, Q.; Baboul, A. G.; Clifford, S.; Cioslowski, J.; Stefanov, B. B.; Liu, G.; Liashenko, A.; Piskorz, P.; Komaromi, I.; Martin, R. L.; Fox, D. J.; Keith, T.; Al-Laham, M. A.; Peng, C. Y.; Nanayakkara, A.; Challacombe, M.; Gill, P. M. W.; Johnson, B.; Chen, W.; Wong, M. W.; Gonzalez, C.; Pople, J. A. *Gaussian 03*; Gaussian, Inc.: Wallingford, CT, 2004.

1H, ArH), 7.38 (m, 3H, ArH), 2.06 (m, 4H, CH₂), 1.09 (m, 20H, CH₂), 0.83 (m, 6H, CH₃), 0.74 (m, 4H, CH₂). ¹³C{¹H} NMR (125 MHz, CDCl₃, ppm): δ 151.5, 151.0, 142.3, 141.9, 140.7, 139.4, 136.9, 130.4, 130.0, 127.6, 127.2, 127.1, 126.8, 126.0, 122.9, 121.5, 120.0, 119.9, 119.8, 61.0, 55.2, 40.4, 31.7, 30.0, 29.2, 23.8, 22.6, 14.0. *m/z* (CD): 594 [M + H]⁺.

Ir(III) Complex Syntheses. [Ir(III)bis(1-(2'-bromophenyl)isoquinolinato-*N,C*)(acetylacetonate)], 2. A mixture of IrCl₃·xH₂O (0.08 g, 0.23 mmol) and 1-(2-(bromophenyl)isoquinoline) (0.30 g, 0.51 mmol) in 2-ethoxyethanol (7.5 mL) and water (2.25 mL) was heated to 110 °C for 18 h. After the mixture cooled to room temperature, the precipitate was filtered and washed with EtOH/H₂O (95:5, 30 mL). The precipitate was then dissolved in CH₂Cl₂ (50 mL), dried (MgSO₄), and concentrated *in vacuo* to yield [bis(Ir(III)di-*μ*-chlorotetrakis(1-(2-(bromophenyl)isoquinolinato-*N,C*))] as a dark red solid (0.11 g, 60%). [Bis(Ir(III)di-*μ*-chlorotetrakis(1-(2-(bromophenyl)isoquinolinato-*N,C*))] (0.11 g, 0.115 mmol) was dissolved in 2-ethoxyethanol (10 mL) in the presence of acetyl acetone (0.09 mL, 0.58 mmol) and Na₂CO₃ (0.12 g, 1.15 mmol). The resulting suspension was stirred at 110 °C for 12 h. The reaction mixture was cooled to room temperature, and water (10 mL) was added. The resulting red precipitate was filtered, washed with H₂O (30 mL), and then dissolved in CH₂Cl₂ (30 mL), dried (MgSO₄), filtered, and concentrated *in vacuo*. Purification by flash column chromatography (silica gel, CH₂Cl₂/hexane, 5:1) afforded [*trans*-Ir(III)bis(1-(2'-bromophenyl)isoquinolinato-*N,C*)(acetyl acetone)] (0.11 g, 57%) and [*cis*-Ir(III)bis(1-(2'-bromophenyl)isoquinolinato-*N,C*)(acetyl acetone)] (0.04 g, 20%) as red solids.

[*trans*-Ir(III)bis(1-(2'-bromophenyl)isoquinolinato-*N,C*)(acetylacetonate)]. Anal. Calcd for C₃₅H₂₅Br₂IrN₂O₂: C 49.02, H 2.94, N 3.27. Found: C 48.99, H 2.95, N 3.25. ¹H NMR (400 MHz, CDCl₃, ppm): δ 8.42 (d, *J* = 8.3 Hz, 2H, ArH), 8.32 (d, *J* = 6.3 Hz, 2H, ArH), 7.90 (d, *J* = 8.1 Hz, 2H, ArH), 7.71 (t, *J* = 7.7 Hz, 2H, ArH), 7.60 (t, *J* = 7.6 Hz, 4H, ArH), 7.11 (d, *J* = 7.1 Hz, 2H, ArH), 6.47 (br, 2H, ArH), 5.245 (br s, 1H, OC(CH₃)CH), 1.773 (br s, 6H, OC(CH₃)CH). ¹³C{¹H} NMR (125 MHz, CDCl₃, ppm): δ 140.3, 140.0, 137.2, 131.3, 131.0, 130.7, 130.2, 129.7, 129.1, 127.7, 127.2, 127.0, 126.8, 125.9, 120.6, 119.9, 100.6, 28.6. *m/z* (FAB): 857 [M + H]⁺.

Ir(III)bis(1-(3'-bromophenyl)isoquinolinato-*N,C*)(acetylacetonate)], 3. This compound was synthesized according to the method used to prepare compound 2. It was isolated as a red solid (0.17 g, 63%).

Anal. Calcd for C₃₅H₂₅Br₂IrN₂O₂: C 49.02, H 2.94, N 3.27. Found: C 48.95, H 2.94, N 3.23. ¹H NMR (400 MHz, CDCl₃, ppm): δ 8.91 (m, 2H, ArH), 8.41 (d, *J* = 6.4 Hz, 2H, ArH), 8.30 (d, *J* = 1.9 Hz, 2H, ArH), 7.96 (m, 2H, ArH), 7.76 (m, 4H, ArH), 7.53 (d, *J* = 6.3 Hz, 2H, ArH), 6.77 (d, *J* = 8.1 Hz, 2H, ArH), 6.23 (d, *J* = 8.2 Hz, 2H, ArH), 5.21 (s, 1H, OC(CH₃)CH), 1.76 (s, 6H, OC(CH₃)CH). ¹³C{¹H} NMR (125 MHz, CDCl₃, ppm): δ 149.50, 148.58, 140.34, 137.16, 135.11, 132.01, 131.68, 130.99, 128.31, 127.45, 126.35, 120.70, 114.14. *m/z* (FAB): 857 [M + H]⁺.

[Ir(III)bis(1-(4'-bromophenyl)isoquinolinato-*N,C*)(acetylacetonate)], 4. This complex was synthesized according to the method used to prepare compound 2. It was isolated as a red solid (0.18 g, 69%).

Anal. Calcd for C₃₅H₂₅Br₂IrN₂O₂: C 49.02, H 2.94, N 3.27. Found: C 48.97, H 2.93, N 3.19. ¹H NMR (400 MHz, CDCl₃, ppm): δ 9.03 (d, *J* = 4.6 Hz, 2H, ArH), 8.51 (d, *J* = 6.3 Hz, 2H, ArH), 8.26 (d, *J* = 8.3 Hz, 2H, ArH), 7.98 (d, *J* = 4.6 Hz, 2H, ArH), 7.77 (m, 4H, ArH), 7.55 (d, *J* = 6.0 Hz, 2H, ArH), 7.11 (d, *J* = 8.0 Hz, 2H, ArH), 6.56 (s, 2H, ArH), 5.26 (s, 1H, OC(CH₃)CH), 1.81 (s, 6H, OC(CH₃)CH). ¹³C{¹H} NMR (125 MHz, CDCl₃, ppm):

δ 184.8, 169.0, 168.8, 151.9, 146.3, 140.6, 137.1, 131.5, 131.3, 130.7, 129.9, 128.7, 127.8, 127.4, 126.7, 126.4, 120.0, 119.5. *m/z* (FAB): 857 [M + H]⁺.

[Ir(III)bis(1-(2-(9',9'-dioctylfluoren-2'-yl)phenyl)isoquinolinato-*N,C*)(acetylacetonate)], 5. This complex was synthesized according to the method used to prepare compound 2. It was isolated as a red solid (0.36 g, 44%).

Anal. Calcd for C₉₃H₁₀₇IrN₂O₂: C 75.62, H 7.30, N 1.90. Found: C 75.63, H 7.35, N 1.92. ¹H NMR (400 MHz, CDCl₃, ppm): δ 8.48 (d, *J* = 6.3 Hz, 2H, ArH), 8.07 (br, m, 2H, ArH), 7.62 (br m, 6H, ArH), 7.46 (br m, 4H, ArH), 7.24 (m, 10H, ArH), 7.01 (br m, 6H, ArH), 6.75 (br m, 2H, ArH), 5.39 (br s, 1H, OC(CH₃)CH), 1.92 (br m, 12H, CH₂/CH₃), 1.28 (br m, 48H, OC(CH₃)CH, CH₃, CH₂), 0.42 (br m, 8H, CH₂). ¹³C{¹H} NMR (125 MHz, CDCl₃, ppm): δ 185.1, 185.1, 171.6, 150.8, 143.1, 143.1, 140.7, 140.3, 138.9, 136.1, 131.7, 129.9, 129.7, 128.8, 128.7, 126.5, 125.6, 125.1, 124.8, 122.9, 120.0, 119.5, 107.9, 100.6, 54.6, 54.5, 39.9, 31.9, 31.7, 30.3, 30.0, 29.7, 29.5, 29.2, 28.7, 23.5, 22.7, 22.6, 14.1. *m/z* (FAB): 1477 [M + H]⁺.

[Ir(III)bis(1-(3-(9',9'-dioctylfluoren-2'-yl)phenyl)isoquinolinato-*N,C*)(acetylacetonate)], 6. This compound was synthesized according to the method used to prepare compound 2. It was isolated as a red solid (0.27 g, 47%).

Anal. Calcd for C₉₃H₁₀₇IrN₂O₂: C 75.62, H 7.30, N 1.90. Found: C 75.6, H 7.18, N 1.91. ¹H NMR (400 MHz, CDCl₃, ppm): δ 9.18 (m, 2H, ArH), 8.59 (d, *J* = 8.6 Hz, 2H, ArH), 8.57 (s, 2H, ArH), 8.01 (m, 2H, ArH), 7.75 (m, 8H, ArH), 7.59 (m, 4H, ArH), 7.53 (s, 2H, ArH), 7.32 (m, 6H, ArH), 7.08 (d, *J* = 7.9 Hz, 2H, ArH), 6.61 (d, *J* = 6.6 Hz, 2H, ArH), 5.31 (s, 1H, OC(CH₃)CH), 1.97 (m, 8H, CH₂), 1.86 (s, 6H, OC(CH₃)CH), 1.11 (m, 40H, CH₂), 0.81 (m, 12H, CH₃), 0.70 (m, 8H, CH₂). ¹³C{¹H} NMR (125 MHz, CDCl₃, ppm): δ 184.9, 169.2, 151.3, 151.2, 150.9, 147.2, 141.4, 141.0, 140.6, 139.3, 137.3, 134.1, 133.9, 130.7, 128.6, 128.3, 127.7, 127.4, 126.8, 126.7, 126.5, 125.3, 122.8, 121.2, 120.0, 119.8, 119.5, 100.6, 54.9, 40.4, 31.7, 30.1, 29.2, 28.8, 23.8, 22.6, 14.0. *m/z* (FAB): 1477 [M + H]⁺.

[Ir(III)bis(1-(4-(9',9'-dioctylfluoren-2'-yl)phenyl)isoquinolinato-*N,C*)(acetylacetonate)], 7. This compound was synthesized according to the method used to prepare compound 2. It was isolated as a red solid (0.21 g, 57%).

Anal. Calcd for C₉₃H₁₀₇IrN₂O₂: C 75.62, H 7.30, N 1.90. Found: C 75.58, H 7.15, N 1.88. ¹H NMR (400 MHz, CDCl₃, ppm): δ 9.09 (m, 2H, ArH), 8.59 (d, *J* = 6.2 Hz, 2H, ArH), 8.33 (d, *J* = 8.5 Hz, 2H, ArH), 7.99 (m, 2H, ArH), 7.81 (m, 4H, ArH), 7.61 (d, *J* = 7.1 Hz, 2H, ArH), 7.55 (d, *J* = 6.3 Hz, 2H, ArH), 7.51 (d, *J* = 7.9 Hz, 2H, ArH), 7.29 (m, 16H, ArH), 7.12 (d, *J* = 1.2 Hz, 2H, ArH), 6.76 (d, *J* = 1.9 Hz, 2H, ArH), 5.32 (s, 1H, OC(CH₃)CH), 1.86 (s, 6H, OC(CH₃)CH), 1.80 (m, 4H, CH₂), 1.61 (m, 4H, CH₂), 0.7–1.7 (m, 52H, CH₂/CH₃), 0.46 (m, 8H, CH₂). ¹³C{¹H} NMR (125 MHz, CDCl₃, ppm): δ 184.8, 169.1, 152.1, 150.8, 150.6, 145.8, 140.8, 140.1, 139.4, 137.1, 131.1, 130.6, 129.9, 127.7, 127.4, 126.7, 126.5, 126.4, 125.6, 122.6, 121.1, 120.9, 119.5, 119.3, 100.6, 99.9, 54.7, 40.5, 40.3, 31.8, 30.1, 30.0, 29.3, 29.2, 28.8, 23.6, 22.6, 14.1. *m/z* (FAB): 1477 [M + H]⁺.

Polyfluorene-Ir(III) Complex Synthesis. [Ir(III)bis(1-(3'-(*o*-bromo-oligo[9',9'-dioctylfluoren-2',7'-diyl])phenyl)isoquinolinato-*N,C*)(acetylacetonate)], 8. A solution of 2-(4',4',5',5'-tetramethyl-1',3',2'-dioxaborolan-2'-yl)-7-bromo-9,9-dioctylfluorene (1.04 g, 1.74 mmol, 18 equiv), Ir(III)bis(1-(3'-bromophenyl)isoquinolinato-*N,C*)(acetylacetonate) (83 mg, 0.097 mmol, 1 equiv), Pd(OAc)₂ (5 mg, 0.022 mmol), and tricyclohexylphosphine (12 mg, 0.044 mmol) in toluene (75 mL) was heated to 90 °C. To this, Et₄NOH (7.50 mL of a 20% solution in water) was added and the solution stirred at 110 °C for 48 h. The reaction mixture was cooled to room temperature and subsequently poured into a large excess of MeOH, which resulted in the precipitation of the polymer. The precipitate was filtered, washed with water

(40 mL), MeOH (40 mL), and acetone (30 mL), and filtered through Celite using toluene as the eluent. The resulting solution was concentrated (to 20 mL), and Na_2CO_3 (0.20 g), acetyl acetone (2.00 mL), and 2-ethoxyethanol (10 mL) were added. The reaction mixture was stirred for 2 h at 110 °C and subsequently cooled to room temperature. The solution was again poured into an excess of MeOH and the precipitate filtered, washed with H_2O (40 mL) and MeOH (40 mL), and dried *in vacuo*. The pure product was isolated as a red powder (0.42 g, 55%).

Anal. Calcd for $\text{C}_{557}\text{H}_{745}\text{Br}_2\text{IrN}_2\text{O}_2$: C 85.19, H 9.56, N 0.36. Found: C 83.42, H 9.68, N 0.26. ^1H NMR (400 MHz, CDCl_3 , ppm): δ 9.14, 8.54, 7.90–7.60 (m, 6H, ArH), 7.04, 6.56, 5.27 (s, $\text{OC}(\text{CH}_3)\text{CH}$), 2.30–2.00 (m, 4H, CH_2), 1.83 (s, $\text{OC}(\text{CH}_3)\text{CH}$), 1.30–1.00 (m, 20H, CH_2), 0.90–0.70 (m, 10H, CH_3CH_2). $^{13}\text{C}\{^1\text{H}\}$ NMR (125 MHz, CDCl_3 , ppm): δ 151.8, 140.5, 140.0, 126.2, 121.5, 119.9, 55.3, 40.5, 40.4, 31.8, 30.1, 29.2, 23.9, 22.6, 14.1. GPC (PS): $M_n = 11\,555$, $M_w = 21\,439$, PDI = 1.85.

[Ir(III)bis(1-(4'-(ω -bromo-oligo[9'',9''-dioctylfluoren-2'',7''-diyl])phenyl)isoquinolinato-*N,C*(acetylacetonate))], 9. This complex was synthesized according to the same procedure used to produce [Ir(III)bis(1-(3'-(ω -bromo-oligo[9'',9''-dioctylfluoren-2'',7''-diyl])phenyl)isoquinolinato-*N,C*(acetylacetonate))] and isolated as a red powder (0.44 g, 58%).

Anal. Calcd for $\text{C}_{557}\text{H}_{745}\text{Br}_2\text{IrN}_2\text{O}_2$: C 85.19, H 9.56, N 0.36. Found: C 83.42, H 9.36, N 0.23. ^1H NMR (400 MHz, CDCl_3 , ppm):

δ 9.10 (ArH), 8.59 (ArH), 8.32 (ArH), 7.90–7.60 (m, 6H, ArH), 7.15 (ArH), 6.78 (ArH), 5.32 (s, $\text{OC}(\text{CH}_3)\text{CH}$), 2.30–2.00 (m, 4H, CH_2), 1.86 (s, $\text{OC}(\text{CH}_3)\text{CH}$), 1.30–1.00 (m, 20H, CH_2), 0.90–0.70 (m, 10H, CH_3CH_2). $^{13}\text{C}\{^1\text{H}\}$ NMR (125 MHz, CDCl_3 , ppm): δ 151.8, 140.5, 140.0, 126.2, 121.5, 119.9, 55.4, 40.4, 31.8, 30.1, 29.2, 23.9, 22.6, 14.1. GPC (PS): $M_n = 12\,112$, $M_w = 21\,266$, PDI = 1.7.

Acknowledgment. The EPSRC is acknowledged for funding the research (EP/C548132/1). Johnson Matthey Plc. is thanked for the donation of $\text{IrCl}_3 \cdot x\text{H}_2\text{O}$. Prof. Henry Rzepa and Dr. Sarah Wilsey at the EPSRC National Service for Computational Chemistry Software (NSCCS) are thanked for their help with the DFT calculations. Dr. Paul Wilde is thanked for the assistance with cyclic voltammetry measurements. Dr. Siva Krishnadasan is thanked for assistance with the thin film quantum yield determination.

Supporting Information Available: Scheme (Figure S1) and experimental protocols for the preparation of the bromine-substituted ligands. Figure S2 shows the variation in calculated orbital energies. This material is available free of charge via the Internet at <http://pubs.acs.org>.

OM800014E

Appendix C

Charge Recombination in Organic Photovoltaic Devices with High Open-Circuit Voltages

Sebastian Westenhoff,^{*,†,‡} Ian A. Howard,[†] Justin M. Hodgkiss,[†] Kiril R. Kirov,[†]
Hugo A. Bronstein,[§] Charlotte K. Williams,[§] Neil C. Greenham,[†] and
Richard H. Friend^{*,†}

OE-Group, Cavendish Laboratory, JJ Thomson Avenue, Cambridge CB3 0HE, U.K., Department of Chemistry, Biochemistry & Biophysics, University of Gothenburg, Box 462, 40530 Gothenburg, Sweden, and Department of Chemistry, Imperial College London, London SW7 2AZ, U.K.

Received May 9, 2008; E-mail: westenho@chem.gu.se; rhf10@cam.ac.uk

Abstract: A detailed charge recombination mechanism is presented for organic photovoltaic devices with a high open-circuit voltage. In a binary blend comprised of polyfluorene copolymers, the performance-limiting process is found to be the efficient recombination of tightly bound charge pairs into neutral triplet excitons. We arrive at this conclusion using optical transient absorption (TA) spectroscopy with visible and IR probes and over seven decades of time resolution. By resolving the polarization of the TA signal, we track the movement of polaronic states generated at the heterojunction not only in time but also in space. It is found that the photogenerated charge pairs are remarkably immobile at the heterojunction during their lifetime. The charge pairs are shown to be subject to efficient intersystem crossing and terminally recombine into F8BT triplet excitons within ~40 ns. Long-range charge separation competes rather unfavorably with intersystem crossing — 75% of all charge pairs decay into triplet excitons. Triplet exciton states are thermodynamically accessible in polymer solar cells with high open circuit voltage, and we therefore suggest this loss mechanism to be general. We discuss guidelines for the design of the next generation of organic photovoltaic materials where separating the metastable interfacial charge pairs within ~40 ns is paramount.

Organic semiconductor heterojunction solar cells are promising candidates for low-cost solar cell devices.^{1–5} The active layer is a partially demixed blend of organic semiconductor materials, where the offsets between the conduction band-edges and valence band-edges are used to ionize photogenerated excitations at the heterojunction. Provided that the maximum phase size is of the order of the exciton diffusion length, excitons can be split across heterojunctions with near unit efficiency, even with minimal band-edge offsets.^{1,2,6} Currently, the most efficient devices are made from blends with high electron affinity materials, such as fullerene derivatives.^{3–5} In these blends, large band-edge offsets reduce the available open-circuit voltage and fundamentally limit the photovoltaic efficiency.⁷ It is therefore

surprising that material combinations with low band-edge offsets have so far failed to outperform the solar cells made from fullerene derivatives, despite the efficient quenching of excitons by charge transfer.⁶ This suggests that a fundamental, performance-limiting process facilitates efficient recombination of charges in these blends.

A lively debate has developed to account for the efficiency limitation of charge collection. On one hand, inefficient bulk charge transport and the convoluted nature of charge-collection pathways are thought to lead to (trap-limited) *nongeminate* recombination as the dominant loss channel,⁸ particularly when long (>μs) time scales are investigated by optical spectroscopy or electrical methods.^{9,10} On the other hand, a number of studies that quantitatively account for all photogenerated charges suggest that intensity-independent *geminate* recombination may significantly deplete the number of long-lived and extractable charges.^{6,11–14} The recent discovery of emission from tightly bound interfacial charge transfer states in blends of conjugated polymers has challenged the assumption that free charge pairs,

[†] Cavendish Laboratory.

[‡] Present address: University of Gothenburg.

[§] Imperial College London.

- (1) Yu, G.; Gao, J.; Hummelen, J. C.; Wudl, F.; Heeger, A. J. *Science* **1995**, *270* (5243), 1789–1791.
- (2) Halls, J. J. M.; Walsh, C. A.; Greenham, N. C.; Marsaglia, E. A.; Friend, R. H.; Moratti, S. C.; Holmes, A. B. *Nature* **1995**, *376* (6540), 498–500.
- (3) Brabec, C. J.; Sariciftci, N. S.; Hummelen, J. C. *Adv. Funct. Mater.* **2001**, *11* (1), 15–26.
- (4) Kim, J. Y.; Lee, K.; Coates, N. E.; Moses, D.; Nguyen, T. Q.; Dante, M.; Heeger, A. J. *Science* **2007**, *317* (5835), 222–225.
- (5) Peet, J.; Kim, J. Y.; Coates, N. E.; Ma, W. L.; Moses, D.; Heeger, A. J.; Bazan, G. C. *Nat. Mater.* **2007**, *6* (7), 497–500.
- (6) McNeill, C. R.; Westenhoff, S.; Groves, C.; Friend, R. H.; Greenham, N. C. *J. Phys. Chem. C* **2007**, *111* (57), 19153–19160.
- (7) Koster, L. J. A.; Mihailetchi, V. D.; Blom, P. W. M. *Appl. Phys. Lett.* **2006**, *88* (9), 093511-1–093511-3.

(8) Nelson, J. *Phys. Rev. B* **2003**, *67* (15), 155209.

(9) Kim, Y.; Cook, S.; Tuladhar, S. M.; Choulis, S. A.; Nelson, J.; Durrant, J. R.; Bradley, D. D. C.; Giles, M.; McCulloch, I.; Ha, C. S.; Rec, M. *Nat. Mater.* **2006**, *5* (3), 197–203.

(10) Montanari, I.; Nogueira, A. F.; Nelson, J.; Durrant, J. R.; Winder, C.; Loi, M. A.; Sariciftci, N. S.; Brabec, C. *Appl. Phys. Lett.* **2002**, *81* (16), 3001–3003.

(11) Mihailetchi, V. D.; Koster, L. J. A.; Hummelen, J. C.; Blom, P. W. M. *Phys. Rev. Lett.* **2004**, *93* (21), 216601.

(12) Offermans, T.; Meskers, S. C. J.; Janssen, R. A. J. *J. Chem. Phys.* **2003**, *119* (20), 10924–10929.

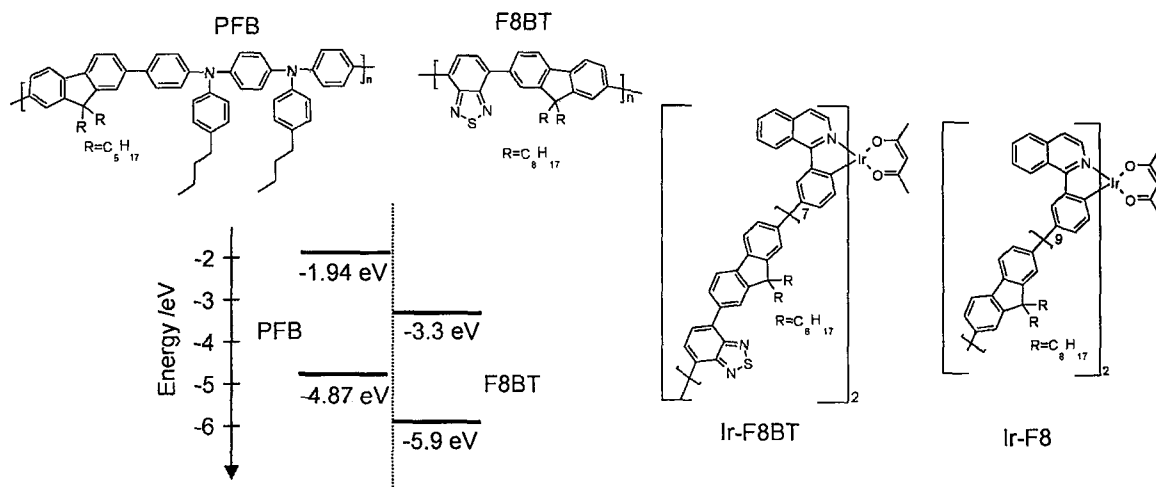


Figure 1. Chemical structures and energy of excited states: The chemical structures of PFB and F8BT are shown together with their highest occupied molecular orbital (HOMO) and lowest unoccupied molecular orbital (LUMO) energies. The HOMO level was deduced from cyclic voltammetry and the LUMO level was calculated based on the HOMO level and the $\pi-\pi^*$ gap. The chemical structure of [iridium(III) bis(1-(3'-(ω -4''',4''',5''',5'''-tetramethyl-1'',3'',2''-dioxaborolan-2''-yl)-oligo[9'',9''-dioctylfluorene-alt-benzothiadiazole)phenyl)isoquinolinato-*N,C'*)(acetylacetonate)] (Ir-F8BT) and [Ir(III)bis(1-(3'-(ω -bromo-oligo[9'',9''-dioctylfluorene-2'',7''-diyl)phenyl)isoquinolinato-*N,C'*)(acetylacetonate))] (Ir-F8) are also displayed.

which are electrons and holes without any wave function overlap, are the inevitable product of exciton quenching at the heterojunction.^{15,16} Furthermore, spectroscopic investigations of blends with low band-edge offsets have shown that triplet excitons are formed with high yields.^{17–19} However, the exact loss mechanism is not clear, mainly because electrical measurements lack time resolution to probe the early (ns) time scales, and it remains challenging to directly obtain spatial information about charge separation from the transient optical spectra of polymer-based polarons and excitons.

To investigate the performance-limiting recombination process in low band-edge offset photovoltaic devices, we introduce polarization-resolved transient absorption (TA) spectroscopy to directly track the movement of photogenerated charges. This measurement takes advantage of three features of bulk heterojunction organic solar cells: i) Electronic states probed by TA spectroscopy are predominantly polarized uniaxially along the chain segments on which they reside; ii) many excitons are ionized in close proximity to the site of photon absorption, thus propagating polarization information to the primary interfacial charge pair; and iii) in amorphous materials, spatial motion of transient states is associated with loss of polarization anisotropy.^{20,21} We observe that most photoexcitations never form fully

separated charges but that they remain as tightly bound and immobile charge pairs at the heterojunction. We combine these measurements with visible and infrared TA data spanning over seven decades in time, supported by an independent spectroscopic assignment of triplet states, to show that 75% of the immobile charge pairs undergo intersystem crossing and recombine terminally into triplet excitons on a 40 ns time scale. This approach should prove valuable to assess the viability of new materials engineered to favor long-range charge separation.

Results and Discussion

In our study, we investigate blends of polyfluorene copolymers poly(9,9-dioctylfluorene-*co*-bis-*N,N'*-(4-butylphenyl)-bis-*N,N'*-phenyl-1,4-phenylene-diamine) (PFB) and poly(9,9-dioctylfluorene-*alt*-benzothiadiazole) (F8BT) (Figure 1). The films were spin cast from chloroform solution, to produce intimately mixed blends, with phase sizes of less than 10 nm.^{6,22} Time-resolved optical TA spectra for pure F8BT and the blend containing 50% F8BT are summarized in parts a and b of Figure 2, respectively. We note that 490 nm excitation is used to selectively excite the low-bandgap material F8BT ($\lambda_{\text{max}} = 460$ nm) over PFB ($\lambda_{\text{max}} = 385$ nm). In both samples, we observe a positive $\Delta T/T$ signal for wavelengths shorter than 620 nm and a negative signal for longer wavelengths at a delay time of 350 fs. These features have been assigned to excitonic stimulated emission and photoinduced absorption of F8BT, respectively.²³ At a delay time of 900 ps, no signal is detected for the pure F8BT sample, whereas the TA spectrum of the blend is dominated by a secondary, spectrally broad absorption. This has been assigned to electrons and holes generated at the heterojunction.^{22,23} We report elsewhere that the charge generation time is limited by diffusion of excitons to the heterojunction and charge generation is completed at ~ 200 and ~ 10 ps for the blends containing 50% and 10% F8BT, respectively.²² Excitons are split with a very high efficiency despite only a ~ 200 meV stabilization of the charge-transfer state relative to the exciton energy.¹⁵

(13) De, S.; Pascher, T.; Maiti, M.; Jespersen, K. G.; Kesti, T.; Zhang, F. L.; Inganäs, O.; Yartsev, A.; Sundström, V. *J. Am. Chem. Soc.* **2007**, *129* (27), 8466–8472.

(14) Marsh, R. A.; Groves, C.; Greenham, N. C. *J. Appl. Phys.* **2007**, *101* (8), 083509.

(15) Morteani, A. C.; Dhoot, A. S.; Kim, J. S.; Silva, C.; Greenham, N. C.; Murphy, C.; Moons, E.; Cina, S.; Burroughes, J. H.; Friend, R. H. *Adv. Mater.* **2003**, *15* (20), 1708–1712.

(16) Offermans, T.; van Hal, P. A.; Meskers, S. C. J.; Koetse, M. M.; Janssen, R. A. *J. Phys. Rev. B* **2005**, *72* (4), 045213.

(17) Ford, T. A.; Avilov, I.; Beljonne, D.; Greenham, N. C. *Phys. Rev. B* **2005**, *71* (12), 125212.

(18) Veldman, D.; Bastiaansen, J.; Langeveld-Voss, B. M. W.; Sweelssen, J.; Koetse, M. M.; Meskers, S. C. J.; Janssen, R. A. *J. Thin Solid Films* **2006**, *511*, 581–586.

(19) Ford, T. A.; Ohkita, H.; Cook, S.; Durrant, J. R.; Greenham, N. C. *Chem. Phys. Lett.* **2008**, 237–241.

(20) Grage, M. M. L.; Pullerits, T.; Ruseckas, A.; Theander, M.; Inganäs, O.; Sundström, V. *Chem. Phys. Lett.* **2001**, *339* (1–2), 96–102.

(21) Westenhoff, S.; Beenken, W. J. D.; Friend, R. H.; Greenham, N. C.; Yartsev, A.; Sundström, V. *Phys. Rev. Lett.* **2006**, *97* (16), 166804.

(22) Westenhoff, S.; Howard, I. A.; Friend, R. H. *Phys. Rev. Lett.* **2008**, *101*, 016102.

(23) Stevens, M. A.; Silva, C.; Russell, D. M.; Friend, R. H. *Phys. Rev. B* **2001**, *63* (16), 165213.

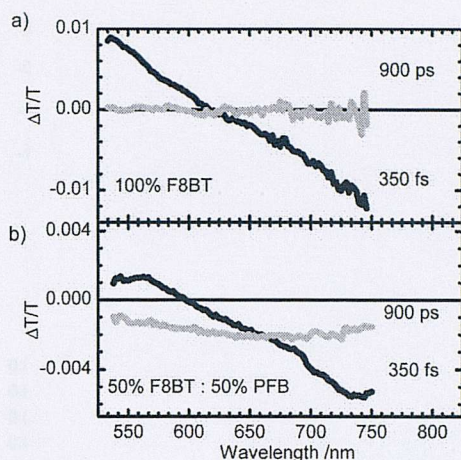


Figure 2. Transient absorption spectroscopy of PFB:F8BT on a femto- to nanosecond time scale: Panels (a) and (b) show the transient transmission spectra of F8BT and 50% PFB:50% F8BT, respectively. The delay times of the spectra were integrated over ± 150 fs and ± 100 ps for the 350 fs and 900 ps spectra, respectively. Excitation was at 490 nm with a fluence of $\sim 3 \times 10^{13}$ photons/cm².

To resolve the fate of the charge pairs on longer time scales, we augmented our femtosecond TA spectrometer with a Nd:YVO₄ laser, Q-switched via an electronically delayed trigger. With this setup, TA can be performed on the nanosecond to millisecond time scales. We simultaneously measured differential absorption signals for parallel and perpendicular polarizations of a single-wavelength probe, yielding both time-resolved polarization anisotropy ($r = (\Delta T/T^{\text{para}} - \Delta T/T^{\text{perp}}) / (\Delta T/T^{\text{para}} + 2 \Delta T/T^{\text{perp}})$) and magic-angle (population) decays ($\Delta T/T^{\text{para}} + 2 \Delta T/T^{\text{perp}}$).²⁴ We recall that the magnitude and decay dynamics of the polarization anisotropy measures the migration of photoexcitations within the disordered polymer films.

Part a of Figure 3 shows the population decay kinetics of the blends containing 50% (red circles) and 10% F8BT (black squares), measured with a probe wavelength of 532 nm. At this wavelength, mainly charged excitations are probed (vide infra). The similarity of the two kinetics traces suggests that their decay dynamics are insensitive to the blend composition. Nevertheless, the polarization anisotropy kinetics, shown in part b of Figure 3, reveals considerable differences between the two blends. First, the anisotropy is higher for the blend with 10% F8BT ($r(1 \text{ ns}) \sim 0.16$) compared to 50% F8BT ($r(1 \text{ ns}) \sim 0.06$). This is in agreement with a diffusion limited charge generation mechanism.²² In the 50% blend, excitons created within the F8BT domain have a longer mean path length to reach a heterojunction, and thus a lower level of polarization anisotropy at the time of charge transfer. Second, the polarization anisotropy of the blends containing 10% F8BT does not decay to zero. This is interpreted to arise from the small size of F8BT domains in this blend ratio, constraining the orientational freedom of transient states residing therein. Importantly, the signal retains significant polarization anisotropy on a time scale exceeding tens of nanoseconds in both blends. This shows conclusively that charge pairs are immobile at the heterojunction for a considerably long time. Indeed, the fact that this time scale approaches or exceeds that of the charge population decay (part a of Figure 3) leads us to the conclusion that most charge pairs

(24) Westenhoff, S.; Daniel, C.; Friend, R. H.; Silva, C.; Sundström, V.; Yartsev, A. *J. Chem. Phys.* **2005**, *122* (9), 094903.

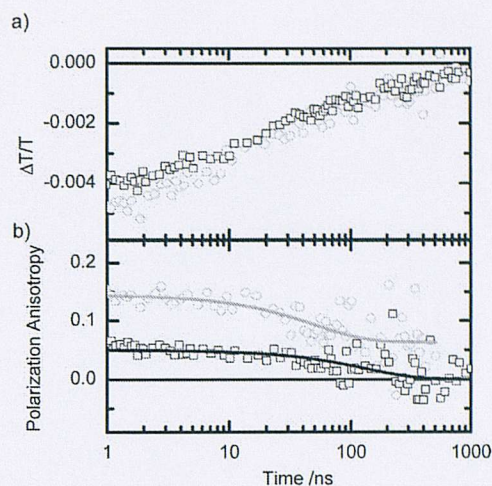


Figure 3. Polarization resolved transient absorption spectroscopy on nano- to microsecond time scale: Panel (a) shows the differential transmission kinetics recorded at 532 nm probe wavelength generated by the second harmonic of the Nd:YVO₄ laser for the two blend ratios with the polarization set to the magic angle to measure the population dynamics. Red open circles and black squares correspond to the blend containing 10% and 50% F8BT, respectively. The excitation fluence was 1×10^{14} and 1×10^{13} at 490 nm, respectively. Panel (b) shows the corresponding polarization anisotropy decays with color coding as in panel (a). The lines are monoexponential fits as a guide to the eye.

must remain at the site of generation until ultimately recombining there geminately.

We continued our investigation by measuring nanosecond TA spectra using a broad-band probe pulse (spanning from 530 to 780 nm) to identify any other states that may participate in the signal evolution. Part a of Figure 4 shows that the spectrum of the F8BT:PFB blend at 5 ns (red circles) resembles the shape of the 900 ps spectrum in part b of Figure 2, assigned to charge pairs. Inspecting the blend spectrum at 75 ns (black squares) reveals a spectral shift, with a new component absorbing in the > 700 nm region. We assign this component (vide infra) to F8BT triplet excitons, which are known to be generated in significant yields in this blend.¹⁷ The triplet formation process has been suggested to occur on submicrosecond time scales, but the exact formation dynamics have proved difficult to distinguish from those of charged states.¹⁹

To unambiguously verify the TA spectral shape of F8BT triplet excitons, we use an F8BT derivative (Ir-F8BT) bearing an iridium moiety (Ir-piq, Figure 1) conjugated with the oligomer backbone (details of the synthesis are provided in the Supporting Information). The large spin-orbit coupling induced by the iridium atom ensures facile intersystem crossing. Photoexcitations transfer to the triplet level on the F8BT unit with $\sim 100\%$ efficiency because it is the excited-state with lowest energy (energy diagram in part a of Figure 5), and charge-transfer intermediate states are avoided. Consequently, no photoluminescence is observed from either the F8BT or Ir-piq chromophores of Ir-F8BT (part b of Figure 5). The photophysical model depicted in part a of Figure 5 is confirmed by the photoluminescence measurements of the related poly-(9,9'-dioctyl-fluorene) (F8) based oligomer, Ir-F8.²⁵ In this case, the F8 triplet exciton is raised due to its larger bandgap compared to F8BT, and the triplet level on the Ir-piq subunit becomes the lowest energy level

(25) Bronstein, H. A.; Finlayson, C. E.; Kirov, K. R.; Friend, R. H.; Williams, C. K. *Organometallics* **2008**, *24* (13), 2980–2989.

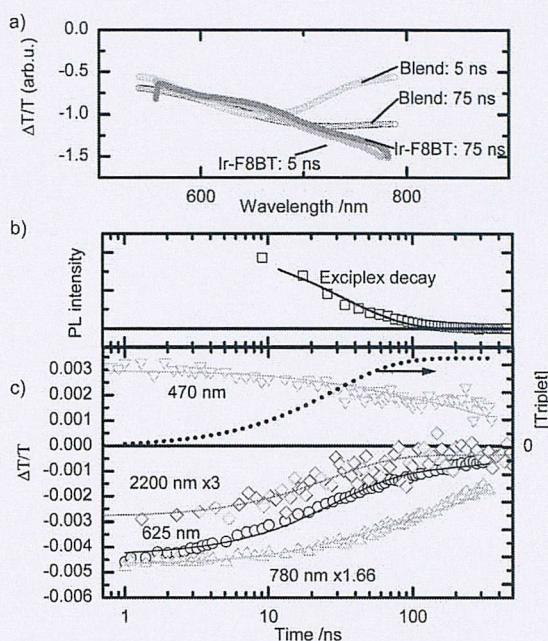


Figure 4. Triplet generation in F8BT:PFB polymer blends: Panel (a) shows time-resolved spectra of a PFB:F8BT (50%/50%) blend and Ir-F8BT films at delay times as indicated in the figure. The spectra are smoothed using a fast Fourier transform filter (Origin 6.0, Originlabs Inc.). Panel (b) shows the photoluminescence decay of the exciplex as measured by time-correlated single-photon counting at 650 nm (symbols) together with a monoexponential fit (line). Panel (c) shows TA kinetics with magic angle polarization between pump and probe at wavelengths as indicated in the figure. Excitation was at 355 nm with fluences of $\sim 5 \times 10^{13}$ photons/cm² (at 650 nm, 775 nm, and 2200 nm probe wavelength), and $\sim 2.5 \times 10^{13}$ photons/cm² (at 475 nm probe wavelength). The dashed black line is the triplet density reconstructed from the global fit.

in the Ir-F8 system. Consequently, strongly red-shifted phosphorescence from the Ir-piq moiety is observed (part b of Figure 5). The spectral signature of triplet excitons in Ir-F8BT is further confirmed by the observation that the TA spectra of the iridium-sensitized F8BT analogue exhibit no spectral shift with decay time (green and blue triangles shown in part a of Figure 4). Importantly, the spectral shapes of the TA spectrum of Ir-F8BT and the delayed TA spectrum of the blends are very similar, which strongly supports our assignment of triplet exciton formation in the blends.

The generation of triplet excitons from charge pairs represents a potential limitation to photovoltaic efficiencies in polymer solar cells. However, the yield of free charge carriers is dependent on the competitive kinetics of long-range charge separation versus recombination. To quantify the branching of primary charge pairs, we have measured the time dependence of the TA signals at the following wavelengths: i) 475 nm (probing the ground-state bleach of F8BT and thus the total number of excited states), ii) 625 nm (probing mainly the photoinduced absorption of polarons), iii) 780 nm (probing the photoinduced absorption of polarons and triplets in F8BT), and iv) 2200 nm (below the bandgap of triplet excitons and thus exclusively probing the photoinduced absorption of polarons²⁶) (part c of Figure 4). Care was taken to use the same excitation fluence and wavelength ($\lambda_{\text{exc}} = 355$ nm) in all measurements. Importantly, the data at the infrared (IR) wavelength shows that most of the charges decay on a nanosecond time scale. Triplets are

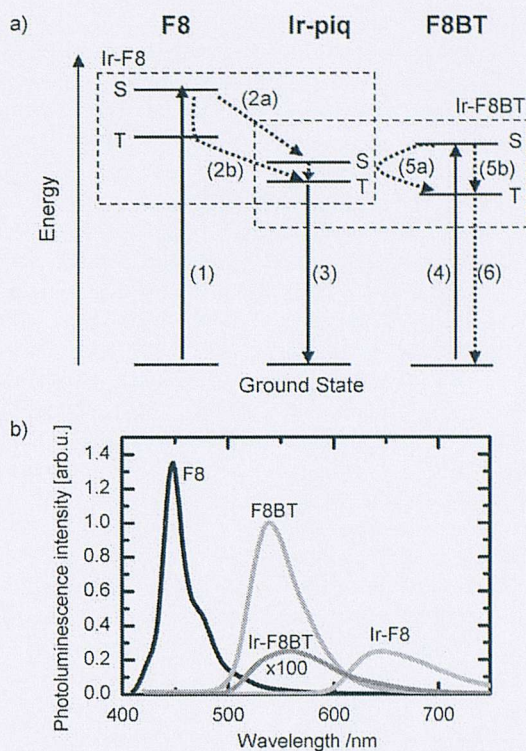


Figure 5. Photophysics of the iridium-oligofluorene copolymers: Panel (a) shows the energy scheme for the lowest-lying excited singlet (S) and triplet (T) states of F8BT, Ir-piq and F8. The singlet-triplet splitting of the charge-transfer excitations in Ir-piq is expected to be much smaller than for F8 and F8BT. The relevant energy levels of the oligomers Ir-F8 and Ir-F8BT are indicated by the boxes. In the photocycle of Ir-F8, (1) light is absorbed to create a singlet exciton on the F8 moiety, (2a) energy transfers to Ir-piq, where efficient intersystem crossing may occur or (2b) triplet excitons are formed on F8 by intersystem crossing and subsequently transfer to the Ir-piq triplet level, and (3) deactivation is by phosphorescence from Ir-piq. In the case of Ir-F8BT, the photocycle involves (4) absorption of light to form singlet excitons on F8BT, (5a) energy transfer to Ir-piq, efficient intersystem crossing, and back transfer to the F8BT triplet exciton or alternatively (5b) enhanced intersystem crossing on F8BT directly, and (6) deactivation by internal conversion. Panel (b) shows the photoluminescence spectra of F8, F8BT, Ir-F8BT, and Ir-F8. The spectra are corrected for the spectral response function of the detector. The integral of the spectra are scaled according to the photoluminescence quantum yield, which were measured using an integrating sphere.

generated on the same time scale as indicated by the dotted line in part c of Figure 4. This confirms that triplet excitons are formed directly from the charge-transfer state. However, $\sim 10\%$ of the IR signal prevails beyond 500 ns, thus we conclude that some charges do not undergo conversion into triplets. As the polarization anisotropy has clearly decayed to zero in the 50% blend at 500 ns delay time (part b of Figure 3), we conclude that at this time the remaining charge pairs must have migrated away from the heterojunction.

On the basis of our observations we propose the photophysical model depicted in Figure 6. Primary interfacial charge pairs (CP) are generated on a picosecond time scale with near unit efficiency.²² The anisotropy measurements (part b of Figure 3) show that these are trapped at the heterojunction. The charge pairs may be emissive exciplexes¹⁵ that can decay directly to the ground state (GS), or nonemissive polaron pairs.²⁷ All interfacial charge pairs may decay into triplet excitons (T), which

(26) Sheng, C. X.; Tong, M.; Singh, S.; Vardeny, Z. V. *Phys. Rev. B* **2007**, *75* (8), 085206.

(27) Huang, Y.-S.; Westenhoff, S.; Avilov, I.; Sreearunothai, P.; Hodgkiss, J. M.; Deleener, C.; Friend, R. H.; Beljonne, D. *Nat. Mater.* **2008**, *7*, 483–489.

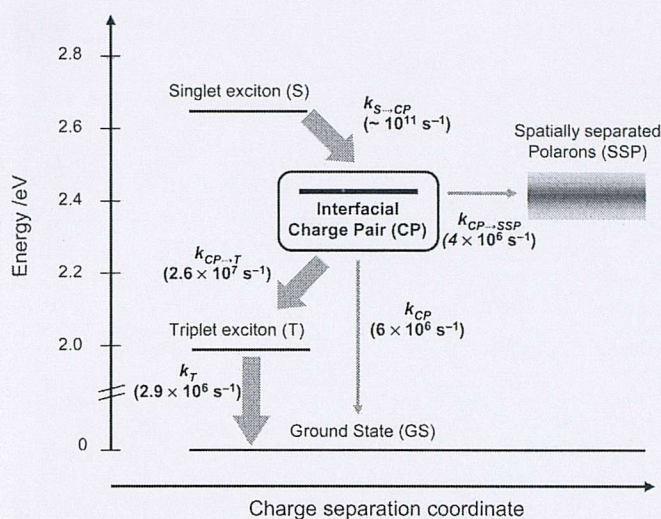


Figure 6. Charge recombination mechanism at the polymer–polymer heterojunction: The energy of the interfacial charge pair and F8BT triplet exciton were taken to be 200 meV (ref 15) and 700 meV (ref 28) below the F8BT singlet exciton energy level, respectively. The bold arrows summarize the main flow of energy.

are thermodynamically available for blend systems with small band edge offsets¹⁸ and high singlet–triplet exchange energies typical of conjugated polymers,²⁸ or further charge separate into spatially separated polarons (SSP). We have assumed that the excited-state absorptions due to interfacial and separated charge pairs are indistinguishable and that the bleaching cross section is similar for triplet, singlet, and charged excitations. The rate equations for the states are: $d[\text{CP}]/dt = -k_{\text{CP}\rightarrow\text{T}}[\text{CP}] - k_{\text{CP}}[\text{CP}] - k_{\text{CP}\rightarrow\text{SSP}}[\text{CP}]$, $d[\text{T}]/dt = k_{\text{CP}\rightarrow\text{T}}[\text{CP}] - k_{\text{T}}[\text{T}]$, $d[\text{SSP}]/dt = k_{\text{CP}\rightarrow\text{SSP}}[\text{CP}]$, and $d[\text{GS}]/dt = k_{\text{T}}[\text{T}] + k_{\text{CP}}[\text{CP}] + k_{\text{SSP}}[\text{SSP}]$. We fit the TA data globally based on these rate equations (see Methods for details) and require $k_{\text{CP}\rightarrow\text{T}} + k_{\text{CP}\rightarrow\text{SSP}} + k_{\text{CP}} = 3.5 \times 10^7 \text{ s}^{-1}$, which is the decay constant of the exciplex photoluminescence (part b of Figure 4). We do not include the decay of the spatially separated polarons in the model, as the relatively small signal from SSP states does not allow us to extract the decay dynamics of this state. We have confirmed that no significant correlation between the parameters exists (Supporting Information). The fit allows us to determine the branching ratios between the three decay channels of interfacial charge-pair state without any further a priori assumptions about the density or cross sections of the states involved. The rate constants yielded are $k_{\text{CP}\rightarrow\text{T}} = (2.6 \pm 0.4) \times 10^7 \text{ s}^{-1}$, $k_{\text{CP}} = (6 \pm 4) \times 10^6 \text{ s}^{-1}$, and $k_{\text{CP}\rightarrow\text{SSP}} = (4 \pm 0.8) \times 10^6 \text{ s}^{-1}$. We note that the intersystem crossing rate from the charge-transfer state ($k_{\text{CP}\rightarrow\text{T}}$) is similar to rates of triplet formation from singlet excitons in pristine F8BT, which was estimated to be $1.2 \times 10^7 \text{ s}^{-1}$.¹⁷ Thus, the increased triplet population in blends is due to the increased lifetime of the charge-transfer state relative to a singlet exciton in a pristine polymer film.

We conclude that immobile, metastable interfacial states are the bottleneck of device efficiency in blends of F8BT and PFB. Seventy-five percent of these charge pairs recombine at the place of their formation into triplet excitons on a time scale of ~ 40 ns. The extractable charges are constrained by a modest 10% geminate pair dissociation yield. This readily explains the modest external quantum efficiency of 3.4% measured in solar

cells under short circuit conditions made from this material system.⁶ The clear implication is that unless open-circuit voltage is sacrificed to make the triplet exciton thermodynamically inaccessible, interfacial charge pairs are vulnerable to terminal loss as triplets if they are not further separated within ~ 40 ns.

Subject to the time-scale constraint imposed by triplet formation, facilitating rapid geminate pair dissociation in organic photovoltaic devices calls for strategies to direct charge transport vectorially away from the interface in opposition to their mutual Coulombic attraction. Nature overcomes a similar kinetic quandary in photosynthesis, where photoexcited electrons are rapidly shuttled away from holes via a cascade of quinone acceptors with appropriately positioned energy levels.²⁹ Likewise, dye-sensitized solar cells owe their impressive quantum efficiency in part to an architecture in which the electron donor and acceptor materials are bridged by a sensitizer to direct charge carriers in opposite directions over a longer length-scale.³⁰ Whereas neither of these examples are optimized with respect to voltage retention, they may yet provide inspiration for heterojunctions engineered to favor long-range charge separation. Current state-of-the-art bulk heterojunction photovoltaic devices comprise blends of P3HT and PCBM.⁵ Here, the charge pairs are stable with respect to triplet excitons (leading to modest open-circuit voltages of ~ 0.6 V).³¹ Notwithstanding, recent experimental evidence suggests that the high performance of PCBM:polymer solar cells could be due to kinetic rather than energetic considerations; with its high local charge mobility allowing charges to readily escape the interface region on a picosecond-to-nanosecond time scale with minimal applied field.^{32,33} This consideration suggests that electron acceptors with lower electron affinities than PCBM ought still to be considered for photovoltaic devices, as long as they exhibit high local electron mobilities. The intersystem crossing time of ~ 40 ns sets a general benchmark against which the kinetics of long-range charge separation must be favorable for efficient charge extraction in the next generation of photovoltaic materials. Polarization-resolved, nanosecond time-resolved TA spectroscopy should prove valuable for directly assessing the interfacial kinetic control in new bulk-heterojunction device architectures.

Methods

Transient Absorption Spectroscopy. Femto- to picosecond TA spectroscopy was performed utilizing two optical paramagnetic amplifiers (OPAs) seeded by the 800 nm output (pulse duration < 80 fs) of a commercially available oscillator/amplifier system (Tsunami and Spitfire Pro, Spectra Physics). Narrow-band pulses were generated using a TOPAS system (Light Conversion). Broad-band pulses spanning from 530 to 800 nm were generated with a home-built non-collinear OPA (Manzoni, C.; Polli, D.; Cerullo, G. *Rev. Sci. Instrum.* **2006**, *77*, 023103). Differential transient transmission spectra were measured by spectrally resolving probe and reference pulses in a spectrograph and recording the light intensity with two diode arrays. The 256 pixel array (S3901256Q, Hamamatsu) was read out using

(29) Wraight, C. A. *Photochem. Photobiol.* **1979**, *30* (6), 767–776.

(30) O'Regan, B.; Gratzel, M. *Nature* **1991**, *353* (6346), 737–740.

(31) Ohkita, H.; Cook, S.; Astuti, Y.; Duffy, W.; Heeney, M.; Tierney, S.; McCulloch, I.; Bradley, D. D. C.; Durrant, J. R. *Chem. Commun.* **2006**, (37), 3939–3941.

(32) Barbour, L. W.; Hegadorn, M.; Asbury, J. B. *J. Phys. Chem. B* **2006**, *110* (48), 24281–24286.

(33) Marsh, R. A.; McNeill, C. R.; Abrusci, A.; Campbell, A. R.; Friend, R. H. *Nano Lett.* **2008**, *8* (5), 1393–1398.

(28) Wilson, J. S.; Dhoot, A. S.; Seeley, A.; Khan, M. S.; Kohler, A.; Friend, R. H. *Nature* **2001**, *413* (6858), 828–831.

Table 1. Fitting Parameters

parameter	cross sections			
	475 nm	650 nm	780 nm	2200 nm
probe wavelength	475 nm	650 nm	780 nm	2200 nm
$\sigma_{CP}^a / 10^{-16} \text{ cm}^2$	—	4.3 ± 0.2	2.8 ± 0.1	1 ± 0.1
$\sigma_T^a / 10^{-16} \text{ cm}^2$	—	1.1 ± 0.3	1.8 ± 0.4	—
$\sigma_{abs}^a / 10^{-16} \text{ cm}^2$	4.0 ± 0.3	—	—	—

parameter	rates
$k_{CP \rightarrow T}^b / 10^7 \text{ s}^{-1}$	2.6 ± 0.4
$k_{CP}^b / 10^6 \text{ s}^{-1}$	6 ± 4
$k_{CP \rightarrow SSP}^b / 10^6 \text{ s}^{-1}$	4 ± 0.8
$k_T / 10^6 \text{ s}^{-1}$	2.9 ± 0.6

^aThe cross sections are referenced to the absorption cross section of F8BT at 475 nm, which was determined to be $\sigma_{abs} = 4 \times 10^{-16} \text{ cm}^{-2}$ in ref 23 ^b $k_{CP \rightarrow T} + k_{CP} + k_{CP \rightarrow SSP} = 3.5 \times 10^{-7} \text{ s}^{-1}$ was required during fitting. The value was determined as the monoexponential lifetime of the delayed exciplex emission.

a commercially available circuit at 2 MFz (C7844, Hamamatsu) and digitized on the fly for each laser pulse using a PXI-6122 card (National Instruments). The transmission with excitation light on and off was calculated using a computer with a real-time operating system (PXI-8175 and Labview real-time) and recorded as a function of optical delay between pump and probe. With this detection system, a complete TA spectrum can be recorded from two subsequent laser pulses. The time-resolved spectra shown in this paper were averaged over several hundred laser shots. They were corrected for chirp of the probe, and offsets at negative time were subtracted. The time resolution was ~ 120 fs, as judged from the rise time of the signal.

For nanosecond- to microsecond TA spectroscopy, a Q-switched Nd:YVO₄ laser (AOT-YVO-25QSPX, Advanced Optical Technology Ltd.) with a pulse length of 500 ps was synchronized electronically with the Ti:Sapphire femtosecond laser by means of a variable delay generator (DG 535, Stanford Research Systems). The instrument response was ~ 0.8 ns, as judged by the rise time of the signal, and the observation window was < 1 ms and was limited only by the repetition rate of the femtosecond laser. The second (532 nm) and third (355 nm) harmonic of the Nd:YVO₄ laser was used as either a

pump or a single-wavelength probe source. For polarization anisotropy measurements, we separated *s* and *p* polarizations with a cube polarizer and detected the $\Delta T/T$ signals with polarization parallel and perpendicular to the excitation source simultaneously.²⁴

Global Fitting Procedure According to the Photophysical Model (Figure 6). The integrated rate laws for the model are

$$[\text{CP}] = [\text{CP}]_0 \exp(-(k_{CP \rightarrow SSP} + k_{CP} + k_{CP \rightarrow T})t) \quad (1)$$

$$[T] = [\text{CP}]_0 \frac{k_{CP \rightarrow T}}{k_{CP} + k_{CP \rightarrow SSP} + k_{CP \rightarrow T}} (1 - [\text{CP}]) \exp(-k_T t) \quad (2)$$

$$[\text{SSP}] = [\text{CP}]_0 \frac{k_{CP \rightarrow SSP}}{k_{CP} + k_{CP \rightarrow SSP} + k_{CP \rightarrow T}} (1 - [\text{CP}]) \quad (3)$$

And the total differential absorption signal is given by

$$\Delta T/T = [-\sigma_{CP}([\text{CP}] + [\text{SSP}]) - \sigma_T[T] + \sigma_{abs}([\text{CP}] + [T] + [\text{SSP}])]d \quad (4)$$

with *d* as the film thickness, σ_{CP} , σ_T , and σ_{abs} respectively being the cross section of the charged excitations (which is assumed to be the same for interfacial charge pairs and spatially separated polarons), cross section of the F8BT triplet excitons, and the absorption cross section of F8BT. See Figure 6 for other assignments. The fitting parameters are summarized in Table 1. The errors were determined by a dependency analysis (Supporting Information).

Acknowledgment. The authors acknowledge financial support from EPSRC. H.A.B. and C.K.W. acknowledge EPSRC grant EP/C548132/1. S.W. thanks Fitzwilliam College Cambridge for a Junior Research Fellowship, and I.A.H. thanks the Cambridge Commonwealth Trust for financial support.

Supporting Information Available: Statistical analysis of the TA global fitting parameters and the synthesis of Ir-F8BT. This material is available free of charge via the Internet at <http://pubs.acs.org>.

JA803054G